VOL. 83, NO. EM3
JUNE 1957

JOURNAL of the

Engineering Mechanics Division

PROCEEDINGS OF THE
AMERICAN SOCIETY OF CIVIL ENGINEERS

Journal of the

ENGINEERING MECHANICS DIVISION

Proceedings of the American Society of Civil Engineers

CONTENTS

June, 1960

Papers

(Over)

Journal of the
ENGINEERING MECHANICS DIVISION
Proceedings of the American Society of Civil Engineers

ANALYSIS OF FRAMES WITH NONLINEAR BEHAVIOR

By Alfredo Hua-Sing Ang,[1] A.M. ASCE

SYNOPSIS

A method for the analysis of frames with nonlinear behavior subjected to lateral deformations is presented. The nonlinear characteristics of both the members and the connections are considered. The relationships needed for the analysis of mild steel frames including strain hardening are derived for use with any structural wide flange sections with an error of less than ± 3% in the resisting moments. Two examples are presented to illustrate the applications of the method.

INTRODUCTION

Analyses of indeterminate frame structures of mild steel subjected to deformations beyond the elastic limit are usually based on moment-curvature relationships that are flat after the fully-plastic resistance of a member has been developed. If the deformations of the members are not restricted by buckling or fracture, the behavior of a structure is largely a function of the stress-strain characteristics of the material, and strengths greater than the fully-plastic resistance can be obtained as a result of strain hardening. Often it is desirable to be able to assess the benefits associated with such increased strength. An example is the case of a structure designed to resist blast loading for which it is desired to determine the energy-absorbing capacity when strain hardening is taken into account. Likewise, in research studies, it is

Note.—Discussion open until November 1, 1960. To extend the closing date one month, a written request must be filed with the Executive Secretary, ASCE. This paper is part of the copyrighted Journal of the Engineering Mechanics Division, Proceedings of the American Society of Civil Engineers, Vol. 86, No. EM 3, June, 1960.

[1] Asst. Prof., Dept. of Civ. Engrg., Univ. of Illinois, Urbana, Ill.

often desirable to have available a means of analyzing the resistance of frames and beams that permits strain hardening to be considered.

The subject of elasto-plastic analysis and pure plastic analysis have been treated extensively by several authors. However, a very limited amount of published material can be found that treats the analysis of statically indeterminate structures when the nonlinear behavior of its component parts is considered. This paper presents a method by which indeterminate frame structures composed of elements (members and connections) having individual resistance-deformation characteristics of any monotonically increasing form subjected to lateral deformations can be analyzed. For indeterminate structures of mild steel, the increased strength and energy-absorbing capacity resulting from strain hardening can, therefore, be calculated. The resistance of structures with riveted and bolted column-base and beam-to-column connections can be evaluated with the nonlinear characteristics of the connections taken into account. The method also may be used to analyze structures of other materials with nonlinear characteristics, such as aluminum, without resorting to linear approximations. The method has been found to be particularly useful in the case of research studies.

The practicability of the method depends upon a convenient means of relating the resistance of a member to a particular deformation. In this method the resisting moments at the ends of a member are related to the corresponding end-slopes. This relationship is called the "moment end-slope relationship."

The resisting moments that correspond to given lateral displacements of the loaded joints in a structure are found by means of an iterative procedure. Such a procedure is made convenient by the use of the moment end-slope curves for the individual members and moment-rotation curves for the nonrigid connections. After the compatible set of resisting moments have been obtained, the corresponding set of loads required to produce the particular joint displacements are computed. By solving a set of such problems, load-joint displacement relationships can be obtained for a range of loads, or conversely, for a range of displacements.

In particular, the application of the method to the analysis of mild-steel frames loaded into the range of strain hardening is presented. Two examples are solved to illustrate the application of the method. The structure of Example A is of rigid joints, while that of Example B is of nonrigid joints.

It is assumed that the ultimate strength of mild steel in a direct tension or compression test, under the particular time-dependent conditions involved, can be fully utilized by the structural members. The stress-strain relationship used in obtaining the moment end-slope relationship is typical of that obtained for ASTM A-7 steel, as shown in Fig. 1. The moment end-slope relationship for mild steel are presented in dimensionless form and can be used for all commonly available structural wide flange sections within an error of $\pm$ 3% in the resisting moments.

Notation.—The letter symbols adopted for use in this paper are defined where they first appear, in the illustrations or in the text, and are arranged alphabetically, for convenience of reference, in the Appendix.

THE METHOD OF ANALYSIS

The assumption underlying the method of analysis are as follows:

1. The moment-curvature relationship corresponds to pure flexure. Effects of axial forces, shearing forces, buckling, and residual stresses on such relationship are neglected.
2. Loadings are concentrated at the joints and are always increasing.
3. Clockwise moments acting on a member are positive.
4. For a rigid joint, moments up to and including the ultimate moment of the members can be transmitted without destroying continuity of the joint. For a nonrigid joint, the moment-rotation characteristics of the connection must be defined up to and including the ultimate moment. In such cases, the rotations of both the connection and the members must be considered.

The analysis of statically indeterminate structures involves, basically, the solutions of the equations of equilibrium and continuity. The equations of equilibrium and physical continuity at a joint j, Fig. 2, in a given structure may be expressed, respectively, as:

$$\sum_{i=1}^{n} M_{ji} = 0 \quad \ldots\ldots\ldots\ldots\ldots\ldots (1)$$

and

$$\Omega_{j1} = \Omega_{j2} = \ldots = \Omega_{ji} = \ldots = \Omega_{jn} \quad \ldots\ldots\ldots\ldots (2)$$

in which

$$\Omega_{ji} = F\left(\psi, \phi_{ji}\right) \qquad \text{for rigid joints}$$

$$\Omega_{ji} = G\left(\psi, \phi_{ji}, \phi^{c}_{ji}\right) \qquad \text{for non-rigid joints}$$

and n denotes the number of members meeting at a joint, M the total moment at a section, and Ω the total rotation. If a simple relationship between the moments, and the end-slopes and connection rotations can be found, the total rotations, Ω_{ji}, may be expressed as

$$\Omega_{ji} = F\left(\psi, M_{ji}, M_{ij}\right) \quad \ldots\ldots\ldots\ldots\ldots (3)$$

and equations of continuity, or conversely, equations of equilibrium, may be written for each joint in a structure that are analogous to the slope-deflection equations for linearly elastic structures. Under such conditions a purely analytical solution is possible. For nonlinear cases, the relationship defined by Eq. 3 usually turns out to be complicated, as in the case of mild steel with strain hardening, and the equations of equilibrium or continuity will involve integral expressions. For such cases, a semi-graphical step-by-step approximation is possible in which the relationships $\phi_{ji} = f\,(M_{ji}, M_{ij})$ and $\phi^{c}_{ji} = g\,(M_{ji})$ are expressed in graphical form. ϕ_{ji} is the end slope at end j of member ji, and ϕ^{c}_{ji} is the rotation of the connection at j of member ji.

The moments at the ends of every member in a structure are assumed at random. These moments, which are in general not compatible with a given deformation pattern of the structure, are corrected iteratively, subject to the conditions of equilibrium and continuity at the joints, until a set of values with convergence to a desired degree of precision has been obtained. It starts out

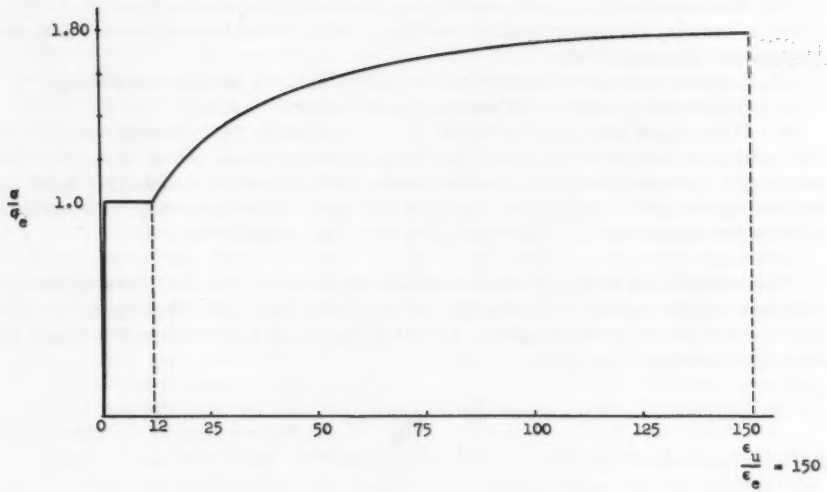

FIG. 1.—TYPICAL STRESS-STRAIN RELATIONSHIP FOR A-7 STEEL

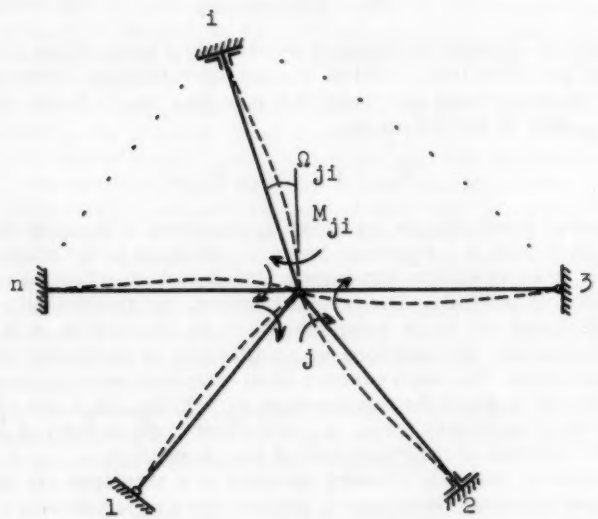

FIG. 2.—MOMENTS AND ROTATIONS AT A JOINT j

by assuming displacements of the loaded joints. From this assumption the general deflected shape of the structure may be determined, and the finding of the appropriate resistance of the structure to that particular deformation pattern is accomplished, assuming that reversal of strain does not occur any place in the structure. This requires a prior knowledge of the correct direction of the moment, which can be determined from the deflected shape of the structure.

The iterative method of correcting the end moments is based on the principle that the moment at the near-end of a member, M_{ji}, as shown in Fig. 2, can be found that will produce the required end-slope, ϕ_{ji}, at the near-end with a known or assumed far-end moment, M_{ij}. The near-end moment, M_{ji}, that corresponds to a given end-slope, ϕ_{ji}, and far-end moment, M_{ij}, can be determined rapidly from the moment end-slope curves given in Figs. 3 and 4 (Fig. 3b is a portion of Fig. 3a to an enlarged scale). Figs. 3 are for members with contraflexure; Fig. 4 is for members without contraflexure. The values of the connection rotation, ϕ^{c}_{ji}, may be determined from moment-rotation curves similar to Figs. 5 and 6. Figs. 5 and 6 are presented herein for purposes of illustration only, but are typical of actual beam-to-column and column-base moment-rotation relationships.

The solution for a joint is obtained once a set of near-end moments and the corresponding near-end rotations is found such that the relationships defined by Eqs. 1 and 2 are satisfied simultaneously.

The moments and rotations at a joint would be the correct values if all the far-end moments, M_{ij}, that were used in determining M_{ji} and ϕ_{ji} were the correct ones. The determination of this tentative solution for a joint is successively carried out for all the joints in a given structure, with the most recently found moments on the opposite ends of the members used as the far-end moments for the joint concerned. The final solution for a structure is found when the tentative solutions of every joint are the correct solutions of the joints. Convergence is quite rapid and, ordinarily, not more than three cycles are required to obtain an accuracy consistent with the accuracy of the moment end-slope curves.

MOMENT-CURVATURE RELATIONSHIP

The moment-curvature relationship for mild steel has been determined in dimensionless form such that the same relationship applies to all commonly available structural wide flange sections of A-7 steel with a maximum possible error resulting from variation in geometrical properties of less than $\pm$ 3% in the resisting moments.

The derivation of the dimensionless moment-curvature relationships is based on the following assumptions:

1. A wide flange section can be idealized as being composed of three rectangular components.
2. Strains are distributed linearly through the depth of a section.
3. The stress-strain relationship for the material is the same in tension and compression, and the resistance of a member in flexure is directly dependent upon this relationship.
4. The average stress in the flange, σ_{fl}, is the stress at the centroidal axis of the flange.

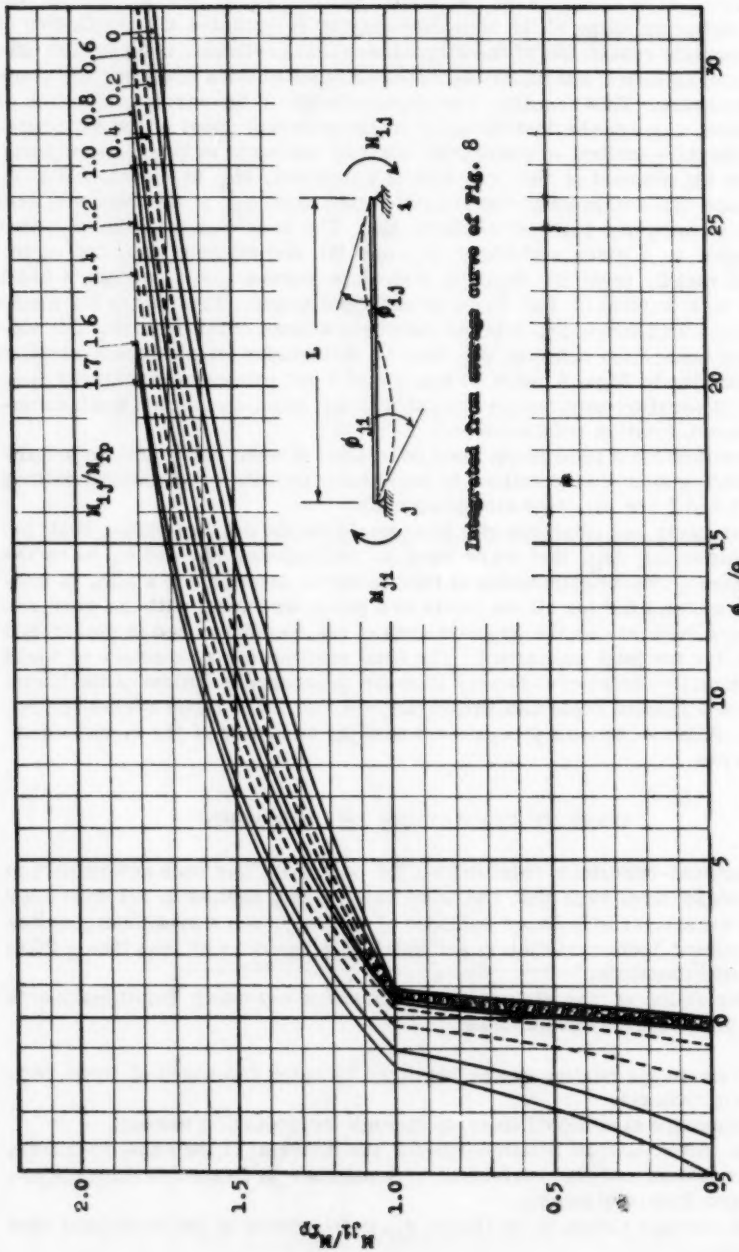

FIG. 3a.—MOMENT-END SLOPE RELATIONSHIPS FOR WF SECTIONS OF ASTM A7 STEEL

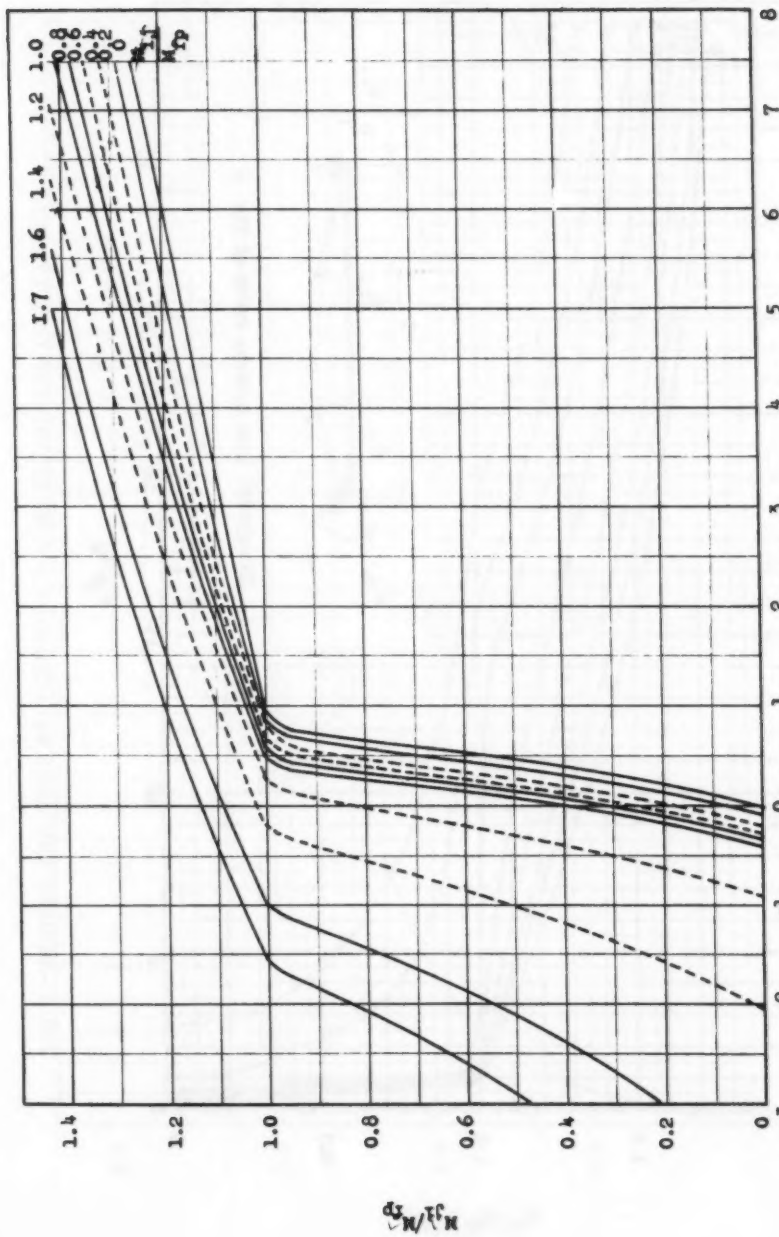

FIG. 3b.—MOMENT-END SLOPE RELATIONSHIPS FOR WF SECTIONS OF ASTM A7 STEEL

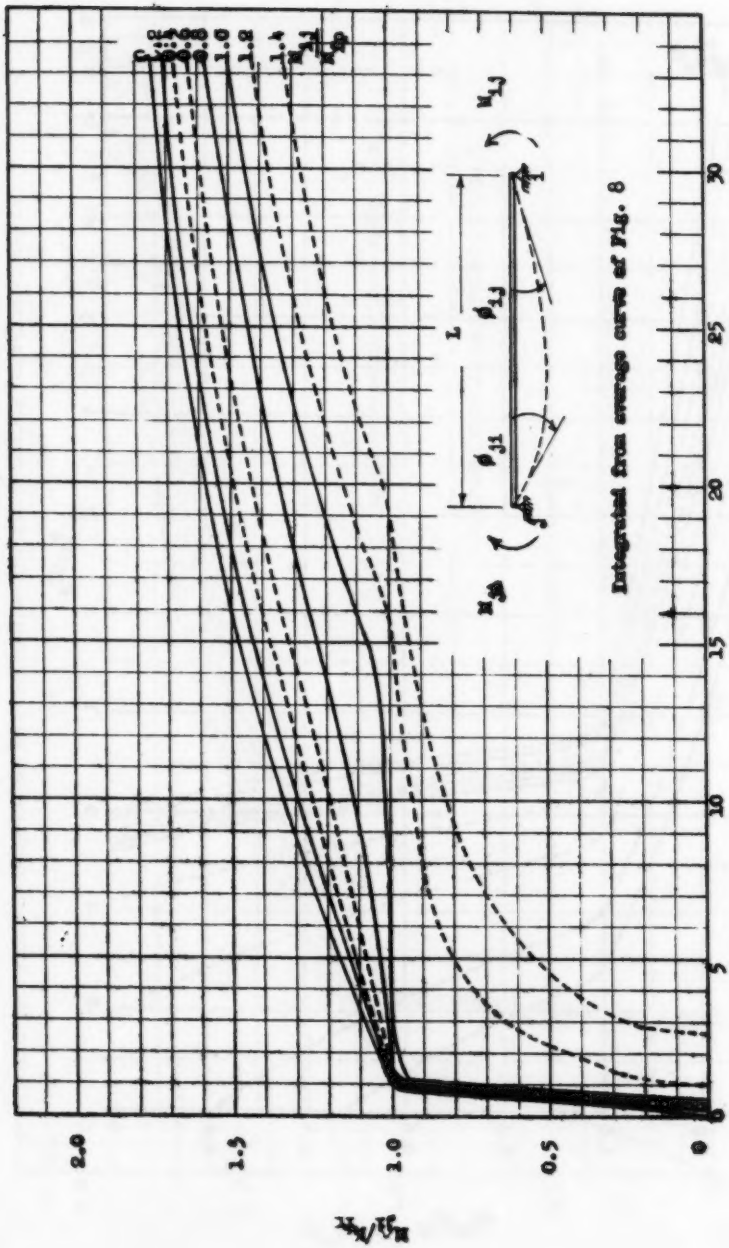

FIG. 4.—MOMENT-END SLOPE RELATIONSHIPS FOR WF SECTIONS OF ASTM A7 STEEL

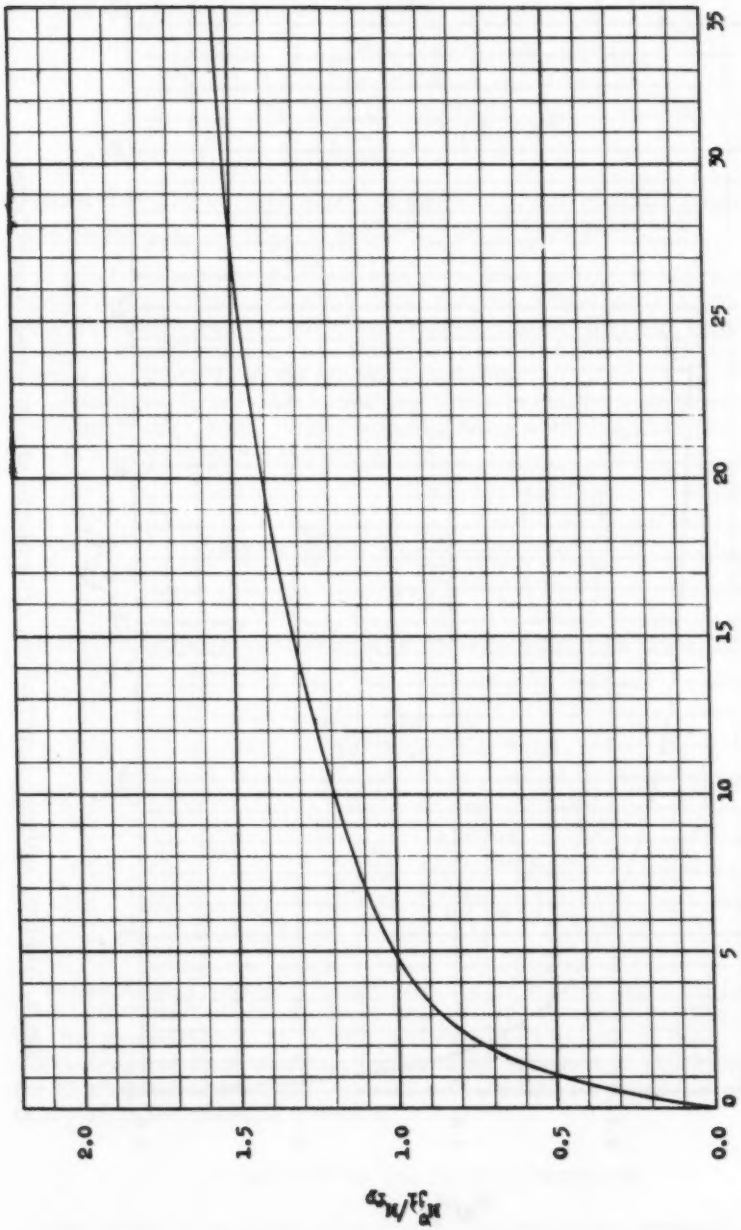

FIG. 5.—ASSUMED MOMENT-ROTATION RELATIONSHIP OF BEAM-TO-COLUMN CONNECTIONS

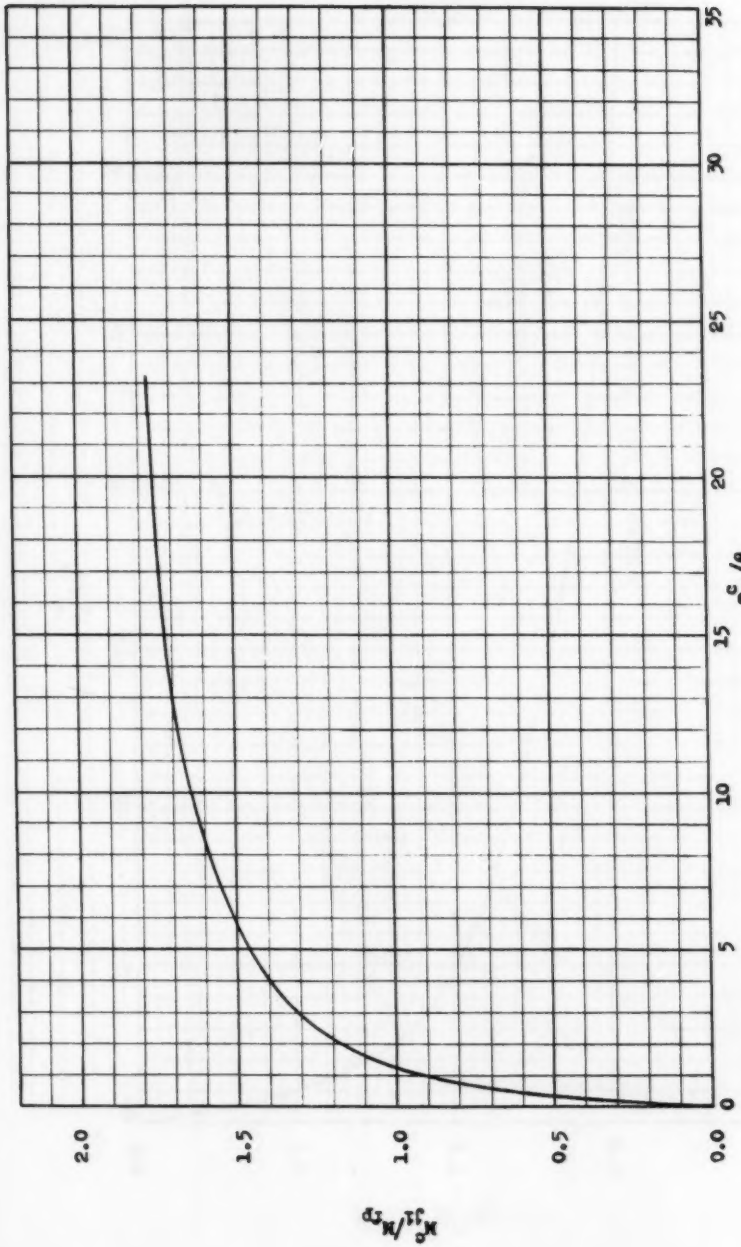

FIG. 6.—ASSUMED MOMENT-ROTATION RELATIONSHIP OF COLUMN-BASE CONNECTIONS

With these assumptions, the dimensionless moment may be expressed in terms of the elastic limit moment of a section, M_e, as

$$\frac{M}{M_e} = \frac{N\,\frac{A_w}{A_{fl}} + \frac{1}{2}\,\frac{\sigma_{fl}}{\sigma_e}\left(\frac{d-t}{d}\right)}{\frac{1}{6}\,\frac{A_w}{A_{fl}} + \frac{1}{2}\left(\frac{d-t}{d}\right)^2} \qquad \ldots\ldots\ldots\ldots (4)$$

in which N is a factor determined by the yield stress level and stress distribution on the web, and is equal to $\frac{\text{moment contributed by the web}}{\sigma_e\, A_w\, d}$

In this form, a study of all commonly available structural wide flange sections of A-7 steel indicates a maximum possible difference in M/M_e of about 12%. An average moment-curvature relationship, shown in Fig. 7, can be used for all commonly available wide flange sections of A-7 steel with a maximum possible error of $\pm$ 7% in the resisting moments.

The variation in the values of M/M_e is closely related with the variation in the shape factors, which is the ratio M_{fp}/M_e of a section. The shape factor, S.F., of a wide flange section is given as

$$\text{S.F.} = \frac{M_{fp}}{M_e} = \frac{\frac{1}{4}\,\frac{A_w}{A_{fl}} + \frac{1}{2}\left(\frac{d-t}{d}\right)}{\frac{1}{6}\,\frac{A_w}{A_{fl}} + \frac{1}{2}\left(\frac{d-t}{d}\right)^2} \qquad \ldots\ldots\ldots (5)$$

The resisting moment can therefore be expressed in terms of the fully-plastic moment of a section, M_{fp}, as

$$\frac{M}{M_{fp}} = \frac{M}{M_e} \times \frac{M_e}{M_{fp}} = \frac{M}{M_e} \times \frac{1}{\text{S.F.}}$$

$$= \frac{N\,\frac{A_w}{A_{fl}} + \frac{1}{2}\,\frac{\sigma_{fl}}{\sigma_e}\left(\frac{d-t}{d}\right)}{\frac{1}{4}\,\frac{A_w}{A_{fl}} + \frac{1}{2}\left(\frac{d-t}{d}\right)} \qquad \ldots\ldots\ldots\ldots (6)$$

In this form, a study of all commonly available structural wide flange sections of A-7 steel indicates a maximum possible difference in M/M_{fp} of about 5%. For moments up to $M/M_{fp} = 1$, this difference is zero, as shown in Fig. 8. The average moment-curvature relationship, as shown in Fig. 8, can be used for all structural wide flange sections with a maximum possible error of less than $\pm$ 3% in the resisting moments.

MOMENT END-SLOPE RELATIONSHIP

The method of analysis utilizes the moment end-slope relationships of the members. These relationships are those of a simply-supported beam with

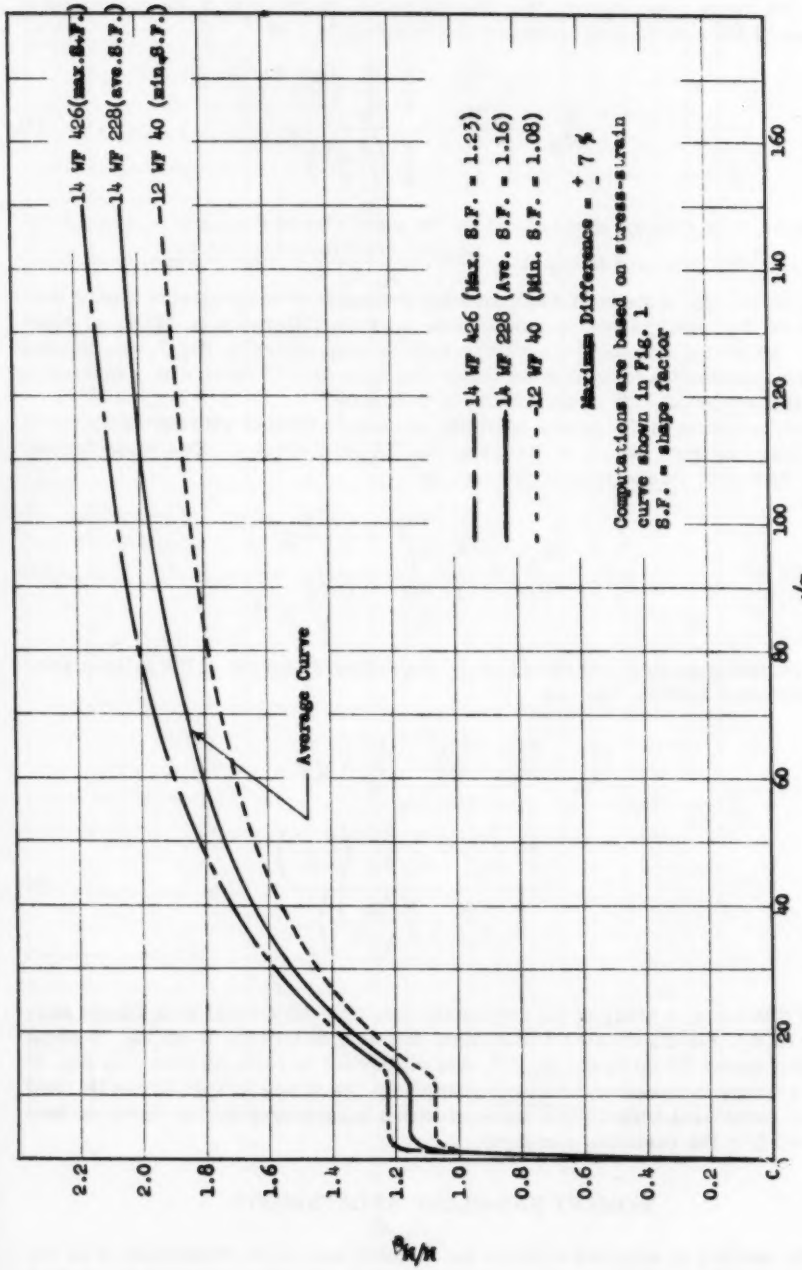

FIG. 7.—RANGE OF MOMENT-CURVATURE RELATIONSHIPS FOR WF SECTIONS OF ASTM A7 STEEL

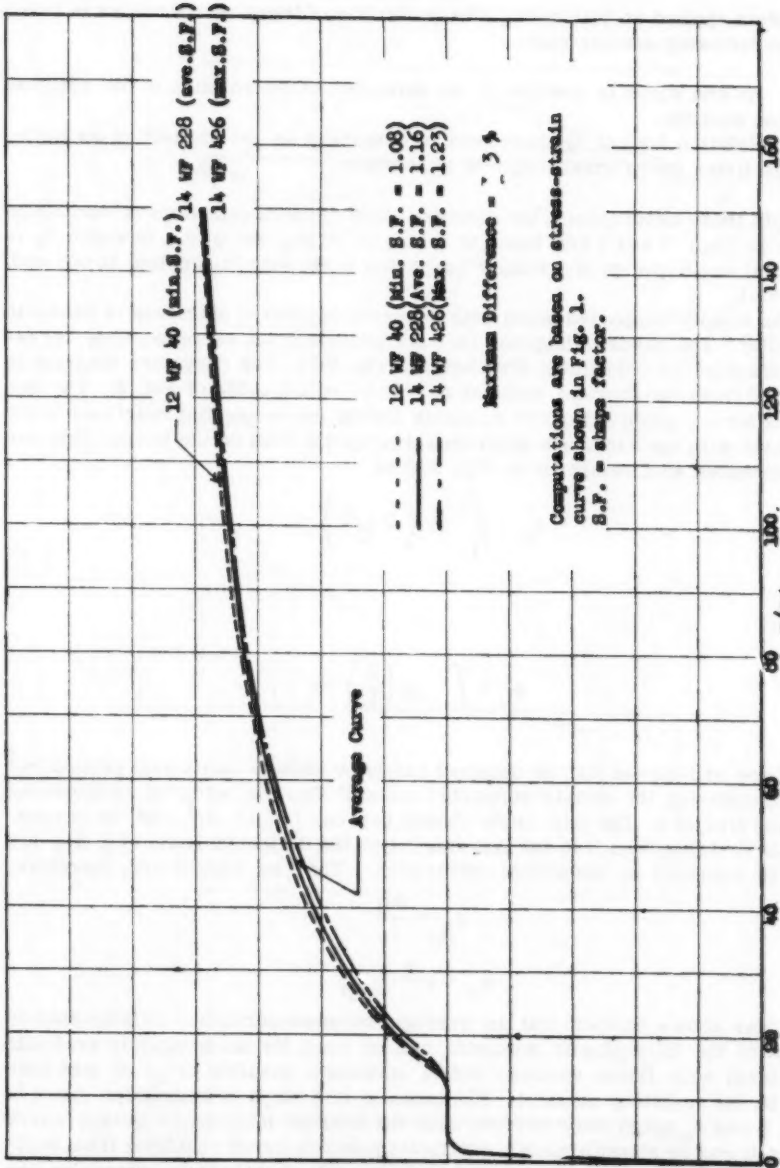

FIG. 8.—RANGE OF MOMENT–CURVATURE RELATIONSHIP FOR WF SECTIONS OF ASTM A7 STEEL

moments applied at both ends. The derivation of these relationships is based on the following assumptions:

1. An end slope is positive if the direction of its rotation is the same as the end moment.
2. Relative lateral displacement is described as the product of an angle-change times the original length of a member.

With these assumptions, the dimensionless moment end-slope relationships given in Figs. 3 and 4 are found in terms of M/M_{fp} and ϕ/θ_e, in which θ_e is the total angle change of a simply-supported beam with M_e applied at one end, Fig. 9(c).

The simply-supported beam with moments applied at both ends is shown in Fig. 9(a). The moment diagram (in dash lines) and its corresponding curvature diagram (in bold lines) are shown in Fig. 9(b). The curvature diagram is deduced from the average moment-curvature relationship of Fig. 8. The end slopes for any given set of end moments are the corresponding reactions at the supports with the curvature diagram acting as the load on the beam. This can be expressed with reference to Fig. 9(b) as

$$\phi_{ji} = \int_j^i \alpha \left(\frac{L - x}{L} \right) dx$$

and

$$\phi_{ij} = \int_j^i \alpha \left(\frac{x}{L} \right) dx$$

These end-slopes can be obtained easily by using a numerical procedure[2] and considering the simply-supported beam of Fig. 9(a) as being cantilevered at j and free at i. The total angle change between j and i, θ^{ji}, and the perpendicular distance from i to the line tangent to the deflected beam at j, Δ_{ij}, are readily obtained by numerical integration. The end slopes are, therefore,

$$\phi_{ji} = \frac{\Delta_{ij}}{L}$$

and

$$\phi_{ij} = \theta^{ji} - \phi_{ji}$$

It was shown earlier that an average moment-curvature relationship in terms of the fully plastic moments can be used for all commonly available structural wide flange sections with a maximum possible error of less than $\pm$ 3% in the resisting moment. The moment-end slope relationships given in Figs. 3 and 4, which were derived with the average moment-curvature curve of Fig. 8, can be shown to have a maximum possible error resulting from variation in geometrical properties of less than $\pm$ 3% when these relationships are used for all commonly available wide flange sections of A-7 steel.

---

[2] "Numerical Procedure for Computing Deflections, Moments, and Buckling Loads," by N. M. Newmark, Transactions, ASCE, Vol. 108, 1945.

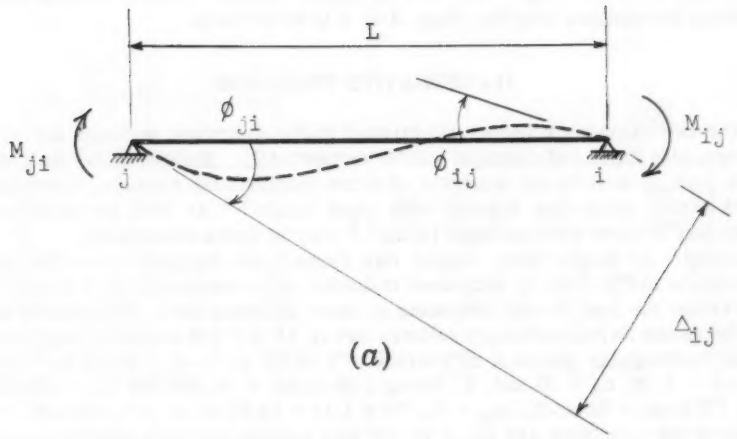

(a)

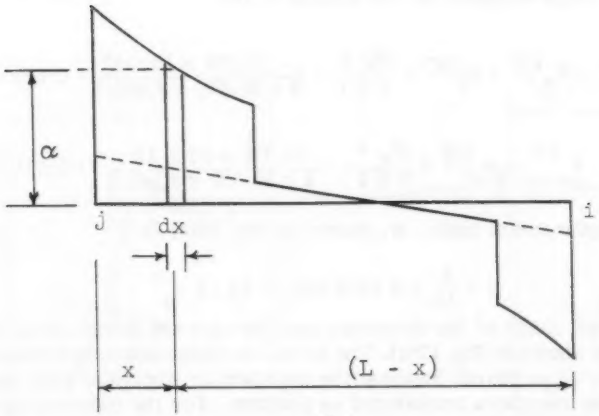

(b)

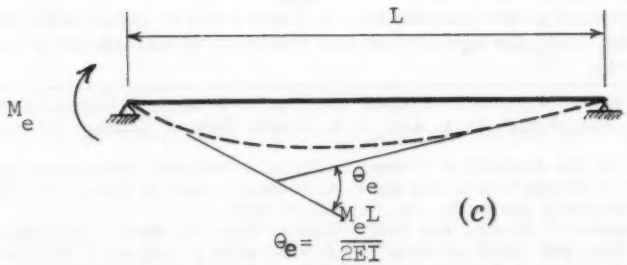

(c)

FIG. 9.—DESIGNATION OF MOMENTS AND DEFORMATIONS OF A SIMPLE SUPPORTED BEAM

The deflected configuration of a member, whether with or without contraflexure, determines whether Figs. 3 or 4 is to be used.

ILLUSTRATIVE PROBLEMS

The two sample problems illustrated in the following sections are simple frames with rigid and nonrigid joints, respectively. However, the method applies just as well to the analysis of more complicated frames. Examples of multi-story, multi-bay frames with rigid joints[3,4] as well as multi-story, multi-bay frames with nonrigid joints[3,5] may be found elsewhere.

Example A; Single Story, Single Bay Frame with Rigid Joints.—The structure shown in Fig. 10(a) is subjected to lateral deformations, $\Delta_{BA} = \Delta_{CD} = 2$ ft. Determine the load P corresponding to these deformations. Properties of the members are as follows: All members are of 14 WF 228 section of mild steel—I, the rectangular moment of inertia = 2,942.4 in.^{4};—S, = 367.8 in.^{3} Shape Factor = 1.16; σ_e = 32 ksi; E, Young's Modulus = 30,000 ksi M_e = 32 x 367.8 = 11,770 k-in. = 981 k-ft. M_{fp} = 11,770 x 1.16 = 13,653 k-in. = 1,138 k-ft. = M_{fp}^o

Since the members are all of 14 WF 228 section, the fully-plastic moments are the same and will be designated by M_{fp}^o in the calculations below. The elastic limit angle-changes for the members are:

$$\theta_e^{AB} = \theta_e^{BA} = \theta_e^{CD} = \theta_e^{DC} = \frac{M_e L}{2 E I} = \frac{11{,}770 \times 15 \times 12}{2 \times 30{,}000 \times 2{,}942.4} = 0.012 \text{ rad.} = \theta_e^o$$

$$\theta_e^{BC} = \theta_e^{CB} = \frac{M_e L}{2 E I} = \frac{11{,}770 \times 20 \times 12}{2 \times 30.000 \times 2{,}942.4} = 0.016 \text{ rad.}$$

The chord displacement angle, ψ, shown in Fig. 10(c) is

$$\psi = \frac{2}{15} = 0.1333 \text{ rad.} = 11.11\ \theta_e^o$$

The deflected shape of the structure and the correct directions of the moments are also shown in Fig. 10(c). The initial assumed end moments are given in the first line of moments (nearest the member) in Fig. 10(b) with clockwise moments on the members considered as positive. For the columns these moments are the fixed end moments due to the given displacements which are found from Fig. 3(a). For column AB, these are determined by taking $\phi ji/\theta_e$ = 11.11 in Fig. 3(a), since $\psi = 11.11\ \theta_e^o$, and rising vertically until $M_{ji}/M_{fp} = M_{ij}/M_{fp}$, and thus giving a value of 1.61 M_{fp}^o.

The first two lines of the computations in Table 1 will be explained in detail. Referring to Fig. 10(c), the equilibrium and continuity requirements at joint B are, respectively,

---

[3] "A Method for the Analysis of Frames Subjected to Inelastic Deformation into the Range of Strain Hardening," by A. Ang, M. S. Thesis, Univ. of Illinois, Urbana, Ill., February, 1957.

[4] "A Method for the Analysis of Frames Subjected to Inelastic Deformation into the Range of Strain Hardening," by A. Ang and J. M. Massard, Univ. of Illinois Civ. Engrg. Studies, Struct. Research Series No. 130, November, 1956.

[5] "An Investigation of Riveted and Bolted Column-Base and Beam-to-Column Connections Under Slow and Rapid Loading," by D. McDonald, A. Ang and J. M. Massard, Univ. of Illinois Civ. Engrg. Studies, Struct. Research Series No. 156, February, 1958.

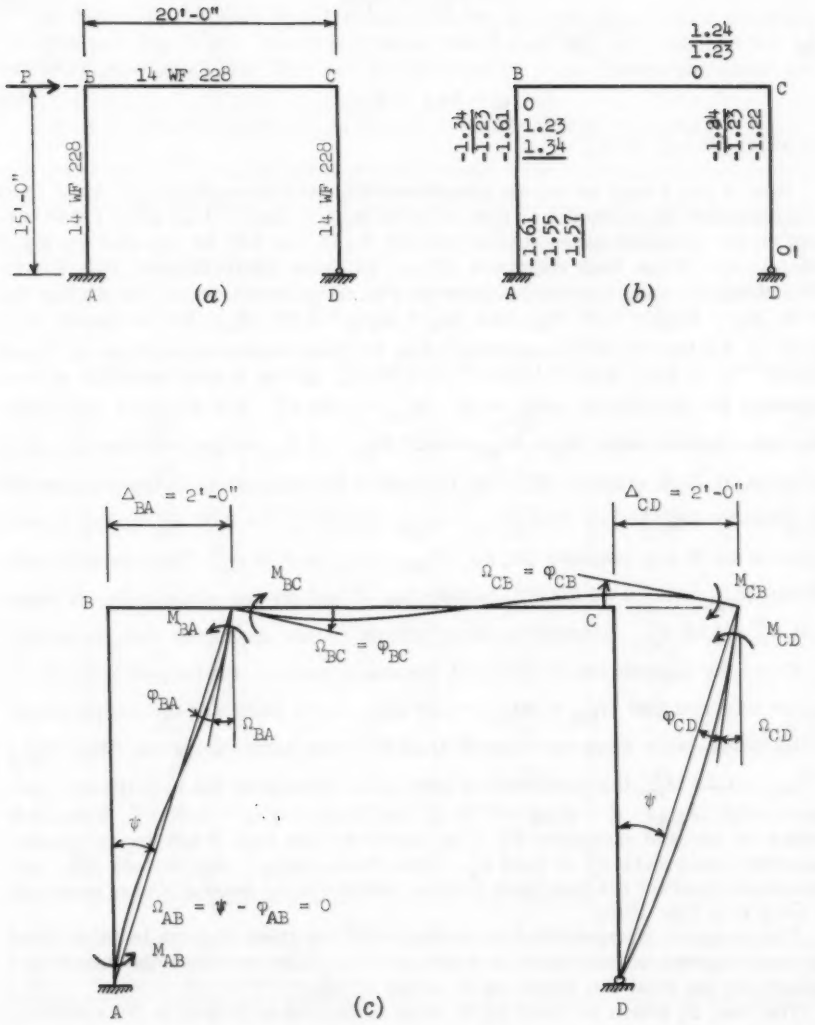

FIG. 10.—SOLUTION OF SINGLE STORY, SINGLE BAY FRAME WITH RIGID JOINTS.

$$M_{BA} = M_{BC} \quad \ldots\ldots\ldots\ldots\ldots\ldots (7)$$

and

$$\Omega_{BA} = \Omega_{BC} \quad \ldots\ldots\ldots\ldots\ldots\ldots (8a)$$

or

$$\Psi - \phi_{BA} = \phi_{BC} \quad \ldots\ldots\ldots\ldots\ldots\ldots (8b)$$

in which $\Psi = 11{,}11\ \theta_e^o$.

Eqs. 7 and 8 may be solved simultaneously by trial-and-error. As a first trial assume the moments at joint B to be $M_{BA} = M_{BC} = 1.20\ M_{fp}^o$ These values of the moments automatically satisfy Eq. 7 and will be checked for Eq. 8 as follows. Since both members AB and BC have contraflexure, Fig. 3(a) or 3(b) should be used for these members. For member BA, enter Fig. 3(a) or 3(b) with $M_{ji} = M_{BA} = 1.20\ M_{fp}$ and $M_{ij} = M_{AB} = 1.61\ M_{fp}$ (the assumed moment at A); the end-slope corresponding to these moments as given by Fig. 3 (a) or 3(b) is $\phi_{ji} = \phi_{BA} = 1.50\ \theta_e^{BA} = 1.50\ \theta_e^o$, giving a total rotation at B of member BA as follows: $\Omega_{BA} = \Psi - \phi_{BA} = 9.61\ \theta_e^o$. For member BC, enter the same figures with $M_{ji} = M_{BC} = 1.20\ M_{fp}$ and $M_{ij} = M_{CB} = 0$ (the assumed moment at C of member BC); the end-slope corresponding to these moments as given by Fig. 3(a) or 3(b) is $\phi_{ji} = \phi_{BC} = 6.00\ \theta_e^{BC} = 8.00\ \theta_e^o$, giving a total rotation at B for member BC as, $\Omega_{BC} = \phi_{BC} = 8.00\ \theta_e^o$. The assumed moments $M_{BA} = M_{BC} = 1.20\ M_{fp}^o$ satisfy Eq. 7 but do not satisfy Eq. 8 since $9.61\ \theta_e^o \neq 8.00\ \theta_e^o$. Therefore these values of the moments are incorrect.

From the magnitudes of the total rotations given in the inequality above, it can be inferred that $M_{BA} = M_{BC} > 1.20\ M_{fp}^o$. Lines 3 and 4 of the computations in the same table show the second trial of these same moments. With $M_{BA} = M_{BC} = 1.23\ M_{fp}^o$, the rotations at joint B for members BA and BC are, respectively, $\Omega_{BA} = \Psi - \phi_{BA} = 9.11\ \theta_e^o$ and $\Omega_{BC} = \phi_{BC} = 9.13\ \theta_e^o$. With these values of the end moments Eq. 7 is satisfied and Eqs. 8 are approximately satisfied since $9.11\ \theta_e^o \cong 9.13\ \theta_e^o$. Therefore, $M_{BA} = M_{BC} = 1.23\ M_{fp}^o$ are considered correct for this cycle and are entered in the second line of moments at joint B in Fig. 10(b).

The complete computation for moments and rotations is given in Table 1 and the convergence of moments is shown in Fig. 10(b), in which the underlined values are the final end moments in terms of M_{fp}^o.

The load P, which is equal to the sum of the shear forces in the columns, may be calculated as

$$P = \frac{1138\ \ (1.57 + 1.34)}{15} + \frac{1138 \times 1.24}{15} = 314.7 \text{ kips.}$$

Example B; Single Story, Single Bay Frame with Non-Rigid Joints.—The same structure used in Example A will be solved considering that the joints are nonrigid (Fig. 11(a)) and have the moment-rotation relationships for beam-to-column and column-base connections given in Figs. 5 and 6, respectively.

These moment-rotation relationships are assumed for purposes of illustration only. For convenience, the moments and rotations are expressed, respectively, in terms of M_{fp} and θ_e of the connected members. The columns are assumed to be continuous across a joint. Joint D is a hinge.

The deflected shape of the structure and the correct direction of moments are shown in Fig. 11(c). Initial end moments of 1.00 M^o_{fp} are assumed for all members, except at joint D where the moment is zero. These moments are

TABLE 1.—COMPUTATION OF MOMENTS AND ROTATIONS FOR EXAMPLE A

Joint	ji	$\frac{M_{ji}}{M^o_{fp}}$	$\frac{\phi_{ji}}{\theta_e^{ji}}$	$\frac{\Omega_{ji}}{\theta_e^{ji}}$	$\frac{\Omega_{ji}}{\theta_e^{o}}$
(1)	(2)	(3)	(4)	(5)	(6)
CYCLE No. 1					
B	BA	Ass. 1.20	1.50	9.61	9.61
	BC	1.20	6.00	6.00	8.00
B	BA	Ass. 1.23	2.00	9.11	9.11
	BC	1.23	6.85	6.85	9.13
A	AB	1.55	11.11	0	0
C	CD	Ass. 1.20	6.00	5.11	5.11
	CB	1.20	2.90	2.90	3.86
C	CD	Ass. 1.23	6.75	4.36	4.36
	CB	1.23	3.35	3.35	4.46
CYCLE No. 2					
B	BA	Ass. 1.30	3.55	7.76	7.76
	BC	1.30	4.55	4.55	6.06
B	BA	Ass. 1.34	4.10	7.01	7.01
	BC	1.34	5.35	5.35	7.13
A	AB	1.57	11.11	0	0
C	CD	Ass. 1.23	6.75	4.36	4.36
	CB	1.23	3.00	3.00	4.00
C	CD	Ass. 1.24	7.00	4.11	4.11
	CB	1.24	3.15	3.15	4.20
CYCLE No. 3					
Cycle No. 3 gives the same values as those found in Cycle No. 2. Therefore the values of Cycle No. 2 are the correct moments.					

the values given closest to the members in Fig. 11(b). Clockwise moments acting on the members are positive.

The first two lines of the computations in Table 2 will be explained in detail. Referring to Fig. 11(c), the equilibrium and continuity requirements at joint B are, respectively,

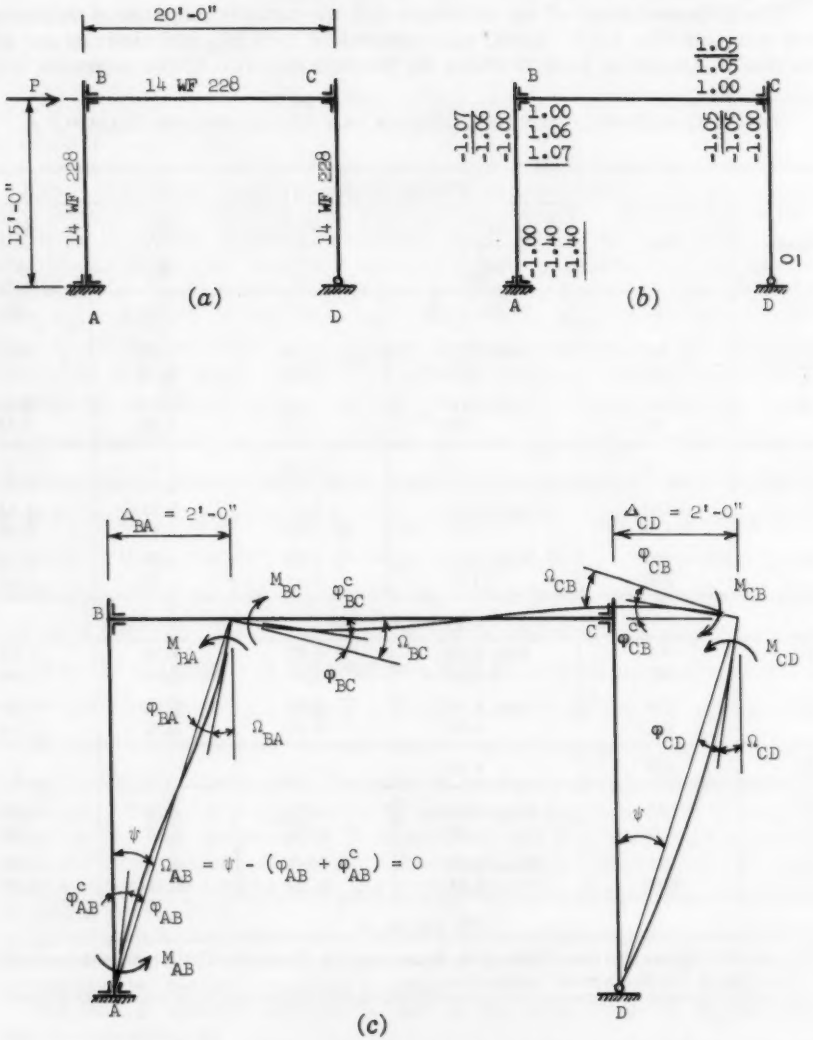

FIG. 11.—SOLUTION OF SINGLE STORY, SINGLE BAY FRAME WITH NON-RIGID JOINTS.

TABLE 2.—COMPUTATION OF MOMENTS AND ROTATIONS FOR EXAMPLE B

Joint	ji	$\frac{M_{ji}}{M^{o}_{fp}}$	$\frac{\phi_{ji}}{\theta^{ji}_{e}}$	$\frac{\phi^{c}_{ji}}{\theta^{ji}_{e}}$	$\frac{\Omega_{ji}}{\theta^{ji}_{e}}$	$\frac{\Omega_{ji}}{\theta^{o}_{e}}$
(1)	(2)	(3)	(4)	(5)	(6)	(7)
CYCLE No. 1						
B	BA	Ass. 1.05	1.10	0	10.01	10.01
	BC	1.05	1.10	5.80	6.90	9.20
B	BA	Ass. 1.06	1.25	0	9.86	9.86
	BC	1.06	1.25	6.00	7.25	9.67
A	AB	Ass. 1.30	5.10	2.90	3.11	3.11
A	AB	Ass. 1.40	7.20	4.00	-0.09	-0.09
C	CB	Ass. 1.05	1.00	5.70	6.70	8.93
	CD	1.05	2.10	0	9.01	9.01
CYCLE No. 2						
B	BA	Ass. 1.06	0.50	0	10.61	10.61
	BC	1.06	1.25	6.00	7.25	9.67
B	BA	Ass. 1.07	0.60	0	10.51	10.51
	BC	1.07	1.40	6.30	7.70	10.27
A	AB	Ass. 1.40	7.20	4.00	-0.09	-0.09
C	CB	Ass. 1.05	1.00	5.70	6.70	8.93
	CD	1.05	2.10	0	9.01	9.01
CYCLE No. 3						
Cycle No. 3 gives the same values as those found in Cycle No. 2. Therefore the values of Cycle No. 2 are the correct moments.						

$$M_{BA} = M_{BC} \quad \ldots\ldots\ldots\ldots\ldots\ldots (9)$$

and

$$\Omega_{BA} = \Omega_{BC} \quad \ldots\ldots\ldots\ldots\ldots\ldots (10a)$$

or

$$\psi - \phi_{BA} = \phi_{BC} + \phi^{c}_{BC} \quad \ldots\ldots\ldots\ldots\ldots\ldots (10b)$$

in which $\psi = 11.11\ \theta^{o}_{e}$.

Eqs. 9 and 10 may be solved simultaneously by trial-and-error. As a first trial assume the moments at joint B to be $M_{BA} = M_{BC} = 1.05\ M^{o}_{fp}$. For member BA, enter Fig. 3(a) or 3(b) with $M_{ji} = M_{BA} = 1.05\ M_{fp}$ and $M_{ij} = M_{AB} = 1.00\ M_{fp}$ (the assumed moment at A); the end-slope corresponding to these

moments as given by Fig. 3(a) or 3(b) is $\phi_{ji} = \phi_{BA} = 1.10\ \theta_e^{BA} = 1.10\ \theta_e^o$, giving a total rotation at B of member BA as follows: $\Omega_{BA} = \psi - \phi_{BA} = 10.01\ \theta_e^o$. For member BC, enter the same figures with $M_{ji} = M_{BC} = 1.05\ M_{fp}$ and $M_{ij} = M_{CB} = 1.00\ M_{fp}$ (the assumed moment at C for member BC). The end-slope corresponding to these moments, as given by Fig. 3(a) or 3(b), is $\phi_{ji} = \phi_{BC} = 1.10\ \theta_e^{BC}$, and the connection rotation at B for member BC is found from Fig. 5 to be $\phi_{ji}^c = \phi_{BC}^c = 5.80\ \theta_e^{BC}$, which is the value corresponding to $M_{ji} = M_{BC} = 1.05\ M_{fp}$. The total rotation at B for member BC is therefore, $\Omega_{BC} = \phi_{BC} + \phi_{BC}^c = 1.10\ \theta_e^{BC} + 5.80\ \theta_e^{BC} = 6.90\ \theta_e^{BC} = 9.20\ \theta_e^o$. The assumed moments $M_{BA} = M_{BC} = 1.05\ M_{fp}^o$ satisfy Eq. 9 but do not satisfy Eq. 10 since $10.01\ \theta_e^o = 9.20\ \theta_e^o$. Therefore these assumed values of the moments are incorrect. The correct values of these moments are found to be $1.06\ M_{fp}^o$ for this cycle, as shown in lines 3 and 4 of the computations in Table 2.

The complete computation for moments and rotations is given in Table 2 and the convergence of moments is shown in Fig. 11(b) in which the underlined values are the final end moments given in terms of M_{fp}^o.

The load P, which is equal to the sum of the shear forces in the columns, may be computed as

$$P = \frac{1138\ \ (1.40 + 1.07)}{15} + \frac{1138 \times 1.05}{15} = 267.0 \text{ kips}$$

ACKNOWLEDGMENTS

The material in this paper was taken from a thesis submitted by the author in partial fulfillment of the requirements for the degree of Master of Science in Civil Engineering at the University of Illinois. The work was undertaken in the Structural Research Laboratory of the University of Illinois under the general direction of Professor N. M. Newmark, Head, Dept. of Civil Engineering, and under the immediate direction of Dr. J. M. Massard, formerly Asst. Prof. of Civil Engineering, as part of a research project sponsored by the United States Air Force Dept. of Defense.

The helpful suggestions of Mr. W. Egger, Research Assoc. in Civil Engineering, concerning the development of the relationships for mild steel, and the assistance and advice of Dr. W. J. Hall, Assoc. Prof. of Civil Engineering, in the preparation of this paper, are gratefully acknowledged.

APPENDIX

NOTATION

The following notation has been adopted in this paper:

Superscripts:
- ji designates the member considered
- c designates the connection considered
- o designates a quantity used as the reference value in a problem

Subscripts:
- e designates elastic limit condition
- fp designates fully-plastic condition
- ji designates end j of member ji

I = moment of inertia about the centroidal axis of the cross section

d = overall depth of structural section

S = section modulus

σ = stress

ϵ = strain

M = total moment at a section

P = applied lateral load

M_e^{ji} = elastic limit resisting moment of member ji

M_{fp}^{ji} = fully-plastic resisting moment of member ji

M_{fp}^{o} = fully-plastic resisting moment of a particular member used as a standard unit of moment in a problem

S.F. = shape factor of a section = M_{fp}/M_e

M_{ji} = total moment at end j of member ji

M_{ji}^{c} = moment of the connection at j of member ji

σ_e = static yield stress of the material

θ^{ji} = total angle-change along the full length of member ji

θ_e^{ji} = total elastic limit angle-change of member ji for a moment M_e applied at one end. (See Fig. 9c.)

θ_e^{o} = total elastic limit angle-change θ_e^{ji} of a particular member used as a standard unit of rotation in a problem

ϕ_{ji} = end slope at end j of member ji

ϕ_{ji}^{c} = rotation of the connection at j of member ji

ψ = chord displacement angle

Ω_{ji} = total rotation at joing j of member ji

Journal of the
ENGINEERING MECHANICS DIVISION
Proceedings of the American Society of Civil Engineers

BEHAVIOR OF VISCOELASTIC PLATES IN BENDING

By George E. Mase[1]

SYNOPSIS

Solutions of the fundamental equation for linear viscoelastic plates in bending are obtained by use of the Laplace transformation. The quasi-static deflection under various lateral loadings and the dynamic response under no load are presented. Specific problems worked out include (a) the Kelvin and Maxwell type plates under proportional loading, (b) a rectangular Maxwell plate under a moving load, and (c) free vibrations of rectangular Maxwell and Kelvin type plates.

INTRODUCTION

A number of solutions of viscoelastic problems involving the concept of differential viscoelastic operators have appeared in the recent literature.[2,3,4,5] Although these papers have been primarily concerned with stress analysis problems, the differential operator concept serves as well in problems for

Note.—Discussion open until November 1, 1960. To extend the closing date one month, a written request must be filed with the Executive Secretary, ASCE. This paper is part of the copyrighted Journal of the Engineering Mechanics Division, Proceedings of the American Society of Civil Engineers, Vol. 86, No. EM 3, June, 1960.

[1] Asst. Prof. of Applied Mechanics, Michigan State Univ., East Lansing, Mich.

[2] "Stress Analysis in Viscoelastic Bodies," by E. H. Lee, Quarterly of Applied Mathematics, Vol. XIII, No. 2, July, 1955, p. 183.

[3] "Stresses in Elastically Reinforced, Viscoelastic Tubes with Internal Pressure," by J. R. M. Radok and E. H. Lee, Technical Report No. 15, Nord 16471, Brown Univ., April, 1956.

[4] "Dynamics of Viscoelastic Anisotropic Media," by M. A. Biot, Proceedings, Second Midwestern Conference on Solid Mechanics, Purdue Univ., September, 1955, p. 94.

[5] "On Transient Thermal Stresses in Linear Viscoelasticity," by Eli Sternberg, Proceedings, Third U. S. National Congress of Applied Mechanics, To be published 1958.

which deformations or deflections are desired. In this paper, the behavior of flat viscoelastic plates in bending is studied. The basic differential equations are established using the operator concept and the solutions obtained by application of the Laplace transform. Two classes of problems are considered. The quasi-static deflection of laterally loaded plates is obtained in terms of the associated elastic deflection of a similar plate. Plate moments for this case are also included and compared with those of the elastic case. The second class considered is that of the dynamic response of simply supported rectangular plates under no load. Here, inertia forces due to deflection are taken into account and the free vibrations of a Maxwell and Kelvin type plate are given. Throughout the work physical constants of the viscoelastic medium are assumed to be constant.

FUNDAMENTAL EQUATIONS

For an isotropic medium linear viscoelastic behavior may be defined by means of the linear differential equations

$$P\,S_{ij} = 2\,Q\,e_{ij} \quad \ldots\ldots\ldots\ldots\ldots\ldots \quad (1a)$$

$$M\,\sigma_{ii} = N\,\epsilon_{ii} \quad \ldots\ldots\ldots\ldots\ldots\ldots \quad (1b)$$

here σ_{ij} and ϵ_{ij} designate the components of the stress and strain tensors, respectively, and s_{ij} and e_{ij} the components of their deviators as given by

$$S_{ij} = \sigma_{ij} - \frac{1}{3}\,\delta_{ij}\,\sigma_{kk} \quad \ldots\ldots\ldots\ldots\ldots\ldots \quad (2a)$$

$$e_{ij} = \epsilon_{ij} - \frac{1}{3}\,\delta_{ij}\,\epsilon_{kk} \quad \ldots\ldots\ldots\ldots\ldots\ldots \quad (2b)$$

in which δ_{ij} stands for the Kronecker delta. In the prior equations and hereafter throughout this paper, subscripts, unless otherwise specified, take on the values x, y and z, and the usual conventions for summation over repeated indices and for space differentiation are in force. The operators P, Q, M and N are linear differential time operators of the form

$$P = \sum_{n=o}^{p} a_n \frac{\partial^n}{\partial t^n}, \quad Q = \sum_{n=o}^{q} b_n \frac{\partial^n}{\partial t^n}, \quad M = \sum_{n=o}^{m} c_n \frac{\partial^n}{\partial t^n}, \quad N = \sum_{n=o}^{s} d_n \frac{\partial^n}{\partial t^n}$$

The coefficients a_n, b_n, etc. which describe the physical properties of the material are assumed to be temperature-independent and are, therefore, taken as constants in the following work.

Experimental evidence indicates that most engineering materials behave elastically under hydrostatic pressure. This permits immediate simplification of Eq. 1b and the viscoelastic stress-strain relations may be given as

$$P\,S_{ij} = 2\,Q\,e_{ij} \quad \ldots\ldots\ldots\ldots\ldots\ldots \quad (3a)$$

$$\sigma_{ii} = 3\,K\,\epsilon_{ii} \quad \ldots\ldots\ldots\ldots\ldots\ldots \quad (3b)$$

in which K is the usual bulk modulus of elasticity theory. This form of the basic equations will be adopted here.

Certain specializations of Eq. 3 are of interest from the point of view of applications. When, for example, P = 1 and Q = G, the shear modulus, the equations define an elastic material. Using operators of first order the equations may be put into suitable forms which define the frequently encountered Maxwell and Kelvin (Voigt) materials. Thus,

$$\dot{S}_{ij} + \frac{G}{\eta} S_{ij} = 2 G \dot{e}_{ij} \quad \ldots\ldots\ldots\ldots\ldots\ldots (4a)$$

$$\sigma_{ii} = 3 K \epsilon_{ij} \quad \ldots\ldots\ldots\ldots\ldots\ldots (4b)$$

define the Maxwell body characterized by instantaneous elastic response followed by viscous flow. Here the dot denotes differentiation with respect to time and η is the coefficient of viscosity. Likewise

$$S_{ij} = 2 G e_{ij} + 2 \eta \dot{e}_{ij} \quad \ldots\ldots\ldots\ldots\ldots\ldots (5a)$$

$$\sigma_{ii} = 3 K \epsilon_{ii} \quad \ldots\ldots\ldots\ldots\ldots\ldots (5b)$$

define a Kelvin body characterized by delayed elastic response. The phenomenological behavior of such viscoelastic media as those defined previously is frequently associated with the response of mechanical models composed of spring and dashpot elements arranged in a suitable fashion. Such models are discussed by T. Alfrey[6] and B. Gross.[7]

The fact that the stress-strain equations of the theory of elasticity are incorporated as a special case of the basic stress-strain relations of viscoelasticity theory has lead to the development of analogies relating the equations of one field to those of the other. Alfrey's analogy[8] for the incompressible case has been extended to cover compressible media by H. S. Tsien.[9] E. H. Lee[2] has established an analogy for isotropic media by using the Laplace transform. More recently, M. A. Biot[4] has given a correspondence principle for anisotropic media based upon the formal analogy of the operational tensor of viscoelastic theory and the elastic moduli of elasticity theory. These various analogies may be interpreted as schemes whereby the elastic constants in a given elasticity equation are replaced by differential time operators to arrive at an analogous viscoelastic equation. For example, as may be seen from Eq. 3, the shear modulus G corresponds to the operator P/Q.

In the particular problem at hand the operational form of the plate flexural rigidity D is required. Recalling that for a plate of thickness h

$$D = \frac{E h^3}{12(1 - \nu^2)} \quad \ldots\ldots\ldots\ldots\ldots\ldots (6)$$

---

6 "Mechanical Behavior of High Polymers," by T. Alfrey, Interscience Publishers, Inc., New York, N. Y., 1948.

7 "Mathematical Structure of the Theories of Viscoelasticity," by B. Gross, Hermann and Cie, Paris, 1953.

8 "Non-homogeneous Stresses in Viscoelastic Media," by T. Alfrey, Quarterly of Applied Mathematics, Vol. 2, May, 1944, pp. 113-119.

9 "A Generalization of Alfrey's Theorem for Viscoelastic Media," by H. S. Tsien, Quarterly of Applied Mathematics, Vol. 8, 1950, p. 104.

or in an equivalent but more appropriate form for this work

$$D = \frac{h^3 G (3K + G)}{3 (3K + 4G)} \quad \ldots\ldots\ldots\ldots\ldots\ldots (7)$$

The operational form based upon Eq. 3 is given as

$$B_1 = \frac{h^3 Q (3 K P + Q)}{3 P (3 K P + 4 Q)} \quad \ldots\ldots\ldots\ldots\ldots\ldots (8)$$

For the purpose of later reference it is convenient to list here the specific forms of this operator for the Maxwell and Kelvin materials. Thus, for a Maxwell material

$$B_1 = \frac{h^3 G p \left[\frac{3K}{\tau} + (3K + G)p\right]}{3\left(p + \frac{1}{\tau}\right)\left[\frac{3K}{\tau} + (3K + 4G)p\right]} \quad \ldots\ldots\ldots\ldots (9)$$

and for a Kelvin material

$$B_1 = \frac{h^3 (G + \eta\, p) (3K + G + \eta\, p)}{3 (3K + 4G + 4\eta\, p)} \quad \ldots\ldots\ldots\ldots (10)$$

In these equations $p \equiv \frac{\partial}{\partial t}$, $\tau = \eta/G$.

In the following, the plates considered are assumed to be thin plates of constant thickness h. Let the x, y plane, referred to a set of right-handed rectangular Cartesian coordinates, be the middle plane of the plate. The positive z direction is taken downward and the deflection of the median plane in this direction is given by w. A distributed load $f = f(x,y,t)$ per unit area of the x,y plane acts in the z direction. ρ is the plate density. Accordingly, the plate equation for elastic plates when inertia forces due to deformation are taken into account is

$$D \nabla^4 w + p^2 \rho h w = f \quad \ldots\ldots\ldots\ldots\ldots\ldots (11)$$

Replacing D in this equation by the operator B_1 gives the fundamental equation for viscoelastic plate response, namely,

$$B_1 \left(\nabla^4 w\right) + p^2 \rho h w = f \ldots\ldots\ldots\ldots\ldots\ldots (12)$$

QUASI-STATIC SOLUTIONS

Proportional Loading.—If inertia forces due to deformation are neglected, Eq. 12 reduces to the basic equation governing the quasi-static deflection of viscoelastic plates. This equation may be written as

$$B_1 \left[\nabla^4 w\,(x,y,t)\right] = f\,(x,y,t) \quad \ldots\ldots\ldots\ldots\ldots (13)$$

When the load function, f, is such that it may be given as the product of a space function multiplied by a time function, the variables may be separated and a solution in terms of the associated elastic solution obtained. Thus, letting

$$f(x,y,t) = F(x,y)\,\theta(t) \quad \ldots\ldots\ldots\ldots\ldots\ldots (14)$$

and taking w to be given by

$$w(x,y,t) = W(x,y)\,\phi(t) \quad \ldots\ldots\ldots\ldots\ldots\ldots (15)$$

yields upon substitution into Eq. 13 the equation

$$\frac{B_1(\phi)}{\theta} = \frac{F}{\nabla^4 W} \quad \ldots\ldots\ldots\ldots\ldots\ldots (16)$$

In this equation, the right hand side is a function of x and y and the left hand side is a function of t, therefore, each side must be equal to the same constant. Taking this constant as D, the flexural rigidity of the plate for purposes of convenience leads to the equations

$$\nabla^4 W(x,y) = \frac{F(x,y)}{D} \quad \ldots\ldots\ldots\ldots\ldots\ldots (17)$$

$$B_1[\phi(t)] = D\,\theta(t) \quad \ldots\ldots\ldots\ldots\ldots\ldots (18)$$

Eq. 17 is simply the elastic plate equation for which solutions are already known. Such solutions may be expressed in the form

$$w_e = \frac{q(x,y)}{D} \quad \ldots\ldots\ldots\ldots\ldots\ldots (19)$$

Solutions of Eq. 18 may be obtained conveniently with the aid of the Laplace transform method of the operational calculus. If it is assumed that the plate is at rest in its undeflected position and free from all stress at the instant of application of the load, the operator B_1 will transform into a rational function of s, the transform variable. Therefore, the transform of Eq. 18 becomes

$$\frac{g(s)}{k(s)}\,\bar{\phi} = D\,\bar{\theta} \quad \ldots\ldots\ldots\ldots\ldots\ldots (20)$$

in which barred quantities indicate the transforms of the same quantity without the bar and g(s) and k(s) are polynomials. Eq. 20 may be solved for $\bar{\phi}$ and the function $\frac{k(s)}{g(s)}$ expanded by partial fractions to give

$$\bar{\phi} = \left[\sum_{i=1}^{n} \frac{A_i}{r_i + s} + A_0\right] D\,\bar{\theta} \quad \ldots\ldots\ldots\ldots\ldots\ldots (21)$$

in which the roots r_i are all real.[10] Their number, n, will depend upon the degree of the polynomial, g(s). Eq. 21 may be inverted at once by the convolution integral to give the general solution of Eq. 18 as

$$\phi = D \int_0^t \left[A_0 \, \delta(T) + \sum_{i=1}^{n} A_i \, e^{-r_i T} \right] \theta(t - T) \, dT \quad \ldots\ldots (22)$$

in which $\delta(t)$ is the Dirac delta function and e is the base of the natural logarithm system. From this and Eq. 15 it follows that

$$w(x,y,t) = w_e \, D \int_0^t \left[A_0 \, \delta(T) + \sum_{i=1}^{n} A_i \, e^{-r_i T} \right] \theta(t - T) \, dT \quad \ldots\ldots (23)$$

As a particular example of the previous solution, consider a plate made of a Kelvin material and having a load distribution for which the elastic solution is known. If the load is assumed to be applied suddenly at time t = 0 and maintained constant thereafter, θ is given by the Heaviside step function defined as

$$\theta(t) = 0 \quad t < 0$$

$$\theta(t) = 1 \quad t > 0$$

The constants A_i and roots r_i may be obtained from the transform of B_1 as given in Eq. 10, and Eq. 23 then integrated directly to give

$$w = w_e \left(1 - \frac{3K + G}{3K + 4G} \, e^{-\frac{t}{\tau}} - \frac{3G}{3K + 4G} \, e^{-\frac{3K + G}{G} \frac{t}{\tau}} \right) \quad \ldots\ldots (24)$$

in which $\tau = \eta/G$ is called the relaxation time of the material.

If the load on the plate in the previous example is suddenly removed at some time $t = t_1$ the expression for the deflection for $t > t_1$ is given by

$$w = w_e \frac{G(3K + G)}{3K + 4G} \left[\frac{\left(e^{\frac{t}{\tau}} - 1 \right)}{G} e^{-\frac{t}{\tau}} + \frac{3 \left(e^{\frac{3K + G}{G} \frac{t_1}{\tau}} - 1 \right)}{3K + G} e^{-\frac{3K + G}{G} \frac{t}{\tau}} \right] \quad \ldots (25)$$

Fig. 1 shows a plot of w/w_e versus t/τ as obtained from Eqs. 24 and 25 for a plate having $\nu = 0.25$ and for which $t_1 = 2\tau$.

In a similar manner expressions for the viscoelastic plate moments $M_{\alpha\beta}(\alpha, \beta = x,y)$ may be obtained from the corresponding equations for the elastic plate moments as given by

---

10 "Theory of Stress-Strain Relations in Anisotropic Viscoelasticity and Relaxation Phenomena," by M. A. Biot, Journal of Applied Physics, Vol. 25, No. 11, November, 1954, p. 1385.

$$M_{\alpha\beta} = -\frac{h^3 G}{6}\left(w_{e,\,\alpha\beta} + \delta_{\alpha\beta}\frac{3K - 2G}{3K + 4G} w_{e,\,\gamma\gamma}\right) \quad (\alpha,\beta = x,y) \quad \ldots\ldots (26)$$

For a Kelvin plate such as was used in the prior example the shear modulus G is given in operational form according to Eq. 5 as $p + \frac{1}{\tau}$. Inserting this in place of G in Eq. 26 and transforming results in

$$\overline{M}_{\alpha\beta} = -\frac{D}{2(3K + G)}\left[\left(\frac{3K + 4G}{s} + \frac{9K}{\frac{3K + G}{G\tau} + s}\right) w_{e,\alpha\beta} + \delta_{\alpha\beta}\left(\frac{3K - 2G}{s} - \frac{9K}{\frac{3K + G}{G\tau} + s}\right) w_{e,\gamma\gamma}\right] \quad \ldots\ldots\ldots (27)$$

which may be inverted at once to give

$$M_{\alpha\beta} = -\frac{D}{2(3K + G)}\left[\left(3K + 4G + 9K\, e^{-\frac{3K + G}{G}\frac{t}{\tau}}\right) w_{e,\,\alpha\beta} + \left(3K - 2G - 9K\, e^{-\frac{3K + G}{G}\frac{t}{\tau}}\right) w_{e,\gamma\gamma}\right] \quad \ldots\ldots\ldots (28)$$

Examination of Eq. 28 reveals that as $t \to \infty$ the viscoelastic plate moments approach the elastic ones and when $t = 0$, the moments are those of an elastic plate having $\nu = -1$ which corresponds to the case of a rigid body.

The analysis of a Maxwell-type plate under the same loading conditions would follow in the same fashion as that for the Kelvin plate as previously given. Omitting the details, the equations are a Maxwell plate corresponding to Eqs. 24, 25, and 28 are given by

$$w = w_e\left(\frac{3K + G}{3K + 4G}\right)\left[\frac{K + G}{K} + \frac{t}{\tau} - \frac{G^2}{(3K + G)K}\, e^{-\frac{3K}{3K + G}\frac{t}{\tau}}\right] \quad \ldots\ldots (29)$$

$$w = w_e\left(\frac{3K + G}{3K + 4G}\right)\left[\frac{t_1}{\tau} + \frac{G^2\left(e^{\frac{3K}{3K + G}\frac{t_1}{\tau}} - 1\right)}{(3K + G)\,K} e^{-\frac{3K}{3K + G}\frac{t}{\tau}}\right] \quad \ldots\ldots\ldots (30)$$

and

$$M_{\alpha\beta} = -\frac{D}{2(3K + G)}\left[\left(3K + G + 3G\, e^{-\frac{3K}{3K + G}\frac{t}{\tau}}\right) w_{e,\,\alpha\beta} + \delta_{\alpha\beta}\left(3K + G - 3G\, e^{-\frac{3K}{3K + G}\frac{t}{\tau}}\right) w_{e,\gamma\gamma}\right] \quad \ldots\ldots\ldots (31)$$

Eqs. 29 and 30 for the Maxwell plate are plotted in Fig. 1 using the same conditions ($\nu = 0.25$ and $t_1 = 2\tau$) employed in plotting the Kelvin plate curves shown there.

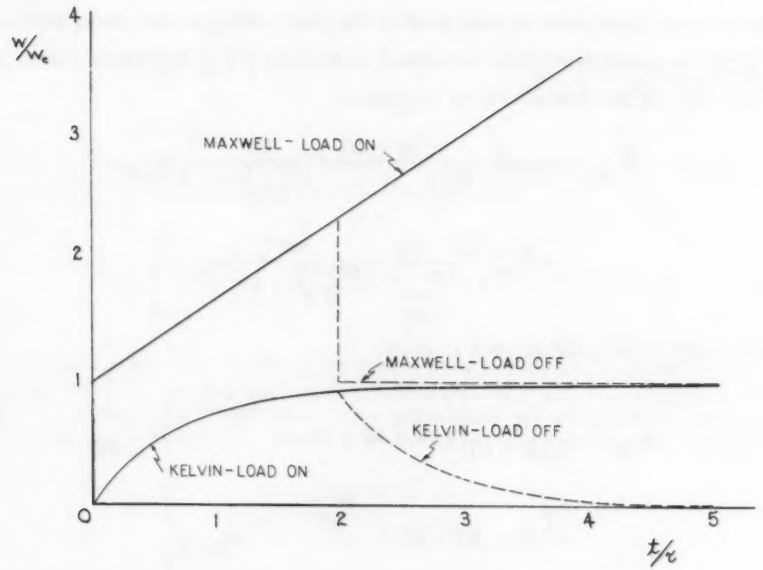

FIG. 1.—MAXWELL AND KELVIN PLATE DEFLECTION

Moving Line Load.—If the load, $f = f(x, y, t)$ cannot be expressed as simply the product of a space function multiplied by a time function, the question of separating the variables in the fundamental equation is not a straight forward operation and a modified approach is required. Consider, for example, the problem of a line load of constant magnitude moving with constant velocity across a simply supported rectangular plate having the dimensions shown in Fig. 2. In view of the boundary conditions on the edge of the plate, it is convenient to take the deflection in the form of the series

$$w(x,y,t) = \sum_{m=1,3,5}^{\infty} \sum_{n=1,3,5}^{\infty} \phi_{mn}(t) \sin \frac{m\pi x}{a} \sin \frac{n\pi y}{b} \quad \ldots\ldots (32)$$

The procedure now is to expand the load function, f, in a similar series and by substituting these series into the fundamental plate equation arrive at an equation from which the coefficients, ϕ_{mn} of the deflection expression may be obtained. To this end let

$$f(x,y,t) = \sum_{m=1}^{\infty} \sum_{n=1}^{\infty} \psi_{mn}(t) \sin \frac{m\pi x}{a} \sin \frac{n\pi y}{b} \quad \ldots\ldots\ldots (33)$$

Considering the line load to be of uniform intensity f_0 over the small interval 2ϵ of the plate and assuming the load is at the left edge of the plate and moving with a constant velocity, v, when t = 0, as indicated in Fig. 3, the functions ψ_{mn}

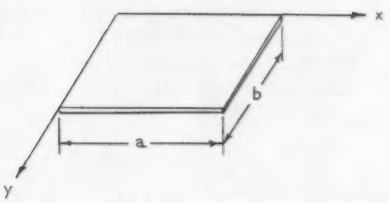

FIG. 2.—RECTANGULAR PLATE

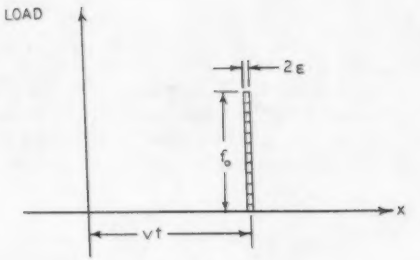

FIG. 3.—MOVING LOAD REPRESENTATION

in Eq. 33 may be determined in the usual manner based upon the orthogonality of the sine functions. For the case at hand the relationship is given by

$$\psi_{mn} = \int_0^b \int_{vt-\epsilon}^{vt+\epsilon} \frac{4}{ab} f_0 \sin\frac{m\pi x}{a} \sin\frac{n\pi y}{b}\, dx\, dy \quad \ldots\ldots\ldots (34)$$

Carrying out the indicated integrations and inserting the limits yields the result

$$\psi_{mn} = \frac{8P_0}{n\pi a} \sin\frac{m\pi v}{a} t \quad (m,n = 1,3,5\ \text{--}) \quad \ldots\ldots\ldots\ldots (35)$$

in which $P_0 = 2 f_0 \epsilon$. Therefore, now

$$f(x,y,t) = \sum_{m=1,3,5}^{\infty} \sum_{n=1,3,5}^{\infty} \frac{8 P_0}{n\pi a} \sin\frac{m\pi v}{a} t \sin\frac{m\pi x}{a} \sin\frac{n\pi y}{b} \quad \ldots\ldots (36)$$

Substitution of this series together with the one given by Eq. 32 into Eq. 13 and matching coefficients produces an ordinary differential equation from which the unknown functions ϕ_{mn} in Eq. 32 may be determined. The equation to be solved is

$$\pi^4\left(\frac{m^2}{a^2} + \frac{n^2}{b^2}\right)^2 B_1 (\varphi_{mn}) = \frac{8 P_0}{n\pi a} \sin\frac{m\pi v}{a} t \quad \ldots\ldots\ldots (

from which ϕ_{mn} in operational form is given by

$$\phi_{mn} = \frac{8\,P_0}{\pi^5\, a\, n\left(\frac{m^2}{a^2} + \frac{n^2}{b^2}\right)^2}\left[\frac{3P\,(3K\,P + 4Q)}{h^3\,Q\,(3K\,P + Q)}\sin\frac{m\pi v}{a}\,t\right] \quad \ldots\ldots (38)$$

Eq. 38 may be solved at once using the Laplace transform method as in the previous work. If, for example, the plate is assumed to be made of a Maxwell type material, the operator B_1 as given by Eq. 9 may be introduced into Eq. 38 and the solution obtained by a direct application of the operational procedure. Omitting the details, the result for such a plate is given by

$$\phi_{mn} = \frac{24\,P_0}{G\,h^3\,\pi^5\, a\, n\left(\frac{m^2}{a^2} + \frac{n^2}{b^2}\right)^2}\left[\frac{3K + 4G}{3K + G}\sin\lambda_m t + \frac{1 - \cos\lambda_m t}{\tau\,\lambda_m}\right.$$

$$\left. + \frac{3G^2}{\tau(3K + G)}\left(\frac{A\sin\lambda_m t - \lambda_m\cos\lambda_m t + \lambda_m e^{-At}}{A^2 + \lambda_m^2}\right)\right] \quad \ldots\ldots (39)$$

in which $A = \frac{3K}{\tau(3K + G)}$ and $\lambda_m = \frac{m\pi v}{a}$.

From this, it is observed that when $t = 0$, $\phi_{mn} = 0$ which corresponds to the undeflected plate before the load has moved upon it.

It is essential to note that the solution given by Eq. 39 is valid only while the load is actually on the plate, that is, when $0 < t < a/v$. At the instant the load leaves the plate the deflection is given by

$$w = \frac{24\,P_0}{G\,h^3\,\pi^5\, a}\sum_{m=1,3,5}^{\infty}\sum_{n=1,3,5}^{\infty}\frac{1}{n\left(\frac{m^2}{a^2} + \frac{n^2}{b^2}\right)^2}\left[\frac{2}{\tau\lambda_m}\right.$$

$$\left. + \frac{3G^2}{\tau\,(3K + G)^2}\,\frac{\lambda_m\left(1 + e^{-\frac{Aa}{v}}\right)}{A^2 + \lambda_m^2}\right]\sin\frac{m\pi x}{a}\,\sin\frac{n\pi y}{b} \quad \ldots\ldots (40)$$

and the plate velocity is given by

$$\dot{w} = \frac{24\,P_0}{G\,h^3\,\pi^5\,a} \sum_{m=1,3,5}^{\infty} \sum_{n=1,3,5}^{\infty} \frac{1}{n\left(\frac{m^2}{a^2} + \frac{n^2}{b^2}\right)^2} \left[-\frac{3K + 4G}{3K + G}\,\lambda_m \right.$$

$$\left. -\frac{3G^2}{\tau(3K + G)} \frac{A\,\lambda_m \left(1 - e^{-\frac{Aa}{v}}\right)}{A^2 + \lambda_m^2} \right] \sin\frac{m\pi x}{a} \sin\frac{n\pi y}{b} \quad \ldots\ldots\ldots (41)$$

Using these expressions as initial conditions the deflection of the plate subsequent to the passing of the load may be determined by the same method as was used for the loaded plate. The operational equation to be solved here is

$$\frac{Q\,(3K\,P + Q)}{P\,(3K\,P + 4Q)}\,\phi_{mn} = 0 \quad \ldots\ldots\ldots\ldots\ldots (42)$$

which for the Maxwell case has the solution

$$\phi_{mn} = -\frac{\dot{\Phi}}{A} + \left(\Phi + \frac{\dot{\Phi}}{A}\right) e^{-At} \quad \ldots\ldots\ldots\ldots\ldots (43)$$

in which

$$\Phi = \phi_{mn}\Big]_{t = a/v} \,, \quad \dot{\Phi} = \dot{\phi}_{mn}\Big]_{t = a/v}$$

Finally, the deflection for $t \geq a/v$ is given by

$$w = \frac{24\,P_0}{G\,h^3\,\pi^5\,a} \sum_{m=1,3,5}^{\infty} \sum_{n=1,3,5}^{\infty} \frac{1}{n\left(\frac{m^2}{a^2} + \frac{n^2}{b^2}\right)^2} \left\langle \left\{ \frac{1}{A} \right\} \frac{3K + 4G}{3K + G}\,\lambda_m \right.$$

$$\left. + \frac{3G^2}{\tau(3K + G)^2} \frac{\lambda_m \left(1 - e^{-\frac{Aa}{v}}\right)}{A^2 + \lambda_m^2} \right\} \left(1 - e^{-At}\right) + \left\{ \frac{2}{\tau\,\lambda_m} \right.$$

$$\left. + \frac{3G^2}{\tau(3K + G)^2} \frac{\lambda_m \left(1 + e^{-\frac{Aa}{v}}\right)}{A^2 + \lambda_m^2} \right\} e^{-At} \Big\rangle \sin\frac{m\pi x}{a} \sin\frac{n\pi y}{b} \quad \ldots\ldots (44)$$

As would be expected from the model representation of a Maxwell material the deflection does not reduce to zero as t increases indefinitely, but some residual deflection remains in the plate. This is given by

$$w = \frac{24\,P_0}{G\,h^3\,\pi^5\,a} \sum_{m=1,3,5}^{\infty} \sum_{n=1,3,5}^{\infty} \frac{1}{n\left(\frac{m^2}{a^2} + \frac{n^2}{b^2}\right)^2} \left\langle \frac{1}{A} \left\{ \frac{3K + 4G}{3K + G} \right\} \lambda_m + \frac{3G^2}{\tau(3K + G)^2} \frac{\lambda_m \left(1 - e^{-\frac{Aa}{v}}\right)}{A^2 + \lambda_m^2} \right\rangle \sin \frac{m\pi x}{a} \sin \frac{n\pi y}{b} \quad \ldots\ldots (45)$$

DYNAMIC SOLUTIONS

Compressible Plate Material.—If inertia effects due to deformation are taken into account, the second term on the left hand side of Eq. 12 must be retained. In the present work only free vibrations are studied. Accordingly, solutions of

$$B_1 \left\{ \nabla^4 w \right\} + p^2 \rho\, h\, w = 0 \quad \ldots\ldots\ldots\ldots\ldots (46)$$

are sought.

Solutions of Eq. 46 may be obtained using the method of the previous section. Consider as an example the free vibrations of a simply supported rectangular plate of the dimensions given in Fig. 2. Taking again the deflection of the plate to be given by the double sine series of Eq. 32 and substituting this into Eq. 46 results in the following equation for determining ϕ_{mn}.

$$\left[p^2 \rho\, h + \pi^4 \left(\frac{m^2}{a^2} + \frac{n^2}{b^2} \right)^2 B_1 \right] \phi_{mn} = 0 \quad \ldots\ldots\ldots (47)$$

If the plate is assumed to be a Maxwell plate this equation becomes

$$p \left\{ (3K + 4G)\, p^3 + \frac{6K + 4G}{\tau}\, p^2 + \left[\frac{3K}{\tau^2} + \pi_{mn}(3K + G) \right] p + \frac{3K\,\pi_{mn}}{\tau} \right\} \phi_{mn} = 0 \quad \ldots (48)$$

in which

$$\pi_{mn} = \frac{G\,h^3\,\pi^4}{3\rho} \left(\frac{m^2}{a^2} + \frac{n^2}{b^2} \right)^2$$

Taking the Laplace transform of Eq. 48 results in

$$\overline{\phi}_{mn} = \frac{\Phi_{mn}(s)}{s\left\{(3K+4G)\,s^3 + \frac{6K+4G}{\tau}\,s^2 + \left[\frac{3K}{\tau^2} + \pi_{mn}(3K+G)\right]s + \frac{3K\,\pi_{mn}}{\tau}\right\}} \quad \ldots (49)$$

in which $\Phi_{mn}(s)$ is a polynomial in s, the transform variable, the exact form of which depends upon the initial conditions of the plate motion. Eq. 49 may be inverted by the method of partial fractions once the roots of the cubic factor of the denominator have been found. Standard procedures for determining these roots are available.[11]

Calling the roots r_1, r_2 and r_3 the solution of Eq. 49 becomes

$$\phi_{mn} = \Phi_{mno} + \sum_{i=1}^{3} \Phi_{mni}\, e^{-r_i t} \quad \ldots (50)$$

in which the Φ_{mni}'s are constants involving the physical parameters of the plate material and initial conditions of the motion. Hence, the response is given by

$$w = \sum_{m=1,3,5}^{\infty} \sum_{n=1,3,5}^{\infty} \left(\Phi_{mno} + \sum_{i=1}^{3} \Phi_{mni}\, e^{-r_i t}\right) \sin\frac{m\pi x}{a} \sin\frac{n\pi y}{b} \quad \ldots (51)$$

From this, if numerical values of G, K and τ are known and the initial conditions are given, the plate response may be expressed in terms of the normal modes. It should be pointed out that because of the presence of π_{mn} in the cubic of Eq. 49 the roots r_i will be different for each mode of vibration. Therefore, considerable calculation would be encountered in carrying out the expansion of Eq. 51 to higher modes.

Incompressible Plate Material.—If the plate material may be assumed to be incompressible, as is frequently done in viscoelastic problems, considerable simplification of Eq. 48 is achieved and general solutions are readily obtained. The condition of incompressibility is expressed by M = 0 and N = 1 in Eq. 1. This is essentially the same as considering $K \to \infty$. Under this assumption the operational form of the flexural rigidity becomes

$$B_1 = \frac{h^3}{3}\frac{Q}{P} \quad \ldots (52)$$

and Eq. 48 is now

$$p\left(p^2 + \frac{1}{\tau}p + \pi_{mn}\right)\phi_{mn} = 0 \quad \ldots (53)$$

11 "Theory of Equations," by L. E. Dickson, John Wiley, and Sons, Inc., New York, 1939, p. 42.

Solutions of Eq. 53 may be obtained at once. Consider, for example, the case of a simply supported Maxwell plate. There is no loss of generality in assuming initial conditions such that when t = 0 the plate has velocity but no displacement or acceleration. For this condition the transform of Eq. 53 is given by

$$\bar{\phi}_{mn} = \dot{\phi}_{mn}\left(\frac{s + \frac{1}{\tau}}{s\left(s^2 + \frac{s}{\tau} + \pi_{mn}\right)}\right) \qquad \ldots\ldots (54)$$

in which $\dot{\phi}_{mn} = \dot{\phi}_{mn}$ at t = 0. Rewriting Eq. 54 in the form best suited for inverting gives

$$\bar{\phi}_{mn} = \dot{\phi}_{mn}\left\{\frac{s + \frac{1}{\tau}}{s\left[\left(s + \frac{1}{2\tau}\right)^2 + \left(\pi_{mn} - \frac{1}{4\tau^2}\right)\right]}\right\} \qquad \ldots\ldots\ldots (55)$$

For this, if $4\tau^2\,\pi_{mn} > 1$, that is, if the "damping effect" of the viscous nature of the plate is small enough the response will be oscillatory. Hence, inverting the equation for this case gives the result

$$\phi = \dot{\phi}_{mn}\left[\frac{1}{\tau\pi_{mn}} + \frac{e^{-\frac{t}{2\tau}}}{\left(\pi_{mn} - \frac{1}{4\tau^2}\right)^{1/2}}\,\sin\left(\sqrt{\pi_{mn} - \frac{1}{4\tau^2}}\;t - \psi_{mn}\right)\right] \qquad \ldots\ldots (56)$$

in which

$$\psi_{mn} = \tan^{-1}\frac{\sqrt{\pi_{mn} - \frac{1}{4\tau^2}}}{\frac{1}{2\tau} - \tau\,\pi_{mn}}$$

Thus, the response consists of a constant term plus a decaying sine term.

Of equal interest to the previous example from a practical point of view is the free response of a Kelvin plate, which corresponds essentially to the concept of internal viscous damping used so often in studying damped vibrations of beams and bars. Assuming that such a plate is started vibrating by giving it an initial displacement and releasing it without velocity the expression for $\bar{\phi}_{mn}$ analogous to Eq. 54 is given by

$$\bar{\phi}_{mn} = \phi_{mn}\left(\frac{s + \eta\,\bar{\pi}_{mn}}{s^2 + \eta\,\bar{\pi}_{mn}\,s + G\,\bar{\pi}_{mn}}\right) \qquad \ldots\ldots\ldots\ldots (57)$$

in which $\bar{\pi}_{mn} = \frac{\pi_{mn}}{G}$. From this the motion is oscillatory if $4G > \eta^2\,\bar{\pi}_{mn}$ and the solution becomes

$$\phi_{mn} = \Phi_{mn}\left[\frac{e^{-\frac{\eta\bar{\pi}_{mn}}{2}t}}{\left(1-\frac{\eta^2\bar{\pi}_{mn}}{4G}\right)^{1/2}}\sin\left(\frac{\eta\bar{\pi}_{mn}}{2}\sqrt{\frac{4G}{\eta^2\bar{\pi}_{mn}}-1}\;t+\psi_{mn}\right)\right] \quad \ldots . (58)$$

in which

$$\psi_{mn} = \tan^{-1}\frac{\sqrt{G\bar{\pi}_{mn}-\frac{\eta^2\bar{\pi}_{mn}^2}{4}}}{\frac{\eta\bar{\pi}_{mn}}{2}}$$

It should be noted in this solution that the higher modes will be rapidly damped out and, therefore, it is the fundamental mode that is of most importance.

ACKNOWLEDGMENT

The paper is based on part of a dissertation submitted to the Virginia Polytechnic Institute, in August, 1958, in partial fulfillment of the requirements for the degree of Doctor of Philosophy.

Journal of the
ENGINEERING MECHANICS DIVISION
Proceedings of the American Society of Civil Engineers

AIRCRAFT STRUCTURAL ANALYSIS ON AN ANALOG COMPUTER[a]

By W. J. Brignac[1] and R. G. Schwendler[2]

SYNOPSIS

It has been known for many years that elastic structures can be represented by electric analogs with passive elements. In recent years this method of analysis has been successfully applied to complex, highly redundant aircraft structures. Presented in this paper is a brief description of this technique and some examples of its practical application in structural analysis.

INTRODUCTION

The structural design refinements required in modern aircraft make it necessary to have accurate deflection and stress data under static and dynamic loads. Present and future design trends require the analysis of highly redundant structures. The principal analytical means in use to handle these problems are either the formulating and solving of a large number of simultaneous equations on a digital computer or the use of electric analog computers of the direct analogy type. Digital computers have experienced rapid development in recent years and solution time and solution accuracy are no longer impediments to large scale structural application. The capabilities of the electric analog method may presently not be as well established. The purpose of this paper is to describe the use of an electric analog computer on structural problems at Convair-Fort Worth and to present the results of some applications in

Note.—Discussion open until November 1, 1960. To extend the closing date one month, a written request must be filed with the Executive Secretary, ASCE. This paper is part of the copyrighted Journal of the Engineering Mechanics Division, Proceedings of the American Society of Civil Engineers, Vol. 86, No. EM 3, June, 1960.

[a] Presented at the October 1959 ASCE Convention in Washington, D. C.

[1] Proj. Structures Engr., Convair, Div. of General Dynamics, Fort Worth, Texas.
[2] Senior Structures Engr., Convair, Div. of General Dynamics, Fort Worth, Texas.

order to show that very satisfactory solutions to extremely complex problems can be obtained with this computer.

GENERAL DESCRIPTION

A direct analogy electric analog computer may be defined as a collection of electrical elements (resistors, capacitors, transformers, etc.) that are used to form circuits analogous to the structure to be analyzed. Solutions are then obtained by testing, or taking measurements on, the electrical model in much the same way that a scale model would be tested. Its principal features are:

(1) It furnishes the user with a readily changeable model and is, therefore, most useful in optimization and parameter variation studies.
(2) It is like an erector set in that the elements can be used over and over again in different arrangements to represent different structures.

The use of analogous electrical circuits as a means of solving pin-connected and rigidly-connected structures was proposed[3] by V. Bush in 1934. Several other instances[4] of analogous circuits for isolated problems also appeared in the literature prior to 1945. Up to that time the rather limited interest in this method of analysis was due to the belief that satisfactory answers could be expected only for relatively simple problems because of the inherent imperfections in the basic passive computer elements. Extensive efforts in recent years at the California Institute of Technology, Pasadena, Calif., and at Computer Engineering Associates of Pasadena, Calif., have resulted in the design of a computer that permits accurate solution of large-scale problems. This computer design is described elsewhere.[5] This reference also lists a large number of papers on the many analogies which have been developed for application to this type of computer.

The computer used in this work, designed for both static and dynamic analyses, is illustrated in Fig. 1. The computer contains the following: 2 control desks; 154 inductors; 320 resistors; 84 steady state current generators; 205 transformers; 69 general purpose amplifiers; and 164 capacitors. To date the computer has been used, alternately, to perform:

(1) Static stress analyses of aircraft wings, fuselages, and tail surfaces.
(2) Static aeroelastic analyses of wings (loads are functions of deflections).
(3) Dynamic analyses including normal mode analyses, flutter and gust response analyses of entire aircraft and individual surfaces.

This report will be limited to discussion on the use of the computer in the static stress analyses field.

BASIC CONCEPTS

The Nodal Analogy.—The force-current, or nodal analogy, is normally used when solving structural problems on the electric analog computer. In the most general application to dynamic problems, force is analogous to current and

[3] "Structural Analysis by Electric Circuit Analogies," by V. Bush, Journal of the Franklin Inst., March, 1934.
[4] "Electrical Analogy for Shear Lag Problems," by R. E. Newton, Experimental Stress Analysis, Vol. II, No. 2, October, 1944.
[5] "The Direct Analogy Electric Analog," by G. D. McCann, ISA Journal, April, 1956.

voltage is analogous to velocity. For the case of purely static stress problems, analogous circuits using only resistors and transformers, in which voltage is analogous to displacement, are used. The basic relationships of a simple spring in tension are summarized in the Fig. 2.

Exact relations are dependent upon the choice of scale factors. The choice of the following basic factors may be used.

$$\text{Mechanical energy} = \frac{1}{2} F X = \frac{1}{2} C^2 I E \quad \ldots\ldots\ldots\ldots \quad (1)$$

$$\text{Mechanical displacement} = X = C a E \quad \ldots\ldots\ldots\ldots\ldots \quad (2)$$

in which C and a are constants, I E denotes electrical power and E is voltage. In the general case of a multi-degree of freedom system, C is the same for all

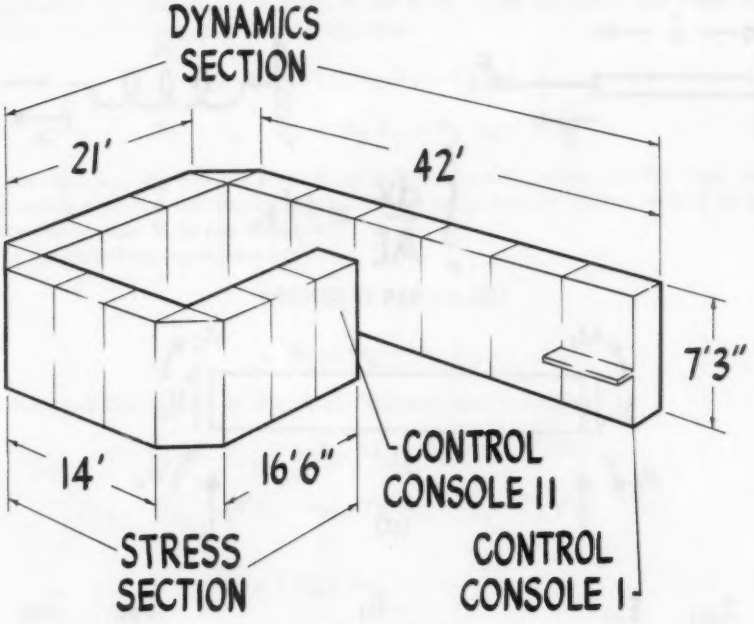

FIG. 1.—LAYOUT OF CONVAIR DAEAC

parts whereas a may be different for every coordinate. I is the current and R is the resistance. The choice of form for the scale factor is largely a convenience in structural problems and leads to the following derived expressions for the example of Fig. 2.

$$F = \frac{C}{a} I \quad \ldots\ldots\ldots\ldots\ldots\ldots \quad (3)$$

$$\frac{1}{K} = a^2 R \quad \ldots\ldots\ldots\ldots\ldots\ldots \quad (4)$$

The constants C and a are chosen as one of the last steps in preparing a problem for solution. They are chosen to give the most practical size of cir-

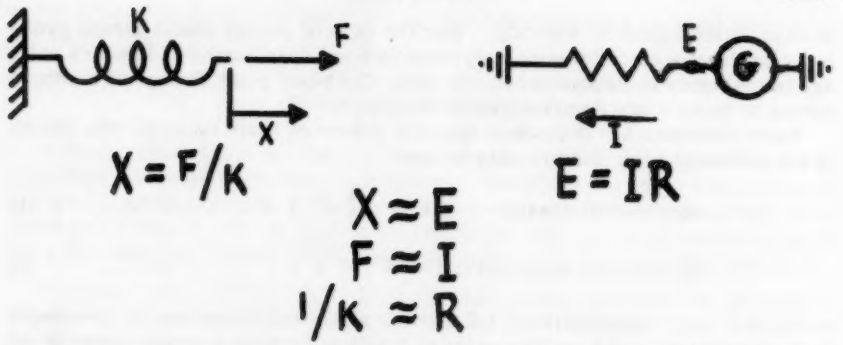

FIG. 2.—SPRING IN TENSION

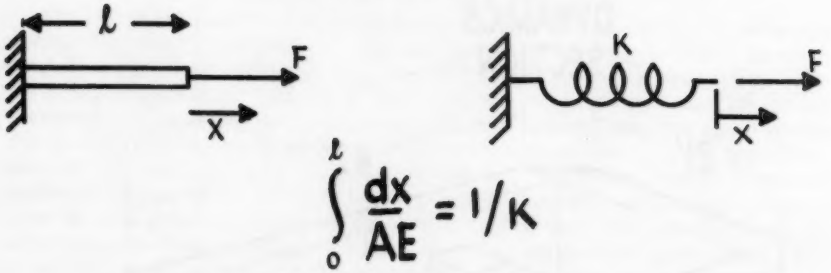

FIG. 3.—BAR IN TENSION

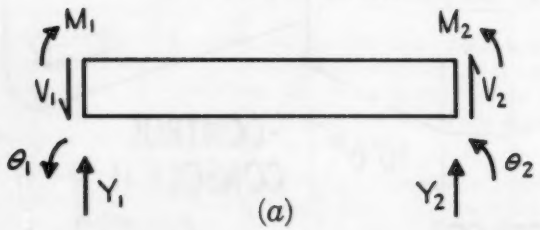

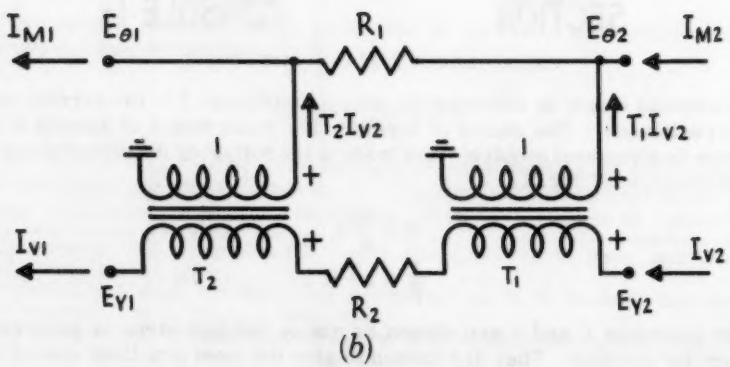

FIG. 4.—BEAM ELEMENT AND ITS ELECTRIC ANALOG

cuit elements and also to minimize parasitic effects. A more complete discussion of scale factors may be found elsewhere.[6]

One-Dimensional Members —In analyzing continuous one-dimensional members (straight or curved bar in tension, torsion, or bending) the only approximation necessary is that distributed loads must be replaced by "equivalent" concentrated loads. For example, the spring previously illustrated represents exactly a rod in tension if the value of K, the spring constant, is as shown in Fig. 3.

An additional example of a one-dimensional member is a straight beam in bending. Many beam analogies of varying degrees of accuracy are in general use. The analogy to follow is exact under the limitations previously applied to loads and is equivalent to the one presented by W. T. Russell and R. H. MacNeal,[7] although the derivation is different.

Shown in Fig. 4(a) is an unloaded segment of a beam of length, L, with internal loads and coordinates defined at the ends. The motion of the right end relative to the left end may be expressed as

$$\theta_2 - \theta_1 = \Delta\theta = M_2 A_1 + V_2 A_2 \quad \ldots\ldots\ldots\ldots (5)$$

$$Y_2 - Y_1 = \Delta y = M_2 A_2 + V_2 A_3 + L\,\theta_1 \quad \ldots\ldots\ldots (6)$$

in which A_1, A_2, A_3 are the flexibility influence coefficients for the right end of the beam with the left end assumed fixed. As indicated in Fig. 4(a) V is the vertical force and M is the moment.

The equilibrium equations are

$$V_1 = V_2 \quad \ldots\ldots\ldots\ldots\ldots\ldots (7)$$

$$M_1 = M_2 + V_2\, L \quad \ldots\ldots\ldots\ldots\ldots (8)$$

Now consider the circuit of Fig. 4(b). Circuit equations are

$$E_{\theta_2} - E_{\theta_1} = \Delta E_\theta = I_{M_2} R_1 + I_{V_2} T_1 R_1 \quad \ldots\ldots\ldots (9)$$

$$E_{y_2} - E_{y_1} = \Delta E_\gamma = I_{M_2} T_1 R_1 + I_{V_2} \left(T_1^2 R_1 + R_2\right) + \left(T_1 + T_2\right) E_{\theta_1} \quad \ldots\ldots\ldots\ldots\ldots\ldots (10)$$

$$I_{V_1} = I_{V_2} \quad \ldots\ldots\ldots\ldots\ldots\ldots (11)$$

and

$$I_{M_1} = I_{M_2} + \left(T_1 + T_2\right) I_{V_2} \quad \ldots\ldots\ldots\ldots (12)$$

---

[6] "The Solution of Aeroelastic Problems by Means of Electrical Analogies," by R. H. MacNeal, G. D. McCann and C. H. Wilts, Journal of Aero Sciences, Vol. 18, December, 1951.

[7] "An Improved Electrical Analogy for the Analysis of Beams in Bending," by W. T. Russell and R. H. MacNeal, Journal of Applied Mechanics, September, 1953.

Standard scale factors used in the analysis are

$$\theta = \frac{C\,a}{P}\ E_\theta \quad \ldots\ldots\ldots\ldots\ldots\ldots\ldots (13)$$

$$Y = C\,a\,E_\gamma \quad \ldots\ldots\ldots\ldots\ldots\ldots\ldots (14)$$

$$M = \frac{C\,P}{a}\ I_M \quad \ldots\ldots\ldots\ldots\ldots\ldots\ldots (15)$$

and

$$V = \frac{C}{a}\ I_V \quad \ldots\ldots\ldots\ldots\ldots\ldots\ldots (16)$$

The "P" factor used in Eqs. 13 and 15 is equivalent to the use of a second constant $a_\theta = \frac{a}{P}$. Substituting Eqs. 13 through 16 into either set of preceding equations gives

$$R_1 = \frac{P^2}{a^2}\ A_1 \quad \ldots\ldots\ldots\ldots\ldots\ldots\ldots (17)$$

$$T_1 = \frac{A_2}{A_1\,P} \quad \ldots\ldots\ldots\ldots\ldots\ldots\ldots (18)$$

$$R_2 = \frac{1}{a^2}\ \left[A_3 - \frac{A_2{}^2}{A_1}\right] \quad \ldots\ldots\ldots\ldots\ldots\ldots\ldots (19)$$

and

$$T_2 = \frac{L}{P} - T_1 \quad \ldots\ldots\ldots\ldots\ldots\ldots\ldots (20)$$

To represent an entire beam, common coordinates of adjacent segments are joined. Supports and loads are introduced into circuits at the appropriate coordinates. The "exactness" of the analogy thus formed is dependent upon the accuracy with which the influence coefficients can be evaluated. It is noted that, in the case of a beam with strain energy due only to bending, the coefficients may be evaluated from

$$A_1 = \int_0^L \frac{dx}{E\,I} \quad \ldots\ldots\ldots\ldots\ldots\ldots\ldots (21)$$

$$A_2 = \int_0^L \frac{x\,dx}{E\,I} \quad \ldots\ldots\ldots\ldots\ldots\ldots\ldots (22)$$

which is the first moment of area about right end, and

$$A_3 = \int_0^L \frac{x^2\,dx}{E\,I} \quad \ldots\ldots\ldots\ldots\ldots\ldots\ldots (23)$$

which is the second moment of one area about right end. A_1 is the rotation due to the unit moment of the $1/E\,I$ diagram, A_2 is the deflection due to the unit moment, and A_3 is the deflection due to the unit force. Additional items such as shear deformation or the effect of tapered flanges may be handled by including these effects in the calculation of the influence coefficients.

Two-Dimensional Elements —Aircraft structures are usually a mixture of one-dimensional elements (spar caps, stiffeners, fuselage frames or rings) and two-dimensional elements such as the flat or curved web and cover panels. The treatment of the two dimensional elements requires additional approximations over the substitution of concentrated loads for distributed loads. These approximations involve the lumping of distributed stiffness or elasticity into effective one-dimensional elements, and the substitution of a finite number of interconnections for the continuous interconnections at boundaries. The result is that the actual structure is replaced by an idealized one consisting of elements which individually can be simulated. The final step is the interconnection of the analogies for the individual elements.

The approach previously described, known as the "lumped parameter" method, is generally more satisfactory on structural problems than an alternate "finite difference" method. In this second approach the differential equations are first replaced by finite difference equations, and circuits analogous to the difference equations are derived.

The treatment of two-dimensional elements may be illustrated by a flat plate in plane stress. The plate shown in Fig. 5 is replaced by a rectangular grid of equivalent bars which carry axial load, and by panels between the bars which carry shear loads only. Further, the panels are assumed to be connected to the bar on each edge by the single point connection shown. Free body diagrams of the bars intersecting at point G are shown in Fig. 6(a) and of panel FLQK are shown in Fig. 6(b).

Consider first the bars intersecting at point G. For the assumed state of uniform stress in the neighborhood of point G, the stress-strain relations are:

$$\epsilon_x = \frac{1}{E}\left(\sigma_x - \upsilon\,\sigma_y\right) \quad \ldots\ldots\ldots\ldots\ldots\ldots (24)$$

$$\epsilon_y = \frac{1}{E}\left(-\upsilon\,\sigma_x + \sigma_y\right) \quad \ldots\ldots\ldots\ldots\ldots\ldots (25)$$

Converting strain to total elongation and writing stress in terms of forces, the equations become:

$$\Delta U_x = U_{x_H} - U_{x_F} = \epsilon_x\,\Delta x = \frac{1}{Et}\left(\frac{Fx}{\Delta y}\,\Delta x - \upsilon\,Fy\right) \quad \ldots\ldots (26)$$

$$\Delta U_y = U_{y_B} - U_{y_L} = \epsilon_y\,\Delta_y = \frac{1}{Et}\left(-\upsilon\,F + Fy\,\frac{\Delta y}{\Delta x}\right) \quad \ldots\ldots (27)$$

The analogous circuit is shown in Fig. 7(a). The requirements for the circuit elements may be established by writing the circuit equations

$$\Delta E_x = E_{x_H} - E_{x_F} = I_x R_x + \left(I_x - T_p\,I_y\right) R_p$$

$$= I_x\left(R_x + R_p\right) - I_y\,T_p\,R_p \quad \ldots\ldots\ldots\ldots\ldots\ldots (28)$$

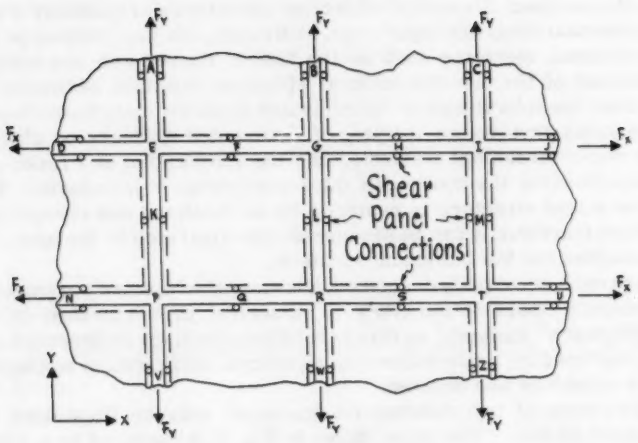

FIG. 5.—FLAT PLATE

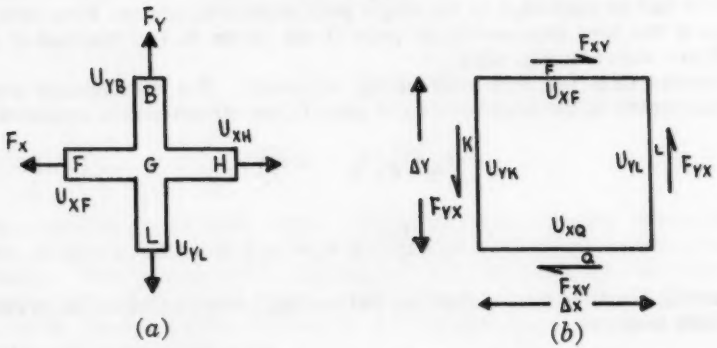

FIG. 6.—FREE BODY DIAGRAM OF BARS INTERSECTING

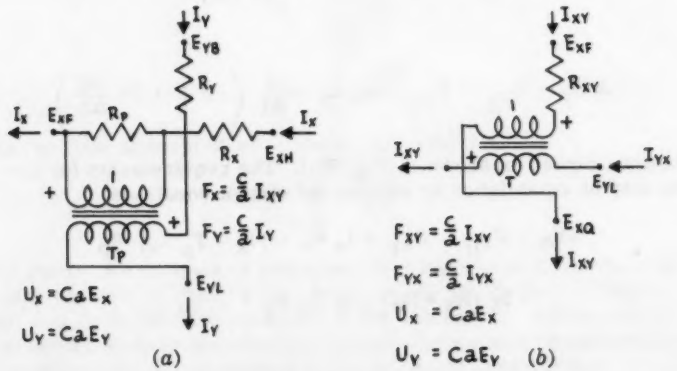

FIG. 7.—ELECTRIC ANALOGS

$$\Delta E_y = E_{y_B} - E_{y_L} = I_y R_y - T_p \left(I_x - T_p I_y\right) R_p$$

$$= I_x T_p R_p + I_y \left(R_y + T_p{}^2 R_p\right) \quad \ldots\ldots\ldots\ldots\ldots\ldots (29)$$

Substitution of the scale factor relations listed on Fig. 7(a) into Eqs. 28 and 29, and letting T_p equal unity gives the following, by comparison with the mechanical Eqs. 26 and 27:

$$R_x = \frac{1}{E\,t\,a^2}\left(\frac{\Delta x}{\Delta y} - \upsilon\right) \quad \ldots\ldots\ldots\ldots\ldots\ldots (30)$$

$$R_y = \frac{1}{E\,t\,a^2}\left(\frac{\Delta y}{\Delta x} - \upsilon\right) \quad \ldots\ldots\ldots\ldots\ldots\ldots (31)$$

and

$$R_p = \frac{1}{E\,t\,a^2}\ \upsilon \quad \ldots\ldots\ldots\ldots\ldots\ldots (32)$$

Analogous circuits for the shear panels will be developed next using energy methods. During the deformation of the panel, the external work done by the edge forces must equal the strain energy stored in the panel. The external work is

$$\text{Work}_{ext} = \frac{1}{2} F_{xy} \left(U_{x_F} - U_{x_Q}\right) + \frac{1}{2} F_{yx} \left(U_{y_L} - U_{y_K}\right)$$

$$= \frac{1}{2} F_{xy} \left[\left(U_{x_F} - U_{x_Q}\right) + \frac{\Delta y}{\Delta x}\left(U_{y_L} - U_{y_K}\right)\right] \quad \ldots\ldots (33)$$

The strain energy also can be expressed in terms of F_{xy}:

$$\text{Strain Energy} = \frac{t}{2G} \iint \tau_{xy}{}^2 \, dx\, dy = \frac{F_{xy}{}^2}{2\,G\,t} \iint \frac{dx\, dy}{\Delta x^2} = \frac{F_{xy}{}^2\, \Delta y}{2\,G\,t} \quad \ldots (34)$$

Equating

$$\left[\left(U_{x_F} - U_{x_Q}\right) + \frac{\Delta y}{\Delta x}\left(U_{y_L} - U_{y_K}\right)\right] = F_{xy}\ \frac{\Delta y}{\Delta x\, G\, t} \quad \ldots\ldots (35)$$

Fig. 7(b) contains the analogous circuit. The turns ratio satisfies the equilibrium equation:

$$I_{xy} = T\, I_{yx} \quad \ldots\ldots\ldots\ldots\ldots\ldots (36)$$

Substituting scale factors

$$\frac{a}{C}\ F_{xy} = T\ \frac{a}{C}\ F_{yx} \quad \ldots\ldots\ldots\ldots\ldots\ldots (37)$$

This is compared with the mechanical equation

$$F_{xy} = F_{yx}\ \frac{\Delta x}{\Delta y} \quad \ldots\ldots\ldots\ldots\ldots\ldots (38)$$

from which

$$T = \frac{\Delta x}{\Delta y} \quad \ldots\ldots\ldots\ldots\ldots\ldots\ldots (39)$$

The electrical equation corresponding to Eq. 33 is

$$\left(E_{x_F} - E_{x_p}\right) + \frac{1}{T}\left(E_{y_L} - E_{y_K}\right) = I_{xy}\, R_{xy} \quad \ldots\ldots\ldots (40)$$

Substitution of scale factors and the value of T from Eq. 39 gives

$$R_{xy} = \frac{1}{a^2}\,\frac{\Delta y}{\Delta x\, G\, t} \quad \ldots\ldots\ldots\ldots\ldots\ldots (41)$$

The combined circuit diagram for a portion of the plate shown in Fig. 5 is given in Fig. 8. Represented are sections of five bars and the two center shear panels.

The process of replacing the actual structure by an idealized one is based mostly on judgment. There is no single method which is applicable to all structures. Each must be treated on an individual basis and many factors including, on large problems, the size of the computer must be considered. An important

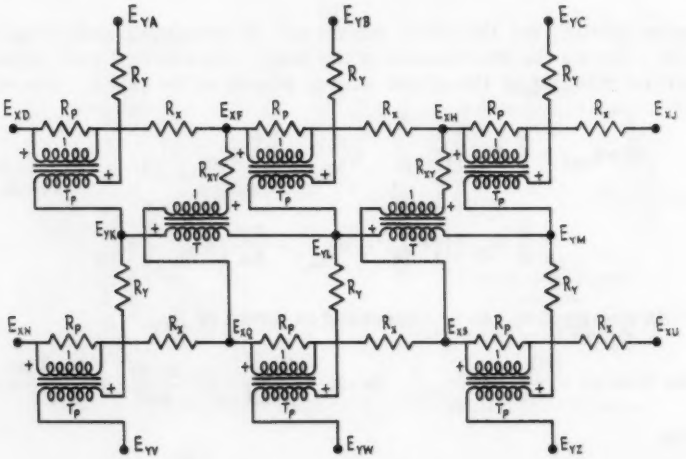

FIG. 8.—FLAT PLATE ANALOGY

feature of the analog computer is that reasonable representations of general two and three-dimensional structures can be built up by methods similar to those used on the preceding example. It has not been the intent of this paper to compile an extensive list of usable analogies. The main purpose has been to illustrate fundamentals which are related to the large scale analyses to be discussed next. The interested reader is referred to other references[5,8] for a comprehensive coverage of analogies.

---

8 "Electrical Analogs of Statically Loaded Structures," by F. C. Ryder, Transactions, ASCE, Vol. 119, 1954.

EXAMPLE BUILDING FRAME PROBLEM

The frame structure shown in Fig. 9 will illustrate the use of the analog computer on composite structures composed of one-dimensional elements. This example will also serve to demonstrate the numerical accuracy which is possible by comparison with the solution obtained by J. S. Archer,[9] on a large scale digital computer.

The frame of Fig. 9 will be represented by the proper connection of six beam segments of the type previously discussed. The connection of the beam segments can be done by inspection of the structure as follows:

(1) The slope of beam AB at point B is identical to the slope of beam BG at point B;

(2) The horizontal deflection of beam AB at point B is identical to the horizontal deflection of beam DC at point D, and so forth throughout the frame.

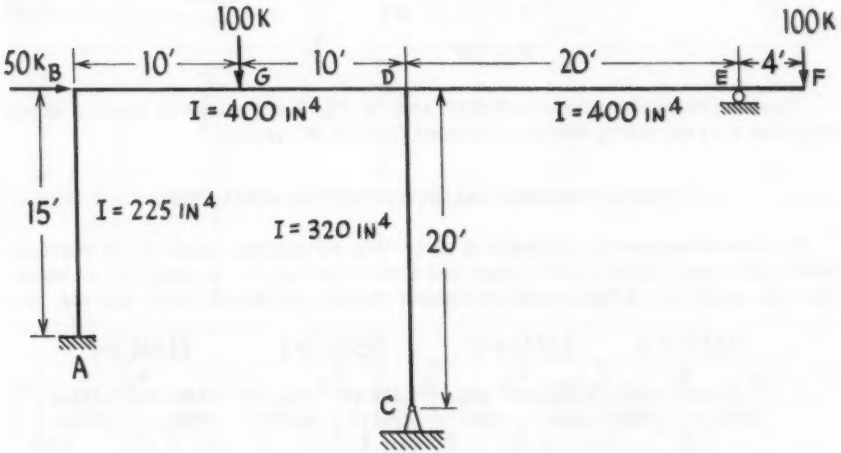

FIG. 9.—EXAMPLE BUILDING FRAME PROBLEM

These identities of slopes and deflections may be accomplished in the analogy of the frame by connecting the corresponding points of the beam segment analogies. It can easily be shown that static equilibrium of the joints of the frame is also maintained in the analogy by the connections discussed above.

The circuit of Fig. 10 shows the electric analogy to the frame of Fig. 9. The beam segment analogies have been kept separated so that they may be individually observed. It should be noted that the number of transformers required in the circuit of Fig. 10 could be reduced to six by combining some of the transformers shown. This reduction in equipment would in no way effect the solution.

The transformer ratios of the circuit of Fig. 10 may be found by combining Eqs. 18, 20, 21 and 22. For a constant EI

$$T_1 = \frac{L}{2P} \quad \ldots\ldots\ldots\ldots\ldots\ldots\ldots\ldots (42)$$

9 "Digital Computations for Stiffness Matrix Analysis," by J. S. Archer, Proceedings, ASCE, Vol. 84, No. ST 6, October, 1958.

$$T_2 = \frac{L}{2P} \quad \ldots\ldots\ldots\ldots\ldots\ldots (43)$$

The values of the resistors of Fig. 10 may be found by combining Eqs. 17, 19, 21, 22 and 23.

$$R_1 = \frac{P^2}{a^2} \frac{L}{E I} \quad \ldots\ldots\ldots\ldots\ldots\ldots (44)$$

$$R_2 = \frac{1}{a^2} \frac{L^3}{12 E I} \quad \ldots\ldots\ldots\ldots\ldots\ldots (45)$$

The numerical values of the transformer ratios and resistors of the circuit of Fig. 10 are evaluated in Tables 1 and 2. The scale factors used are:

$$\left.\begin{aligned} a &= \sqrt{10} \times 10^{-4} \\ C &= 1.5 \times 10^{4} \\ P &= 100 \end{aligned}\right\} \quad \ldots\ldots\ldots\ldots\ldots\ldots (46)$$

The results of the analysis of the frame of Fig. 9 are shown in Table 3 along with the corresponding results obtained from J. S. Archer.[9]

TWO-DIMENSIONAL STRUCTURAL ANALYSIS

In a two-dimensional analysis of plate-like structures, made up of vertical webs with cover skins on the upper and lower surface, the assumption is made that the structure is symmetrical about a central, or chord plane, and that the

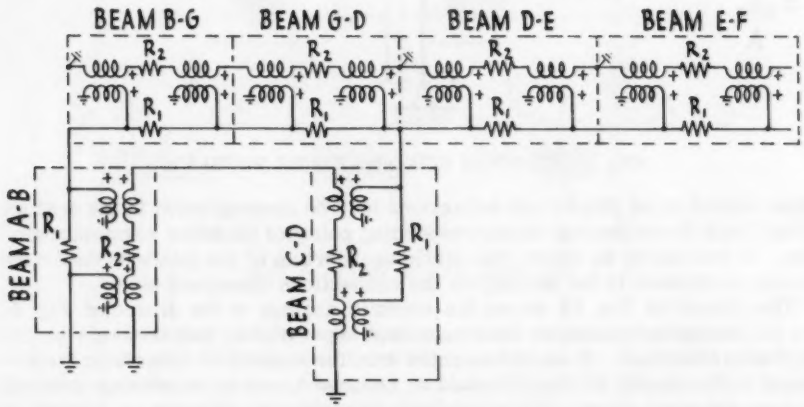

FIG. 10.—ANALOG CIRCUIT-BUILDING FRAME PROBLEM

surface stresses and deformations are antisymmetrical about the same central plane. Forces and deformations in the cover skins can then be represented as moments and rotations, respectively, about the central plane. The result is that the skin representation is reduced to a system of beams and torque boxes acting in conjunction with a second beam network, representing the spars and ribs.

The analysis of a triangular airplane wing on the analog computer that was used in this work is a good example of a large scale analysis of this type. The planform arrangement of the vertical webs of the structure is shown in Fig. 11. The structure is covered by stiffened skin panels on the top and bottom.

Due to the excessive size of the overall problem, the structure of Fig. 11 was reduced in complexity to the one shown in Fig. 12 for an initial analysis. The cover skins of the structure were lumped into a rectangular grid of equivalent bars and shear panels as discussed in the section on two-dimensional elements. The shear panels are connected to the spars and ribs at the points shown in Fig. 12.

TABLE 1.—RESISTOR CALCULATIONS

Beam	Length, in inches	I in.^{4}	Resistance R_1, in ohms	Resistance R_2, in ohms
AB	180	225	2667	720
BG	120	400	1000	120
GD	120	400	1000	120
DE	240	400	2000	960
EF	48	400	400	7.7
CD	240	320	2500	1200

TABLE 2.—TRANSFORMER CALCULATIONS

Beam	Length, in inches	$T_1 = T_2$ P/S	P, Number of turns	S Number of turns
AB	180	.90	90	100
BG	120	.60	60	100
GD	120	.60	60	100
DE	240	1.20	96	80
EF	48	.24	24	100
CD	240	1.20	96	80

It may be noted in Fig. 12 that many of these connections are not on the periphery of a shear panel. For these cases a modification, which considers the structural element shown in Fig. 13, is made to the conventional shear panel analogy described under two-dimensional elements. Fig. 13(a) indicates skewed spans with orthogonal skin lumping and Fig. 13(b) indicates a shear panel with interior forces.

In order to obtain more detailed stress information on the portion of the structure of Fig. 11 aft of line BB, a second analysis was made of that portion of the structure only. The structural elements used in this second analysis are identical in nature to those of the first. The structure was, however, represented in much finer detail due to the reduction in overall size. Fig. 14 shows

the structural representation used in this analysis. Along the line BB, where the wing is "cut" for this analysis, boundary conditions obtained from the first analysis were applied.

Extensive comparisons of results from the second analysis with experimental results for several load conditions show good agreement. Analysis and

TABLE 3.—DEFLECTIONS FROM BUILDING FRAME ANALYSIS

Point	Analog Solution			Digital Solution		
	Vertical Deflection, in inches	Horizontal Deflection, in inches	Slope, in radians	Vertical Deflection, in inches	Horizontal Deflection, in inches	Slope, in radians
A	0	0	0	0	0	0
B	0	5.17	.0307	0	5.120	.0304
C	0	0	.0385	0	0	.0383
D	0	5.17	-.0124	0	5.120	-.0125
E	0	5.17	.0307	0	5.120	.0303
F	1.77	5.17	.0400	1.760	5.120	.0399
G	1.91	5.17	-.0046	1.889	5.120	-.0048

TABLE 4.—INTERNAL LOADS FROM BUILDING FRAME ANALYSIS

Member	Analog Solution			Digital Solution		
	Moment (L.E.), in in.-lb	Shear, in pounds	Moment (R.E.), in in.-lb	Moment (L.E.), in in.-lb	Shear, in pounds	Moment (R.E.), in in.-lb
AB	$.415 \times 10^7$	- 33,300	$-.186 \times 10^7$	$.4118 \times 10^7$	- 33,074	$-.1835 \times 10^7$
BG	$-.186 \times 10^7$	- 27,200	$-.516 \times 10^7$	$-.1835 \times 10^7$	- 27,603	$-.5148 \times 10^7$
GD	$-.516 \times 10^7$	71,600	$.352 \times 10^7$	$-.5148 \times 10^7$	72,397	$.3540 \times 10^7$
DE	$-.525 \times 10^6$	22,100	$.470 \times 10^7$	$-.5224 \times 10^6$	22,176	$.4800 \times 10^7$
EF	$.470 \times 10^7$	-100,000	0	$.4800 \times 10^7$	-100,000	0
CD	0	- 16,400	$-.404 \times 10^7$	0	- 16,126	$-.4062 \times 10^7$

experimental test results for a typical condition are shown in Figs. 15 and 16. Items presented for comparison are skin span-wise normal stress and spar cap stress.

THREE DIMENSIONAL STRUCTURAL ANALYSIS

The analysis of the inboard portion of a swept wing, also performed on this analog computer, demonstrates the utility of this type of computer on a large scale three-dimensional structure. The idealized representation of the structure analyzed is shown in Fig. 17.

The structure includes the inboard portion of the airplane wing and simplified representation of a portion of the fuselage. The fuselage structure was not the subject of this analysis, but was included in this analysis to give a proper support to the wing.

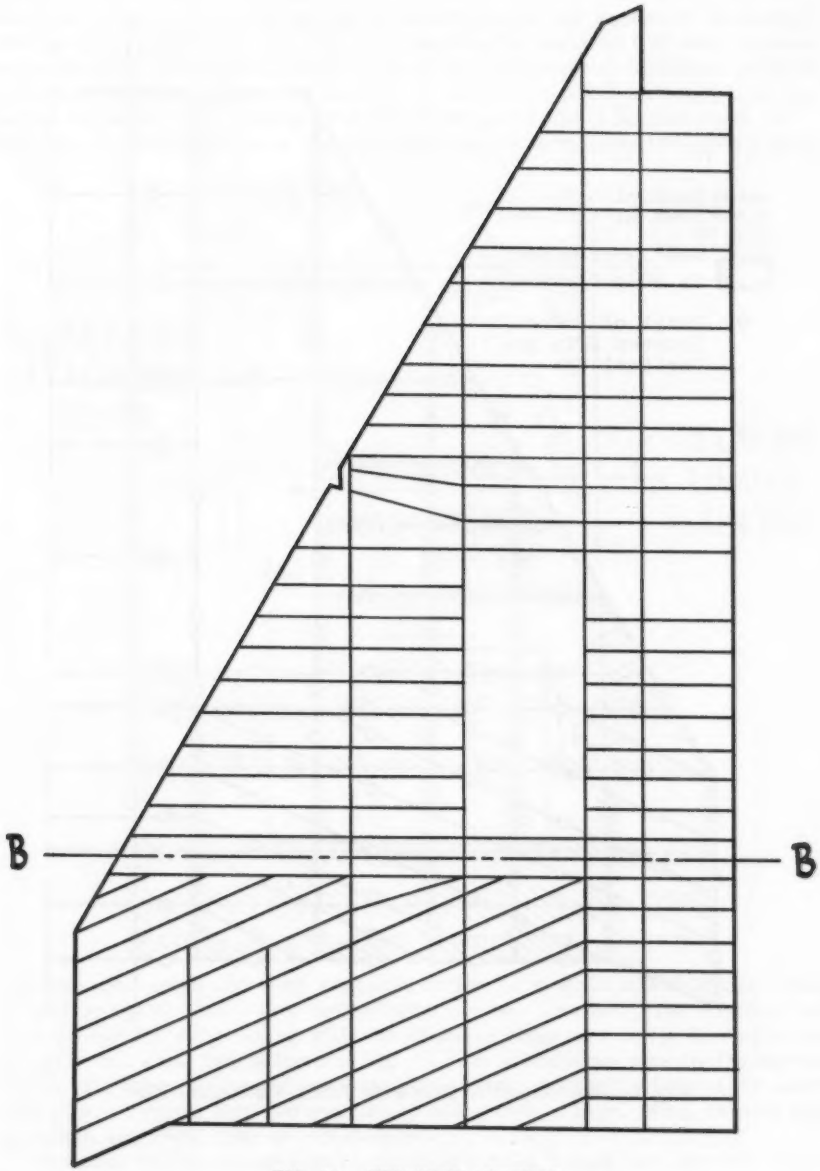

FIG. 11.—TRIANGULAR WING

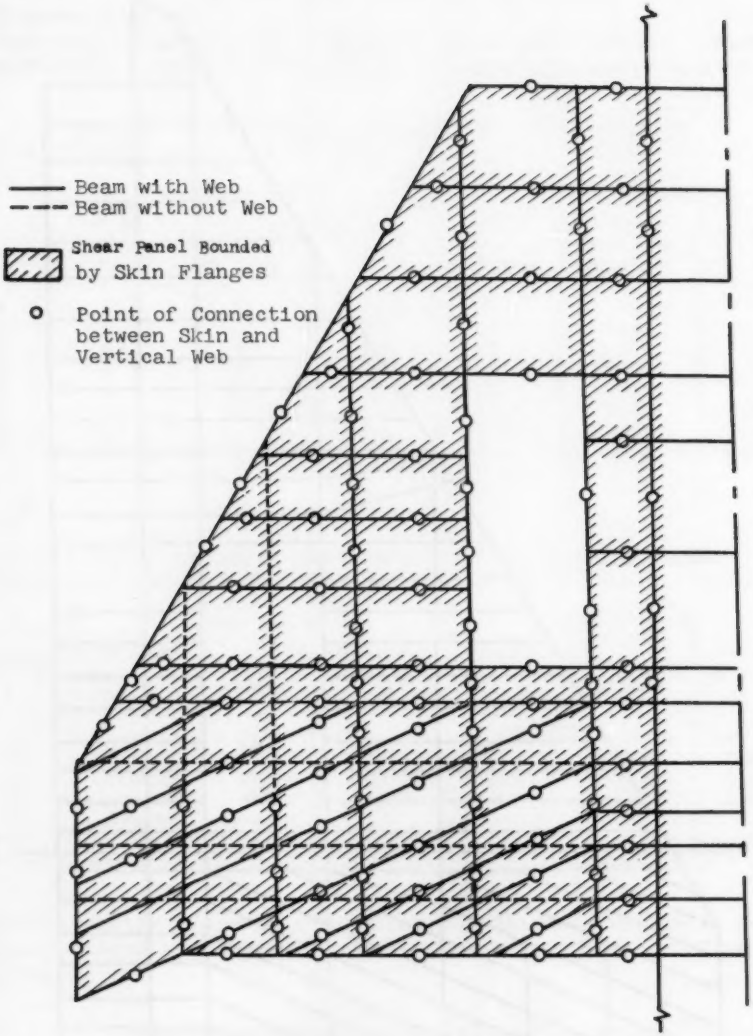

FIG. 12.—REPRESENTATION FOR FIRST WING ANALYSIS

The wing structure consists of three main spars and a number of ribs which intersect non-orthogonally and have a considerable amount of taper. Further, the cover skins are curved and the structure lacks any degree of symmetry about a chord plane. Accuracy of analysis results required individual representation of all principal structural elements. Idealization consisted of first replacing the cover skins by a number of flat planes which approximated the curved surfaces. The treatment of the cover skins which seemed most suitable was, in this instance, to lump the skin tensile properties into bars fitting

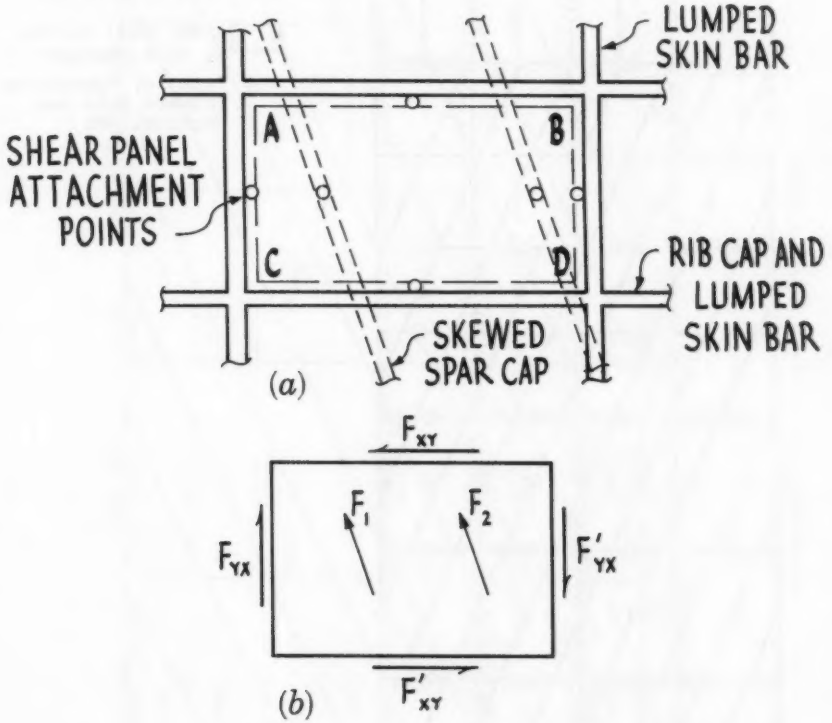

FIG. 13.—MODIFICATIONS TO STRUCTURAL ELEMENT

into the non-orthogonal spar-rib pattern. The bars which coincide with either a spar or rib cap were then lumped with the cap member. The effective bar pattern for the wing, along with the effective longerons in the fuselage, are given by the solid line pattern of Fig. 17. Between these bars lie the skewed cover skin shear panels and the shear panels representing the webs of the spars and ribs. Typical skin and web panels are shown in Figs. 18(a), skewed skin element, and 18(b), spar or rib element.

Because the span-wise and chord-wise axially loaded bars are not orthogonal to each other, it was considered necessary to account for the coupling which exists between axial stresses and strains in these bars and the shearing stress and strain in the cover panels. This coupling can best be described by considering the elemental area of skin shown in Fig. 19.

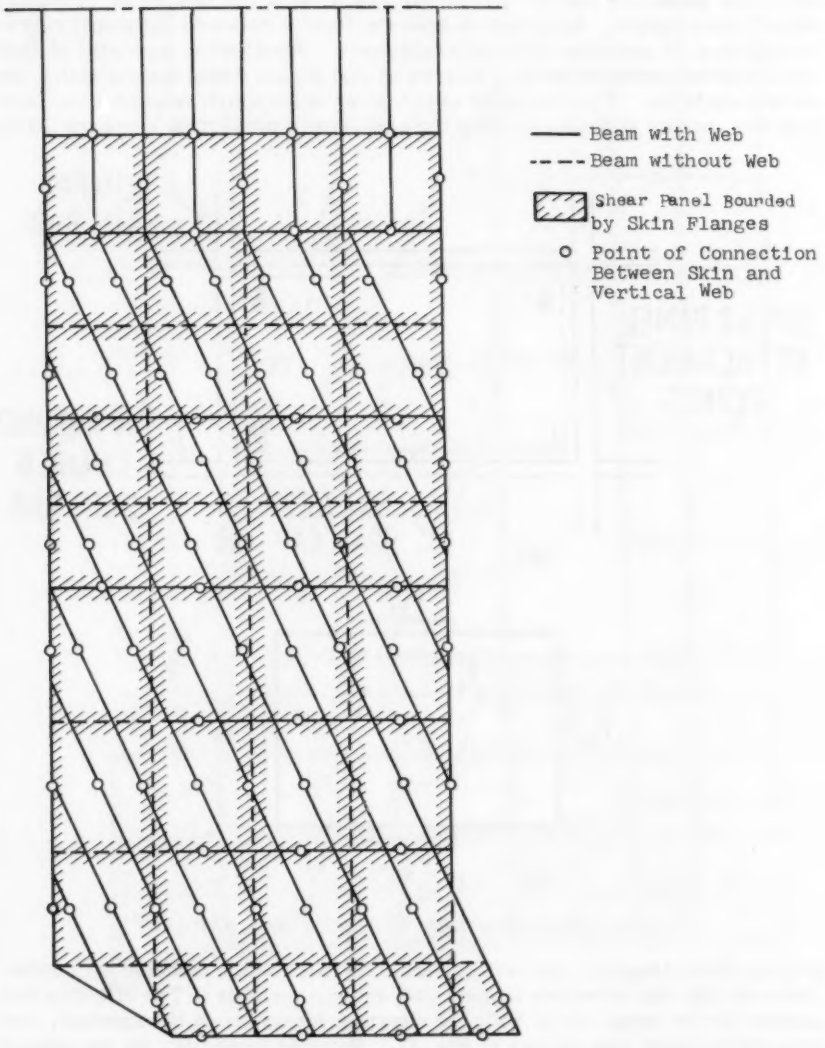

FIG. 14.—REPRESENTATION FOR SECOND WING ANALYSIS

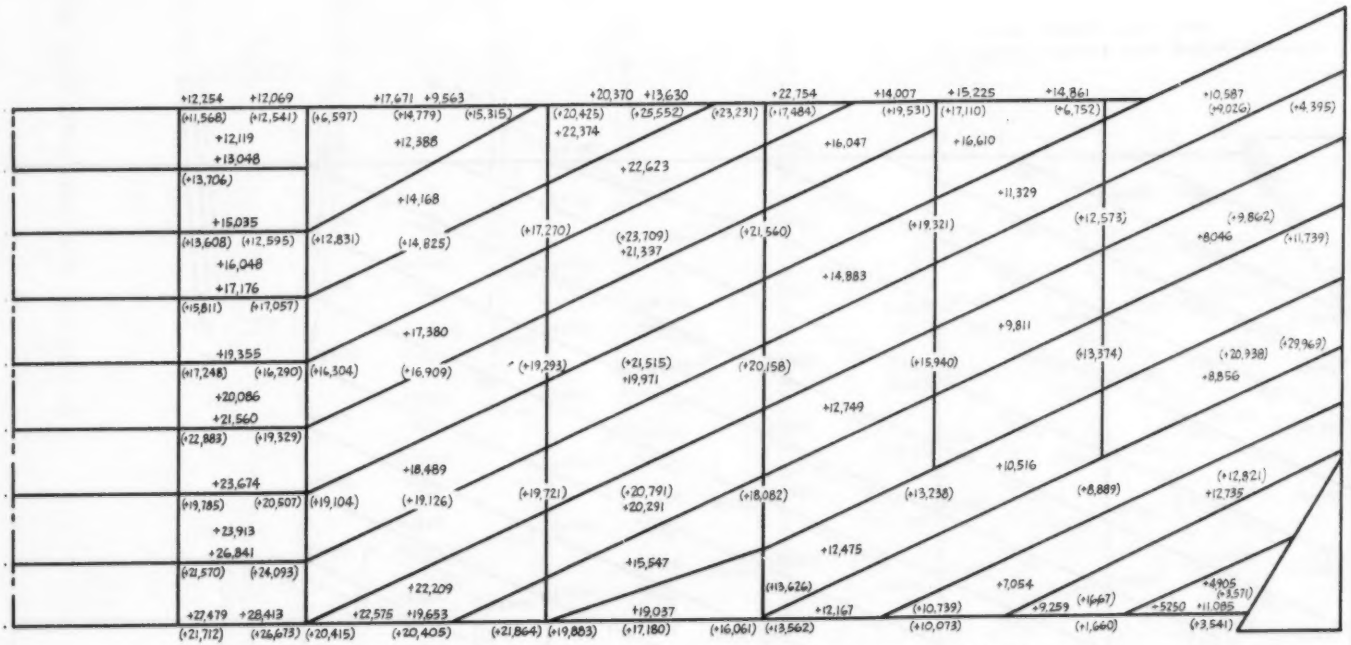

LEGEND:

(0000) Stress From Analog Analysis
0000 Stress From Test

FIG. 15.—COMPARISON OF SPANWISE SKIN STRESSES

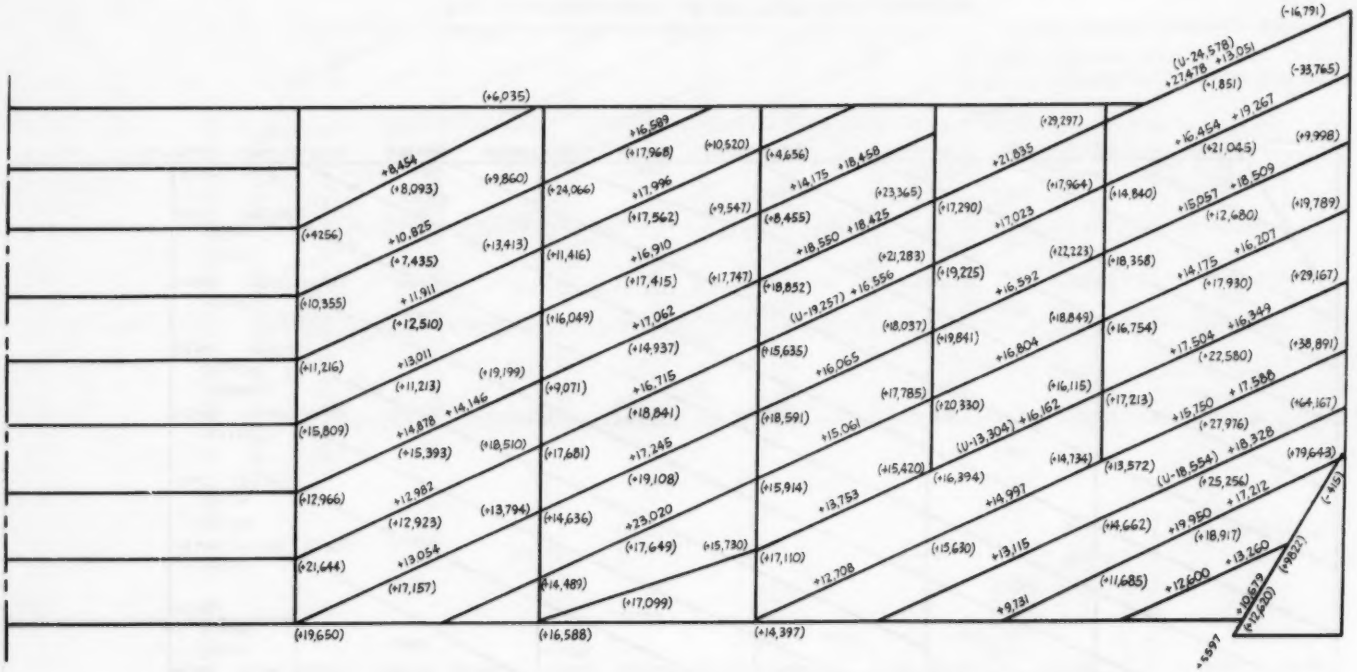

LEGEND:

(0000) Stress From Analog Analysis
0000 Stress From Test

FIG. 16.—COMPARISON OF SKEWED SPAR CAP STRESSES

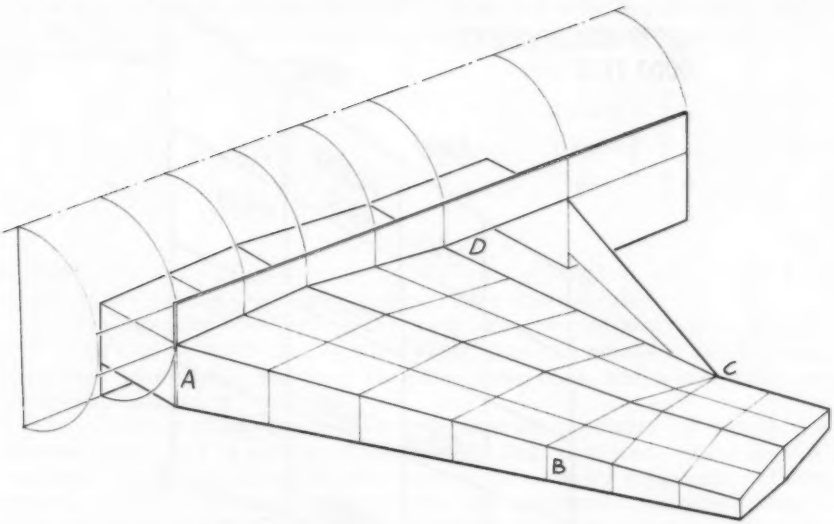

FIG. 17.—STRUCTURAL REPRESENTATION FOR SWEPT WING ANALYSIS

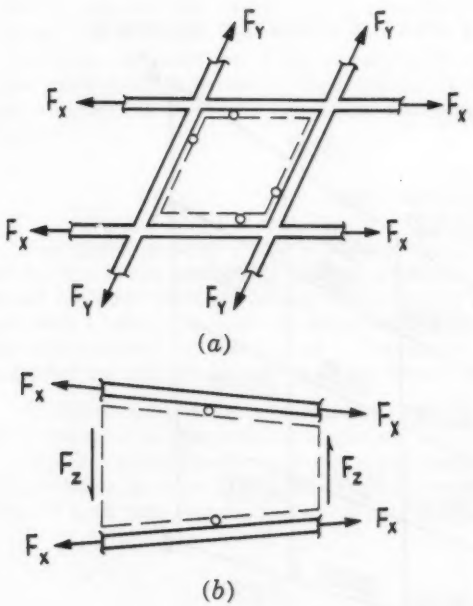

FIG. 18.—TYPICAL SKIN AND WEB PANELS

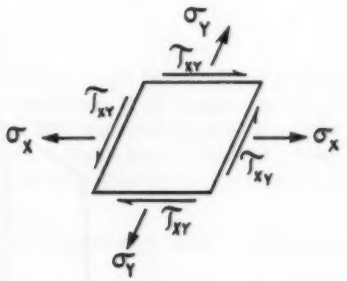

FIG. 19.—SKIN STRESS IN SKEWED COORDINATES

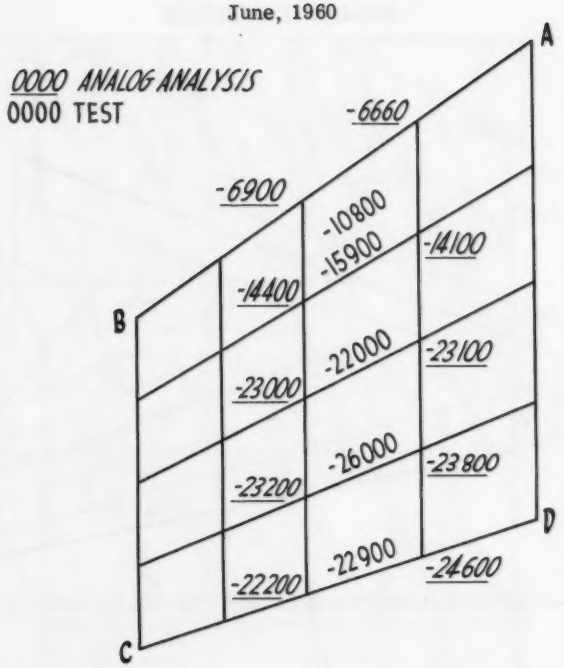

FIG. 20.—COMPARISON OF SPANWISE UPPER SURFACE STRESS

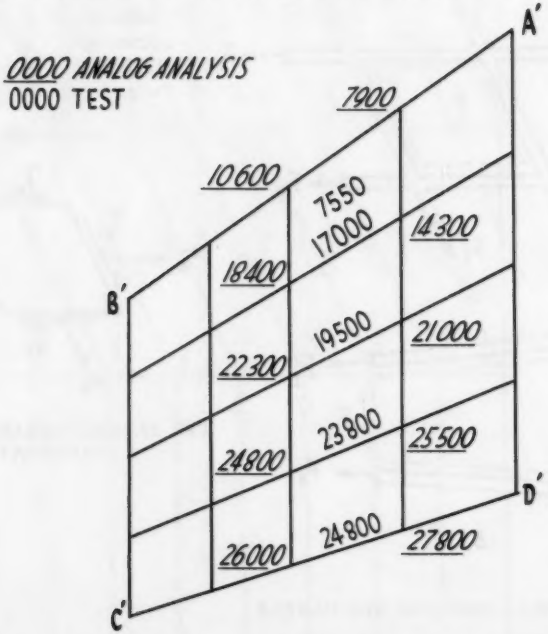

FIG. 21.—COMPARISON OF SPANWISE LOWER SURFACE STRESS

The stress-strain relationships of Fig. 19 are given by Eq. 47, which shows that the shear and normal stresses are not independent as in the case of a rectangular element.

$$\begin{bmatrix} \epsilon_x \\ \epsilon_y \\ \gamma_{xy} \end{bmatrix} = \frac{1}{E \cos \delta} \begin{bmatrix} 1 & -\mu & 2 \sin \delta \\ -\mu & 1 & 1 \sin \delta \\ 2 \sin \delta & 2 \sin \delta & g^1 \end{bmatrix} \begin{bmatrix} \alpha_x \\ \alpha_y \\ \tau_{xy} \end{bmatrix} \quad \ldots (47)$$

in which $\mu = \upsilon - (1 + \upsilon) \sin \delta$; υ = Poisson's ratio, $g^1 = 2 [1 + \upsilon + (1 - \upsilon) \sin^2 \delta]$; ϵ_x and ϵ_y are axial strains and γ_{xy} denotes the shear strain.

The analogy used to represent the cover skins in this analysis is derived from the foregoing equation. The effect of the coupling amounts to an off-center connection between the panel and the surrounding bars, and is illustrated on the skewed element of Fig. 18(a).

The purpose of this analysis was to determine the structural deflections and internal loads due to a number of different loading conditions. Each loading condition included calculated internal loads at the outboard wing section of this analysis. A second purpose of this analysis was to determine the internal loads in the structure due to a given loading condition after the presumed failure of any chosen single structural member. This portion of the analysis is used to demonstrate the safety of the structure in the event of an unobserved fatigue failure. The failure of one structural member can easily and quickly be simulated in this analysis by effectively removing the portion of the circuit representing that member.

Limited comparisons of the results of the analysis with available test data show very good agreement. Figs. 20 and 21 show a comparison of some normal stresses in the upper and lower cover skin areas ABCD and A'B'C'D' of Fig. 17.

CONCLUSIONS

The direct analogy electric analog computer has been found to be a very useful tool in the analysis of highly redundant structures. It is emphasized that in the authors' work the analog computer and the high speed digital computers are both extensively used for structural analysis. Each has a class of problems for which it is best suited. The analog computer has been used principally for the following classes of problems:

(1) On design problems when many changes or refinements may be required in arriving at an optimum arrangement.

(2) On some problems for which a satisfactory digital solution was not readily available. In these cases the use of the analog computer has resulted in savings of both time and costs.

Journal of the
ENGINEERING MECHANICS DIVISION
Proceedings of the American Society of Civil Engineers

VIBRATIONS AND STABILITY OF PLATES UNDER INITIAL STRESS

By George Herrmann,[1] M. ASCE and Anthony E. Armenakas,[2] M. ASCE

SYNOPSIS

A linear theory of the motion of elastic plates is established which, in addition to initial membrane forces, takes into account initial moments and transverse shear forces. The equations of motion are obtained by linearizing the appropriate nonlinear plate equations and, in the absence of initial stresses, they are reduced, depending on the order of approximation, to either the classical (elementary) or the Mindlin plate theory (classical theory extended to include the effects of transverse shear deformation and rotatory inertia). These equations are applied to the solution of particular problems and the effect of uniform initial compression, bending moment and transverse shear force on the frequencies of the flexural, longitudinal, thickness-shear and the first two face-shear modes is discussed.

In the course of this investigation it was found that a plate under a uniform transverse shear force may buckle in a fashion similar to a plate under compression.

INTRODUCTION

It is well-known that a state of initial stress may significantly change the static and dynamic response of an elastic body. One of the most familiar examples concerns flexural vibrations of a hinged elastic beam. The funda-

Note.—Discussion open until November 1, 1960. To extend the closing date one month, a written request must be filed with the Executive Secretary, ASCE. This paper is part of the copyrighted Journal of the Engineering Mechanics Division, Proceedings of the American Society of Civil Engineers, Vol. 86, No. EM 3, June, 1960.

[1] Assoc. Prof. of Civ. Engrg., Inst. of Flight Structures, Columbia Univ.

[2] Assoc. Prof. of Civ. Engrg., The Cooper Union for the Advancement of Science and Art, New York.

mental frequency of free vibrations is diminished by an initial compression and may even vanish, if the initial compression reaches the value of the buckling stress.

General, three-dimensional theories of elasticity of a body under initial stress were formulated by M. A. Biot (1)[3] and J. N. Goodier (2). A variety of other studies have dealt with particular problems. For example, the effect of initial stress on the torsional stiffness was considered by Biot (3) and by Goodier (2), and the influence of initial stress on elastic waves by Biot (4).

In plate theory, the interest in the influence of initial stress is of long standing. The equilibrium of plates, under initial stresses uniformly distributed across the plate thickness, has been studied by B. de Saint-Venant (5, 6), who derived the governing equations by considering an isolated plate element. A correlation between Saint-Venant's plate equations and the three-dimensional theory has been established (7). This existing theory of plates is limited to initial "membrane" stresses. The possibility of initial moments or initial transverse shear forces has not, as yet, been considered.

It appears that a more complete theory of equilibrium and motion of plates, subjected to a more general state of initial stress may be useful, for it should describe phenomena not contained in Saint-Venant's theory and should provide additional insight as to the reasons why only initial "membrane" stresses were considered in previous investigations.

In addition to generalizing the Saint-Venant plate theory, the intent of this study is to establish a more inclusive theory of plates under initial stress, analogous to the R. D. Mindlin plate theory (8), by retaining in the equations of motion the effects of transverse shear deformation and rotatory inertia.

Notation.—The letter symbols adopted for use in this paper are defined where they first appear, in the illustrations or in the text, and are arranged alphabetically, for the convenience of reference, in the Appendix.

COMPONENTS OF STRAIN

The equations of motion for the isotropic elastic plate, that include the influence of initial stresses, will be obtained by linearizing non-linear plate equations, that will in turn be derived from basic relations of non-linear elasticity. The form of these non-linear equations is dependent upon the specification of stress of strain and upon the order of approximation. With regard to strain, for example, Biot (1) has established a second order theory wherein the strain components are linearly related to the actual change of length, rather than to the change of the square of the length—as are the classical Lagrangian or Eulerian components of strain (see, for example, V. V. Novozhilov (9) and I. S. Sokolnikoff (10)). The results obtained by using Biot's theory are not simpler, however, than those obtained by using the classical non-linear theory of elasticity with Lagrangian strain components (15). For this reason, the latter will be utilized in this work.

To define the components of strain, we consider a material element whose Cartesian coordinates before deformation are x, y, z and whose coordinates after deformation, in the same Cartesian system, are ξ, η, ζ. The components

---

[3] Numerals in parentheses, thus (1), refer to corresponding items in the Bibliography. (see Appendix I)

of displacement u_x, u_y, u_z are also dependent on time, t, and are defined by

$$\left.\begin{aligned} \xi &= x + u_x(x, y, z, t) \\ \eta &= y + u_y(x, y, z, t) \\ \zeta &= z + u_z(x, y, z, t) \end{aligned}\right\} \quad \ldots\ldots\ldots\ldots\ldots\ldots (1)$$

and the Lagrangian components of strain by

$$\epsilon_{xx} = \frac{\partial u_x}{\partial x} + \frac{1}{2}\left[\left(\frac{\partial u_x}{\partial x}\right)^2 + \left(\frac{\partial u_y}{\partial x}\right)^2 + \left(\frac{\partial u_z}{\partial x}\right)^2\right] \quad \ldots\ldots\ldots\ldots (2a)$$

$$\epsilon_{yy} = \frac{\partial u_y}{\partial y} + \frac{1}{2}\left[\left(\frac{\partial y_x}{\partial y}\right)^2 + \left(\frac{\partial u_y}{\partial y}\right)^2 + \left(\frac{\partial u_z}{\partial y}\right)^2\right] \quad \ldots\ldots\ldots\ldots (2b)$$

$$\epsilon_{zz} = \frac{\partial u_z}{\partial z} + \frac{1}{2}\left[\left(\frac{\partial u_x}{\partial z}\right)^2 + \left(\frac{\partial u_y}{\partial z}\right)^2 + \left(\frac{\partial u_z}{\partial z}\right)^2\right] \quad \ldots\ldots\ldots\ldots (2c)$$

$$2\epsilon_{xy} = \frac{\partial u_x}{\partial y} + \frac{\partial u_y}{\partial x} + \frac{\partial u_x}{\partial x}\frac{\partial u_x}{\partial y} + \frac{\partial u_y}{\partial x}\frac{\partial u_y}{\partial y} + \frac{\partial u_z}{\partial x}\frac{\partial u_z}{\partial y} \quad \ldots\ldots (2d)$$

$$2\epsilon_{xz} = \frac{\partial u_x}{\partial z} + \frac{\partial u_z}{\partial x} + \frac{\partial u_x}{\partial x}\frac{\partial u_x}{\partial z} + \frac{\partial u_y}{\partial x}\frac{\partial u_y}{\partial z} + \frac{\partial u_z}{\partial x}\frac{\partial u_z}{\partial z} \quad \ldots\ldots (2e)$$

$$2\epsilon_{yz} = \frac{\partial u_y}{\partial z} + \frac{\partial u_z}{\partial y} + \frac{\partial u_x}{\partial y}\frac{\partial u_x}{\partial z} + \frac{\partial u_y}{\partial y}\frac{\partial u_y}{\partial z} + \frac{\partial u_z}{\partial y}\frac{\partial u_z}{\partial z} \quad \ldots\ldots\ldots (2f)$$

DEFORMATIONS

A plate of constant thickness, h, is referred to an x, y, z Cartesian coordinate system, with the x, y plane being the middle plane of the plate.

First, a theory of plates will be established that includes the influence of initial stresses, and that could be reduced to Mindlin's theory (8) (classical theory, extended to include the effects of transverse shear deformation and rotatory inertia) if the initial stresses vanish.

As has been done in many previous investigations, the displacement components u_x, u_y, u_z are expanded in infinite series of powers of the thickness coordinate z, and approximate displacement components $\bar{u}_x$, $\bar{u}_y$, $\bar{u}_z$, are introduced by truncating the infinite series. Only those terms are retained that contribute to the modes of vibration that will be investigated.

For this reason it will suffice to consider the following expansions;

$$\bar{u}_x(x,y,z,t) = u(x,y,t) + z\psi_x(x,y,t) \quad \ldots\ldots\ldots\ldots (3a)$$

$$\bar{u}_y(x,y,z,t) = v(x,y,t) + z\psi_y(x,y,t) \quad \ldots\ldots\ldots\ldots (3b)$$

$$\bar{u}_z(x,y,z,t) = w(x,y,t) \quad \ldots\ldots\ldots\ldots\ldots\ldots (3c)$$

STRAIN ENERGY

We consider a body of original volume V in some general deformed position, specified by displacement components u_x, u_y, u_z and shall calculate the increment δW_{int} of the strain energy W_{int} due to arbitrary increments δu_x, δu_y, δu_z of the displacement components. Since the strain energy is a function of the strains, (more specifically of the strain invariants) we have

$$\delta W_{int} = \int_V \delta\phi \; dx\, dy\, dz = \int_V \left[\sigma_{ij} \; \delta\epsilon_{ij}\right] dx\, dy\, dz \quad \ldots\ldots\ldots (4)$$

in which σ_{ij} (i, j = x, y, z) are defined as the partial derivatives of the strain energy density with respect to the corresponding components of strain (ϵ_{ij}). Since the significance of σ_{ij} is not immediately apparent, it is necessary to consider the geometry of deformation. In general, three initially perpendicular line elements d_x, d_y, d_z, are displaced and strained due to the deformation

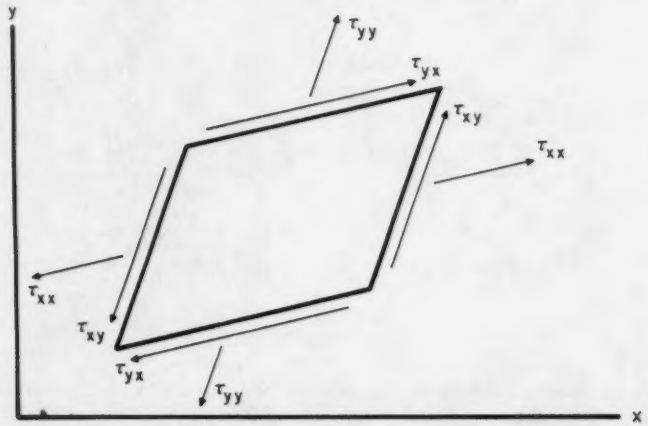

FIG. 1.—DEFORMED ELEMENT AND COMPONENTS OF STRESS

into a non-orthogonal parallelepiped. The force vector on any one face of this parallelepiped may be resolved into (non-orthogonal) components parallel to its edges, which, divided by the face area before deformation, define the stress components τ_{ij}. It is obvious that the components τ_{ij} do not form a symmetric stress tensor, since the moment condition of equilibrium (Fig. 1) required that

$$\tau_{ij}\left(1 + E_i\right) = \tau_{ji}\left(1 + E_j\right) \quad \ldots\ldots\ldots\ldots\ldots (5)$$

E_x is the relative elongation of a line element that, before deformation, was parallel to the x-axis.

A symmetric stress tensor σ^*_{ij} may be formed by the relations

$$\sigma^*_{ij} = \frac{\tau_{ij}}{\left(1 + E_j\right)} \quad \ldots\ldots\ldots\ldots\ldots\ldots\ldots (6)$$

It can be shown (9) that σ^*_{ij}, which are Trefftz's components of stress (2), are identical to σ_{ij} introduced previously as $\partial\phi / \partial\epsilon_{ij}$.

Using the approximate expressions (Eq. 3), approximate increments of the components of strain (Eq. 2) are established and substituted into Eq. 4. Since the dependence on the z-coordinate is specified, integration through the thickness, h, is readily carried out. This process leads to the plate stresses

$$\left.\begin{aligned}
&N_{xx} = \int_{-h/2}^{h/2} \sigma_{xx}\, dz \qquad N_{yy} = \int_{-h/2}^{h/2} \sigma_{yy}\, dz \qquad N_{xy} = \int_{-h/2}^{+h/2} \sigma_{xy}\, dz \\
&M_{xx} = \int_{-h/2}^{h/2} \sigma_{xx}\, z\, dz \qquad M_{yy} = \int_{-h/2}^{h/2} \sigma_{yy}\, z\, dz \qquad M_{xy} = \int_{-h/2}^{h/2} \sigma_{xy}\, z\, dz \\
&K_{xx} = \int_{-h/2}^{h/2} \sigma_{xx}\, z^2\, dz \qquad K_{yy} = \int_{-h/2}^{h/2} \sigma_{yy}\, z^2\, dz \qquad K_{xy} = \int_{-h/2}^{h/2} \sigma_{xy}\, z^2\, dz \\
&Q_{xx} = \int_{-h/2}^{h/2} \sigma_{xz}\, dz \qquad Q_y = \int_{-h/2}^{h/2} \sigma_{yz}\, dz \qquad N_{zz} = \int_{-h/2}^{h/2} \sigma_{zz}\, dz \\
&T_x = \int_{-h/2}^{h/2} \sigma_{xz}\, z\, dz \qquad T_y = \int_{-h/2}^{h/2} \sigma_{yz}\, z\, dz
\end{aligned}\right\} \quad \ldots (7)$$

Integration by parts of Eq. 4 results in

$$\delta W_{int} = -\int_A \left[\frac{\partial N_{xx}}{\partial x}\, \delta u + \frac{\partial M_{xx}}{\partial x}\, \delta\psi_x + \frac{\partial}{\partial x}\left(N_{xx}\, \frac{\partial v}{\partial x}\right)\delta v + \frac{\partial}{\partial x}\left(M_{xx}\, \frac{\partial v}{\partial x}\right)\, \delta\psi_y \right.$$

$$+ \frac{\partial}{\partial x}\left(M_{xx}\, \frac{\partial \psi_y}{\partial x}\right)\delta v + \frac{\partial}{\partial x}\left(N_{xx}\frac{\partial w}{\partial x}\right)\, \delta w + \frac{\partial}{\partial x}\left(N_{xx}\, \frac{\partial u}{\partial x}\right)\, \delta u$$

$$\left. + \frac{\partial}{\partial x}\left(M_{xx}\, \frac{\partial u}{\partial x}\right)\, \delta\psi_x + \frac{\partial}{\partial x}\left(M_{xx}\, \frac{\partial \psi_x}{\partial x}\right)\, \delta u + \frac{\partial N_{yy}}{\partial y}\, \delta v \right.$$

$$+\frac{\partial M_{yy}}{\partial y}\delta\psi_y+\frac{\partial}{\partial y}\left(N_{yy}\frac{\partial u}{\partial y}\right)\delta u+\frac{\partial}{\partial y}\left(M_{yy}\frac{\partial u}{\partial y}\right)\delta\psi_x+\frac{\partial}{\partial y}\left(M_{yy}\frac{\partial\psi_x}{\partial y}\right)\delta u$$

$$+\frac{\partial}{\partial y}\left(N_{yy}\frac{\partial w}{\partial y}\right)\delta w+\frac{\partial}{\partial y}\left(N_{yy}\frac{\partial v}{\partial y}\right)\delta v+\frac{\partial}{\partial y}\left(M_{yy}\frac{\partial v}{\partial y}\right)\delta\psi_y+\frac{\partial}{\partial y}\left(M_{yy}\frac{\partial\psi_y}{\partial y}\right)\delta v$$

$$+\frac{\partial}{\partial x}\left(N_{xy}\frac{\partial u}{\partial y}\right)\delta u+\frac{\partial}{\partial x}\left(M_{xy}\frac{\partial u}{\partial y}\right)\delta\psi_x+\frac{\partial}{\partial x}\left(M_{xy}\frac{\partial\psi_x}{\partial y}\right)\delta u+\frac{\partial N_{xy}}{\partial x}\delta v$$

$$+\frac{\partial M_{xy}}{\partial x}\delta\psi_y+\frac{\partial}{\partial x}\left(N_{xy}\frac{\partial w}{\partial y}\right)\delta w+\frac{\partial}{\partial x}\left(N_{xy}\frac{\partial v}{\partial y}\right)\delta v+\frac{\partial}{\partial x}\left(M_{xy}\frac{\partial v}{\partial y}\right)\delta\psi_y$$

$$+\frac{\partial}{\partial x}\left(M_{xy}\frac{\partial\psi_y}{\partial y}\right)\delta v+\frac{\partial}{\partial y}\left(N_{xy}\frac{\partial u}{\partial x}\right)\delta u+\frac{\partial}{\partial y}\left(M_{xy}\frac{\partial u}{\partial x}\right)\delta\psi_x$$

$$+\frac{\partial}{\partial y}\left(M_{xy}\frac{\partial\psi_x}{\partial x}\right)\delta u+\frac{\partial N_{xy}}{\partial y}\delta u+\frac{\partial M_{xy}}{\partial y}\delta\psi_x+\frac{\partial}{\partial y}\left(N_{xy}\frac{\partial v}{\partial x}\right)\delta v$$

$$+\frac{\partial}{\partial y}\left(M_{xy}\frac{\partial v}{\partial x}\right)\delta\psi_y+\frac{\partial}{\partial y}\left(M_{xy}\frac{\partial\psi_y}{\partial x}\right)\delta v+\frac{\partial}{\partial y}\left(N_{xy}\frac{\partial w}{\partial x}\right)\delta w$$

$$+\frac{\partial}{\partial x}\left(Q_x\psi_x\right)\delta u+\frac{\partial}{\partial x}\left(Q_x\psi_y\right)\delta v+\frac{\partial Q_x}{\partial x}\delta w-Q_x\delta\psi_x$$

$$-\left(Q_x\frac{\partial v}{\partial x}\right)\delta\psi_y-\left(Q_x\frac{\partial u}{\partial x}\right)\delta\psi_x+\frac{\partial}{\partial y}\left(Q_y\psi_y\right)\delta v+\frac{\partial}{\partial y}\left(Q_y\psi_x\right)\delta u$$

$$+\frac{\partial Q_y}{\partial y}\delta w=Q_y\delta\psi_y=\left(Q_y\frac{\partial u}{\partial y}\right)\delta\psi_x-\left(Q_y\frac{\partial v}{\partial y}\right)\delta\psi_y\Bigg]dx\,dy$$

$$+\int_S\Big[N_{nn}\delta u_n+N_{ns}\delta u_s+Q_n\delta w+M_{nn}\delta\psi_n+M_{ns}\delta\psi_s$$

$$+N_{nn}\frac{\partial u_n}{\partial n}\delta u_n+N_{ns}\frac{\partial u_n}{\partial s}\delta u_n+N_{nn}\frac{\partial u_s}{\partial n}\delta u_s+N_{ns}\frac{\partial u_s}{\partial s}\delta u_s$$

$$+N_{nn}\frac{\partial w}{\partial n}\delta w+N_{ns}\frac{\partial w}{\partial s}\delta w+M_{nn}\frac{\partial u_n}{\partial n}\delta\psi_n+M_{ns}\frac{\partial u_n}{\partial s}\delta\psi_n$$

$$+M_{nn}\frac{\partial u_s}{\partial n}\delta\psi_s+M_{ns}\frac{\partial u_s}{\partial s}\delta\psi_s+M_{nn}\frac{\partial\psi_n}{\partial n}\delta u_n+M_{ns}\frac{\partial\psi_n}{\partial s}\delta u_n$$

$$+M_{nn}\frac{\partial\psi_s}{\partial n}\delta u_s+M_{ns}\frac{\partial\psi_s}{\partial s}\delta u_s+Q_n\psi_n\delta u_n+Q_n\psi_s\delta u_s\Big]ds\quad\ldots.(8)$$

The surface integral $\int_S$ extends over the face area A of the plate before deformation; the line integral extends over the total undeformed cylindrical boundary of the plate; n and s are coordinates measured along the outward normal and along the tangent to the undeformed boundary, respectively. Notice that in Eq. 8 the contribution of the plate stresses N_{zz}, K_{xx}, K_{yy}, K_{xy}, T_x, T_y, to the increment of the strain energy, is disregarded.

WORK OF EXTERNAL FORCES

The external forces consist of boundary tractions, taken for convenience per unit undeformed boundary area, and of body forces taken per unit undeformed volume. These external forces will be, in general, functions of the spatial coordinates and of time.

We consider again some deformed state of the body and decompose the boundary traction in this state into Cartesian components f_ξ, f_η, f_ζ parallel to the fixed x, y, z-axes, respectively. The work done by these forces, due to increments δu_x, δu_y, δu_z, of the displacement components, is in all generality

$$\delta W_e = \int_S \left[f_\xi \, \delta u_x + f_n \, \delta u_y + f_\zeta \, \delta u_z \right] ds \quad \ldots\ldots\ldots (9)$$

The integral has to be extended over the whole surface bounding the body in the initial state.

In the case of a plate, the expression for the work of the surface traction is, therefore,

$$\delta W_e = \int_A \left[f_\xi \, \delta u_x + f_\eta \, \delta u_y + f_\zeta \, \delta u_z \right] dx \, dy \Big|_{z=-h/2}^{z=h/2}$$

$$+ \int_S \int_{-h/2}^{h/2} \left[f_n \, \delta u_n + f_s \, \delta u_s + f_\zeta \, \delta u_z \right] dz \, ds \quad \ldots\ldots\ldots (10)$$

As in the preceding section, the line integral is to be taken around the total undeformed cylindrical boundary of the plate, while the subscripts n and s indicate components referred to coordinates measured outwardly normal to and along the undeformed boundary, respectively.

Substitution of the approximations $\bar{u}_x$, $\bar{u}_y$, $\bar{u}_z$ for the displacements u_x, u_y, u_z results in an approximate expression $\delta \bar{W}_e$ for the increment of the work done by the boundary tractions, which, employing the notations

$$F_\xi = f_\xi \Big|_{z=-/h2}^{z=h/2} \qquad F_\eta = f_\eta \Big|_{z=-h/2}^{z=h/2} \qquad q = f_\zeta \Big|_{z=-h/2}^{z=h/2}$$

$$m_\xi = f_\xi \, z \Big|_{z=-h/2}^{z=h/2} \qquad m_\eta = f_\eta \, z \Big|_{z=-h/2}^{z=h/2}$$

$$N^*_{nn} = \int_{-h/2}^{h/2} f_n \, dz \qquad N^*_{ns} = \int_{-h/2}^{h/2} f_s \, dz \qquad Q^*_n = \int_{-h/2}^{h/2} f_\zeta \, dz$$

$$M^*_{nn} = \int_{-h/2}^{h/2} f_n \, z \, dz \qquad M^*_{ns} = \int_{-h/2}^{h/2} f_s \, z \, dz \quad \ldots\ldots\ldots\ldots\ldots (11)$$

may be written as

$$\delta \overline{W}_e = \int_A \left[F_\xi \, \delta u + m_\xi \, \delta \psi_x + F_\eta \, \delta v + m_\eta \, \delta \psi_y + q \, \delta w \right] dx \, dy$$

$$+ \int_S \left[N^*_{nn} \, \delta u_n + M^*_{nn} \, \delta \psi_n + N^*_{ns} \, \delta u_s + M^*_{ns} \, \delta \psi_s + Q^*_n \, \delta w \right] ds \quad \ldots (12)$$

In order to calculate the work done by body forces, let b_ξ, b_η, b_ζ, designate the x, y, z components in the deformed position, of the body force per unit original volume. The work done by these forces is, in general,

$$\delta W_B = \int_V \left[b_\xi \, \delta u_x + b_\eta \, \delta u_y + b_\zeta \, \delta u_z \right] dx \, dy \, dz \quad \ldots\ldots (13)$$

Substituting for the displacements u_x, u_y, u_z the approximations $\bar{u}_x$, $\bar{u}_y$, $\bar{u}_z$, and integrating through the thickness, the approximate expression $\delta \overline{W}_B$ for the work done by body forces becomes

$$\delta \overline{W}_B = \int_A \left[B_\xi \, \delta u + B_\eta \, \delta v + B_\zeta \, \delta w \right] dx \, dy \quad \ldots\ldots\ldots (14)$$

where

$$B_\xi = \int_{-h/2}^{h/2} b_\xi \, dz \qquad B_\eta = \int_{-h/2}^{h/2} b_\eta \, dz \qquad B_\zeta = \int_{-h/2}^{h/2} b_\zeta \, dz \quad \ldots (15)$$

In obtaining Eq. 14 it was assumed, for simplicity, that

$$\int_{-h/2}^{h/2} b_\xi \, z \, dz = 0 \qquad \int_{-h/2}^{h/2} b_\eta \, z \, dz = 0$$

KINETIC ENERGY

The kinetic energy T of a body occupying, before deformation, a volume V, and having a mass density ρ, is given by

$$T = \frac{1}{2} \int_V \rho \left[\dot{u}_x^2 + \dot{u}_y^2 + \dot{u}_z^2 \right] dx \, dy \, dz \quad \ldots\ldots\ldots\ldots (16)$$

The dot indicates differentiation with respect to time. Using for the velocities expressions based on the approximate displacements (Eq. 3), assuming that ρ

is independent of z and integrating through the thickness, h, of the plate, an approximate expression for the increment of the kinetic energy $\delta \overline{T}$ is obtained

$$\delta \overline{T} = \int_A \rho\, h \left[\dot{u}\, \delta\dot{u} + \frac{h^2}{12} \dot{\psi}_x\, \delta\dot{\psi}_x + \dot{v}\, \delta\dot{v} + \frac{h^2}{12} \dot{\psi}_y\, \delta\dot{\psi}_y + \dot{w}\, \delta\dot{w} \right] dx\, dy \quad \ldots (17)$$

Integrating by parts with respect to time and assuming that the initial velocities of the displacement components are specified, we obtain

$$\delta \overline{T} = -\int_A \rho\, h \left[\ddot{u}\, \delta u + \ddot{v}\, \delta v + \frac{h^2}{12} \ddot{\psi}_x\, \delta\psi_x + \frac{h^2}{12} \ddot{\psi}_y\, \delta\psi_y + \ddot{w}\, \delta w \right] dx\, dy \quad \ldots (18)$$

NON-LINEAR PLATE THEORY

Hamilton's principle is applied to derive the equations of motion and the boundary conditions. The principle states that for an arbitrary time interval t_1 to t_2, the kinetic potential L has to satisfy

$$\delta \int_{t_1}^{t_2} L\, dt = 0 \quad \ldots (19)$$

In the present case, since partial integration with respect to time has already been carried out,

$$\delta L = \delta \overline{T} - \delta \overline{W}_{int} + \delta \overline{W}_e + \delta \overline{W}_B \quad \ldots (20)$$

The variation of the kinetic potential δL must vanish for arbitrary values of δu, δv, and so forth. Thus, we obtain from the integrand of the double integrals (Eqs. 8, 12, 14 and 18) the following five equations of motion

$$\frac{\partial N_{xx}}{\partial x} + \frac{\partial N_{xy}}{\partial y} + \frac{\partial}{\partial x}\left(N_{xx}\frac{\partial u}{\partial x}\right) + \frac{\partial}{\partial y}\left(N_{yy}\frac{\partial u}{\partial y}\right) + \frac{\partial}{\partial x}\left(N_{xy}\frac{\partial u}{\partial y}\right)$$

$$+ \frac{\partial}{\partial y}\left(N_{xy}\frac{\partial u}{\partial x}\right) + \frac{\partial}{\partial x}\left(M_{xx}\frac{\partial \psi_x}{\partial x}\right) + \frac{\partial}{\partial y}\left(M_{yy}\frac{\partial \psi_x}{\partial y}\right) + \frac{\partial}{\partial x}\left(M_{xy}\frac{\partial \psi_x}{\partial y}\right)$$

$$+ \frac{\partial}{\partial y}\left(M_{xy}\frac{\partial \psi_x}{\partial x}\right) + \frac{\partial}{\partial x}\left(Q_x \psi_x\right) + \frac{\partial}{\partial y}\left(Q_y \psi_x\right) + F_\xi + B_\xi = \rho\, h\, \ddot{u} \quad \ldots (21a)$$

$$\frac{\partial N_{yy}}{\partial y} + \frac{\partial N_{xy}}{\partial x} + \frac{\partial}{\partial y}\left(N_{yy}\frac{\partial v}{\partial y}\right) + \frac{\partial}{\partial x}\left(N_{xx}\frac{\partial v}{\partial x}\right) + \frac{\partial}{\partial y}\left(N_{xy}\frac{\partial v}{\partial x}\right)$$

$$+ \frac{\partial}{\partial x}\left(N_{xy}\frac{\partial v}{\partial y}\right) + \frac{\partial}{\partial y}\left(M_{yy}\frac{\partial \psi_y}{\partial y}\right) + \frac{\partial}{\partial x}\left(M_{xx}\frac{\partial \psi_y}{\partial x}\right) + \frac{\partial}{\partial y}\left(M_{xy}\frac{\partial \psi_y}{\partial x}\right)$$

$$+\frac{\partial}{\partial x}\left(M_{xy}\frac{\partial \psi_y}{\partial y}\right)+\frac{\partial}{\partial y}\left(Q_y\psi_y\right)+\frac{\partial}{\partial x}\left(Q_x\psi_y\right)+F_\eta+B_\eta=\rho\, h\,\ddot{v} \quad \ldots\ldots \text{(21b)}$$

$$\frac{\partial Q_x}{\partial x}+\frac{\partial Q_y}{\partial y}+\frac{\partial}{\partial x}\left(N_{xx}\frac{\partial w}{\partial x}\right)+\frac{\partial}{\partial y}\left(N_{yy}\frac{\partial w}{\partial y}\right)+\frac{\partial}{\partial x}\left(N_{xy}\frac{\partial w}{\partial y}\right)$$

$$+\frac{\partial}{\partial y}\left(N_{xy}\frac{\partial w}{\partial x}\right)+q+B_\zeta=\rho\, h\,\ddot{w} \quad \ldots\ldots \text{(21c)}$$

$$\frac{\partial M_{xx}}{\partial x}+\frac{\partial M_{xy}}{\partial y}-Q_x+\frac{\partial}{\partial x}\left(M_{xx}\frac{\partial u}{\partial x}\right)+\frac{\partial}{\partial y}\left(M_{yy}\frac{\partial u}{\partial y}\right)$$

$$+\frac{\partial}{\partial x}\left(M_{xy}\frac{\partial u}{\partial y}\right)+\frac{\partial}{\partial y}\left(M_{xy}\frac{\partial u}{\partial x}\right)-Q_x\frac{\partial u}{\partial x}-Q_y\frac{\partial u}{\partial y}$$

$$+m_\xi=\rho\,\frac{h^3}{12}\,\ddot{\psi}_x \quad \ldots\ldots \text{(21d)}$$

$$\frac{\partial M_{yy}}{\partial y}+\frac{\partial M_{xy}}{\partial x}-Q_y+\frac{\partial}{\partial y}\left(M_{yy}\frac{\partial v}{\partial y}\right)+\frac{\partial}{\partial x}\left(M_{xx}\frac{\partial v}{\partial x}\right)$$

$$+\frac{\partial}{\partial y}\left(M_{xy}\frac{\partial v}{\partial x}\right)+\frac{\partial}{\partial x}\left(M_{xy}\frac{\partial v}{\partial y}\right)-Q_y\frac{\partial v}{\partial y}-Q_x\frac{\partial v}{\partial x}$$

$$+m_\eta=\rho\,\frac{h^3}{12}\,\ddot{\psi}_y \quad \ldots\ldots \text{(21e)}$$

From the line integrals we obtain the following boundary conditions

$$\left.\begin{aligned}
N^*_{nn} &= N_{nn}+N_{nn}\frac{\partial u_n}{\partial n}+N_{ns}\frac{\partial u_n}{\partial s}+M_{nn}\frac{\partial \psi_n}{\partial n}+M_{ns}\frac{\partial \psi_n}{\partial s}+Q_n\psi_n\\
N^*_{ns} &= N_{ns}+N_{nn}\frac{\partial u_s}{\partial n}+N_{ns}\frac{\partial u_s}{\partial s}+M_{nn}\frac{\partial \psi_s}{\partial n}+M_{ns}\frac{\partial \psi_s}{\partial s}+Q_n\psi_s\\
M^*_{nn} &= M_{nn}+M_{nn}\frac{\partial u_n}{\partial n}+M_{ns}\frac{\partial u_n}{\partial s}\\
M^*_{ns} &= M_{ns}+M_{nn}\frac{\partial u_s}{\partial n}+M_{ns}\frac{\partial u_s}{\partial s}\\
Q^*_n &= Q_n+N_{nn}\frac{\partial w}{\partial n}+N_{ns}\frac{\partial w}{\partial s}
\end{aligned}\right\} \quad \ldots\ldots \text{(22)}$$

PLATE UNDER INITIAL STRESS

It is assumed that the state of initial stress is given by the Cartesian components, S_{ij}, which form a symmetric tensor. The plate deforms to its final

configuration, specified by the displacement components u_x, u_y, u_z, due to additional stresses designated by t_{ij}. These additional stresses are assumed to be related to the displacements in accordance with Hooke's law for a three-dimensional isotropic solid. As indicated by Biot (1), and also by A. Pflüger (12), this is an approximation which introduces an error of the order of magnitude of the ratio of initial stress to the elastic modulus. This error is due to the fact that the deformations associated with initial stresses are neglected, which make the body both heterogeneous and anisotropic (12) in its response to the additional stresses. In order to introduce the above stresses into the non-linear equations of motion (Eq. 21), we may approximate

$$\left.\begin{aligned} \sigma_{xx} &= S_{xx} + t_{xx} & \sigma_{yy} &= S_{yy} + t_{yy} & \sigma_{zz} &= S_{zz} + t_{zz} \\ \sigma_{xy} &= S_{xy} + t_{xy} & \sigma_{yz} &= S_{yz} + t_{yz} & \sigma_{xz} &= S_{xz} + t_{xz} \end{aligned}\right\} \quad . . (23)$$

or we may approximate

$$\left.\begin{aligned} \tau_{xx} &= S_{xx} + t_{xx} & \tau_{yy} &= S_{yy} + t_{yy} & \tau_{zz} &= S_{zz} + t_{zz} \\ \tau_{xy} &= S_{xy} + t_{xy} & \tau_{yz} &= S_{yz} + t_{yz} & \tau_{zx} &= S_{zx} + t_{zx} \\ \tau_{yx} &= \tau_{xy}\left[\frac{1+E_x}{1+E_y}\right] & \tau_{zy} &= \tau_{yz}\left[\frac{1+E_y}{1+E_z}\right] & \tau_{xz} &= \tau_{zx}\left[\frac{1+E_z}{1+E_x}\right] \end{aligned}\right\} . (24)$$

Both relations, as indicated by Pflüger (12), have their advantages and drawbacks, which briefly may be summarized as follows: Fig. 23 has the disadvantage of not describing satisfactorily the case of uniaxial initial and additional tension since they reduce to $\tau_{xx} = (1 + Ex)\,(S_{xx} + t_{xx})$ instead of the anticipated $\tau_{xx} = S_{xx} + t_{xx}$. In Eq. 24, the tensor τ_{ij} is unsymmetrical, resulting in non-symmetric equations of motion. Furthermore, some terms in the equations of motion are dependent upon the arbitrary choice of specifying $\tau_{xy} = S_{xy} = t_{xy}$ and so forth, instead of $\tau_{yx} = S_{yx} + t_{yx}$ and so forth.

These deficiencies can be circumvented by using only the top three relations of Eq. 24, combined with the last three of Eq. 23. Thus, taking $\frac{1}{1+E_j} \simeq \left(1 - \frac{\partial u_j}{\partial x_j}\right)$ we obtain

$$\left.\begin{aligned} \sigma_{xx} &= (S_{xx} + t_{xx})\left(1 - \frac{\partial u_x}{\partial x}\right) & \sigma_{yy} &= (S_{yy} + t_{yy})\left(1 - \frac{\partial u_y}{\partial y}\right) & \sigma_{zz} &= (S_{zz} + t_{zz})\left(1 - \frac{\partial u_z}{\partial z}\right) \\ \sigma_{xy} &= S_{xy} + t_{xy} & \sigma_{yz} &= S_{yz} + t_{yz} & \sigma_{zx} &= S_{zx} + t_{zx} \end{aligned}\right\} . . (25)$$

Defining the initial plate stresses by

$$N^i_{xx} = \int_{-h/2}^{h/2} S_{xx}\, dz \qquad M^i_{xx} = \int_{-h/2}^{h/2} S_{xx}\, z\, dz \qquad Q^i_x = \int_{-h/2}^{h/2} S_{xz}\, dz \text{ e.t.c.} \quad . . (26)$$

and the additional plate stresses by

$$N^a_{xx} = \int_{-h/2}^{h/2} t_{xx}\, dz \quad M^a_{xx} = \int_{-h/2}^{h/2} t_{xx}\, z\, dz \quad Q^a_x = \int_{-h/2}^{h/2} t_{xz}\, dz \text{ e.t.c. . . } (27)$$

and using the relations of Eq. 25 we have

$$\left.\begin{aligned}
N_{xx} &= \left(N^i_{xx} + N^a_{xx}\right)\left(1 - \frac{\partial u}{\partial x}\right) - \left(M^i_{xx} + M^a_{xx}\right)\frac{\partial \psi_x}{\partial x} \\
N_{yy} &= \left(N^i_{yy} + N^a_{yy}\right)\left(1 - \frac{\partial v}{\partial y}\right) - \left(M^i_{yy} + M^a_{yy}\right)\frac{\partial \psi_y}{\partial y} \\
M_{xx} &= \left(M^i_{xx} + M^a_{xx}\right)\left(1 - \frac{\partial u}{\partial x}\right) \\
M_{yy} &= \left(M^i_{yy} + M^a_{yy}\right)\left(1 - \frac{\partial v}{\partial y}\right) \\
N_{xy} &= N^i_{xy} + N^a_{xy} \\
Q_x &= Q^i_x + Q^a_x \qquad Q_y = Q^i_y + Q^a_y
\end{aligned}\right\} \quad \ldots . (28)$$

It is noted that, depending on their physical nature, the initial surface tractions and body forces may change themselves in the course of deformation. The following notation is, therefore, introduced

$$\left.\begin{aligned}
F_\xi &= F_x{}^i + \Delta F_x{}^i + F_x{}^a & N^*_{nn} &= N^{*i}_{nn} + \Delta N^{*i}_{nn} + N^{*a}_{nn} \\
F_\eta &= F_y{}^i + \Delta F_y{}^i + F_y{}^a & N^*_{ns} &= N^{*i}_{ns} + \Delta N^{*i}_{ns} + N^{*a}_{ns} \\
q &= q^i + \Delta q^i + q^a & Q^*_n &= Q^{*i}_n + \Delta Q^{*i}_n + Q^{*a}_n \\
m_\xi &= m^i_x + \Delta m^i_x + m^a_x & M^*_{nn} &= M^{*i}_{nn} + \Delta M^{*i}_{nn} + M^{*a}_{nn} \\
m_\eta &= m^i_y + \Delta m^i_y + m^a_y & M^*_{ns} &= M^{*i}_{ns} + \Delta M^{*i}_{ns} + M^{*a}_{ns}
\end{aligned}\right\} \quad \ldots . (29)$$

in which F_ξ is the x-component of the total surface traction per unit original area in the deformed state. $F_x{}^a$ is the x-component of the additional surface traction which induces the deformation. $F_x{}^i$ is the x-component of the initial surface traction in the undeformed state. $\Delta F_x{}^i$ is the x-component of the change of $F_x{}^i$, due to the deformation expressed per unit original area. N^*_{nn} is the n-component of the total traction on the deformed cylindrical surface per

unit undeformed area, n being the outward normal to the undeformed boundary; N^{*i}_{nn} is the n-component of the initial surface traction in the undeformed state; ΔN^{*i}_{nn} is the n-component of the change of N^{*i}_{nn}, due to the deformation, per unit original area; N^{*a}_{nn} is the n-component of the additional traction on the deformed cylindrical surface.

For the body forces we may put, analogously,

$$\left.\begin{aligned} B_\xi &= B^i_x + \Delta B^i_x + B^a_x \\ B_\eta &= B^i_y + \Delta B^i_y + B^a_y \\ B_\zeta &= B^i_z + \Delta B^i_z + B^a_z \end{aligned}\right\} \quad \ldots\ldots\ldots\ldots (30)$$

Since initially, the plate is assumed to be in equilibrium, the initial stresses must satisfy the following equilibrium equations

$$\left.\begin{aligned} &\frac{\partial N^i_{xx}}{\partial x} + \frac{\partial N^i_{xy}}{\partial y} + F^i_x + B^i_x = 0 \\ &\frac{\partial N^i_{yy}}{\partial y} + \frac{\partial N_{xy}}{\partial x} + F^i_y + B^i_y = 0 \\ &\frac{\partial Q^i_x}{\partial x} + \frac{\partial Q^i_y}{\partial y} + q^i + B^i_z = 0 \\ &\frac{\partial M^i_{xx}}{\partial x} + \frac{\partial M^i_{xy}}{\partial y} - Q^i_x + m^i_x = 0 \\ &\frac{\partial M^i_{yy}}{\partial y} + \frac{\partial M^i_{xy}}{\partial x} - Q^i_y + m^i_y = 0 \end{aligned}\right\} \quad \ldots\ldots\ldots\ldots (31)$$

and the following boundary conditions

$$\left.\begin{aligned} N^{*i}_{nn} &= N^i_{nn} \qquad & M^{*i}_{nn} &= M^i_{nn} \\ N^{*i}_{ns} &= N^i_{ns} \qquad & M^{*i}_{ns} &= M^i_{ns} \\ Q^{*i}_n &= Q^i_n \end{aligned}\right\} \quad \ldots\ldots\ldots\ldots (32)$$

By substituting Eqs. 28, 29, 30 into Eqs. 21 and 22, and by taking into account Eqs. 31 and 32, we obtain the five equations of motion, as well as the boundary conditions of a plate under initial stress. These equations will be linearized by disregarding all non-linear terms involving the additional stresses. Thereby, we are postulating that the unit elongations, shears, and rotations associated with the displacements u_x, u_y, u_z, are small as compared to unity. Therefore, we disregard the terms involving products of the derivatives of the components of the displacement and the additional stresses, for they are negligible in comparison with the additional stresses. However, the initial stresses are assumed to be of higher order of magnitude than the additional stresses. Consequently, higher order terms involving initial stresses may be of the same order of magnitude than the additional stresses. Consequently, higher order terms involving initial stresses may be of the same order of magnitude as the additional stresses and shall, therefore, be retained.

The linearized equations of motion for a plate under initial stress are

$$\frac{\partial N^a_{xx}}{\partial x} + \frac{\partial N^a_{xy}}{\partial y} + \frac{\partial}{\partial y}\left(N^i_{yy}\frac{\partial u}{\partial y}\right) + \frac{\partial}{\partial x}\left(N^i_{xy}\frac{\partial u}{\partial y}\right) + \frac{\partial}{\partial y}\left(N^i_{xy}\frac{\partial u}{\partial x}\right)$$

$$+ \frac{\partial}{\partial y}\left(M^i_{yy}\frac{\partial \psi_x}{\partial y}\right) + \frac{\partial}{\partial x}\left(M^i_{xy}\frac{\partial \psi_x}{\partial y}\right) + \frac{\partial}{\partial y}\left(M^i_{xy}\frac{\partial \psi_x}{\partial x}\right)$$

$$+ \frac{\partial}{\partial x}\left(Q^i_x \psi_x\right) + \frac{\partial}{\partial y}\left(Q^i_y \psi_x\right) + \Delta F^i_x + \Delta B^i_x + F^a_x + B^a_x = \rho\, h\, \ddot{u} \quad \ldots\ldots \text{(33a)}$$

$$\frac{\partial N^a_{yy}}{\partial y} + \frac{\partial N^a_{xy}}{\partial x} + \frac{\partial}{\partial x}\left(N^i_{xx}\frac{\partial v}{\partial x}\right) + \frac{\partial}{\partial y}\left(N^i_{xy}\frac{\partial v}{\partial x}\right) + \frac{\partial}{\partial x}\left(N^i_{xy}\frac{\partial v}{\partial y}\right)$$

$$+ \frac{\partial}{\partial x}\left(M^i_{xx}\frac{\partial \psi_y}{\partial x}\right) + \frac{\partial}{\partial x}\left(M^i_{xy}\frac{\partial \psi_y}{\partial y}\right) + \frac{\partial}{\partial y}\left(M^i_{xy}\frac{\partial \psi_y}{\partial x}\right)$$

$$+ \frac{\partial}{\partial y}\left(Q^i_y \psi_y\right) + \frac{\partial}{\partial x}\left(Q^i_x \psi_y\right) + \Delta F^i_y + \Delta B^i_y + F^a_y + B^a_y = \rho\, h\, \ddot{v} \quad \ldots\ldots \text{(33b)}$$

$$\frac{\partial Q^a_x}{\partial x} + \frac{\partial Q^a_y}{\partial y} + \frac{\partial}{\partial x}\left(N^i_{xx}\frac{\partial w}{\partial x}\right) + \frac{\partial}{\partial y}\left(N^i_{yy}\frac{\partial w}{\partial y}\right) + \frac{\partial}{\partial x}\left(N^i_{xy}\frac{\partial w}{\partial y}\right)$$

$$+ \frac{\partial}{\partial y}\left(N^i_{xy}\frac{\partial w}{\partial x}\right) + q^a + \Delta q^i + \Delta B^i_z + B^a_z = \rho\, h\, \ddot{w} \quad \ldots\ldots\ldots\ldots \text{(33c)}$$

$$\frac{\partial M^a_{xx}}{\partial x} + \frac{\partial M^a_{xy}}{\partial y} - Q^a_x + \frac{\partial}{\partial y}\left(M^i_{yy}\frac{\partial u}{\partial y}\right) + \frac{\partial}{\partial x}\left(M^i_{xy}\frac{\partial u}{\partial y}\right)$$

$$+ \frac{\partial}{\partial y}\left(M^i_{xy}\frac{\partial u}{\partial x}\right) - Q^i_x\frac{\partial u}{\partial x} - Q^i_y\frac{\partial u}{\partial y} + \Delta m^i_x + m^a_x = \rho\,\frac{h^3}{12}\,\ddot{\psi}_x \quad \ldots\ldots\ldots \text{(33d)}$$

$$\frac{\partial M^a_{yy}}{\partial y} + \frac{\partial M^a_{xy}}{\partial x} - Q^a_y + \frac{\partial}{\partial x}\left(M^i_{xx}\frac{\partial v}{\partial x}\right) + \frac{\partial}{\partial y}\left(M^i_{xy}\frac{\partial v}{\partial x}\right)$$

$$+ \frac{\partial}{\partial x}\left(M^i_{xy}\frac{\partial v}{\partial y}\right) - Q^i_y\frac{\partial v}{\partial y} - Q^i_x\frac{\partial v}{\partial x} + \Delta m^i_y + m^a_y = \rho\frac{h^3}{12}\ddot{\psi}_y \quad \ldots\ldots\ldots (33e)$$

The boundary conditions are

$$\left.\begin{aligned}
&N^{*a}_{nn} + \Delta N^{*i}_{nn} = N^a_{nn} + N^i_{ns}\frac{\partial u_n}{\partial s} + M^i_{ns}\frac{\partial \psi_n}{\partial s} + Q^i_n\psi_n \\
&N^{*a}_{ns} + \Delta N^{*i}_{ns} = N^a_{ns} + N^i_{ns}\frac{\partial u_s}{\partial s} + N^i_{nn}\frac{\partial u_s}{\partial n} + M^i_{ns}\frac{\partial \psi_s}{s} \\
&+ M^i_{nn}\frac{\partial \psi_s}{\partial n} + Q^i_n\psi_s \\
&M^{*a}_{nn} + \Delta M^{*i}_{nn} = M^a_{nn} + M^i_{ns}\frac{\partial u_n}{\partial s} \\
&M^{*a}_{ns} + \Delta M^{*i}_{ns} = M^a_{ns} + M^i_{ns}\frac{\partial u_s}{\partial s} + M^i_{nn}\frac{\partial u_s}{\partial n} \\
&Q^{*a}_n + \Delta Q^{*i}_n = Q^a_n + N^i_{nn}\frac{\partial w}{\partial n} + N^i_{ns}\frac{\partial w}{\partial s}
\end{aligned}\right\} \quad \ldots\ldots (34)$$

It might be noted, that identical equations of motion including the boxed terms could be obtained by appropriate integration of the three-dimensional equations of motion that include initial stresses, (2). In the sequel, the boxed terms, however, will not be retained for reasons given at the beginning of this section.

STRESS-DISPLACEMENT RELATIONS

The relations between the additional plate stresses and the displacements will be taken the same as in the absence of initial stresses. As mentioned earlier, this procedure introduces an error of the order of the ratio of an initial stress component to an elastic modulus.

For an isotropic material the pertinent stress-displacement relations (11) are

$$N^a_{xx} = E_p\left(\frac{\partial u}{\partial x} + \nu\frac{\partial v}{\partial y}\right) \qquad M^a_{xx} = D\left(\frac{\partial \psi_x}{\partial x} + \nu\frac{\partial \psi_y}{\partial y}\right)$$

$$N^a_{yy} = E_p\left(\frac{\partial v}{\partial y} + \nu\frac{\partial u}{\partial x}\right) \qquad M^a_{yy} = D\left(\frac{\partial \psi_y}{\partial y} + \nu\frac{\partial \psi_x}{\partial x}\right)$$

$$N^a_{xy} = G\,h\left(\frac{\partial u}{\partial y} + \frac{\partial v}{\partial x}\right) \qquad M^a_{xy} = G\,I\left(\frac{\partial \psi_x}{\partial y} + \frac{\partial \psi_y}{\partial x}\right)$$

$$Q^a_x = \kappa^2\,G\,h\left(\psi_x + \frac{\partial w}{\partial x}\right) \qquad Q^a_y = \kappa^2\,G\,h\left(\psi_y + \frac{\partial w}{\partial y}\right) \quad \ldots\ldots\ldots (35)$$

in which $E_p = E\,h/(1-\nu^2)$ is the plate compressional modulus, $I = h^3/12$ is the moment of inertia, $D = E\,h^3/12(1-\nu^2)$ is the plate flexural modulus, E is Young's modulus, G is the shear modulus, ν is Poisson's ratio, and κ^2 is a factor used for adjustment. Its value can be taken as equal to $\pi^2/12$, (8) and (11).

Relations of Eq. 35 are readily derived from Hooke's law for an isotropic three-dimensional solid, by eliminating the z-component of strain, integrating over the thickness coordinate and setting the integrals involving t_{zz} equal to zero.

DISPLACEMENT EQUATIONS OF MOTION

The stress equations of motion (Eq. 33) can now be converted to the following displacement equations of motion:

$$E_p\frac{\partial^2 u}{\partial x^2} + G\,h\frac{\partial^2 u}{\partial y^2} + \left(E_p\,\nu + G\,h\right)\frac{\partial^2 v}{\partial x\,\partial y} + \frac{\partial}{\partial y}\left(N^i_{yy}\frac{\partial u}{\partial y}\right)$$

$$+\frac{\partial}{\partial x}\left(N^i_{xy}\frac{\partial u}{\partial y}\right) + \frac{\partial}{\partial y}\left(N^i_{xy}\frac{\partial u}{\partial x}\right) + \frac{\partial}{\partial y}\left(M^i_{yy}\frac{\partial \psi_x}{\partial y}\right)$$

$$+\frac{\partial}{\partial x}\left(M^i_{xy}\frac{\partial \psi_x}{\partial y}\right) + \frac{\partial}{\partial y}\left(M^i_{xy}\frac{\partial \psi_x}{\partial x}\right) + \frac{\partial}{\partial x}\left(Q^i_x\,\psi_x\right) + \frac{\partial}{\partial y}\left(Q^i_y\,\psi_x\right)$$

$$+\Delta F^i_x + \Delta B^i_x + F^a_x + B^a_x = \rho\,h\,\ddot{u} \quad \ldots\ldots\ldots\ldots\ldots\ldots\ldots\ldots (36a)$$

$$E_p\frac{\partial^2 v}{\partial y^2} + G\,h\frac{\partial^2 v}{\partial x^2} + \left(E_p\,\nu + G\,h\right)\frac{\partial^2 u}{\partial x\,\partial y} + \frac{\partial}{\partial x}\left(N^i_{xx}\frac{\partial v}{\partial x}\right)$$

$$+\frac{\partial}{\partial y}\left(N^i_{xy}\frac{\partial v}{\partial x}\right) + \frac{\partial}{\partial x}\left(N^i_{xy}\frac{\partial v}{\partial y}\right) + \frac{\partial}{\partial x}\left(M^i_{xx}\frac{\partial \psi_y}{\partial x}\right) + \frac{\partial}{\partial y}\left(M^i_{xy}\frac{\partial \psi_y}{\partial x}\right)$$

$$+\frac{\partial}{\partial x}\left(M^i_{xy}\frac{\partial \psi_y}{\partial y}\right) + \frac{\partial}{\partial y}\left(Q^i_y\,\psi_y\right) + \frac{\partial}{\partial x}\left(Q^i_x\,\psi_y\right) + \Delta F^i_y + \Delta B^i_y$$

$$+F^a_y + B^a_y = \rho\,h\,\ddot{v} \quad \ldots\ldots\ldots\ldots\ldots\ldots\ldots\ldots\ldots\ldots (36b)$$

$$\kappa^2\,G\,h\left(\frac{\partial \psi_x}{\partial x} + \frac{\partial \psi_y}{\partial y}\right) + \kappa^2\,G\,h\left(\frac{\partial^2 w}{\partial x^2} + \frac{\partial^2 w}{\partial y^2}\right) + \frac{\partial}{\partial x}\left(N^i_{xx}\frac{\partial w}{\partial x}\right)$$

$$+\frac{\partial}{\partial y}\left(N^i_{yy}\frac{\partial w}{\partial y}\right)+\frac{\partial}{\partial x}\left(N^i_{xy}\frac{\partial w}{\partial y}\right)+\frac{\partial}{\partial y}\left(N^i_{xy}\frac{\partial w}{\partial x}\right)+q^a+\Delta q^i$$

$$+\Delta B^i_z+B^a_z=\rho\, h\,\ddot{w} \quad \ldots\ldots\ldots\ldots\ldots\ldots\ldots\ldots\ldots\ldots \text{(36c)}$$

$$D\frac{\partial^2\psi_x}{\partial x^2}+G\,I\frac{\partial^2\psi_x}{\partial y^2}+(D\nu+G\,I)\frac{\partial^2\psi_y}{\partial x\,\partial y}-\kappa^2 G\,h\left(\psi_x+\frac{\partial w}{\partial x}\right)$$

$$+\frac{\partial}{\partial y}\left(M^i_{yy}\frac{\partial u}{\partial y}\right)+\frac{\partial}{\partial x}\left(M^i_{xy}\frac{\partial u}{\partial y}\right)+\frac{\partial}{\partial y}\left(M^i_{xy}\frac{\partial u}{\partial x}\right)-Q^i_x\frac{\partial u}{\partial x}$$

$$-Q^i_y\frac{\partial u}{\partial y}+m^a_x+\Delta m^i_x=\rho\frac{h^3}{12}\ddot{\psi}_x \quad \ldots\ldots\ldots\ldots\ldots\ldots\ldots\ldots \text{(36d)}$$

$$D\frac{\partial^2\psi_y}{\partial y^2}+G\,I\frac{\partial^2\psi_y}{\partial x^2}+(D\nu+G\,I)\frac{\partial^2\psi_x}{\partial x\,\partial y}-\kappa^2 G\,h\left(\psi_y+\frac{\partial w}{\partial y}\right)$$

$$+\frac{\partial}{\partial x}\left(M^i_{xx}\frac{\partial v}{\partial x}\right)+\frac{\partial}{\partial y}\left(M^i_{xy}\frac{\partial v}{\partial x}\right)+\frac{\partial}{\partial x}\left(M^i_{xy}\frac{\partial v}{\partial y}\right)-Q^i_y\frac{\partial v}{\partial y}$$

$$-Q^i_x\frac{\partial v}{\partial x}+m^a_y+\Delta m^i_y=\rho\frac{h^3}{12}\ddot{\psi}_y \quad \ldots\ldots\ldots\ldots\ldots\ldots\ldots\ldots \text{(36e)}$$

In an isotropic plate without initial stresses, the face-extensional motion (involving u and v), and the flexural motion are not coupled, while in an anisotropic plate, such as a crystal, they are coupled. It is noted here that the initial moments and transverse shear forces couple the u-equation to the ψ_x-equation, and the v-equation to the ψ_y - equation. By contrast, initial membrane forces N^i_{xx}, N^i_{yy} and N^i_{xy} do not introduce any coupling. Thus, the initial stresses make the plate, in a certain sense, anisotropic. Inasmuch as the initial stresses depend, in general, on the space coordinates, the plate also becomes heterogeneous.

CLASSICAL PLATE THEORY IN THE PRESENCE OF INITIAL STRESS

The passage from the non-linear plate theory discussed in preceding sections to the classical non-linear plate theory (absence of rotatory inertia and shear effects) can be accomplished as follows: Disregarding the rotatory inertia terms, $\rho\,(h^3/12)\,\ddot{\psi}_x$ and $\rho\,(h^3/12)\,\ddot{\psi}_y$ in the last two of Eqs. 21, the plate shear Q_x and Q_y may be obtained in terms of the other plate stresses, and the resulting expressions may be introduced into the remaining equations of motion; thus, a set of three equations is obtained that does not involve the shear stresses.

Since the effect of shear is disregarded, we may find by setting $\bar{\epsilon}_{xz} = 0$ and $\bar{\epsilon}_{yz} = 0$ at $z = 0$, the following expressions:

$$\psi_x = -\frac{\partial w}{\partial x} + \frac{\partial w}{\partial x}\frac{\partial u}{\partial x} + \frac{\partial w}{\partial y}\frac{\partial v}{\partial x}$$

$$\psi_y = -\frac{\partial w}{\partial y} + \frac{\partial w}{\partial y}\frac{\partial v}{\partial y} + \frac{\partial w}{\partial x}\frac{\partial u}{\partial y} \quad \ldots\ldots\ldots\ldots\ldots (37)$$

Substituting the above relations in Eq. 21, a set of three equations of motion is obtained which excludes the effect of transverse shear deformation and rotatory inertia. It is noted that the second order terms in Eq. 37 contribute only higher order terms to the previously-mentioned equations and can be disregarded.

The same equations could have been obtained by using Eq. 37 and setting $\bar{\epsilon}_{xz} = \bar{\epsilon}_{yz} = 0$ directly in the variation of the strain energy (Eq. 4). In this case, however, the higher order terms in Eq. 37 cannot be disregarded.

These equations, if linearized, for the case of a plate under initial stress, in the manner discussed previously, are

$$\frac{\partial N^a_{xx}}{\partial x} + \frac{\partial N_{xy}}{\partial y} + \frac{\partial}{\partial y}\left(N^i_{yy}\frac{\partial u}{\partial y}\right) + \frac{\partial}{\partial x}\left(N^i_{xy}\frac{\partial u}{\partial y}\right) + \frac{\partial}{\partial y}\left(N^i_{xy}\frac{\partial u}{\partial x}\right)$$

$$- \frac{\partial}{\partial y}\left(M^i_{yy}\frac{\partial^2 w}{\partial x\,\partial y}\right) - \frac{\partial}{\partial x}\left(M^i_{xy}\frac{\partial^2 w}{\partial x\,\partial y}\right) - \frac{\partial}{\partial y}\left(M^i_{xy}\frac{\partial^2 w}{\partial x^2}\right)$$

$$- \frac{\partial}{\partial x}\left[\left(\frac{\partial M^i_{xx}}{\partial x} + \frac{\partial M^i_{xy}}{\partial y} + m^i_x\right)\frac{\partial w}{\partial x}\right] - \frac{\partial}{\partial y}\left[\left(\frac{\partial M^i_{yy}}{\partial y} + \frac{\partial M^i_{xy}}{\partial x} + m^i_y\right)\frac{\partial w}{\partial x}\right]$$

$$+ \Delta F^i_x + F^a_x + B^a_x + \Delta B^i_x = \rho\, h\, \ddot{u} \quad \ldots\ldots\ldots\ldots\ldots\ldots\ldots (38a)$$

$$\frac{\partial N^a_{yy}}{\partial y} + \frac{\partial N^a_{xy}}{\partial x} + \frac{\partial}{\partial x}\left(N^i_{xx}\frac{\partial v}{\partial x}\right) + \frac{\partial}{\partial y}\left(N^i_{xy}\frac{\partial v}{\partial x}\right) + \frac{\partial}{\partial x}\left(N^i_{xy}\frac{\partial v}{\partial y}\right)$$

$$- \frac{\partial}{\partial x}\left(M^i_{xx}\frac{\partial^2 w}{\partial x\,\partial y}\right) - \frac{\partial}{\partial y}\left(M^i_{xy}\frac{\partial^2 w}{\partial x\,\partial y}\right) - \frac{\partial}{\partial x}\left(M^i_{xy}\frac{\partial^2 w}{\partial y^2}\right)$$

$$- \frac{\partial}{\partial y}\left[\left(\frac{\partial M^i_{yy}}{\partial y} + \frac{\partial M^i_{xy}}{\partial x} + m^i_y\right)\frac{\partial w}{\partial y}\right] - \frac{\partial}{\partial x}\left[\left(\frac{\partial M^i_{xx}}{\partial x} + \frac{\partial M^i_{xy}}{\partial y} + m^i_x\right)\frac{\partial w}{\partial y}\right]$$

$$+ \Delta F^i_y + F^a_y + B^a_y + \Delta B^i_y = \rho\, h\, \ddot{v} \quad \ldots\ldots\ldots\ldots\ldots\ldots\ldots (38b)$$

$$\frac{\partial^2 M^a_{xx}}{\partial x^2} + \frac{\partial^2 M^a_{yy}}{\partial y^2} + 2\frac{\partial^2 M^a_{xy}}{\partial x\,\partial y} + \frac{\partial}{\partial x}\left(N^i_{xx}\frac{\partial w}{\partial x}\right) + \frac{\partial}{\partial y}\left(N^i_{yy}\frac{\partial w}{\partial y}\right)$$

$$+\frac{\partial}{\partial x}\left(N^i_{xy}\frac{\partial w}{\partial y}\right)+\frac{\partial}{\partial y}\left(N^i_{xy}\frac{\partial w}{\partial x}\right)+\frac{\partial^2}{\partial x\,\partial y}\left(M^i_{xx}\frac{\partial v}{\partial x}\right)+\frac{\partial^2}{\partial x\,\partial y}\left(M^i_{yy}\frac{\partial u}{\partial y}\right)$$

$$+\frac{\partial^2}{\partial x^2}\left(M^i_{xy}\frac{\partial u}{\partial y}\right)+\frac{\partial^2}{\partial y^2}\left(M^i_{xy}\frac{\partial v}{\partial x}\right)+\frac{\partial^2}{\partial x\,\partial y}\left(M^i_{xy}\frac{\partial u}{\partial x}\right)+\frac{\partial^2}{\partial x\,\partial y}\left(M^i_{xy}\frac{\partial v}{\partial y}\right)$$

$$-\frac{\partial}{\partial y}\left[\left(\frac{\partial M^i_{xx}}{\partial x}+\frac{\partial M^i_{xy}}{\partial y}+m^i_x\right)\frac{\partial v}{\partial x}\right]-\frac{\partial}{\partial x}\quad\frac{\partial M^i_{xx}}{\partial x}+\frac{\partial M^i_{xy}}{\partial y}+m^i_x\frac{\partial u}{\partial x}$$

$$-\frac{\partial}{\partial x}\left[\left(\frac{\partial M^i_{yy}}{\partial y}+\frac{\partial M^i_{xy}}{\partial x}+m^i_y\right)\frac{\partial u}{\partial y}\right]-\frac{\partial}{\partial y}\left[\left(\frac{\partial M^i_{yy}}{\partial y}+\frac{\partial M^i_{xy}}{\partial x}+m^i_y\right)\frac{\partial v}{\partial y}\right]$$

$$+\frac{\partial m^a_x}{\partial x}+\frac{\partial m^a_y}{\partial y}+\frac{\partial \Delta m^i_x}{\partial x}+\frac{\partial \Delta m^i_y}{\partial y}+q^a+\Delta q^i+B^a_z+\Delta B^i_z=\rho\,h\,\ddot{w}\quad\ldots.\ (38c)$$

The boundary conditions are

$$N^{*a}_{nn}=N^a_{nn}-\Delta N^{*i}_{nn}+N^i_{ns}\frac{\partial u_n}{\partial s}-M^i_{ns}\frac{\partial^2 w}{\partial s\,\partial n}-\left(\frac{\partial M^i_{nn}}{\partial n}+\frac{\partial M^i_{ns}}{\partial s}+m^i_n\right)\frac{\partial w}{\partial n}$$

$$N^{*a}_{ns}=N^a_{ns}-\Delta N^{*i}_{ns}+N^i_{ns}\frac{\partial u_s}{\partial s}+N^i_{nn}\frac{\partial u_s}{\partial n}-M^i_{ns}\frac{\partial^2 w}{\partial s^2}-M^i_{nn}\frac{\partial^2 w}{\partial s\,\partial n}$$

$$-\left(\frac{\partial M_{nn}}{\partial n}+\frac{\partial M_{ns}}{\partial s}+m^i_n\right)\frac{\partial w}{\partial s}$$

$$M^{*a}_{nn}=M^a_{nn}=\Delta M^{*i}_{nn}+M^i_{ns}\frac{\partial u_n}{\partial s}$$

$$Q^{*a}_n+\frac{\partial M^{*a}_{ns}}{\partial s}=-\Delta Q^{*i}_n-\frac{\partial \Delta M^{*i}_{ns}}{\partial s}+\frac{\partial M^a_{nn}}{\partial n}+2\frac{\partial M^a_{ns}}{\partial s}+\frac{\partial}{\partial n}\left(M^i_{nn}\frac{\partial u_n}{\partial n}\right)$$

$$+\frac{\partial}{\partial n}\left(M^i_{ns}\frac{\partial u_n}{\partial s}\right)+\frac{\partial}{\partial s}\left(M^i_{sn}\frac{\partial u_n}{\partial n}\right)+\frac{\partial}{\partial s}\left(M^i_{ss}\frac{\partial u_n}{\partial s}\right)+\frac{\partial}{\partial s}\left(M^i_{ns}\frac{\partial u_s}{\partial s}\right)$$

$$+\frac{\partial}{\partial s}\quad M^i_{nn}\frac{u_s}{n}\quad-\left(\frac{\partial M^i_{nn}}{\partial n}+\frac{\partial M^i_{ns}}{\partial s}+m^i_n\right)\frac{\partial u_n}{\partial n}-\left(\frac{\partial M^i_{ss}}{\partial s}+\frac{\partial M^i_{ns}}{\partial n}+m^i_s\right)\frac{\partial u_n}{\partial s}$$

$$+N^i_{nn}\frac{\partial w}{\partial n}+N^i_{ns}\frac{\partial w}{\partial s}+m^i_n\qquad\ldots\ (39)$$

The equations of motion reveal that membrane stresses do not introduce any coupling between compressional and flexural motions, while initial moments do introduce such coupling.

Equations of motion (Eq. 38) could also have been obtained by disregarding the inertia terms $\rho(h^3/12)\ddot{\psi}_x$ and, $\rho(h^3/12)\ddot{\psi}_y$ in the last two of Eq. 33, and by introducing the obtained expressions for Q_x^a and Q_y^a into the remaining equations of motion; in addition to replacing ψ_x and ψ_y by $\left(-\frac{\partial w}{\partial x}\right)$ and $\left(-\frac{\partial w}{\partial y}\right)$, respectively.

Using Eqs. 37 the stress displacement relations of Eq. 35 reduce to

$$\left.\begin{aligned} N_{xx}^a &= E_p\left(\frac{\partial u}{\partial x} + \nu\frac{\partial v}{\partial y}\right) & M_{xx}^a &= -D\left(\frac{\partial^2 w}{\partial x^2} + \nu\frac{\partial^2 w}{\partial y^2}\right) \\ N_{yy}^a &= E_p\left(\frac{\partial v}{\partial y} + \nu\frac{\partial u}{\partial x}\right) & M_{yy}^a &= -D\left(\frac{\partial^2 w}{\partial y^2} + \nu\frac{\partial^2 w}{\partial x^2}\right) \\ N_{xy}^a &= G\,h\left(\frac{\partial u}{\partial y} + \frac{\partial v}{\partial x}\right) & M_{xy}^a &= -2\,G\,I\,\frac{\partial^2 w}{\partial x \partial y} \end{aligned}\right\} \quad \ldots\ldots (40)$$

and the displacement equations of motion can readily be obtained by the substitution of these in relations into the stress equations of motion (Eq. 38).

APPLICATIONS

In order to study the influence of initial stresses on the frequencies of the modes of motion considered in this investigation (Fig. 2), a series of particular solutions of the newly derived equations is presented and discussed in this section. In Fig. 2 the modes are as follows: A = flexural, B = lower face-shear, C = longitudinal, D = upper face-shear, and E = thickness shear.

Initial Normal Stress.—As a first example, we consider the case of initial constant normal stress $N_{xx}^i = N$. It is well known that initial tension raises, while initial compression lowers the frequency of the flexural vibrations. For the sake of completeness, however, it may be stated that in the case of cylindrical vibrations $\left(\frac{\partial}{\partial y} = v = \psi_y = 0\right)$ the flexural frequency is calculated from the equation

$$-D\,\frac{\partial^4 w}{\partial x^4} + N\,\frac{\partial^2 w}{\partial x^2} = \rho\,h\,\ddot{w} \quad \ldots\ldots\ldots\ldots (41)$$

which is obtained from the set of Eqs. 38.

Letting

$$w = W \sin\frac{\pi x}{L}\, e^{i\omega t} \quad \ldots\ldots\ldots\ldots (42)$$

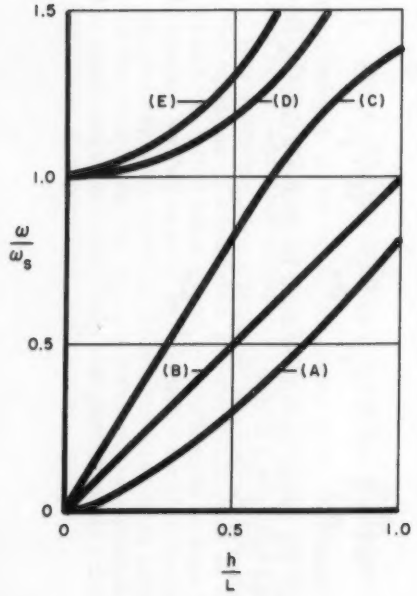

FIG. 2.—FREQUENCIES OF THE FIRST FIVE MODES OF VIBRATION FOR AN ISOTROPIC PLATE, SEE (14)

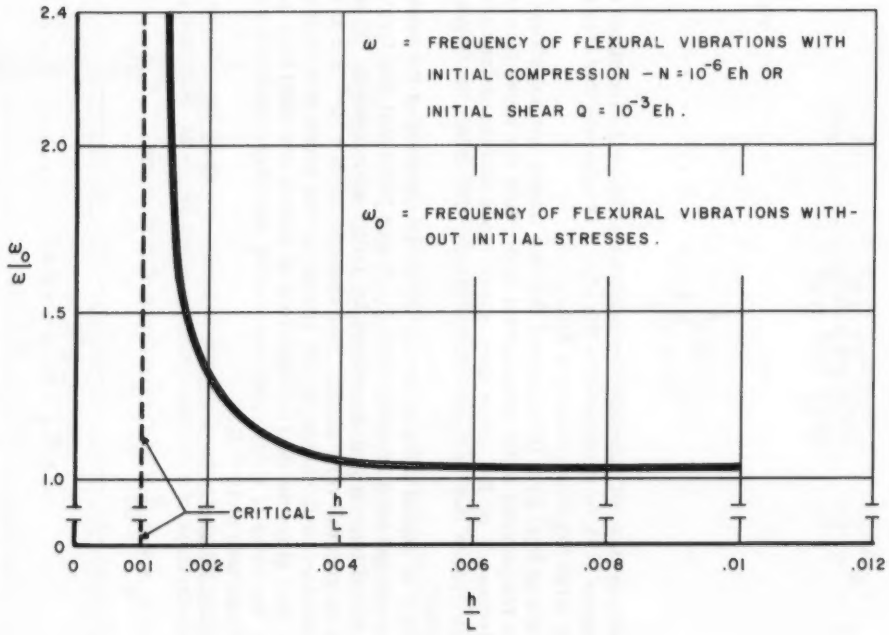

FIG. 3.—RELATIVE EFFECT OF INITIAL COMPRESSION AND TRANSVERSE SHEAR ON THE FREQUENCY OF THE PREDOMINANTLY FLEXURAL MODE

results in

$$\left(\frac{\omega}{\omega_f}\right)^Z = 1 + \frac{N L^2}{D \pi^2} \quad \ldots\ldots\ldots\ldots\ldots\ldots (43)$$

in which

$$\omega_f^2 = \frac{D \pi^4}{\rho h L^4} \quad \ldots\ldots\ldots\ldots\ldots\ldots (44)$$

is the frequency of flexural vibration for small h/L. The relative effect of initial compression (-N) is illustrated in Fig. 3. It is apparent that this effect becomes very large for small values of h/L.

By inspection of Eqs. 38 it is concluded that the initial normal stress does not effect the frequencies of the longitudinal mode, and the upper face-shear mode. The frequency of the lower face-shear mode increases due to initial tension and decreases due to initial compression; this effect is, in general, exceedingly small.

The influence of initial normal stress on the frequencies of the predominantly shear mode has been investigated (15). It was found that this frequency increases by initial tension and decreases by initial compression. However this effect is in general very small. For example for $N = 10^{-3}$ E h and $h/L = 10^{-2}$ the frequency will change by an amount of the order of magnitude of 10^{-7}. Notice that since the derived equations of motion are valid only in the elastic range, the value of N for most engineering materials could not exceed the order of magnitude of 10^{-3} E h.

Initial Bending Moment.—As a second example, we study the influence, on frequencies of vibration, of a constant initial moment $M^i_{xx} = M$. For face shear vibrations $\left(u = \psi_x = w = \frac{\partial}{\partial y} = 0\right)$ the equations of motion are

$$G h \frac{\partial^2 v}{\partial x^2} + M \frac{\partial^2 \psi_y}{\partial x^2} = \rho h \ddot{v} \quad \ldots\ldots\ldots\ldots\ldots (45a)$$

$$G I \frac{\partial^2 \psi_y}{\partial x^2} - \kappa^2 G h \psi_y + M \frac{\partial^2 u}{\partial x^2} = \rho \frac{h^3}{12} \ddot{\psi}_y \quad \ldots\ldots\ldots\ldots (45b)$$

It is apparent that the initial bending moment introduces a coupling between the upper and lower face-shear modes.

We seek a solution of the above equations in the form

$$v = V \sin \frac{\pi x}{L} e^{i\omega t} \quad \ldots\ldots\ldots\ldots\ldots\ldots (46a)$$

$$\psi_y = \Psi_y \sin \frac{\pi x}{L} e^{i\omega t} \quad \ldots\ldots\ldots\ldots\ldots\ldots (46b)$$

and we obtain the frequency equation

$$\omega^4 - \omega_s^2\left(1 + 2\frac{h^2}{L^2}\right)\omega^2 + \omega_s^4\frac{h^2}{L^2}\left(1 + \frac{h^2}{L^2}\right) - \frac{12\,\pi^4\,M^2}{\rho^2\,h^4\,L^4} = 0 \quad \ldots\ldots (47)$$

in which

$$\omega_s^2 = \frac{G\,\pi^2}{\rho\,h^2} \quad \ldots\ldots\ldots\ldots\ldots\ldots (48)$$

is the frequency of the thickness-shear vibration. The solution of Eq. 47 is

$$\left(\frac{\omega}{\omega_s}\right)^2 = \frac{1}{2} + \frac{h^2}{L^2} + \frac{1}{2}\left(1 + \frac{48\,M^2}{L^4\,G^2}\right)^{\frac{1}{2}} \quad \ldots\ldots\ldots\ldots (49)$$

Noting that, in order that the stress does not exceed the elastic limit, **M** must not exceed the order of magnitude $10^{-3}\,G\,\frac{h^2}{2}$, we conclude that the frequency of the upper face-shear mode increases due to the initial moment. This effect increases with h/L, but is, in general, exceedingly small. We also observe

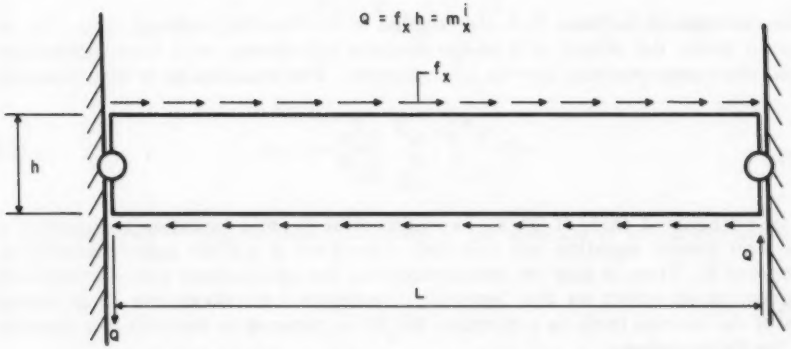

FIG. 4.—PLATE SUBJECTED TO INITIAL TRANSVERSE SHEAR

that the frequency of the lower face-shear mode decreases due to the initial moment. This effect also, increases with h/L but is generally very small.

Initial Shear.—As a last example, we consider the influence, on the frequencies of free vibration, of a uniform initial shear force, $Q_x^i = Q$. As is seen from the equations of equilibrium for the initial state of stress (Eq. 31), a state of uniform initial shear cannot be produced by an edge loading, but only by an external bending moment m_x^i, uniformly distributed over the plate (Fig. 4). This moment may be the result of surface shear tractions uniformly distributed over the two plate faces. As the plate deforms, the applied moment m_x^i, or the surface shear tractions constituting this moment, could change in both magnitude and direction, depending on their physical nature.

For this example it will be assumed that the magnitude of the applied shear tractions could change during deformation in such a manner that for any element the resulting bending moment remains constant. It can be shown that this force system is conservative.

As an alternative, the magnitude of the surface shear tractions could remain constant during deformation. In this case, however, the force system is nonconservative. It is more specifically, in Ziegler's (13) terminology, "circulatory."

In regard to the deformed direction of the applied surface shear tractions, we could assume that the resulting shear forces either rotate with the element or do not change direction after deformation. The resulting applied bending moment, within the accuracy of the present theory, will be the same in both cases.

For the above mentioned conservative loading, $m_x^i = Q$ and $\Delta m_x^i = 0$. Considering only free cylindrical vibrations $\left(\frac{\partial}{\partial y} = v = \psi_y = 0\right)$, the equations of motion (Eq. 38) reduce to

$$E_p \frac{\partial^2 u}{\partial x^2} - Q \frac{\partial^2 w}{\partial x^2} = \rho h \ddot{u}$$

$$- D \frac{\partial^4 w}{\partial x^4} - Q \frac{\partial^2 u}{\partial x^2} = \rho h \ddot{w} \quad \ldots\ldots\ldots\ldots\ldots (50)$$

The extensional motions in u are coupled to the flexural motions in w. In order to study the effect of Q on the flexural vibrations, as a first approximation, the compressional inertia is neglected. The equation on w then becomes

$$- D \frac{\partial^4 w}{\partial x^4} - \frac{Q^2}{E_p} \frac{\partial^2 w}{\partial x^2} = \rho h \ddot{w} \quad \ldots\ldots\ldots\ldots\ldots (51)$$

It is recognized that, if Q^2/E_p is replaced by N, this equation is identical to the well known equation for cylindrical motions of a plate under initial compression N. Thus, it may be anticipated that the initial shear force Q will have a pronounced effect on the flexural frequencies. Furthermore, it is noticed that if the inertia term is neglected, Eq. 51 is reduced to the buckling equation of the Euler column.

Assuming the solution of Eq. 51 in the form

$$w = W \sin\left(\frac{\pi}{L} x\right) e^{i\omega t} \quad \ldots\ldots\ldots\ldots\ldots (52)$$

We obtain the frequency equation

$$\left(\frac{\omega}{\omega_f}\right)^2 = 1 - \frac{12\left(1 - \nu^2\right)^2}{\pi^2} \frac{Q^2 L^2}{E^2 h^4} \quad \ldots\ldots\ldots\ldots (53)$$

If the vibrations are to remain finite, all the values of ω must be real. Therefore, buckling occurs for

$$Q_{crit.} = \frac{\pi \sqrt{D E_P}}{L} \quad \ldots\ldots\ldots\ldots\ldots\ldots (54)$$

For the stresses in the plate not to exceed the elastic limit, Q must not be larger than the order of magnitude 10^{-3} E h. For the sake of simplicity, we choose $\nu = 0.305$ and $Q = 10^{-3}$ E h and obtain

$$\left(\frac{\omega}{\omega_f}\right)^2 = 1 - 10^{-6} \frac{L^2}{h^2} \quad \ldots\ldots\ldots\ldots\ldots\ldots (55)$$

From this relation it becomes apparent that the initial shear force decreases the frequency of the flexural mode. The relative effect becomes large for small value of h/L; this is illustrated in Fig. 3, in which, from the above equation, the ratio ω_f/ω is plotted as a function of h/L.

For the chosen value of Q the plate will buckle if $h/L = 10^{-3}$. This indicates that a plate must have a very small h/L ratio in order to buckle in the elastic range, due to constant transverse shear.

If the longitudinal inertia ρ h $\ddot{u}$ is not neglected, the frequency equation is

$$\left(\omega^2 - \omega_f^2\right)\left(\omega^2 - \omega_c^2\right) - K^2 = 0 \quad \ldots\ldots\ldots\ldots\ldots\ldots (56)$$

where

$$\omega_c^2 = \frac{E_P \pi^2}{\rho h L^2} \quad \ldots\ldots\ldots\ldots\ldots\ldots (57)$$

is the frequency of longitudinal vibrations in the absence of initial stresses,

$$K^2 = \frac{Q^2 \pi^4}{\rho^2 h^2 L^4} \quad \ldots\ldots\ldots\ldots\ldots\ldots (58)$$

and ω_f^2 is given by Eq. 44.

The two roots of the Eq. 56 are

$$\omega_{1,2}^2 = \frac{\omega_c^2 + \omega_f^2}{2} \pm \frac{\omega_c^2 - \omega_f^2}{2} \left(1 + \frac{4 K^2}{\left(\omega_c^2 - \omega_f^2\right)^2}\right)^{1/2} \quad \ldots\ldots (59)$$

If Q is again assumed to be of the order 10^{-3} E h, and for values of h/L which are small as compared to unity, the second term under the square root in the

above expression is small compared to one, and binomial expansion results in

$$\omega_{1,2}^2 = \frac{\omega_c^2 + \omega_f^2}{2} \pm \frac{\omega_c^2 - \omega_f^2}{2} \pm \frac{K^2}{\omega_c^2 - \omega_f^2} \quad \ldots\ldots\ldots\ldots (60)$$

The higher frequency ω_1^2 can then be written approximately, as

$$\frac{\omega_1^2}{\omega_f^2} = \frac{L^2}{h^2}\frac{12}{\pi^2} + 10^{-6}\frac{\pi^2}{12} \quad \ldots\ldots\ldots\ldots\ldots\ldots (61)$$

It is seen that the initial shear stress raises the higher (longitudinal) frequency, but only by a small amount. This effect increases with h/L but is, in general, exceedingly small. The lower (flexural) frequency ω_2^2 is

$$\left(\frac{\omega_2}{\omega_f}\right)^2 = 1 - 10^{-6}\frac{L^2}{h^2}\left(1 + \frac{h^2}{L^2}\frac{\pi^2}{12}\right) \quad \ldots\ldots\ldots\ldots (62)$$

The second term in the parenthesis above represents the influence of longitudinal inertia and is seen to be small as compared to unity. If this term is dropped, the expression for ω_2^2 becomes identical to the one given by Eq. 55.

As evidenced from this example, the initial shear stress has a large effect only on the flexural frequencies of vibration for very slender plates ($h/L \ll 1$). The effect of initial shear on the longitudinal frequency is exceedingly small.

In the case of face shear vibrations, the frequency equation for motion under the influence of initial shear is analogous to the one obtained for motion under the influence of initial bending moment. We may, therefore, conclude that initial shear increases the frequency of the upper face-shear mode, and decreases the frequency of the lower. These effects increase with h/L but are, in general, exceedingly small.

The influence of an initial transverse shear stress on the frequency of the predominantly thickness-shear mode has been investigated (Eq. 15). It was found that an initial shear stress raises this frequency by a very small amount, even for relatively large values of h/L.

CONCLUSIONS

On the basis of the results obtained by applying the equations of motion derived in this paper to a number of specific cases, we may conclude that the effect of initial stresses on the frequencies of the two face shear modes and on the predominantly compressional and thickness shear modes is exceedingly small. The relative effect of initial membrane stresses $\left(N_{xx}^i\ N_{xy}^i\right)$ and of transverse shear stress Q on the frequencies of the predominantly flexural mode increases as h/L decreases. In the elastic region, however, the effect of initial membrane stresses becomes large in a range of h/L that has great practical importance, while the effect of initial transverse shear becomes

significant for values of h/L too small to be of great practical importance. For instance, the frequency of the predominantly flexural mode changes by 50% for a plate with h/L = 0.03 when under the influence of initial tension of magnitude 10^{-3} E h. To produce the same change when a plate is subjected to initial transverse shear of the same magnitude, the ratio h/L has to be approximately 0.0017.

The qualitative influence of uniform initial stresses, on the frequencies of cylindrical vibration, is summarized in Table 1.

TABLE 1.—QUALITATIVE INFLUENCE OF UNIFORM INITIAL STRESS OF THE FREQUENCIES OF CYLINDRICAL VIBRATIONS

Initial Stress	Flexural	Lower face-shear	Longitudinal	Upper face-shear	Thickness shear
Tension	increases	increases	———	———	increases
Moment	———	decreases	———	increases	———
Shear	decreases	decreases	increases	increases	increases

ACKNOWLEDGMENTS

This investigation was supported by the United States Air Force, through the Office of Scientific Research of the Air Research and Development Command, under contract with Columbia University.

APPENDIX - NOTATION

List of symbols used in this paper:

x, y, z = Initial Cartesian coordinates of an element.

ξ, η, ζ = Final Cartesian coordinates of an element.

u_x, u_y, u_z = Displacement components in the x, y, z direction, respectively.

h = Plate thickness.

u, v, w = Displacement components of middle plane.

ψ_x, ψ_y = Angles of rotation of a normal to the middle plane in the z-x and z-y planes, respectively.

W_{int} = Total strain energy.

σ_{ij} $(i, j = x, y, z)$ = Trefftz's components of stress per unit original area defined by Eq. 6.

τ_{ij} $(i, j = x, y, z)$ = Components of stress per unit original area (Fig. 1).

E_x, E_y, E_z = Unit elongation of a line element originally in the x, y, z-direction, respectively.

ϕ = Strain energy density.

$N_{xx}, N_{yy}, N_{zz}, N_{xy}$, M_{xx}, M_{yy}, M_{xy}, Q_x, Q_y, T_x, T_y, K_{xx}, K_{yy}, K_{xy} = Plate stresses defined by Eq. 7.

n, s = Coordinates measured along the outward normal and along the tangent to the undeformed cylindrical boundary respectively.

f_ξ, f_η, f_ζ = Components of boundary traction.

W_e = Work done by boundary tractions.

S = Surface of a body before deformation.

A = Plate area before deformation.

F_ξ, F_η, q, $N^*_{nn}, N^*_{ns}, Q^*_n$, $m_\xi, m_\eta, M^*_{nn}, M^*_{ns}$ = Boundary plate forces and moments defined by Eq. 11.

b_ξ, b_η, b_ζ = Components of body force.

W_B = Work done by body forces.

B_ξ, B_η, B_ζ = Components of body force defined by Eq. 15.

T = Kinetic energy.

ρ = Mass density.

t = Time.

L = Kinetic potential.

S_{ij} (i, j = x, y, z) = Components of initial stress.

t_{ij} (i, j = x, y, z) = Components of additional stress.

ΔF^i_x = x component of the change, due to deformation, of the initial boundary plate force

E_p = Plate compressional modulus.

D = Plate flexural modulus.

E = Young's modulus.

ν = Poisson's ratio.

G = Shear modulus.

κ^2 = Adjustment factor.

ω = Circular frequency.

ω_o = Circular frequency in the absence of initial stress.

ω_s = Frequency of the first thickness-shear mode in the absence of initial stress.

ω_f = Frequency of the flexural mode for large wave-lengths in the absence of initial stress.

ω_c = Frequency of the compressional mode for large wavelengths in the absence of initial stress.

Superscripts:

—	= approximate
a	= additional
i	= initial
*	= on the boundary

APPENDIX - BIBLIOGRAPHY

1. "Nonlinear Theory of Elasticity and the Linearized Case for a Body under Initial Stress," by M. A. Biot, Philosophical Magazine, Vol. 27, 1940, pp. 468-489.
2. "Elastic Torsion in the Presence of Initial Axial Stress," by J. N. Goodier, Journal of Applied Mechanics, Vol. 17, 1950, pp. 383-387.
3. "Increase of Torsional Stiffness of a Prismatical Bar Due to Axial Tension," by M. A. Biot, Journal of Applied Physics, Vol. 10, 1939, pp. 860-864.
4. "The Influence of Initial Stress on Elastic Waves," by M. A. Biot, Journal of Applied Physics, Vol. 11, 1940, pp. 522-530.
5. "Théorie de l'Elasticité des Corps Solides," by A. Clebsch and B. de Saint-Venant, 1883, p. 689.
6. "Theory of Plates and Shells," by S. Timoshenko, McGraw-Hill Book Co., New York, 1940, p. 301.
7. "The Influence of Initial Stress on the Dynamic Behavior of Elastic and Viscoelastic Plates," by G. Herrmann, Publication of the Interntl. Assn. for Bridge and Structural Engrg., Vol. 16, 1956, pp. 275-294.
8. "Influence of Rotatory Inertia and Shear on Flexural Motions of Isotropic Elastic Plates," by R. D. Mindlin, Journal of Applied Mechanics, Vol. 18, 1951, pp. 31-38.
9. "Foundations of the Nonlinear Theory of Elasticity," by V. V. Novozhilov, Graylock Press, Rochester, New York, 1953.
10. "Mathematical Theory of Elasticity," by I. S. Sokolnikoff, McGraw-Hill Book Co., New York, 1956.
11. "An Introduction to the Mathematical Theory of Vibrations of Elastic Plates," by R. D. Mindlin, Monograph, U. S. Army Signal Corps Engrg. Labs., Fort Monmouth, New Jersey, 1955.
12. "Stabilitätsprobleme der Elastostatik," by A. Pflüger, Springer, Berlin/Göttingen/Heidelberg, 1950.
13. "On the Concept of Elastic Stability," by H. Ziegler, Advances in Applied Mechanics, Volume IV, Academic Press, New York, 1956, pp. 351-402.
14. "Waves and Vibrations in Isotropic Elastic Plates," by R. D. Mindlin, Proceedings of 1st Symposium on Naval Structural Mechanics, Pergamon Press, 1959.

15. "Vibrations and Stability of Plates under Initial Stress," by G. Herrmann and A. Armenakas, Air Force Office of Scientific Research, Tech. Note 59-189, ASTIA Document 211 220, February, 1959.

Journal of the
ENGINEERING MECHANICS DIVISION
Proceedings of the American Society of Civil Engineers

ULTIMATE STRENGTH OF OVER-REINFORCED BEAMS

By Ladislav B. Kriz,[1] M. ASCE and Seng-Lip Lee,[2] M. ASCE

SYNOPSIS

The flexural strength of rectangular reinforced concrete beams controlled by compression is investigated analytically, using stress distribution derived from experimental stress-strain curves. Empirical expression for the ultimate bending moment is presented and the calculated moments of fifty-nine test beams that failed in compression are compared with the ultimate test moments.

INTRODUCTION

In American design practice, the ultimate flexural strength of reinforced concrete beams is determined by means of empirical design formulas based on the results of numerous tests.[3,4] For beams controlled by yielding of the

Note.—Discussion open until November 1, 1960. To extend the closing date one month, a written request must be filed with the Executive Secretary, ASCE. This paper is part of the copyrighted Journal of the Engineering Mechanics Division, Proceedings of the American Society of Civil Engineers, Vol. 86, No. EM 3, June, 1960.

[1] Graduate Student, Civ. Engrg. Dept., Northwestern Univ., Evanston, Ill., and Assoc. Development Engr., Structural Development Sect., Portland Cement Assn. Labs., Skokie, Ill.

[2] Assoc. Prof. of Civ. Engrg., Northwestern Univ., Evanston, Ill.

[3] "Ultimate Strength of Reinforced Concrete in American Design Practice," by E. Hognestad, Proceedings, Symposium on the Strength of Concrete Structures, London, May, 1956. Also, Portland Cement Assn. Development Dept. Bulletin D12.

[4] "Report of ASCE-ACI Joint Committee on Ultimate Strength Design," Proceedings ASCE, Vol. 81, October, 1955.

tensile reinforcement these formulas, which were also derived analytically,[5] give a close approximation of the ultimate strength. The flexural strength of beams controlled by crushing of concrete may be estimated, assuming that the strength of the beams is proportional to the concrete cylinder strength.[4,6] Because of the undesirability of compression failures, formulas based on this assumption are designed to give a conservative value for the calculated strength.

When greater accuracy of the calculated strength of beams controlled by compression is required, other methods may be used. An analysis based on an assumed rectangular stress distribution and an ultimate concrete strain gives satisfactory results.[7] In the present paper the flexural strength of rectangular beams controlled by compression is investigated analytically, using stress distribution derived from experimental stress-strain curves.[8]

CONCRETE STRESS DISTRIBUTION IN FLEXURE

The stress-strain relationship of concrete in flexure was determined experimentally for concrete of various strength at the ages of 7, 14, 28, and 90 days.[8] For the purpose of this investigation, these stress-strain curves were approximated by second-degree curves having the general equation

$$f^2 + A\epsilon^2 + B f \epsilon + C f + D\epsilon = 0 \quad \ldots\ldots\ldots\ldots \quad (1)$$

in which f denotes the stress, ϵ the strain, and A, B, C, and D are coefficients which are functions of f'_c. Solving for the stress f yields

$$f = \sqrt{\frac{(B\epsilon + C)^2}{4} - A\epsilon^2 - D\epsilon} - \frac{B\epsilon + C}{2} \quad \ldots\ldots\ldots (2)$$

The coefficients in Eq. 1 are determined by solving four simultaneous equations, obtained by substituting in Eq. 1 four given values of strain ϵ and the corresponding values of stress f. The values of strain used, in inches per inch, were 0.0006, 0.0012, 0.0018, and 0.0024.

The values of stress corresponding to each value of strain were first expressed as a function of the cylinder strength f'_c by means of the equation

$$f = F + G f'_c + H \left(f'_c\right)^2 \quad \ldots\ldots\ldots\ldots\ldots \quad (3)$$

The coefficients F, G, and H of Eq. 3, which are functions of ϵ, were determined from the twenty stress-strain curves given by E. Hognestad, et al,[8] by the method of least squares, and are presented in Table 1.

With the coefficients given in Table 1, the values of stress f corresponding to the four given values of strain ϵ were determined for concrete strength varying in 1,000-psi increments up to 6,000 psi. Then the coefficients in Eq. 1

---

5 "Ultimate Strength Criteria for Reinforced Concrete," by L. B. Kriz, Proceedings, ASCE, Vol. 85, No. EM 3, July, 1959.

6 "Plastic Theory in Reinforced Concrete Design," by C. S. Whitney, Transactions, ASCE, Vol. 107, 1942, pp. 251-282.

7 "Rectangular Concrete Stress Distribution in Ultimate Strength Design," by A. H. Mattock, L. B. Kriz, E. Hognestad and "Rectangular Concrete Stress Distribution in Ultimate Strength Design," to be published.

8 "Concrete Stress Distribution in Ultimate Strength Design," by E. Hognestad, N. W. Hanson and D. McHenry, Proceedings, ACI, Vol. 52, 1955, pp. 455-479. Also, Portland Cement Assn. Development Dept. Bulletin D6.

were calculated, and the results are given in Table 2. The strains in Eq. 1 are to be given in 10^{-3} inches per inch, and the stresses in kips per square inch. The stress-strain curves obtained in this manner are shown in Fig. 1.

TABLE 1.

ϵ (1)	F (3)	G (3)	H (4)
0.0006	0.1134	0.6820	-0.04644
0.0012	0.04016	1.036	-0.04800
0.0018	0.05359	1.016	-0.01559
0.0024	0.08964	0.9737	-0.02019

TABLE 2.

f'_c, in psi (1)	A (2)	B (3)	C (4)	D (5)
1,000	-0.07042	-1.421	-1.262	1.746
2,000	-0.8454	-2.552	-3.291	8.109
3,000	-3.434	-3.434	-6.751	22.58
4,000	-11.51	-6.603	-14.26	56.99
5,000	-34.35	-1.196	-31.41	137.8
6,000	-56.31	3.780	-44.13	199.9

The following properties of the stress-strain curves were determined for later use by numerical integration using the trapezoidal rule and strain increments of 0.0002 in. per in.:

$$\int_0^{\epsilon} f \, d\epsilon \quad \ldots\ldots\ldots\ldots\ldots\ldots \quad (a)$$

$$\int_0^{\epsilon} f \, \epsilon \, d\epsilon \quad \ldots\ldots\ldots\ldots\ldots\ldots \quad (b)$$

and

$$1 - \frac{\int_0^{\epsilon} f \, \epsilon \, d\epsilon}{\epsilon \int_0^{\epsilon} f \, d\epsilon} \quad \ldots\ldots\ldots\ldots\ldots\ldots \quad (c)$$

ULTIMATE STRENGTH ANALYSIS OF RECTANGULAR BEAMS

The ultimate flexural strength of rectangular reinforced concrete beams, shown in Fig. 2 was determined by computing the resisting moment of the beams, assuming increasing values of the strain in the extreme compressive

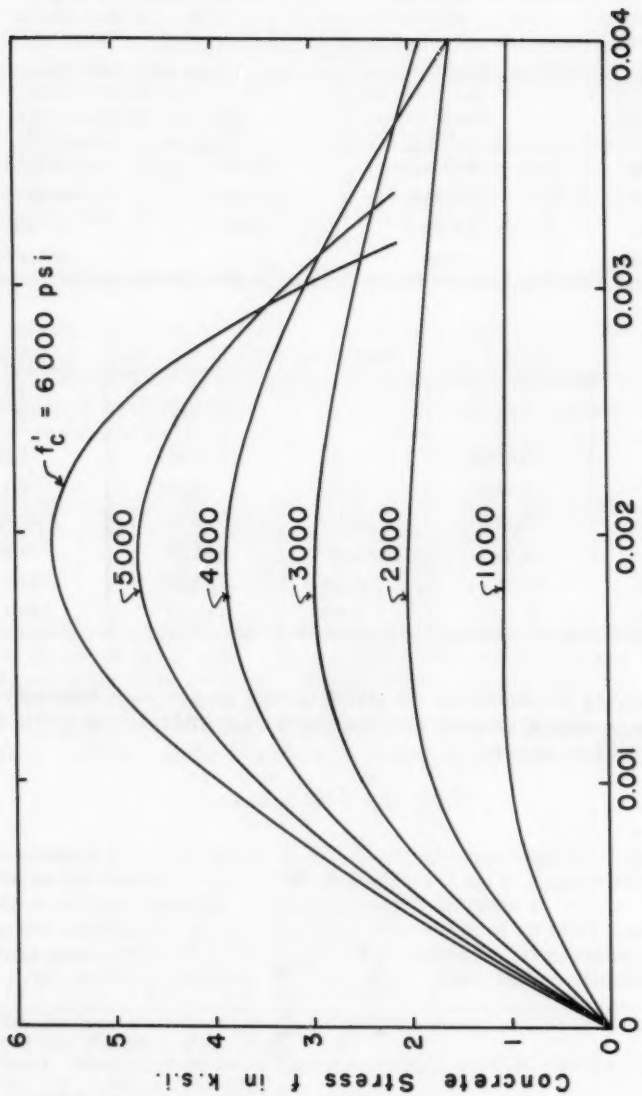

FIG. 1.—CONCRETE STRESS STRAIN RELATIONSHIP

fibers ϵ_c, with $\epsilon_c = 0.004$ in. per in. maximum. The highest value of the resisting moment thus obtained was designated M_u, the ultimate bending moment.

The following assumptions were made in the computations:

(a) Plane sections normal to the axis remain plane after bending.
(b) Tensile strength of concrete may be neglected.
(c) The stress-strain relationship of concrete in flexure is as shown in Fig. 1.
(d) The modulus of elasticity of the reinforcement is 30×10^6 psi.
(e) The stress in the reinforcement is constant after the yield stress is reached.

The yield strength of the reinforcement was assumed to be $f_y = 60{,}000$ psi, the maximum stress recommended by the ACI Building Code (ACI 318-56), Section A603.

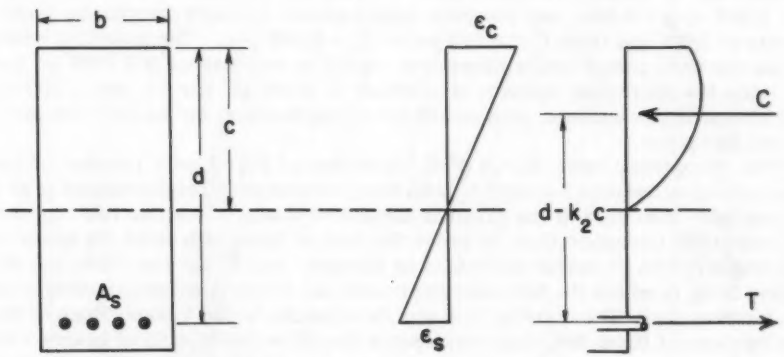

FIG. 2.—CONDITIONS IN REINFORCED CONCRETE BEAM IN BENDING

With these assumptions, the equations of equilibrium and of compatibility of strains give the resisting moment M as

$$M = p\ b\ d^2\ f_s \left(1 - k_2\ k\right) \quad \ldots\ldots\ldots\ldots \quad (4)$$

in which

$$k = \frac{\epsilon_c}{\epsilon_s + \epsilon_c} \quad \ldots\ldots\ldots\ldots\ldots\ldots \quad (5)$$

$$f_s = E_s\ \epsilon_s \quad \ldots\ldots\ldots\ldots\ldots\ldots\ldots \quad (6)$$

and

$$\epsilon_s = \sqrt{\frac{\epsilon_c^2}{4} + \frac{\int_0^{\epsilon_c} f\ d\epsilon}{p\ E_s}} - \frac{\epsilon_c}{2} \quad \ldots\ldots\ldots\ldots \quad (7)$$

if the reinforcement is in the elastic stage $\left(f_s < f_y\right)$, or

$$k = p\ f_y \frac{\epsilon_c}{\int_0^{\epsilon_c} f\ d\epsilon} \quad \ldots\ldots\ldots\ldots\ldots \quad (8)$$

and

$$f_s = f_y \quad \ldots\ldots\ldots\ldots\ldots\ldots \quad (9)$$

when the reinforcement yields. In either case, k_2 is given by

$$k_2 = 1 - \frac{\int_0^{\epsilon_c} f\,\epsilon\,d\epsilon}{\epsilon_c \int_0^{\epsilon_c} f\,d\epsilon} \quad \ldots\ldots\ldots\ldots\ldots \quad (10)$$

By means of Eqs. 4 through 10 and the properties of the approximate stress-strain curves, the ultimate strength in flexure was determined for beams with percentage of tensile reinforcement varying in increments of 0.005 from p = 0.005 to p = 0.050, and concrete compressive strength varying in increments of 1,000 psi from f'_c = 1,000 psi to f'_c = 6,000 psi. The assumed strain in the extreme compressive fibers was varied in increments of 0.0002 in. per in. until the maximum moment or a strain of 0.004 in. per in. was reached. All computations outlined previously were programmed for an LGP-30 electronic computer.

The theoretical ratio $M_u/\left(b\,d^2\,f'_c\right)$ is shown in Fig. 3 as a function of the concrete compressive strength f'_c with the percentage of reinforcement p as a parameter. The area of the graph is divided by a heavy line into two regions: (a) one below the heavy line, in which the dashed lines represent the ultimate bending strength of beams controlled by tension, and (b) the one above the dividing line, in which the full lines represent the strength of beams controlled by compression. The dividing line was determined by the intersections of the two systems of lines, and, thus, represents the ultimate strength of beams with balanced reinforcement for the yield stress f_y = 60,000 psi. The ultimate strength of beams controlled by tension, as obtained by the present method, is in close agreement with the values obtained by Eq. A1 of the ACI Building Code (ACI 318-56).

The variation of the ratio $M_u/\left(d\,b^2\,f'_c\right)$ suggests the possibility of approximating the ultimate flexural strength of rectangular reinforced concrete beams controlled by compression by means of the expression

$$M_u/\left(b\,d^2\,f'_c\right) = R + S\,p - T\,f'_c \quad \ldots\ldots\ldots\ldots \quad (11a)$$

or, specifically,

$$M_u/\left(b\,d^2\,f'_c\right) = 1.64\,p + 0.45\left(1 - 10^{-4}\,f'_c\right) \ldots\ldots\ldots \quad (11b)$$

Eq. 11b was used to compute the ultimate strength of fifty-nine test beams which failed in compression.[9,10,11,12] The results are presented in Table 3 and in Fig. 4. The distribution of the ratio between the test and the calculated

---

9 "Compressive Strength of Concrete in Flexure as Determined from Tests of Reinforced Beams," by W. A. Slater and I. Lyse, Proceedings, ACI, Vol. 26, 1930, pp. 831-874.

10 "Comparative Tests of Concrete Beams Reinforced with Isteg and Hot Rolled Deformed Bars," Columbia University, Report No. 2507, 1941.

11 "Test of Reinforced Concrete Beams with Recommendations for Attaining Balanced Design," by K. C. Cox, Proceedings, ACI, Vol. 38, 1942, pp. 65-80.

12 "The Ultimate Strength of Reinforced Concrete Beams," by S. D. Lash and J. W. Brison, Proceedings, ACI, Vol. 46, 1950, pp. 457-470.

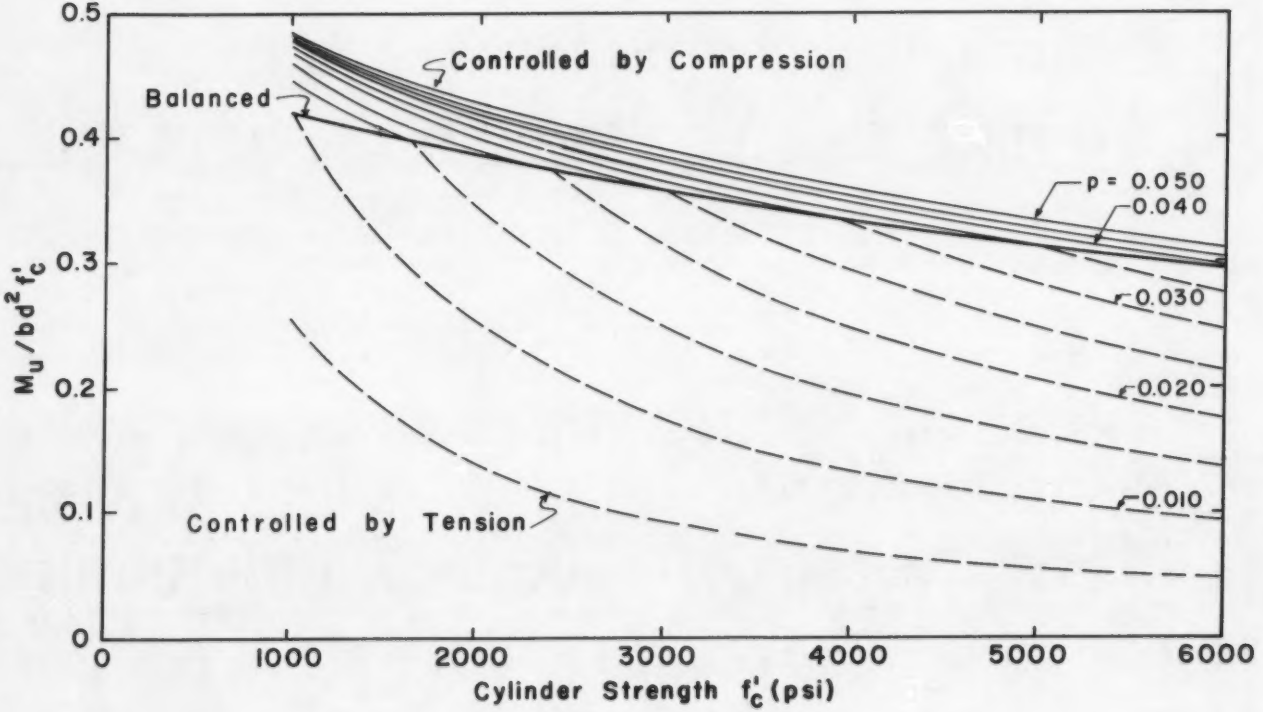

FIG. 3.—THEORETICAL VALUES OF $M_u/(b\,d^2\,f'_c)$

TABLE 3.—COMPRESSION FAILURES OF REINFORCED CONCRETE BEAMS REINFORCED IN TENSION

Source	Beam Number	f'_c, in psi	f_y, in psi	p	$\frac{M_u}{b\,d^2\,f'_c}$		Col. 6 ÷ Col. 7
					Test	Calculated	
(1)	(2)	(3)	(4)	(5)	(6)	(7)	
W. A. Slater and I. Lyse	1	1,390	64.8	0.021	0.506	0.422	1.20
	2	2,790	64.8	0.028	0.337	0.370	0.91
	3	4,070	64.8	0.037	0.326	0.328	0.99
	4	4,800	64.8	0.047	0.339	0.311	1.09
	5	5,740	64.8	0.056	0.320	0.284	1.13
	6	2,590	64.8	0.030	0.422	0.382	1.10
	6A	4,130	64.8	0.039	0.327	0.328	1.00
	7	2,950	64.8	0.028	0.341	0.363	0.94
	8	2,760	64.8	0.031	0.380	0.377	1.01
	9	2,820	64.8	0.032	0.391	0.376	1.04
	10	2,820	64.8	0.030	0.346	0.372	0.93
	10A	3,810	64.8	0.040	0.354	0.344	1.03
Columbia University	C1	3,550	61.37	0.0341	0.406	0.346	1.17
	C11	3,550	62.00	0.0345	0.394	0.347	1.14
	C2	3,550	63.04	0.0334	0.386	0.345	1.12
	C12	3,550	64.28	0.0328	0.365	0.344	1.06
K. C. Cox	122	1,700	53.4	0.0176	0.405	0.402	1.01
	123	1,700	53.4	0.0264	0.423	0.417	1.01
	124	1,700	53.4	0.0352	0.455	0.431	1.06
	125	1,700	53.4	0.0440	0.471	0.446	1.06
	142	1,700	48.1	0.0244	0.442	0.414	1.07
	143	1,700	48.1	0.0368	0.426	0.434	0.98
	144	1,700	48.1	0.0488	0.490	0.454	1.08
	224	3,100	53.4	0.0352	0.343	0.368	0.93
	225	3,100	53.4	0.0440	0.353	0.383	0.92
	243	3,100	48.1	0.0368	0.370	0.371	1.00
	244	3,100	48.1	0.0488	0.375	0.390	0.96
	214	3,100	55.2	0.0308	0.374	0.361	1.04
	215	3,100	55.2	0.0388	0.372	0.374	0.99
	235	3,100	48.1	0.0388	0.381	0.374	1.02
	252	3,100	50.6	0.0348	0.379	0.368	1.03
	253	3,100	50.6	0.0520	0.388	0.395	0.98
	325	4,500	53.4	0.0440	0.320	0.320	1.00
	343	4,500	48.1	0.0368	0.297	0.308	0.96
	344	4,500	48.1	0.0488	0.342	0.328	1.04
	425	5,800	53.4	0.0440	0.293	0.261	1.12
	444	5,800	48.1	0.0488	0.300	0.269	1.12
S. D. Lash and J. W. Brison	4205	1,970	39.2	0.0400	0.449	0.427	1.05
	4206	1,930	44.4	0.0475	0.464	0.441	1.05
	4308	3,330	42.8	0.0454	0.367	0.375	0.98
	4407	4,170	40.8	0.0367	0.305	0.322	0.95
	4408	4,490	43.4	0.0471	0.346	0.325	1.06
	6203	2,150	88.0	0.0140	0.346	0.376	0.92
	6204	2,150	75.8	0.0200	0.333	0.386	0.86
	6205	1,950	75.8	0.0225	0.415	0.399	1.04
	6206	2,080	73.5	0.0284	0.400	0.403	0.99
	6207	1,915	75.2	0.0385	0.391	0.427	0.92
	6208	2,120	75.2	0.0391	0.407	0.419	0.97
	6303	3,290	72.0	0.0147	0.270	0.326	0.83
	6304	2,760	75.8	0.0233	0.347	0.364	0.95
	6305	3,200	74.0	0.0286	0.338	0.352	0.96
	6306	2,760	75.2	0.0394	0.359	0.390	0.92
	6404	4,490	75.8	0.0226	0.263	0.285	0.92
	6405	4,140	74.0	0.0280	0.293	0.310	0.94
	6406	4,190	75.2	0.0390	0.317	0.325	0.98
	6407	4,190	62.1	0.0408	0.314	0.328	0.96
	6504	4,870	75.8	0.0233	0.247	0.269	0.92
	6505	4,450	65.0	0.0371	0.299	0.310	0.96
	6506	5,450	75.8	0.0458	0.292	0.280	1.04
					Average, all beams		1.007
					Standard Deviation, all beams		±0.076

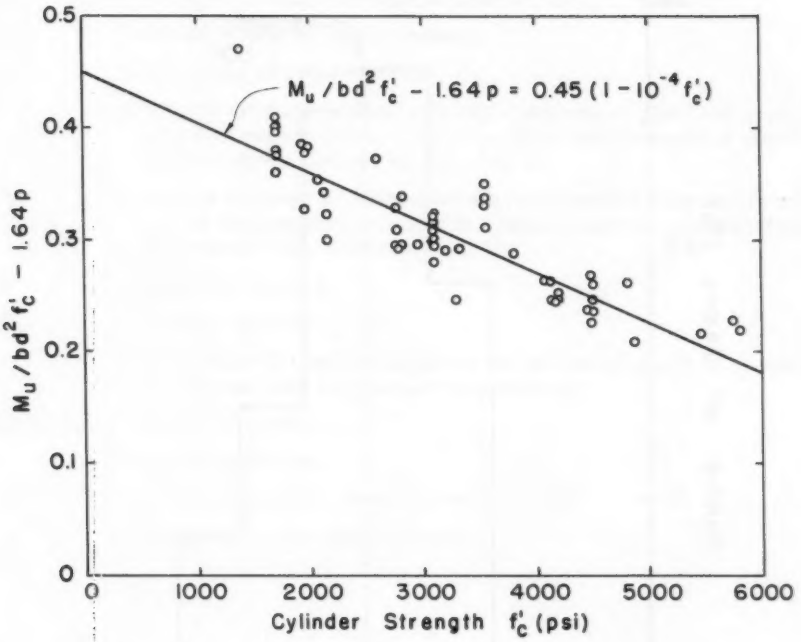

FIG. 4.—TESTS OF FIFTY NINE BEAMS CONTROLLED BY COMPRESSION

moment is shown in a histogram, Fig. 5. The average value of this ratio for the fifty-nine beams is 1.007, with a standard deviation $\pm$ 0.076.

CONCLUSIONS

The ultimate strength of rectangular reinforced concrete beams, when controlled by compression, depends primarily on concrete strength and, to a lesser degree, on the percentage of tensile reinforcement. The relationship between the ultimate strength in bending and the two factors is nonlinear. However, the ratio $M_u/(b\,d^2\,f'_c)$ may be assumed to decrease linearly with increasing concrete strength (within the practical range 2,000 psi to 6,000 psi) for a constant percentage of reinforcement. Similarly, the ratio $M_u/(b\,d^2\,f'_c)$, at a given concrete strength, may be assumed to be proportional to the percentage of reinforcement. An equation based on these two assumptions gives a close approximation of the ultimate bending moment, as confirmed by comparison of test values with the computed values of ultimate moment of fifty-nine test beams, which failed in compression.

ACKNOWLEDGMENT

Most of the numerical computations involved in the preparation of this paper were carried out by means of an electronic computer at the Research and De-

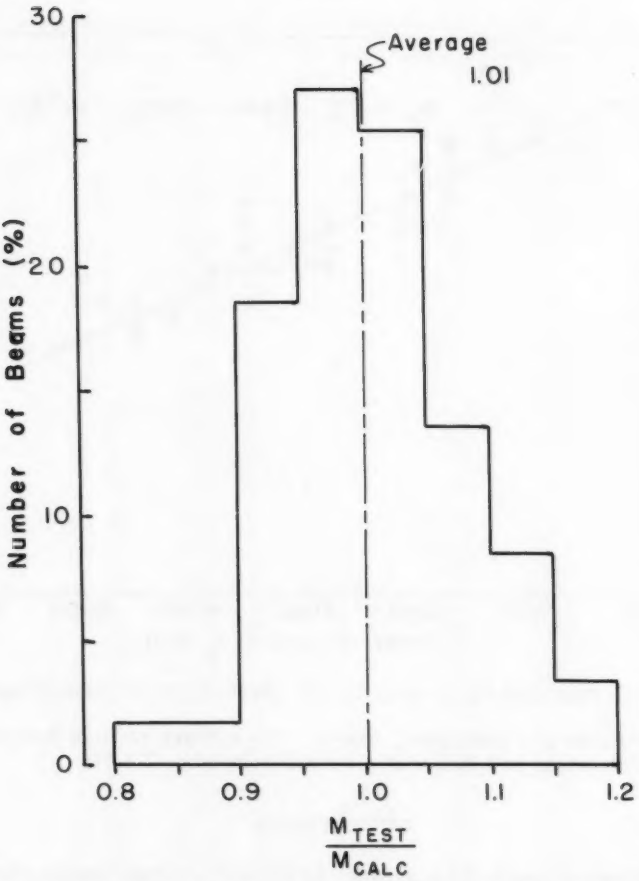

FIG. 5.—HISTOGRAM FOR COMPRESSION FAILURES OF SINGLY REINFORCED REINFORCED CONCRETE BEAMS

velopment Laboratories of the Portland Cement Association. This courtesy is gratefully acknowledged.

NOTATION

A, B, C, D = coefficients which are functions of f'_c;

b = width of rectangular section;

d = distance of extreme compressive fiber to centroid of tensile reinforcement;

E_s = modulus of elasticity of tensile reinforcement;

F, G, H = coefficients which are functions of ϵ;

f = stress in concrete;

f'_c = concrete cylinder strength at time of test;

f_s = stress in tensile reinforcement;

f_y = yield point of reinforcement;

k = ratio of distance between extreme compressive fiber and neutral axis to distance between extreme fiber and centroid of tensile reinforcement, defined by Eqs. 5 or 8;

k_2 = ratio of distance between extreme compressive fiber and resultant of compressive stresses to distance between extreme fiber and neutral axis, defined by Eq. 10;

M = resisting moment;

M_u = ultimate moment;

p = percentage of tensile reinforcement defined by $A_s/(b\ d)$ in which A_s denotes area of tensile reinforcement;

R, S, T = constant coefficients;

ϵ = strain in concrete;

ϵ_c = strain in extreme compressive fiber; and

ϵ_s = strain in tensile reinforcement.

Journal of the
ENGINEERING MECHANICS DIVISION
Proceedings of the American Society of Civil Engineers

EXPERIMENTAL STUDY OF BEAMS ON ELASTIC FOUNDATIONS

By Robert L. Thoms[1]

SYNOPSIS

The design and use of a structural model for the solution of shear and moment in a beam on an elastic foundation is presented. Through use of the model, a typical problem of a laterally loaded pile foundation is solved as an example.

THE PROBLEM

Shear and moment in a loaded beam on an elastic foundation can be calculated if the solution of the differential equation relating beam deflection and load is available and if the deflection-reaction characteristics of the supporting foundation are known. It will be assumed in this study that deflection-reaction characteristics of the supporting foundation are known. The differential equation relating load and deflection[2] is of the form,

$$q = \frac{d^4y}{dx^4} \quad \ldots\ldots\ldots\ldots\ldots\ldots \quad (1)$$

Numerical methods of solving Eq. 1 for the bending of a beam on a continuous elastic foundation generally make use of an assumption by Winkler, that the reaction forces of the foundation at any point are proportional to the deflection of the beam at that same point.[3] The effect of this assumption is to represent

Note.—Discussion open until November 1, 1960. To extend the closing date one month, a written request must be filed with the Executive Secretary, ASCE. This paper is part of the copyrighted Journal of the Engineering Mechanics Division, Proceedings of the American Society of Civil Engineers, Vol. 86, No. EM 3, June, 1960.

[1] Inst. of Engrg. Mechanics, The Univ. of Texas, Austin, Texas.

[2] "Strength of Materials, Part II," by S. Timoshenko, New York, Van Nostrand, p. 2.

[3] Ibid., p. 1.

the beam as being supported by closely spaced coil springs acting independently of each other. The solution of a foundation problem based on the Winkler assumption neglects any existing shear between adjacent supports. It is also assumed that negative reactions may exist on the elastic beam.

The method of solution presented herein is an alternate procedure to numerical methods for finding deflections of a beam on an elastic foundation. This method has the advantage of being more rapid than numerical computation by means of desk computers, and less expensive than computation involving large electronic computers. Foundation problems with any pattern of variation of reaction modulus with distance along the beam can be solved. Further-

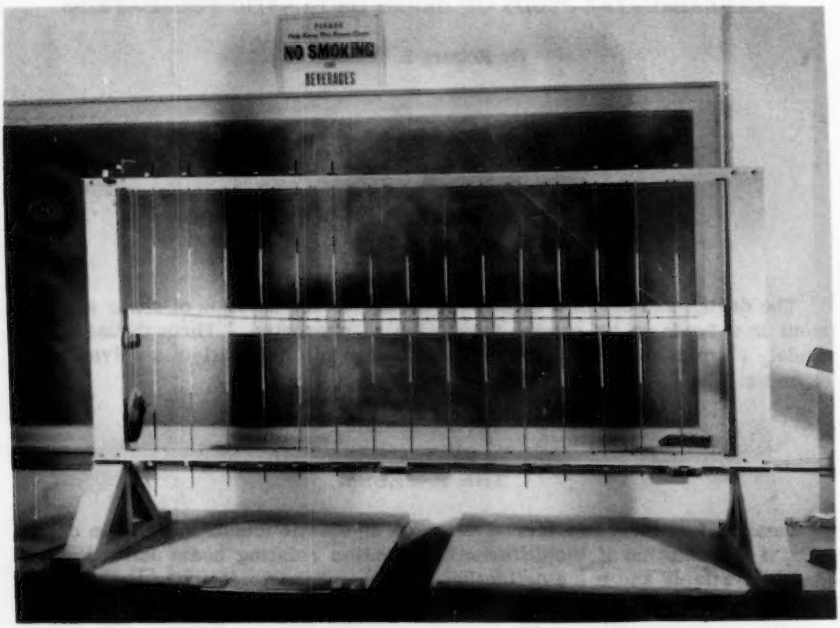

FIG. 1.—MODEL LOADED

more, this method can readily accommodate changes in E I in the elastic beam, and could be extended to provide solutions where structural restraints are involved in the beam. Although this method has the property of being less exact than numerical methods, it should be noted than the accuracy with which soil reaction characteristics can be determined does not necessitate a more exact solution.

METHOD OF SOLUTION

The method used involves a structural model that is a physical adaptation of the Winkler beam. Basically, the model consists of an elastic beam support-

ed by closely spaced coil springs. The model was designed for the purpose of predicting the deflection curve of a loaded elastic beam on an elastic foundation. Reactions on the beam may be found by use of the predicted deflection curve of the beam and the reaction modulus of the supporting foundation. Shear and moment in the beam may then be calculated by successive integration of the reactions on the beam.

A problem with a supporting foundation possessing non-linear deflection-reaction characteristics can be solved by use of an iteration process. The iteration process is necessary for the model, essentially a linear system, to represent non-linear effects.

In the example problem of this study the model was designed for the purpose of predicting the deflection curve of a laterally loaded pile foundation. The predicted deflections of the pile, obtained by use of the model, were used in an iteration process to determine the effective secant soil reaction moduli, E'_s, of the supporting soil. The iteration process was used in adjusting the model to represent the non-linear effects of the supporting soil reaction on the pile. Supporting soil reactions on the pile were then obtained by multiplying the predicted pile deflections by the determined effective secant soil reaction moduli. With the reactions on the pile available, a complete solution of the problem was possible.

The method of solution described for the example pile problem is different from existing numerical methods only in that the model was used to obtain the deflection curve of the loaded pile. The advantage of the model is that it may be used to obtain the deflection curve quite rapidly, thereby greatly reducing the time spent in the iteration process used in determining the effective secant soil reaction moduli, E'_s.

SIMILITUDE REQUIREMENTS

The system to be represented by the model consists of (1) the elastic beam and (2) the supporting foundation. The elastic beam was represented in the model by a cylindrical steel rod with a flexural rigidity and length determined by flexural similitude requirements. The supporting foundation was represented in the model by a series of closely spaced elastic supports. Each support consisted of a pair of coil springs in opposing tension as shown in Fig. 1. Providing there are n model supports equally spaced, each model support represents an increment of supporting foundation of length, L_p/n.

It is required that the model have a deflection curve similar to that of the actual pile or prototype undergoing study. If it is to do this, the model must satisfy certain similitude requirements. These requirements may be determined by the methods of dimensional analysis.[4]

The deflection y at a distance x from the loaded end of the beam, in Fig. 2, depends on P, E I, x, j, and L.

Let $(P)_m$, $(E\,I)_m$, $(x)_m$, $(j)_m$, and $(L)_m$ be the model factors; and $(P)_p$, $(E\,I)_p$, $(x)_p$, $\left(E_r \frac{L_p}{n}\right)$, and $(L)_p$, be the prototype factors.

By dimensional analysis:

$$\left(\frac{y}{L}\right)_p = Q\left(\frac{P\,L^2}{E\,I}\,,\ \frac{E_r\,\frac{L}{n}}{\frac{P}{L}}\,,\ \frac{x}{L}\right)_p \qquad (2)$$

4 "Similitude in Engineering," by Glen Murphy, New York, The Ronald Press Co., 1950, pp. 112-113, 118-123.

and

$$\left(\frac{y}{L}\right)_m = Q\left(\frac{P\,L^2}{E\,I}\,,\ \frac{j}{\frac{P}{L}}\,,\ \frac{x}{L}\right)_m \quad \ldots\ldots\ldots\ldots (3)$$

It is required that $Q_p = Q_m$, therefore

$$\left(\frac{P\,L^2}{E\,I}\right)_p = \left(\frac{P\,L^2}{E\,I}\right)_m \quad \ldots\ldots\ldots\ldots\ldots (4)$$

$$\left(\frac{E_r\,\frac{L}{n}}{\frac{P}{L}}\right)_p = \left(\frac{j}{\frac{P}{L}}\right)_m \quad \ldots\ldots\ldots\ldots\ldots (5)$$

and

$$\left(\frac{x}{L}\right)_p = \left(\frac{x}{L}\right)_m \quad \ldots\ldots\ldots\ldots\ldots (6)$$

Eqs. 4 and 5 may be combined to give,

$$\left(\frac{\frac{E\,I}{L^3}}{j}\right)_m = \left(\frac{\frac{E\,I}{L^3}}{E_r\,\frac{L}{n}}\right)_p \quad \ldots\ldots\ldots\ldots (7)$$

Eq. 7 was the basic relation observed, along with Eq. 6, in design and adjustment of the model. It should be remarked that the structural model referred to in this study is not generally a simple scaled-down version of a prototype beam, as this would have limited its versatility. The basic requirements, Eqs. 4 and 5, were combined into Eq. 7 to permit convenient representation of any prototype by the model.

PREDICTION EQUATIONS

The relation between deflection of the model and prototype may be established on the basis of dimensional analysis. This relation is generally referred to as the prediction equation for the model.[5]

Since

$$\left(\frac{y}{L}\right)_p = \left(\frac{y}{L}\right)_m \quad \ldots\ldots\ldots\ldots\ldots (8)$$

and Eq. 4 must be true, the combination of Eqs. 4 and 8 yields the prediction equation for the model:

$$\left(\frac{y}{\frac{P\,L^3}{E\,I}}\right)_p = \left(\frac{y}{\frac{P\,L^3}{E\,I}}\right)_m \quad \ldots\ldots\ldots\ldots (9)$$

---

5 Ibid., p. 99.

or

$$y_p = y_m \left(\frac{P L^3}{E I}\right)_p \left(\frac{E I}{P L^3}\right)_m \quad \ldots\ldots\ldots\ldots (10)$$

In a similar fashion, the prediction equation for the model loaded with an applied concentrated moment is,

$$\frac{y_p}{y_m} = \frac{\left(\frac{M L^2}{E I}\right)_p}{\left(\frac{M L^2}{E I}\right)_m} \quad \ldots\ldots\ldots\ldots\ldots (11)$$

Eq. 11 may be written as

$$y_p = y_m \left(\frac{M L^2}{E I}\right)_p \left(\frac{E I}{M L^2}\right)_m \quad \ldots\ldots\ldots\ldots (12)$$

DESCRIPTION OF THE MODEL

The model used for this study consists of a cylindrical steel rod representing a beam and a series of adjustable coil spring supports representing the

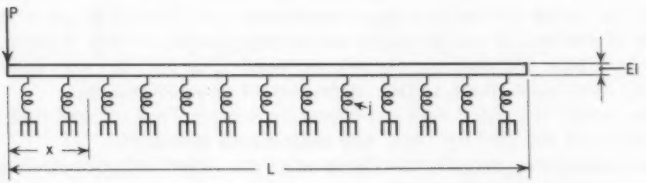

FIG. 2.—TYPICAL BEAM

foundation support. Fig. 1 shows the model with a load applied at one end. The elastic rod seen in the center of the supporting frame of the model represents the beam. This particular rod is 60 in. in length. Outside dimensions of the relatively rigid supporting frame are 31 in. by 6 ft. Each coil spring is connected to the supporting frame of the model with a device by means of which the length of the coil spring supporting the elastic rod can be quickly and conveniently changed, thereby allowing any support a range of spring constants.

The model may be loaded by a weight suspended over a pulley or by a free-hanging weight. Care must be taken that a closure of any coil springs is avoided. Deflections of the rod are obtained by recording, both before and after loading, the vertical positions of pointers clamped on the rod. To eliminate reading parallax, an engineers transit was used at approximately 15 ft from the model to note the positions of the pointers on the grid immediately behind the rod.

USE OF MODEL IN PROBLEM SOLUTIONS

The model may be used to solve for the deflection of a beam on an elastic foundation possessing (a) linear deflection-reaction characteristics, or (b) non-linear deflection-reaction characteristics.

The following procedure is used to solve the linear case:

(1) Preliminary calculations are used in selecting a suitable elastic rod to represent the beam. Prototype characteristics and initial arbitrarily fixed model characteristics are substituted in Eq. 7 to determine the approximate dimensions of a satisfactory rod.

(2) On the basis of the prototype conditions and the selected elastic rod, the coil springs may be adjusted to represent the foundation reaction moduli.

(3) The model is loaded with any convenient magnitude of load that does not cause closure of the coil springs, and deflections measured.

(4) The deflections may be used to predict prototype deflections through use of prediction equations.

(5) The predicted deflections of the prototype may be used to find the foundation reactions on the elastic beams through use of the reaction moduli.

(6) The moment and shear diagrams can be obtained by successive integration of the reactions on the beam, and then used to calculate stress in the beam.

The non-linear case is solved with the model by the following procedure:

(a) This step is identical to step 1 for the linear case.

(b) On the basis of the prototype conditions and the selected elastic rod, estimates of deflection can be made and corresponding secant moduli obtained from the available foundation reaction curves. The coil springs may then be adjusted to represent these initial estimates of reaction moduli.

(c) The model is loaded with any convenient magnitude of load that does not cause closure of the coil springs, and deflections measured.

(d) The deflections may be used to predict prototype deflections through use of prediction equations. The predicted prototype deflections are plotted on the foundation reaction curves and new estimates of the reaction moduli determined.

(e) The model supports are adjusted to represent the second estimate of the effective foundation reaction moduli.

(f) Steps c, d, and e are repeated until the effective secant foundation reaction moduli are determined completely. The effective secant foundation reaction moduli are determined when the reaction moduli obtained in the course of the trial and adjustment process converge to sufficiently constant values.

(g) The final deflection of the model with supports correctly adjusted is used to predict deflections of the prototype. The predicted deflection of the prototype is transformed into foundation reaction on the pile by use of the effective secant foundation reaction moduli determined previously.

(h) This step is identical to step 6 in the solution of the linear case.

EXAMPLE PROBLEM

The following example illustrates the solution of a hypothetical problem through use of the model. The hypothetical problem is the analysis of moment and shear in a laterally loaded pile foundation.

The analysis entailed in designing a laterally loaded pile involves two major problems: (1) Soil reaction curves must be obtained, and (2) the deflection of the pile must be calculated in order to solve for shear and moment.[6] This study is concerned primarily with the second problem, and soil characteristics are assumed to be known.

There are, generally, two methods of solving for the shear and moment in a laterally loaded pile: (1) methods involving limit analysis, and (2) methods based on elastic characteristics.[7] Although a physical model may be adjusted

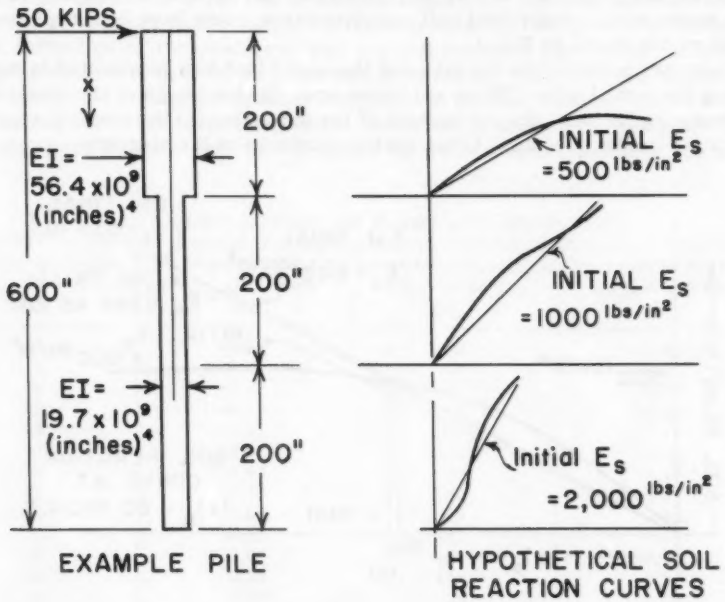

P = 50 KIPS APPLIED LATERALLY AT x = 0.

L = 600 INCHES.

$EI = 56.4 \times 10^9 (\text{INCHES})^4$ FOR $0 \le x \le 200$ INCHES.

$EI = 19.7 \times 10^9 (\text{INCHES})^4$ FOR $200 \le x \le 600$ INCHES.

INITIAL ASSUMED VALUES OF E_s =

$500^{\text{lbs./in.}}$ PER INCH FOR $0 \le x \le 200"$,

$1000^{\text{lbs./in.}}$ PER INCH FOR $200 \le x \le 400"$,

$2000^{\text{lbs./in.}}$ PER INCH FOR $400 \le x \le 600"$.

FIG. 3.—DATA ASSUMED FOR PROTOTYPE PILE

[6] "Non-Dimensional Solutions for Laterally-Loaded Piles With Soil Modulus Assumed Proportional to Depth," by Lymon C. Reese and Hudson Matlock, Proceedings of Eighth Texas Conference on Soil Mechanics and Foundation Engineering, 1956, pp. 4-5.

[7] Ibid., p. 13.

so as to use either approach, this study will be restricted to an analysis based on a representation of the pile foundation as an elastic beam on an elastic foundation.

Fig. 3 shows the given prototype data and the hypothetical available soil reaction curves at various depths in the soil. The soil was divided into three layers, each layer possessing the soil reaction curve shown. As the soil reaction curves are non-linear, it follows that the procedure previously described for use of the model in representing non-linear foundation systems will be used in solving the problem. It may be pointed out that up to fifteen layers of soil, each possessing an individual soil reaction curve, could have been represented by the model shown in Fig. 1.

There are initially four variables of the model that may be adjusted in representing the actual pile. These variables are: (1) the length of the elastic rod representing the pile, (2) the spacing of the supports, (3) the flexural rigidity, E I, of the model pile, and (4) the spring constants of the supports.

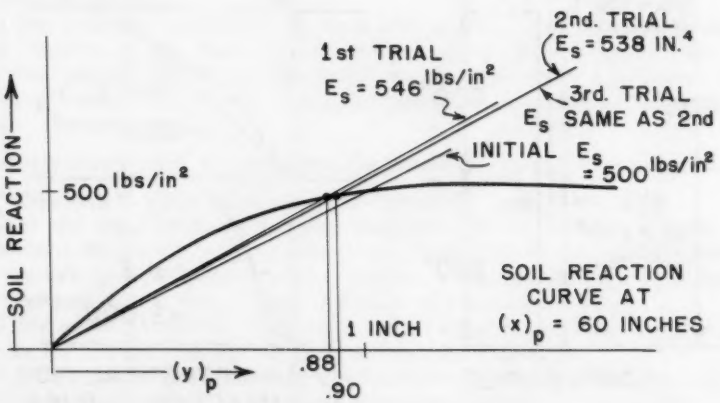

FIG. 4.—SOIL REACTION CURVE

The length of the elastic rod representing the pile was arbitrarily selected as 60 in., thereby establishing a scale ratio of 10 between prototype and model. The supports were arbitrarily spaced at 4-in. equal intervals, with the first and last support being 2 in. from the ends of the elastic rod. This gave a total of fifteen supports. The length of soil support on the prototype represented by each model support was then 40 in. The remaining two variables, the flexural rigidity of the elastic rod and the spring constants of the model supports, were determined from Eq. 7 with prototype data substituted, and a consideration of properties of available coil springs and rods. Coil springs with a range of spring constants from approximately 0.55 lb per in. to 7.00 lb per in. depending on the length of coil spring active in supporting load were used for the model supports. A steel cylindrical rod, 60 in. in length, with a change in section at x_m = 20 in., and with $E I_m$ = 4,930 lb.-in.^{2} for 0 in. $\leqq x \leqq$ 20 in. and $E I_m$ = 1,720 lb-in.^{2} for 20 in. $\leqq x \leqq$ 60 in., was selected to represent the prototype pile.

With the establishment of the dimensions of the steel rod and the spacing of supports, it was possible to use Eq. 7 to determine the spring constants of the model supports such that the initial estimated secant soil reaction moduli shown in Fig. 3 would be represented. After all spring constants had been determined, the model supports were adjusted to possess the necessary constants on the basis of the assumption that the spring constant of any coil spring was inversely proportional to the length of spring active in supporting load.

The model was loaded with a concentrated lateral force of 2 lb at the end of the rod corresponding to the top of the prototype pile. Deflections were measured and used to predict prototype deflections with Eq. 10. By use of the predicted deflection of the prototype and the soil reaction curves for each soil support, a new soil reaction modulus was determined. This modulus was taken as the slope of a straight line from the origin of the soil reaction curve to the point on the curve corresponding to the predicted deflection. This procedure generally gave a better estimate of the effective secant soil reaction modulus

TABLE 1.—DEFLECTIONS OF MODEL AND PROTOTYPE

Location on Model $(x)_m$, in inches (1)	Measured Deflection $(y)_m$, in inches (2)	Location on Prototype $(x)_p$, in inches (3)	Predicted Deflection $(y)_p$, in inches (4)
0	-0.68	0	-1.49
4	-0.51	40	-1.11
8	-0.32	80	-0.70
12	-0.18	120	-0.39
16	-0.08	160	-0.17
20	-0.01	200	-0.02
24	0.03	240	0.07
28	0.03	280	-0.07
32	0.03	320	0.06
36	0.01	360	0.02
40	0.01	400	0.02
44	0.00	440	0.00
48	0.00	480	0.00
52	0.00	520	0.00
56	-0.01	560	-0.01
60	-0.01	600	-0.02

than the initial assumed value. The model supports were then readjusted so as to reproduce the effect of the newer soil reaction moduli. The model was reloaded and deflections recorded. Prototype deflections were predicted on the basis of the second set of model deflections, and soil reaction moduli again determined. This procedure was repeated until the secant soil reaction moduli converged to effectively constant values.

The soil reaction curve of the soil support at $x_p = 60$ in. is shown in Fig. 4. The initial and subsequent soil reaction moduli used in the calculations are also shown. Only three trials were necessary to determine the effective secant soil reaction modulus, E'_s, illustrating the rapid convergence of the method of this study.

Table 1 shows measured deflections of the model pile. Soil reactions on the actual pile obtained from the soil reaction curve and the final values of the predicted deflections are shown in Col. 4 of Table 2.

The shear and moment diagrams computed from the soil reactions for the laterally-loaded pile are shown in Figs. 5 and 6. The diagrams were obtained by integrating successively the reactions from the loaded end of the pile.

Apparent error of this solution is indicated by the failure of the moment and shear diagrams to close to zero at x_p = 580 in. The magnitude of error shown is typical of the method of solution of this study. It may be pointed out that as the reactions were integrated successively from the loaded end of the beam, any small errors shear at the loaded end would have become a magnified error in moment at the unloaded end. In the neighborhood of the more important maximum moment, the value of moment obtained by the integration process is not so easily affected as the moment near the unloaded end of the pile.

TABLE 2.—RESULTS FOR THE PROTOTYPE PILE

Location on Prototype $(x)_p$, in inches	Predicted Average Deflections Over Soil Supports $(y)_p$, in inches	Effective Secant Soil Reaction Moduli E_s' in psi	Soil Reactions on Pile $\left[(y)_p E_s' \frac{(L)_p}{n}\right]$ in kips
20	-1.30	382	19.8
60	-0.91	538	19.6
100	-0.55	640	14.1
140	-0.29	800	9.3
180	-0.10	892	3.6
220	0.03	1000	-1.2
260	0.07	1750	-4.9
300	0.06	2000	-4.8
340	0.04	1820	-2.9
380	0.02	1540	-1.2
420	0.01	640	-0.3
460	0.00	910	0.0
500	0.00	850	0.0
540	0.00	1250	0.0
580	-0.01	1250	0.5

With the shear and moment in the pile obtained to a reasonable degree of accuracy, the stress could be calculated in the conventional manner.

After some experience in use of the model, no doubt closer initial estimates of the effective secant soil reaction moduli could be made, thereby reducing the time required to obtain a satisfactory solution.

CONCLUSIONS AND FURTHER USES OF THE MODEL

The major advantage of the model is that it makes possible a reasonably accurate solution of a complicated problem with a small amount of labor and expense. The model can be used to solve for shear and moment in an elastic beam on an elastic foundation with any of the following characteristics: (1) any variation of E_r with x, (2) changes in E I of the beam, and (3) structural restraints on the beam. Shear and moment in an elastic beam with the foregoing characteristics can be solved by numerical or computer methods. However, these methods are not generally simple and convenient to use.

A difficult problem that may be solved by use of the model is a laterally loaded pile foundation with all of the previously listed characteristics. This problem cannot be readily analyzed by non-dimensional solutions such as are available for pile foundations with E_S = constant and E_S = k x.

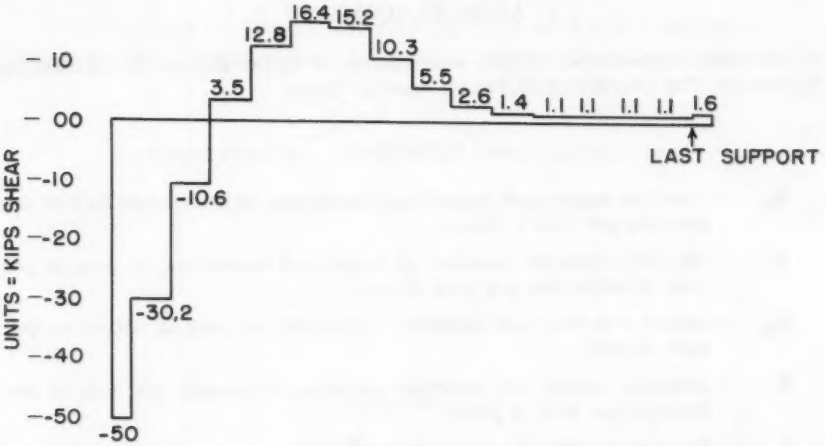

FIG. 5.—SHEAR DIAGRAM FOR TYPICAL PROBLEM

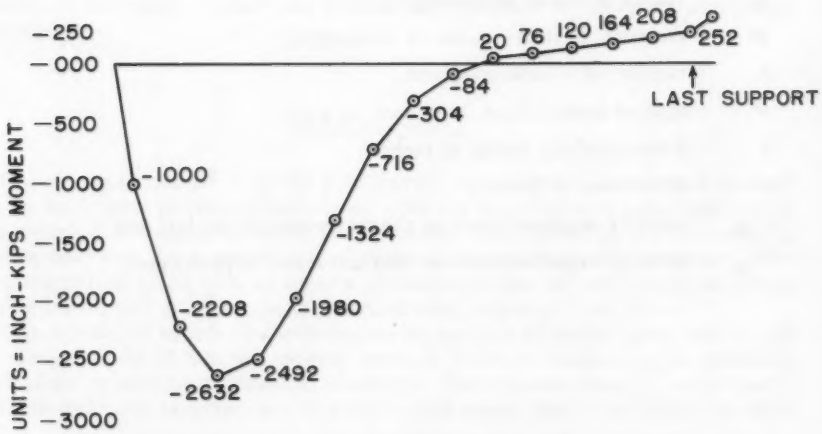

FIG. 6.—MOMENT DIAGRAM FOR TYPICAL PROBLEM

It would also be possible for the model to be extended to solve problems of grid-type beams. In this case, the model would be a more exact representation of the prototype than in the case of a prototype involving a continuous supporting foundation.

A benefit obtained through experience with the model would be insight into the action of the beam-foundation system. The model could also be used as a supplement to numerical methods. Gross errors in computation could be detected rapidly from a rough check obtained with the model.

ACKNOWLEDGMENTS

The work reported on herein was sponsored by the Bureau of Engineering Research, The University of Texas, Austin, Texas.

NOTATION

E_r = reaction modulus of supporting foundation, in pounds per inch of deflection per inch of beam;

E'_r = effective reaction modulus of supporting foundation, in pounds per inch of deflection per inch of pile;

E_s = secant soil reaction modulus, in pounds per inch of deflection per inch of pile;

E'_s = effective secant soil reaction modulus, in pounds per inch of deflection per inch of pile;

EI = flexural rigidity, in pound-inches^2;

j = spring constant of an elastic support, in pounds per inch of deflection;

L = length of beam, in inches;

M = moment, in inch-pounds or inch-kips;

n = number of elastic supports;

P = applied lateral load, in pounds or kips;

x = distance along beam, in inches;

y = deflection, in inches;

$( )_m$ = quantity in parenthesis is characteristic of model; and

$( )_p$ = quantity in parenthesis is characteristic of prototype.

Journal of the
ENGINEERING MECHANICS DIVISION
Proceedings of the American Society of Civil Engineers

ASYMMETRICAL BENDING OF CONICAL SHELLS

By Bayard Wilson,[1] J. M. ASCE

SYNOPSIS

The equations of Goldenveizer's theory are specialized to the case of conical shells. A method of solution is developed applicable to truncated cones of finite length simply supported along two generators and having any type of support at the ends. Numerical results are obtained by using an electronic computer.

INTRODUCTION

Recent publications[2,3] on the problem of asymmetrical bending of conical shells have been primarily concerned with the derivation of equations, while it appears that relatively little progress has been made in the direction of finding solutions from which numerical results can be readily obtained. The purpose of this paper is to present a practical method by which such solutions can be found, and to illustrate the method with numerical examples.

The method is based on a well-known separation of variables technique and the development of a power series form of solution relative to an ordinary part of the system of differential equations. The series converge very slowly, but this difficulty is overcome by using a high speed digital computer for their

Note.—Discussion open until November 1, 1960. To extend the closing date one month, a written request must be filed with the Executive Secretary, ASCE. This paper is part of the copyrighted Journal of the Engineering Mechanics Division, Proceedings of the American Society of Civil Engineers, Vol. 86, No. EM 3, June, 1960.

[1] Asst. Prof., Engrg. Mechanics, Univ. of Kansas, Lawrence, Kans.

[2] "Thin Circular Conical Shells Under Arbitrary Loads," by N. J. Hoff, Journal of Applied Mechanics, Vol. 22, No. 4, 1955, pp. 557-562.

[3] "A Donnell Type Theory for Asymmetrical Bending and Buckling of Thin Conical Shells," by P. Seide, Journal of Applied Mechanics, Vol. 24, No. 4, 1957, pp. 547-552.

evaluation. The method is applicable to cases where cross-sections are complete circles, and to the special case of axial symmetry, although the present work shall not be concerned with the latter.

Before a particular problem can be attacked, a general theory of shells must be accepted. The question of what constitutes a suitable theory has been the source of considerable disagreement in the literature, but for present purposes, the point of view expounded by the Russian theoretician A. L. Goldenveizer[4] shall be accepted. Although it has some rather appealing qualities, this point of view seems not to have attracted much attention among Western theoreticians (perhaps because of an unfortunate language barrier). It is proposed to apply the simplest possible theory, based on the Kirchhoff hypothesis, for which a unique theorem can be proved in the same manner as was done by Kirchhoff for the classical theory of elasticity, and for which a (Rayleigh-Betti) theorem of reciprocity of work can be proved. The formal requirements of such a theory were first established in an important theoretical paper.[5]

One of the principal points of departure in the development of a Kirchhoffean theory of shells is the choice of stress-strain relations, that is, relations between the stress resultants and components of deformation. Goldenveizer contends that the most suitable choice is the simplest one which satisfies the requirements of the previously mentioned theorems, and is therefore free of formal contradiction. A variety of stress-strain relations will fulfill these requirements, and it is suggested that the variant most convenient for the solution of the particular problem at hand be chosen.[6] When the stress-strain relations have been chosen, a basic system of differential equations governing the displacements of the middle surface of a shell can be easily obtained from equations governing the equilibrium of stress resultants.

BASIC DIFFERENTIAL EQUATIONS

Let x_1 and x_2 be coordinates in the middle surface of a shell along lines of principal curvature having radii R_1 and R_2. If z is the coordinate on an outward normal to the middle surface, then the length of a line element in space can be expressed in the form

$$(ds)^2 = A_1^2 \left(1 + \frac{z}{R_1}\right)^2 (dx_1)^2 + A_2^2 \left(1 + \frac{z}{R_2}\right)^2 (dx_2)^2 + (dz)^2 \quad \ldots\ldots (1)$$

The stress resultants may be defined in terms of stress as follows:

$$N_1 = \int_{-h}^{h} \sigma_1 \left(1 + \frac{z}{R_2}\right) dz \quad \ldots\ldots\ldots\ldots\ldots (2a)$$

$$N_2 = \int_{-h}^{h} \sigma_2 \left(1 + \frac{z}{R_1}\right) dz \quad \ldots\ldots\ldots\ldots\ldots (2b)$$

---

[4] "Theory of Thin Elastic Shells," by A. L. Goldenveizer, Gostekhteoretizdat, 1953. (in Russian).

[5] "On the Applicability of General Theorems of the Theory of Elasticity to Thin Shells," by A. L. Goldenveizer, Prit. Mat, i Mekh., Vol. 8, No. 1, 1944, pp. 1-14 (in Russian with English summary).

[6] "Theory of Thin Elastic Shells," pp. 70-71, 80-82.

$$N_{12} = \int_{-h}^{h} \tau_{12} \left(1 + \frac{z}{R_2}\right) dz \quad \ldots\ldots\ldots\ldots\ldots (2c)$$

$$N_{21} = \int_{-h}^{h} \tau_{21} \left(1 + \frac{z}{R_1}\right) dz \quad \ldots\ldots\ldots\ldots\ldots (2d)$$

$$M_1 = \int_{-h}^{h} \sigma_1 \left(1 + \frac{z}{R_2}\right) z\, dz \quad \ldots\ldots\ldots\ldots\ldots (2e)$$

$$M_2 = \int_{-h}^{h} \sigma_2 \left(1 + \frac{z}{R_1}\right) z\, dz \quad \ldots\ldots\ldots\ldots\ldots (2f)$$

$$M_{12} = \int_{-h}^{h} \tau_{12} \left(1 + \frac{z}{R_2}\right) z\, dz \quad \ldots\ldots\ldots\ldots\ldots (2g)$$

$$M_{21} = \int_{-h}^{h} \tau_{21} \left(1 + \frac{z}{R_1}\right) z\, dz \quad \ldots\ldots\ldots\ldots\ldots (2h)$$

$$Q_1 = \int_{-h}^{h} \tau_{1z} \left(1 + \frac{z}{R_2}\right) dz \quad \ldots\ldots\ldots\ldots\ldots (2i)$$

$$Q_2 = \int_{-h}^{h} \tau_{2z} \left(1 + \frac{z}{R_1}\right) dz \quad \ldots\ldots\ldots\ldots\ldots (2j)$$

in which 2h is the thickness of the shell. The positive sense of the stresses δ_1, τ_{12}, etc., is that customarily taken in the theory of elasticity.

With these definitions, the equations governing the equilibrium of the stress resultants are

$$\left(A_2 N_1\right)_{,1} + \left(A_1 N_{21}\right)_{,2} + A_{1,2}\, N_{12} - A_{2,1}\, N_2 + \frac{A_1 A_2}{R_1}\, Q_1 + A_1 A_2 X_1 = 0 \quad \ldots (3a)$$

and

$$\left(A_1 N_2\right)_{,2} + \left(A_2 N_{12}\right)_{,1} + A_{2,1}\, N_{21} - A_{1,2}\, N_1 + \frac{A_1 A_2}{R_2}\, Q_2 + A_1 A_2 X_2 = 0 \quad \ldots (3b)$$

$$\left(A_2 Q_1\right)_{,1} + \left(A_1 Q_2\right)_{,2} - \frac{A_1 A_2}{R_1}\, N_1 - \frac{A_1 A_2}{R_2}\, N_2 + A_1 A_2 Z = 0 \quad \ldots (3c)$$

$$\left(A_2 M_1\right)_{,1} + \left(A_1 M_{21}\right)_{,2} - A_{2,1}\, M_2 + A_{1,2}\, M_{12} - A_1 A_2\, Q_1 = 0 \quad \ldots (3d)$$

$$\left(A_1 M_2\right)_{,2} + \left(A_2 M_{12}\right)_{,1} - A_{1,2}\, M_1 + A_{2,1}\, M_{21} - A_1 A_2\, Q_2 = 0 \quad \ldots \quad (3e)$$

and

$$N_{12} - N_{21} + \frac{1}{R_1}\, M_{12} - \frac{1}{R_2}\, M_{21} = 0 \quad \ldots \quad (3f)$$

in which X_1, X_2, and Z are components of the lateral load per unit of middle surface area in the positive x_1, x_2, and z directions respectively. A comma followed by a subscript denotes partial differentiation with respect to the indicated variable. Eq. 3f is the "sixth" equilibrium equation which expresses the equilibrium of moments about an axis normal to the middle surface.

The development of a theory of thin shells is based on the Kirchhoff hypothesis, which is equivalent to assuming that the z components of the strain tensor vanish, that is,

$$e_{1z} = e_{2z} = e_z = 0 \quad \ldots \quad (4)$$

It follows from this, without further approximation, that the remaining components of the strain tensor can be expressed in the form

$$e_1 = \frac{\epsilon_1 + z\, X_1}{1 + \frac{z}{R_1}} \quad \ldots \quad (5a)$$

$$e_2 = \frac{\epsilon_2 + z\, X_2}{1 + \frac{z}{R_2}} \quad \ldots \quad (5b)$$

and

$$e_{12} = \frac{\left(1 - \frac{z^2}{R_1 R_2}\right) \epsilon_{12} + \left[2 + z\left(\frac{1}{R_1} + \frac{1}{R_2}\right)\right] z\, X_{12}}{\left(1 + \frac{z}{R_1}\right)\left(1 + \frac{z}{R_2}\right)} \quad \ldots \quad (5c)$$

in which

$$\epsilon_1 = \frac{1}{A_1}\, u_{,1} + \frac{A_{1,2}}{A_1 A_2}\, v + \frac{1}{R_1}\, w \quad \ldots \quad (6a)$$

$$\epsilon_2 = \frac{1}{A_2}\, v_{,2} + \frac{A_{2,1}}{A_1 A_2}\, u + \frac{1}{R_2}\, w \quad \ldots \quad (6b)$$

$$\epsilon_{12} = \frac{A_1}{A_2}\left(\frac{u}{A_1}\right)_{,2} + \frac{A_2}{A_1}\left(\frac{v}{A_2}\right)_{,1} \quad \ldots \quad (6c)$$

$$X_1 = \frac{1}{A_1}\left(\frac{u}{R_1} - \frac{w_{,1}}{A_1}\right)_{,1} + \frac{A_{1,2}}{A_1 A_2}\left(\frac{v}{R_2} - \frac{w_{,2}}{A_2}\right) \quad \ldots \quad (6d)$$

$$X_2 = \frac{1}{A_2}\left(\frac{v}{R_2} - \frac{w,_2}{A_2}\right),_2 + \frac{A_{2,1}}{A_1 A_2}\left(\frac{u}{R_1} - \frac{w,_1}{A_1}\right) \quad \ldots\ldots (6e)$$

and

$$2X_{12} = \frac{1}{A_2}\left[\left(\frac{u}{R_1}\right),_2 + \frac{u,_2}{R_1} - \left(\frac{w,_1}{A_1}\right),_2\right]$$

$$+ \frac{1}{A_1}\left[\left(\frac{v}{R_2}\right),_1 + \frac{v,_1}{R_2} - \left(\frac{w,_2}{A_2}\right),_1\right]$$

$$+ \frac{A_{2,1}}{A_1 A_2}\left[\frac{w,_2}{A_2} - \left(\frac{1}{R_1} + \frac{1}{R_2}\right) v\right]$$

$$+ \frac{A_{1,2}}{A_1 A_2}\left[\frac{w,_1}{A_1} - \left(\frac{1}{R_1} + \frac{1}{R_2}\right) u\right] \quad \ldots\ldots (6f)$$

with u, v, and w being the displacements of the middle surface in the positive x_1, x_2, and z directions respectively.

It is further assumed that δ_z can be neglected in Hooke's law, which then takes the form

$$\sigma_1 = \frac{E}{1 - \nu^2}\left(e_1 + \nu\, e_2\right) \quad \ldots\ldots (7a)$$

$$\sigma_2 = \frac{E}{1 - \nu^2}\left(e_2 + \nu\, e_1\right) \quad \ldots\ldots (7b)$$

$$\tau_{12} = \frac{E}{2(1+\nu)}\, e_{12} \quad \ldots\ldots (7c)$$

where E is Young's modulus and ν is Poisson's ratio.

The stress-strain relations for a theory of shells can now be obtained by substituting Eqs. 7 and 5 into Eq. 2 and performing the indicated integrations. If the integrations are carried out with all terms containing the factor h^3 being retained, the result is of the Flügge-Vlasov type.[7,8,9] On the other hand, if the terms z/R are neglected in comparison to unity, and then the integrations are carried out, the result corresponds to Love's first approximation.[10]

---

7 "Statik und Dynamik der Schalen," by W. Flügge, Julius Springer, 1934.

8 "Basic Differential Equations in General Theory of Elastic Shells," by V. Z. Vlasov, NACA TM 1241, February, 1951.

9 "General Theory of Shells," by V. Z. Vlasov, Gostekhizdat, 1949 (in Russian).

10 "Treatise on the Mathematical Theory of Elasticity," by A. E. H. Love, Dover, 4th Edition, 1927, Article 329.

When considered from the point of view of what Goldenveizer[11] calls "authentic" accuracy, it is concluded that the latter procedure should be adopted. Because of the inexactness of the fundamental hypothesis, one cannot expect to improve the accuracy of a Kirchhoffean theory of shells by merely applying the more complicated Flügge-Vlasov type stress-strain relations.

Having agreed that the approximations involved in Love's stress-strain relations and the other approximations of the theory are commensurate, what is needed now is a convenient modification of Love's relations to eliminate the contradictions they imply. Applying the following system, suggested by Goldenveizer,[12] which satisfies the requirements of an internally consistent theory,

$$N_1 = \frac{3D}{h^2}\left(\epsilon_1 + \nu\,\epsilon_2\right) \quad \ldots\ldots\ldots\ldots\ldots\ldots (8a)$$

$$N_2 = \frac{3D}{h^2}\left(\epsilon_2 + \nu\,\epsilon_1\right) \quad \ldots\ldots\ldots\ldots\ldots\ldots (8b)$$

$$N_{12} = \frac{3D(1-\nu)}{2h^2}\left(\epsilon_{12} + \frac{2h^2}{3R_2}\,X_{12}\right) \quad \ldots\ldots\ldots\ldots (8c)$$

$$N_{21} = \frac{3D(1-\nu)}{2h^2}\left(\epsilon_{12} + \frac{2h^2}{3R_1}\,X_{12}\right) \quad \ldots\ldots\ldots\ldots (8d)$$

$$M_1 = D\left(X_1 + \nu\,X_2\right) \quad \ldots\ldots\ldots\ldots\ldots\ldots (8e)$$

$$M_2 = D\left(X_2 + \nu\,X_1\right) \quad \ldots\ldots\ldots\ldots\ldots\ldots (8f)$$

$$M_{12} = M_{21} = D(1-\nu)\,X_{12} \quad \ldots\ldots\ldots\ldots\ldots\ldots (8g)$$

where

$$D = \frac{2\,E\,h^3}{3\left(1-\nu^2\right)} \quad \ldots\ldots\ldots\ldots\ldots\ldots (9)$$

These particular stress-strain relations were first written down by V. V. Novozhilov[13,14] and independently by L. I. Balabukh.[15] (The title of this last paper indicates that it may have an important bearing on the present work with conical shells, but in spite of considerable effort, the author has thus far been unable to locate a copy in this country.) It can be seen that these relations satisfy the sixth equilibrium Eq. 3 identically. This is necessary for the proof of the theorems previously mentioned.

The principal difference between the system (Eq. 8) and Love's first approximation is the X_{12} term in the expressions for N_{12} and N_{21}. This term has an important effect on the system of differential equations to be solved for u, v, and w, but it does not imply that there will be a significant difference in the calculated values of N_{12} and N_{21}.

---

11 "Theory of Thin Elastic Shells," p. 71.

12 Ibid., p. 81.

13 "A New Method of Calculating Thin Shells," by V. V. Novozhilov, Akad. Nauk SSSR, Otd. Tekh. Nauk, Izvestiia, No. 1, 1946, pp. 35-48 (in Russian).

14 "Theory of Thin Shells," by V. V. Novozhilov, Sudpromgiz, 1951, p. 50 (in Russian).

15 "Bending of Torsion of Conical Shells," by L. I. Balabukh, Tsentral'ni Aero-Gidrodinam. Inst., Trudy, No. 577, Moscow, 1946 (in Russian).

When Q_1 and Q_2 are eliminated from the first three equilibrium equations (Eq. 3), and then Eqs. 8 and 6 are substituted, a system of three differential equations governing u, v, and w is obtained. Instead of writing down this system of equations for the general case, conical shells will be specialized, which

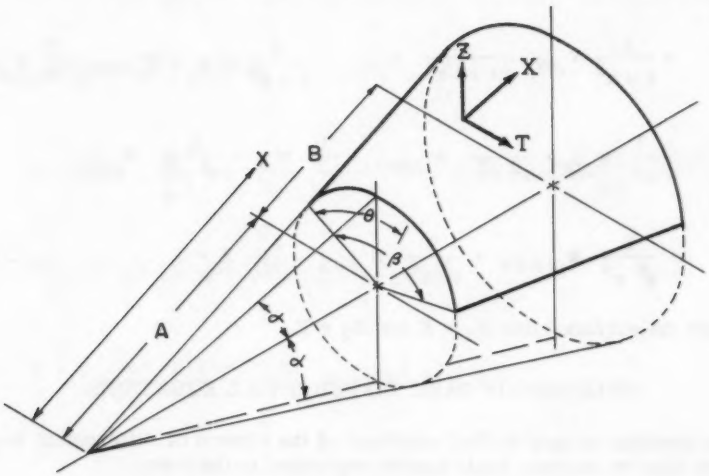

FIG. 1

is the case most concerned with here. This can be achieved by setting (Fig. 1) $x_1 = x$, $x_2 = \theta$, $\frac{1}{R_1} = 0$, $R_2 = t\,x$, $A_1 = 1$, and $A_2 = s\,x$ in which $s = \sin\alpha$, and $t = \tan\alpha$. With these substitutions, the following system of basic differential equations for conical shells is obtained from Eqs. 3, 8, and 6:

$$U_{,xx} + \frac{1}{x}\,u_{,x} - \frac{1}{x^2}\,u + \frac{1-\nu}{2\,s^2x^2}\,u_{,\theta\theta} + \frac{1+\nu}{2\,s\,x}\,v_{,x\theta}$$

$$- \frac{3-\nu}{2\,s\,x^2}\,v_{,\theta} + \frac{\nu}{t\,x}\,w_{,x} - \frac{1}{t\,x^2}\,w + \frac{h^2}{3D}\,X = 0 \quad \ldots\ldots (10a)$$

$$\frac{1+\nu}{2\,s\,x}\,u_{,x\theta} + \frac{3-\nu}{2\,s\,x^2}\,u_{,\theta} + \frac{1-\nu}{2}\,v_{,xx} + \frac{1-\nu}{2x}\,v_{,x} + \frac{1}{s^2x^2}\,v_{,\theta\theta}$$

$$- \frac{1-\nu}{2x^2}\,v + \frac{1}{t\,s\,x^2}\,w_{,\theta} + \frac{h^2}{3}\left[\frac{2(1-\nu)}{t^2\,x^2}\,v_{,xx} - \frac{2(1-\nu)}{t^2\,x^3}\,v_{,x}\right.$$

$$+ \frac{1}{t^2\,s^2\,x^4}\,v_{,\theta\theta} + \frac{2(1-\nu)}{t^2\,x^4}\,v - \frac{2-\nu}{t\,s\,x^2}\,w_{,xx\theta} + \frac{1-2\nu}{t\,s\,x^3}\,w_{,x\theta}$$

$$\left. - \frac{1}{t\,s^3\,x^4}\,w_{,\theta\theta\theta} - \frac{2(1-\nu)}{t\,s\,x^4}\,w_{,\theta}\right] + \frac{h^2}{3D}\,T = 0 \quad \ldots\ldots\ldots (10b)$$

and

$$\frac{\nu}{t\,x}\,u_{,x} + \frac{1}{t\,x^2}\,u + \frac{1}{t\,s\,x^2}\,v_{,\theta} + \frac{1}{t\,x^2}\,w + \frac{h^2}{3}\left[-\frac{2-\nu}{t\,s\,x^2}\,v_{,xx\theta}\right.$$

$$+ \frac{3}{t\,s\,x^3}\,v_{,x\theta} - \frac{1}{t\,s^3\,x^4}\,v_{,\theta\theta\theta} - \frac{4}{t\,s\,x^4}\,v_{,\theta} + w_{,xxxx} + \frac{2}{x}\,w_{,xxx}$$

$$- \frac{1}{x^2}\,w_{,xx} + \frac{2}{s^2\,x^2}\,w_{,xx\theta\theta} + \frac{1}{x^3}\,w_{,x} - \frac{2}{s^2\,x^3}\,w_{,x\theta\theta}$$

$$\left. + \frac{1}{s^4\,x^4}\,w_{,\theta\theta\theta\theta} + \frac{4}{s^2\,x^4}\,w_{,\theta\theta}\right] - \frac{h^2}{3D}\,Z = 0 \quad \ldots\ldots\ldots (10c)$$

in which the surface loads $X_1 = X$ and $X_2 = T$.

SOLUTION OF BASIC DIFFERENTIAL EQUATIONS

The problem is now to find solutions of the system of differential Eq. 10. Suppose that the surface loads can be expressed in the form

$$X = \frac{3D}{h\,x^2}\,X(x)\,\sin ms\theta \quad \ldots\ldots\ldots\ldots\ldots (11a)$$

$$T = \frac{3D\,h}{x^4}\,T(x)\,m\,\cos ms\theta \quad \ldots\ldots\ldots\ldots (11b)$$

and

$$Z = \frac{3D\,h}{x^4}\,Z(x)\,\sin ms\,\theta \quad \ldots\ldots\ldots\ldots\ldots (11c)$$

in which $m = \frac{n\,\pi}{s\,\beta}$, and $n = 1, 2, 3, \ldots$

and β is the angle indicated in Fig. 1. Solutions of Eq. 10 can now be written in the form

$$u = h\,U(x)\,\sin ms\theta \quad \ldots\ldots\ldots\ldots\ldots (12a)$$

$$v = h\,V(x)\,m\,\cos ms\theta \quad \ldots\ldots\ldots\ldots\ldots (12b)$$

and

$$w = h\,W(x)\,\sin ms\theta \quad \ldots\ldots\ldots\ldots\ldots (12c)$$

provided U, V, and W satisfy the following system of ordinary differential equations:

$$x^2\,U'' + x\,U' - \left[1 + \frac{(1-\nu)m^2}{2}\right] U - \frac{(1+\nu)m^2}{2}\,x\,V' + \frac{(3-\nu)m^2}{2}\,V + \frac{\nu}{t}\,x\,W' - \frac{1}{t}\,W + X(x) = 0 \quad \ldots\ldots\ldots (13a)$$

$$(1+\nu)\,x^3\,U' + (3-\nu)\,x^2\,U + (1-\nu)\left(x^2 + \frac{4h^2}{3t^2}\right) x^2\,V'' + (1-\nu)\left(x^2 - \frac{4h^2}{3t^2}\right) x\,V' - \left[\left(2m^2 + 1 - \nu\right)x^2 + \frac{2\left(m^2 - 2 + 2\nu\right)h^2}{3t^2}\right] V - \frac{2(2-\nu)}{3t}\,h^2\,x^2\,W'' + \frac{2(1-2\nu)}{3t}\,h^2\,x\,W' + \frac{2}{t}\left[x^2 + \frac{m^2 - 2(1-\nu)}{3}\,h^2\right] W + 2h^2\,T(x) = 0 \quad \ldots\ldots\ldots\ldots (13b)$$

and

$$\frac{3\nu}{t}\,x^3\,U' + \frac{3}{t}\,x^2\,U + \frac{(2-\nu)m^2}{t}\,h^2\,x^2\,V'' - \frac{3m^2}{t}\,h^2\,x\,V' - \left[3\,x^2 + (m^2 - 4)\,h^2\right]\frac{m^2}{t}\,V + h^2\,x^4\,W'''' + 2h^2\,x^3\,W''' - \left(2m^2 + 1\right)h^2\,x^2\,W'' + \left(2m^2 + 1\right)h^2\,x\,W' + \left[\frac{3x^2}{t^2} + m^2\left(m^2 - 4\right)h^2\right] W - 3h^2\,Z(x) = 0 \quad \ldots\ldots\ldots\ldots (13c)$$

in which primes denote differentiation with respect to x.

It is not difficult to see that solutions in the form (Eq. 12) identically satisfy the boundary conditions for simple support on the generators $\theta = 0$ and $\theta = \beta$ (Fig. 1). By setting $\beta = \pi$, then this form can also be applied to complete cones.

If we can find the solution of Eq. 13 which satisfies some prescribed boundary conditions at the ends x = A and x = A + B, then the problem of the bending of a truncated conical shell which is simply supported along two generators and which is under the action of the loads (Eq. 11) will be completely solved. Hence, the next task is to develop solutions of the system of ordinary differential equations (Eq. 13).

A. E. H. Love[10] suggests the use of an asymptotic development of solutions while N. J. Hoff[2] proposes to apply the method of Frobenius.[16] Both of these methods are discussed by F. V. Pohle[17] who asserts that neither is useful for the purpose of obtaining numerical results.

The Frobenius method will be briefly considered. Solutions of the homogeneous equations (Eq. 13) are sought relative to the singular point $x = 0$ in the form

$$U(x) = \sum_{n=o}^{\infty} U_n \, x^{n+r} \quad \ldots\ldots\ldots\ldots\ldots \quad (14a)$$

$$V(x) = \sum_{n=o}^{\infty} V_n \, x^{n+r} \quad \ldots\ldots\ldots\ldots\ldots \quad (14b)$$

and

$$W(x) = \sum_{n=o}^{\infty} W_n \, x^{n+r} \quad \ldots\ldots\ldots\ldots\ldots \quad (14c)$$

This will represent a solution if r is a root of an indicial equation. The point $x = 0$ is said to be a regular singular point since the degree of the indicial equation is equal to the order of the system of differential equations, namely, eight. Certain of the roots will differ by an integer, and hence the general solution of Eq. 13 will contain logarithmic terms. In order to estimate the interval of convergence of the solutions (Eq. 14) the system (Eq. 13) is transformed into a system of eight first order differential equations by setting $U_1 = U$, $U_2 = U'$, $U_3 = V$, $U_4 = V'$, $U_5 = W$, $U_6 = W'$, $U_7 = W'$, and $U_8 = W'''$. Then the homogeneous system (Eq. 13) can be written in the form

$$U_i' = \sum_{j=1}^{8} P_{ij}(x) \, U_j \quad i = 1,2, \ldots, 8 \ldots\ldots \quad (15)$$

The radius of the circle of convergence of the solutions of Eq. 15 and hence Eq. 13 is determined by the singularities of the coefficients p_{ij}. Certain of these have in the denominator the factor $\left[x^2 + (4/3)(h/t)^2\right]$ which arises from the coefficient of V'' in the second member of Eq. 13. If x is thought of as being a complex variable, and the view is extended to that of the Fuchsian theory,[18] then it can be concluded that convergence of the series solutions (Eq. 4) is assured only when $|x| < (2h)/(t\sqrt{3})$. This can hardly be considered a useful range for x. However, it is not unreasonable to argue that, in the coefficients p_{ij}, quantities of the order $(h/t)^2$ can be neglected in comparison to x^2. In this event the solution will converge for all finite x. But if these quantities are neglected, then the differential equations will no longer conform to the requirements of an internally consistent theory. This can be serious under

---

16 "Ordinary Differential Equations," by E. L. Ince, Dover, 1956, p. 396.

17 F. V. Pohle, Journal of Applied Mechanics, Vol. 23, No. 2, 1956, pp. 322-323.

18 E. L. Ince, Chapter XV.

some circumstances, see, for example,[19] where it is shown that improper modification of the stress-strain relations within the frame work of the Kirchhoff hypothesis can lead to an arbitrarily large error in the calculation of long cylindrical shells. But such circumstances for conical shells need not be examined here since the indicated quantities will not be neglected in the solutions to follow.

Instead of attempting to apply the method of Frobenius, observe that since the theory is valid for thin shells only, it follows that solutions of the differential equations (Eq. 10) are not applicable in the neighborhood of the apex of a conical shell. Consequently, it seems logical to seek solutions of the system (Eq. 13) relative to some point away from the apex rather than the point $x = 0$. Such a point will be an ordinary point of the differential equations, and there will be no loss of generality if it is chosen to be the value of x at a transverse boundary of the shell. In order to achieve this, let the distance $A = a\,h$ and the length $B = b\,a\,h$, where a and b are dimensionless parameters with $a >> 1$, and introduce a new independent variable y such that

$$y = \frac{x}{a\,h} - 1 \qquad \ldots\ldots\ldots\ldots\ldots\ldots (16)$$

the differential equations (Eq. 13) now become

$$(y+1)^2\ U'' + (y+1)\ U' - \left[1 + \frac{(1-\nu)m^2}{2}\right] U - \frac{(1+\nu)m^2}{2}\ (y+1)\ V' + \frac{(3-\nu)m^2}{2}\ V + \frac{\nu}{t}\ (y+1)\ W' - \frac{1}{t}\ W + X(y) = 0 \qquad \ldots\ldots\ldots\ldots (17a)$$

$$(1+\nu)(y+1)^3\ U' + (3-\nu)(y+1)^2\ U + (1-\nu)\left[(y+1)^2 + \frac{4}{3t^2\,a^2}\right](y+1)^2\ V'' + (1-\nu)\left[(y+1)^2 - \frac{4}{3t^2\,a^2}\right](y+1)\ V' - \left[\left(2m^2 + 1 - \nu\right)(y+1)^2 + \frac{2\left(m^2 - 2 + 2\nu\right)}{3t^2\,a^2}\right] V - \frac{2(2-\nu)}{3\,t\,a^2}\ (y+1)^2\ V'' + \frac{2(1-2\nu)}{3\,t\,a^2}\ (y+1)\ W' + \frac{2}{t}\left[(y+1)^2 + \frac{m^2 - 2(1-\nu)}{3a^2}\right] W + \frac{2}{a^2}\ T(y) = 0 \qquad \ldots\ldots\ldots\ldots\ldots (17b)$$

---

[19] "Theory of Thin Elastic Shells," p. 236.

and

$$\frac{3\nu a^2}{t}(y+1)^3 U' + \frac{3a^2}{t}(y+1)^2 U + \frac{(2-\nu)m^2}{t}(y+1)^2 V''$$

$$- \frac{3m^2}{t}(y+1) V' - \frac{m^2}{t}\left[3a^2(y+1)^2 + m^2 - 4\right] V + (y+1)^4 W''''$$

$$+ 2(y+1)^3 W''' - (2m^2+1)(y+1)^2 W'' + \left(2m^2+1\right)(y+1) W'$$

$$+ \left[\frac{3a^2}{t^2}(y+1)^2 + m^2\left(m^2-4\right)\right] W - 3 Z(y) = 0 \quad \ldots\ldots\ldots\ldots (17c)$$

in which the primes denote differentiation with respect to y, and X(y), T(y), Z(y) are obtained from Eq. 11 by making the substitution Eq. 15. The transverse boundries of the conical shell are at y = 0 and y = b.

Solutions of Eq. 17 relative to the ordinary point y = 0 are now sought in the form

$$U(y) = \sum_{n=0}^{\infty} u_n y^n, \quad V(y) = \sum_{n=0}^{\infty} v_n y^n, \quad W(y) = \sum_{n=0}^{\infty} w_n y^n \quad \ldots\ldots (18)$$

Reasoning analagous to that indicated in the foregoing shows that solutions in this form will converge for all $|y| < 1$, which includes the region of interest for all conical shells of finite length when the parameters a and b are properly chosen.

It is assumed that the surface loads can be expressed in the form

$$X(y) = \sum_{n=0}^{\infty} X_n y^n \quad \ldots\ldots\ldots\ldots\ldots\ldots\ldots\ldots\ldots\ldots (19a)$$

$$T(y) = \sum_{n=0}^{\infty} T_n y^n \quad \ldots\ldots\ldots\ldots\ldots\ldots\ldots\ldots\ldots\ldots (19b)$$

$$Z(y) = \sum_{n=0}^{\infty} Z_n y^n \quad \ldots\ldots\ldots\ldots\ldots\ldots\ldots\ldots\ldots\ldots (19c)$$

By substituting Eq. 19 and Eq. 18 into Eq. 17, the following recurrence relations are obtained:

$$u_{n+2} = -\frac{1}{(n+1)(n+2)}\left\{(2n+1)(n+1)\, u_{n+1} + \left(n^2 - 1 - \frac{1-\nu}{2} m^2\right) u_n \right.$$

$$- \frac{(1+\nu)m^2}{2}(n+1)\, v_{n+1} - \frac{m^2}{2}\left[(1+\nu)n - 3 + \nu\right] v_n$$

$$\left. + \frac{\nu}{t}(n+1)\, w_{n+1} + \frac{1}{t}(\nu n - 1) w_n + X_n \right\} \quad \ldots\ldots\ldots\ldots\ldots (20a)$$

$$v_{n+2} = -\frac{1}{(1-\nu)\left(1+\frac{4}{3\,t^2\,a^2}\right)(n+1)(n+2)}\Bigg\{(1+\nu)(n+1)u_{n+1}$$

$$+\,[3(1+\nu)n+3-\nu]u_n + [3(1+\nu)n+3-5\nu]u_{n-1}$$

$$+\,[(1+\nu)n+1-3\nu]u_{n-2} + (1-\nu)(n+1)\left[4\left(1+\frac{2}{3\,t^2\,a^2}\right)n+1\right.$$

$$\left.-\frac{4}{3\,t^2\,a^2}\right]v_{n+1} + (1-\nu)\left[2\left(3+\frac{2}{3\,t^2\,a^2}\right)n^2 - \left(3+\frac{8}{3\,t^2\,a^2}\right)n\right.$$

$$\left.-\frac{2m^2}{1-\nu}\left(1+\frac{1}{3\,t^2\,a^2}\right) - 1 + \frac{4}{3\,t^2\,a^2}\right]v_n + \left[(1-\nu)\left(4n^2 - 9n+3\right)\right.$$

$$\left.-4m^2\right]v_{n-1} + \left[(1-\nu)(n-1)(n-3) - 2m^2\right]v_{n-2}$$

$$-\frac{2(2-\nu)}{3\,t\,a^2}(n+2)(n+1)\,w_{n+2} - \frac{2}{3\,t\,a^2}[2(2-\nu)n-1+2\nu](n+1)w_{n+1}$$

$$-\frac{2}{3\,t\,a^2}\left[(2-\nu)n^2 - (1-\nu)(3n-2) - m^2 - 3a^2\right]w_n$$

$$+\frac{4}{t}\,w_{n-1} + \frac{2}{t}\,w_{n-2} + \frac{2}{a^2}\,T_n\Bigg\} \quad \ldots\ldots\ldots\ldots\ldots\ldots (20b)$$

and

$$w_{n+4} = -\frac{1}{(n+1)(n+2)(n+3)(n+4)}\Bigg\{\frac{3\,\nu\,a^2}{t}(n+1)\,u_{n+1} + \frac{3a^2}{t}(3\,\nu\,n+1)\,u_n$$

$$+\frac{3a^2}{t}(3\,\nu\,n+2-3\nu)\,u_{n-1} + \frac{3a^2}{t}(\nu\,n+1-2\nu)\,u_{n-2}$$

$$+\frac{(2-\nu)m^2}{t}(n+1)(n+2)\,v_{n+2} + \frac{m^2}{t}[2(2-\nu)n-3](n+1)\,v_{n+1}$$

$$+\frac{m^2}{t}\left[(2-\nu)n^2 - (5-\nu)n+4 - m^2 - 3a^2\right]v_n - \frac{6a^2\,m^2}{t}\,v_{n-1}$$

$$-\frac{3a^2\,m^2}{t}\,v_{n-2} + 2(2n+1)(n+1)(n+2)(n+3)\,w_{n+3}$$

$$+\left(6n^2 - 1 - 2m^2\right)(n+1)(n+2)\,w_{n+2} + \left[2n(n-1) - 1 - 2m^2\right](2n-1)(n+1)w_{n+1}$$

$$+\left[n^2(n-2)^2 - 2n(n-2)m^2 + \frac{3a^2}{t^2} + m^2\left(m^2-4\right)\right]w_n$$

$$+\frac{6a^2}{t^2}\,w_{n-1} + \frac{3a^2}{t^2}\,w_{n-2} - 3\,Z_n\Bigg\} \quad \ldots\ldots\ldots\ldots\ldots\ldots (20c)$$

for all n = 0,1,2,... Quantities with negative subscripts are taken to be zero.

Eight linearly independent solutions of the homogeneous system in Eq. 17 can be constructed in the following manner: Set $X_n = T_n = Z_n = 0$ and the leading coefficients $u_0 = 1$, $u_1 = v_0 = v_1 = w_0 = w_1 = w_2 = w_3 = 0$ and then calculate the coefficients u_n, v_n, w_n from Eq. 20. The solution obtained from Eq. 18 with these coefficients will be denoted $U_1(y)$, $V_1(y)$, $W_1(y)$. Similarly, $U_2(y)$, $V_2(y)$, $W_2(y)$ can be constructed by setting all of the leading coefficients equal to zero except $u_1 = 1$. This process can be continued until the solution $U_8(y)$, $V_8(y)$, $W_8(y)$ has been obtained. A particular solution $U_9(y)$, $V_9(y)$, $W_9(y)$ can be found in the same way by setting all the leading coefficients $u_0 = u_1 = v_0 = v_1 = w_0 = w_1 = w_2 = w_3 = 0$ and letting X_n, T_n, Z_n take on some prescribed values.

Hence, the general solution of Eq. 17 can be written in the form

$$U(y) = u_0\, U_1(y) + u_1\, U_2(y) + v_0\, U_3(y) + v_1\, U_4(y) + w_0\, U_5(y) + w_1\, U_6(y) + w_2\, U_7(y) + w_3\, U_8(y) + U_9(y) \quad \ldots\ldots\ldots \text{(21a)}$$

$$V(y) = u_0\, V_1(y) + u_1\, V_2(y) + v_0\, V_3(y) + v_1\, V_4(y) + w_0\, V_5(y) + w_1\, V_6(y) + w_2\, V_7(y) + w_3\, V_8(y) + V_9(y) \quad \ldots\ldots\ldots \text{(21b)}$$

and

$$W(y) = u_0\, W_1(y) + u_1\, W_2(y) + v_0\, W_3(y) + v_1\, W_4(y) + w_0\, W_5(y) + w_1\, W_6(y) + w_2\, W_7(y) + w_3\, W_8(y) + W_9(y) \quad \ldots\ldots\ldots \text{(21c)}$$

The values of u_0, u_1,..., w_3 can be adjusted to satisfy a system of boundary conditions at y = 0 and y = b. When the values of the leading coefficients u_0, u_1,..., w_3 have been determined, then the solutions U(y), V(y), and W(y) satisfying the boundary conditions can be obtained from Eq. 21 or from Eq. 18 by making use of Eq. 20. With this solution, the magnitudes of the stress resultants are determined by the following equations which are obtained by making obvious substitutions into Eqs. 8 and 3:

$$N_x = \frac{3D}{h^2 a}\, N_x(y) \sin ms\theta \quad \ldots\ldots\ldots\ldots \text{(22a)}$$

$$N_\theta = \frac{3D}{h^2 a}\, N_\theta(y) \sin ms\theta \quad \ldots\ldots\ldots\ldots \text{(22b)}$$

$$N_{\theta x} = \frac{3D}{h^2 a}\, N_{\theta x}(y)\, m \cos ms\theta \quad \ldots\ldots\ldots\ldots \text{(22c)}$$

$$M_x = \frac{D}{h\, a^2}\, M_x(y) \sin ms\theta \quad \ldots\ldots\ldots\ldots \text{(22d)}$$

$$M_\theta = \frac{D}{h\,a^2}\ M_\theta(y)\ \sin ms\theta \quad \ldots\ldots\ldots\ldots (22e)$$

$$M_{x\theta} = \frac{D}{h\,a^2}\ M_{x\theta}(y)\ m\ \cos ms\theta \quad \ldots\ldots\ldots (22f)$$

$$Q_x = \frac{D}{h^2\,a^3}\ Q_x(y)\ \sin ms\theta \quad \ldots\ldots\ldots\ldots (22g)$$

and

$$Q_\theta = \frac{D}{h^2\,a^3}\ Q_\theta(y)\ m\ \cos ms\theta \quad \ldots\ldots\ldots\ldots (22h)$$

where

$$N_x(y) = U' + \frac{\nu}{y+1}\left(U - m^2\,V + \frac{1}{t}\,W\right) \quad \ldots\ldots\ldots (23a)$$

$$N_\theta(y) = \nu\,U' + \frac{1}{y+1}\left(U - m^2\,V + \frac{1}{t}\,W\right) \quad \ldots\ldots\ldots (23b)$$

$$N_{\theta x}(y) = \frac{1-\nu}{2}\left[\frac{1}{y+1}\,(U-V) + V'\right] \quad \ldots\ldots\ldots\ldots (23c)$$

$$M_x(y) = -\,W'' - \frac{\nu}{(y+1)^2}\left[(y+1)\,W' - m^2\,W + \frac{m^2}{t}\,V\right] \quad \ldots\ldots (23d)$$

$$M_\theta(y) = -\,\nu\,W'' - \frac{1}{(y+1)^2}\left[(y+1)\,W' - m^2\,W + \frac{m^2}{t}\,V\right] \quad \ldots\ldots (23e)$$

$$M_{x\theta}(y) = -\,\frac{1-\nu}{(y+1)^2}\left[(y+1)\,W' - W - \frac{y+1}{t}\,V' + \frac{1}{t}\,V\right] \quad \ldots\ldots (23f)$$

$$Q_x(y) = -\,\frac{1}{(y+1)^3}\left[(y+1)^3\,W''' + (y+1)^2\,W'' - \left(m^2+1\right)(y+1)\,W' + 2m^2\,W + \frac{m^2}{t}\,(y+1)\,V' - \frac{2m^2}{t}\,V\right] \quad \ldots\ldots\ldots (23g)$$

$$Q_\theta(y) = -\,\frac{1}{(y+1)^3}\left[(y+1)^2\,W'' + (y+1)\,W' - m^2\,W - \frac{1-\nu}{t}\,(y+1)^2\,V'' + \frac{m^2}{t}\,V\right] \quad \ldots\ldots\ldots\ldots (23h)$$

NUMERICAL EXAMPLES

Now there is available at least a formal solution of the indicated class of problems, but the objective of obtaining numerical results is still some distance away. The series in Eq. 18 converge slowly, and calculating the coefficients from the recurrence relations in Eq. 20 is at best a slow and tedious task if ordinary methods are to be used. In order to overcome these practical difficulties, an IBM 650 computer has been used to evaluate solutions. The calculation proceeds in three stages which are outlined as follows:

Stage I. General Solution.—The terms t, a, b, ν, m, X_n, T_n, and Z_n are given. Set y = b and using the recurrence relations in Eq. 20 as described previously, calculate the nine solutions $U_1(b)$, $V_1(b)$, $W_1(b)$, etc., appearing in Eq. 21.

Stage II. Boundary Conditions.—Four boundary conditions must be satisfied at each end y = 0 and y = b. The conditions at y = b are stated in terms of the results of Stage I. It is unnecessary to use the computer to develop a statement of conditions at y = 0. In general, the boundary conditions lead to eight non-homogeneous algebraic equations in the eight unknown u_0, u_1, v_0, v_1, w_0, w_1, w_2, w_3 which are solved by using a standard program for the computer.

Stage III. Final Results.—Having determined the leading coefficients in the power series solution (Eq. 18), from Stage II, these are now entered into the same program used in Stage I, and the solution satisfying the boundary conditions is evaluated for various values of y between y = 0 and y = b. The stress resultants are then calculated according to Eq. 23.

Example I.—(Fig. 2.) The terms t = 0.25, a = 100, b = 0.5, ν = 0.25, m = $\sqrt{17}$ X = T = 0, $Z_0 = 1$, $Z_1 = 4$, $Z_2 = 6$, $Z_3 = 4$, $Z_4 = 1$, and $Z_5 = Z_6 \ldots = 0$. This corresponds to a surface load $Z = (3D/h^3) \times 10^{-8} \sin \theta$. The shell is assumed to be simply supported at each end. This requires that $V = W = N_X = M_X = 0$ at y = 0 and y = b. The results of the calculation are given in Table 1(a) and are plotted in Fig. 3 and Fig. 4.

Example II.—(Fig. 5.) The terms t = 1, a = 200, b = -0.6, ν = 0.25, m = $\sqrt{8}$, X = T = 0, $Z_0 = 1$, $Z_1 = 4$, $Z_2 = 6$, $Z_3 = 4$, $Z_4 = 1$, and $Z_5 = Z_6 = \ldots = 0$. This corresponds to a surface load $Z = (3/16)(D/h^3) \times 10^{-8} \sin 2\theta$. The shell is assumed to be simply supported at y = 0 and y = b. Results are given in Table 1(b) and are plotted in Fig. 6 and Fig. 7.

These examples are intended to illustrate what can be accomplished with the method described in this paper. With the program which has been constructed for the IBM 650, any meaningful values of the parameters t, a, b, ν, and m can be used, while the loads X(y), T(y), and Z(y) appearing in Eq. 19 can be polynomials of degree nineteen. It should be clear that problems with other boundary conditions such as free or fixed at the ends y = 0 and y = b can be solved in the same manner.

Calculations were carried out to eight decimal digits and as many as 78 terms were summed depending on the value of y for which the series were being evaluated. However, because the calculations involve subtracting quantities having similar magnitudes, our final results cannot be correct to eight significant figures. Independent calculations were made using different programs for the computer and, at least for the examples considered, the results were found to be consistent to within 2%, or 3%. As far as engineering applications are concerned, no apology is needed for this degree of accuracy since

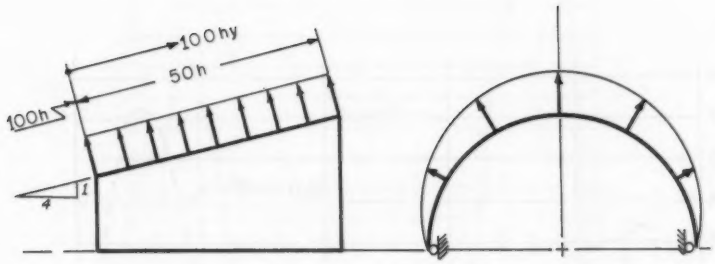

FIG. 2.—SKETCH FOR EXAMPLE I

TABLE 1.—RESULTS FOR EXAMPLES 1 AND 2

y	U(y) x 10^6	V(y) x 10^6	W(y) x 10^6	$N_x(y)$ x 10^6	$N_\theta(y)$ x 10^6	$N_{x\theta}(y)$ x 10^6	$M_x(y)$ x 10^4	$M_\theta(y)$ x 10^4	$M_{x\theta}(y)$ x 10^4	$Q_x(y)$ x 10^2	$Q_\theta(y)$ x 10^4
(a) RESULTS FOR EXAMPLE I.											
0.00	-3.79	0	0	0	- 3.6	4.15	0	-1.94	-1.10	9.81	- 1.63
0.05	-3.81	0.71	9.0	3.52	18.9	3.34	17.1	3.91	-0.59	- 0.19	14.45
0.10	-3.86	1.29	14.2	6.53	27.9	1.95	10.4	3.18	-0.16	- 1.49	7.90
0.15	-3.85	1.70	16.7	8.43	30.0	0.54	4.3	1.98	-0.02	- 0.79	2.51
0.20	-3.78	1.92	18.2	9.26	30.7	-0.75	1.8	1.41	-0.03	- 0.27	0.41
0.25	-3.70	1.98	19.2	9.23	32.1	-1.91	1.2	1.31	-0.07	0.06	0.04
0.30	-3.67	1.87	20.0	8.54	34.3	-3.02	2.7	1.78	-0.10	0.65	1.28
0.35	-3.71	1.60	20.1	7.29	36.2	-4.09	8.2	3.35	-0.03	1.67	5.48
0.40	-3.84	1.18	18.1	5.51	34.0	-5.06	18.4	6.19	0.24	2.23	12.88
0.45	-4.00	0.62	11.7	3.12	21.7	-5.71	24.4	8.01	0.74	- 0.59	-17.31
0.50	-4.04	0	0	0	- 2.9	-5.69	0	1.79	1.09	-11.07	- 1.50
(b) RESULTS FOR EXAMPLE II.											
0.00	-0.69	0	0	0	- 0.6	-5.69	0	3.8	2.95	-12.40	0.032
-0.05	-0.66	0.73	18.7	2.15	12.5	-5.97	31.3	12.4	2.51	- 1.70	0.367
-0.10	-0.60	1.42	30.5	3.93	20.3	-5.68	28.0	11.4	1.52	2.17	0.347
-0.15	-0.56	2.00	35.8	5.41	22.5	-5.05	16.2	8.2	0.77	2.25	0.225
-0.20	-0.59	2.45	37.2	6.71	21.5	-4.27	7.6	6.0	0.39	1.16	0.131
-0.25	-0.71	2.76	36.9	7.85	19.5	-3.44	4.1	5.4	0.25	0.25	0.095
-0.30	-0.90	2.91	35.7	8.80	17.6	-2.58	3.8	5.6	0.18	- 0.16	0.101
-0.35	-1.17	2.90	33.9	9.49	16.1	-1.64	4.7	6.1	0.07	- 0.23	0.125
-0.40	-1.47	2.72	31.3	9.73	15.0	-0.58	5.9	6.4	-0.13	- 0.27	0.154
-0.45	-1.79	2.35	27.5	9.27	14.0	0.70	8.1	6.7	-0.49	- 0.59	0.203
-0.50	-2.07	1.77	21.9	7.70	12.5	2.25	13.5	6.8	-1.25	- 1.16	0.311
-0.55	-2.27	0.98	13.1	4.62	7.3	4.01	20.6	5.0	-2.94	0.27	0.442
-0.60	-2.39	0	0	0	- 6.7	5.27	0	-7.3	-5.34	13.96	- 0.150

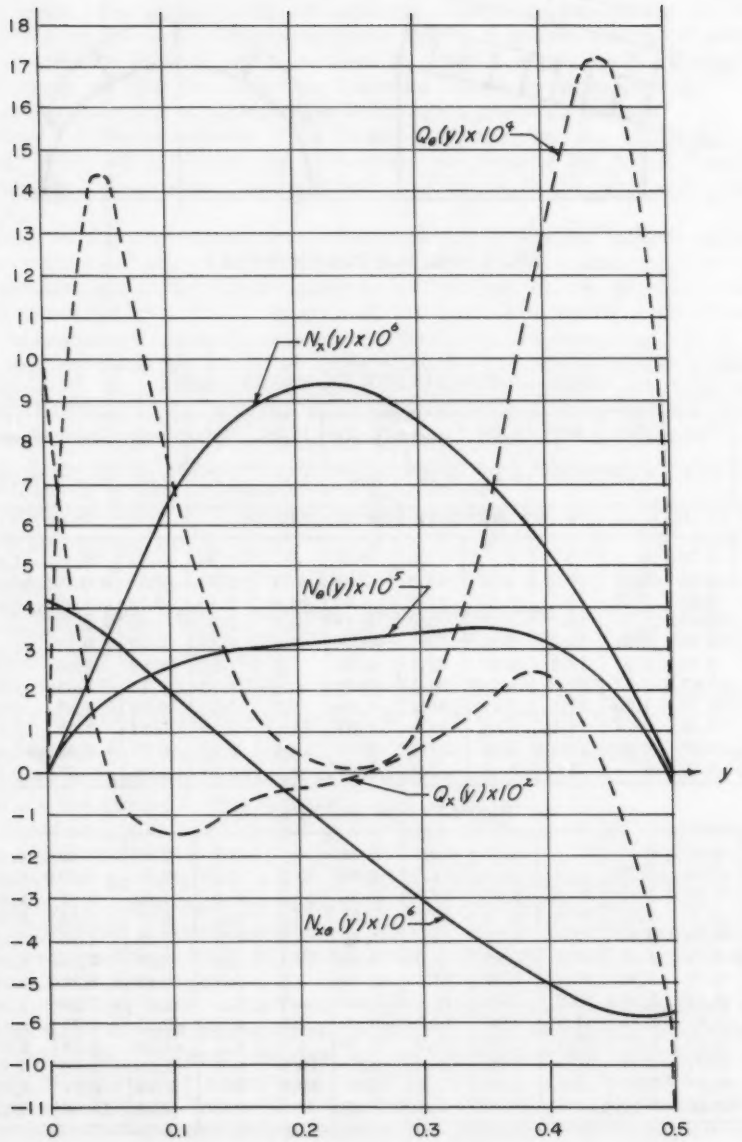

FIG. 3.—RESULTS FOR EXAMPLE I

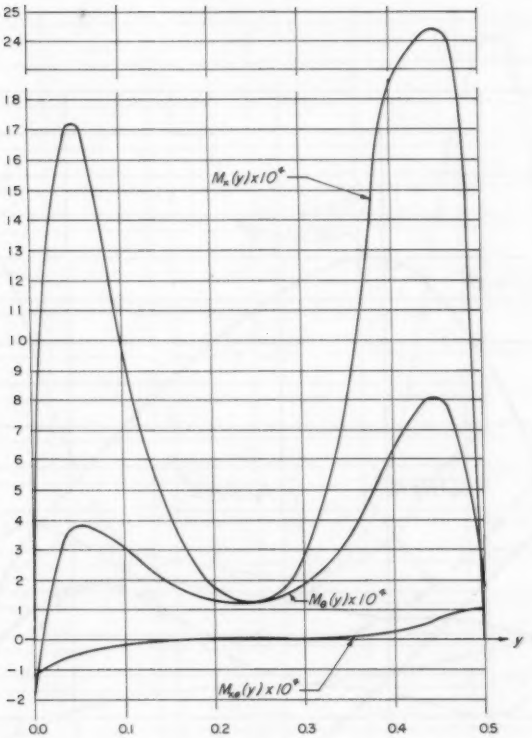

FIG. 4.—RESULTS FOR EXAMPLE I

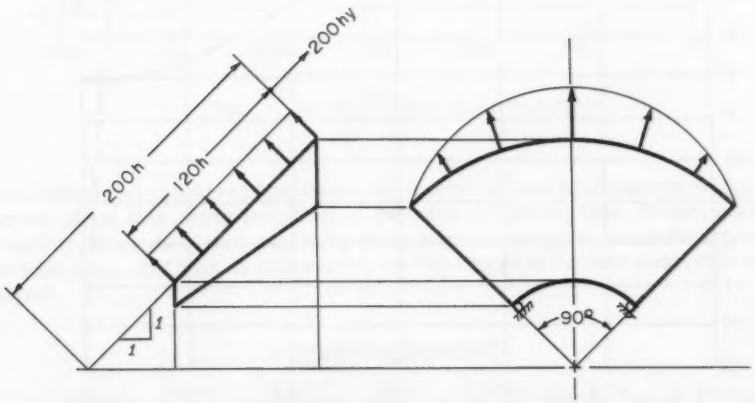

FIG. 5.—SKETCH FOR EXAMPLE II

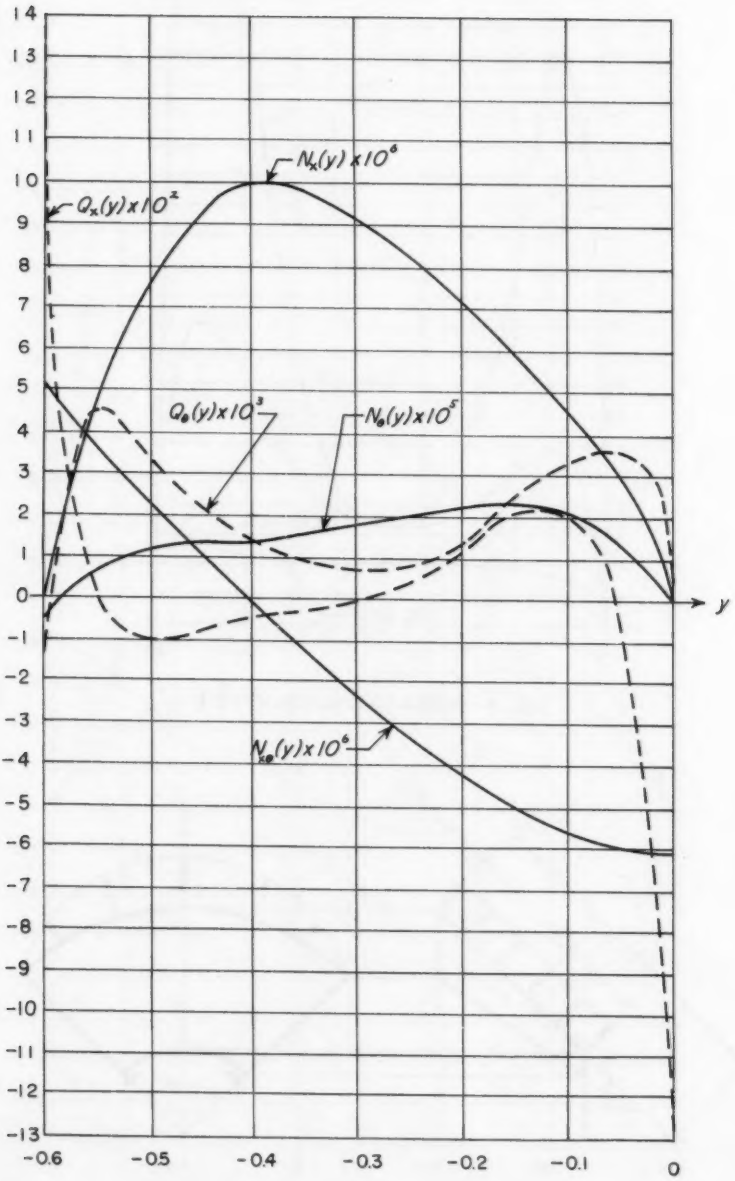

FIG. 6.—RESULTS FOR EXAMPLE II

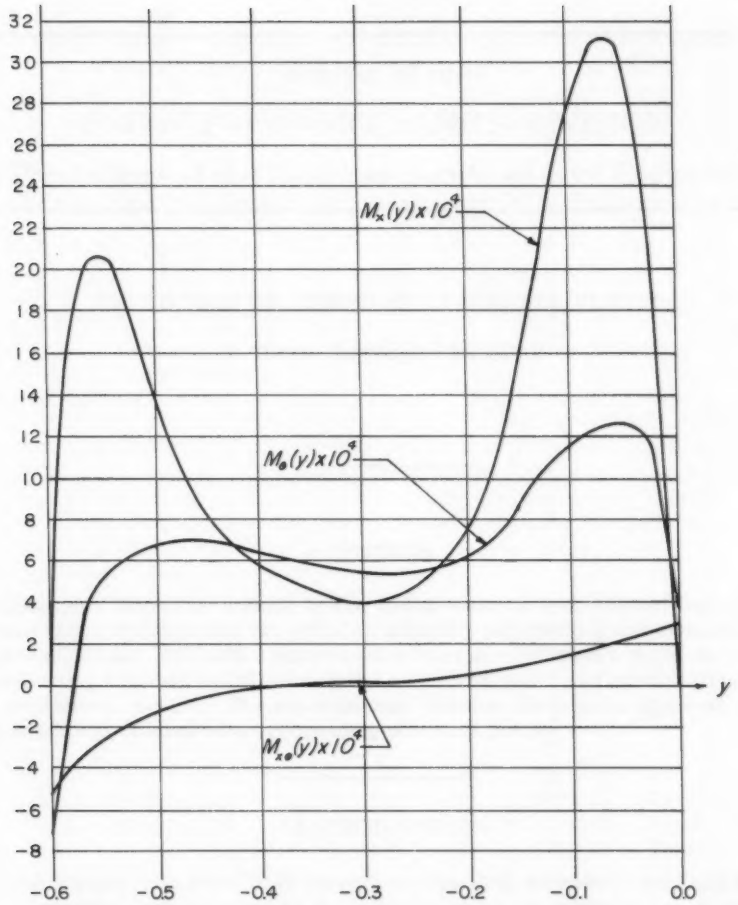

FIG. 7.—RESULTS FOR EXAMPLE II

the fundamental hypothesis on which the theory is based introduces an inaccuracy of about this same magnitude. Because of the expense of operating the computer, the author was unable to make a more extensive numerical study of the solutions, but this is expected to be the object of further research on the subject.

ACKNOWLEDGMENTS

The results of this paper were obtained during the course of a research project sponsored by the University of Kansas, Lawrence, Kans.

Journal of the
ENGINEERING MECHANICS DIVISION
Proceedings of the American Society of Civil Engineers

ADDED MASS OF LENSES AND PARALLEL PLATES

By Turgut Sarpkaya,[1] M. ASCE

SYNOPSIS

Contained herein is a study of the added mass of lens-shaped bodies, two parallel square plates, and two parallel, infinitely long rectangular plates of various thicknesses. The added masses were determinded from a mass-frequency relationship obtained by immersing the objects in water and accelerating them in oscillatory motion. The experimental results are in good agreement with the analytical studies of corresponding potential flows.

INTRODUCTION

The motion of a solid body through an infinitely extended real fluid at rest is, in general, accompanied by the following three interdependent, as well as time dependent, occurences: boundary layer, wake, and fluid mass transport. Consequently, the object is subjected to a resistance. In steady motion, boundary layer and the characteristics of the wake and, hence, the total resistance depend on the velocity, on some physical properties of the fluid, and on the geometrical characteristics of the object. Although, the fluid mass transported or the mass of fluid entrained by the body, including the wake-induced mass, also depends on the cited variables, it does not contribute to total resistance. In unsteady motion, however, the total resistance is affected in several ways. The velocity dependent drag is so affected that it is not the same as for steady flow. An inertial force occurs because of the acceleration of the additional mass en-

Note.—Discussion open until November 1, 1960. To extend the closing date one month, a written request must be filed with the Executive Secretary, ASCE. This paper is part of the copyrighted Journal of the Engineering Mechanics Division, Proceedings of the American Society of Civil Engineers, Vol. 86, No. EM 3, June, 1960.

[1] Assoc. Prof. of the Engrg. Mechanics Dept., Univ. of Nebraska, Lincoln, Nebr.

trained by the body. Finally, the geometry of the wake varies with time, and both the drag and the inertial force are affected markedly. For oscillatory as well as unidirectional, unsteady motion, therefore, the analytical determination of the inertial force and the drag appears to be very difficult. Studies[2] made on the vortex shedding seem to throw some light on the understanding of the general problem.

The inertial force can, however, be computed for the irrotational flow produced in an ideal incompressible fluid by the vibratory motion of an immersed object. The usefulness of the preceding theoretical prediction, of inertial force or the inertia coefficient, is obviously limited by the very severe restrictions made in its evaluation. At the moment of zero velocity there is no wake and the flow pattern closely resembles that for irrotational flow without separation. Therefore, the inertia coefficient obtained from irrotational flow theory constitutes a single point on the general drag-inertia-coefficient curve,[2] which is the approximate starting point of motion. Approximate, because the fluid accumulated in the boundary layer prior to separation causes the actual inertial forces to be slightly higher than what the theory would predict.

Since the time of Du Buat, the added mass has been the subject of many experimental and analytical investigations. For three-dimensional flows however, the added mass has been determined explicitly only for a very limited category of geometrically prescribed objects. For all elliptic cylinders with one axis parallel to the direction of flow, the virtual mass is equal to the mass displaced by a circular cylinder for which the diameter is the transverse axis of the ellipse.[3] An expression in elliptic functions was developed[4] by D. Riabouchinsky for cylinders with rectangular cross sections. Also available in terms of elliptic integrals are coefficients for any ellipsoid, provided only that one axis is parallel to the direction of motion.[3] For all of these cases, irrotational flow without separation is assumed.

Because separation occurs in flow past any body which is not well streamlined, the theoretical results are not necessarily useful in analyzing flows past structures of conventional design. A more realistic representation of flow past a flat plate was proposed[4] by Riabouchinsky, in which a second plate downstream of the first closes the flow. The cavity, bounded by the two plates and the connecting streamlines, is a mathematical approximation to actual wakes. G. Birkhoff et al. extended[5] this analysis and presented drag coefficients for various cases. The method was again extended recently to include the evaluation of the virtual mass coefficients for systems with various spacings of the plates.[6] Other ways of achieving finite cavities are the reentrant jet[7] of D. Gilbarg and D. H. Rock and the parallel after-body[8] of A. Roshko.

---

2 "Vortex Formation and Resistance in Periodic Motion," by J. S. McNown and G. H. Keulegan, EM 1, January, 1959, pp. 1-6.

3 "Hydrodynamics," by H. Lamb, Dover Publications, Inc., New York, 6th Edition, 1945.

4 "Sur la Resistance des Fluides," by D. Riabouchinsky, Comptes Rendus, Conres International des Mathematiciens, Strasbourg, 1920, pp. 568-585.

5 "Wall Effects in Cavity Flow-II," by G. Birkhoff, M. Plesset and N. Simmons, Quarterly of Applied Mathematics, January, 1952.

6 "Note on Estimation of Virtual Mass Coefficient," by J. S. McNown, (April 17, 1955, Unpublished, Sandia Corp.)

7 Naval Ordnance Lab. Memorandum 8717, by D. Gilbarg and D. H. Rock, 1945.

8 "A New Hodograph for Free-Streamline Theory," by A. Roshko, NACA TN-3168, 1954.

The classical theory without separation is appropriate for motions in which the displacement is small. It has been used for determining the forces on dams during earthquakes,[9,10] for studies of bodies vibrating in liquids,[11,12] and for computations of gust and vibration loadings of airplane wings. Considerable discrepancy is found between the results of this type and those obtained for flows in which the amplitude of the motion is large enough for a separation pocket to occur. A wake-induced mass which varies continuously during the period of vortex shedding had to be taken into consideration.

In the present study, the experimentally determined added-mass coefficients for a lenticular object formed by two intersecting spheres, for two completely separated spheres, for two parallel square plates, and finally for two parallel, infinitely long rectangular plates of various thicknesses have been added to the existing list of added mass coefficients.

At this time, it is appropriate to discuss briefly the evolution of the idea of added mass. Definitions of virtual mass have been presented from several points of view all leading to the same result. H. Lamb presented[3] a method in which the integral of the Euler equation, including the term for unsteady flow, is used. Another method requires the integration throughout the fluid of the incremental force which is the product of an elementary mass and the local acceleration. Then, the quotient of the total force required to produce the accelerations throughout the fluid divided by the acceleration of the body defines the virtual mass. The usual derivation of virtual mass, however, is from kinetic energy which suffers from the inherent weakness that it assumes a constant velocity for the confined solid body, whereas all outward manifestations of mass are associated with acceleration. Therefore, velocity must be allowed to vary and the fact should be recognized that the added mass can yield momentum as well as energy. Sir Charles Darwin has shown[13] that an object moving in an infinitely extended ideal fluid, besides pushing the particles aside temporarily in passing, also displaces the fluid particles permanently in the direction of its motion and that this displaced mass of fluid enclosed between the initial and final positions of fluid particles, is in fact, the added mass itself. Although, Darwin's physical interpretation of the added mass is quite different from what was known, it does not in any way disprove the well-known kinetic-energy concept nor does it constitute a simpler method to determine the added-mass coefficients theoretically.

THEORY

Since the time rate of change of kinetic energy is equal to the rate of doing work, upon integrating, there results

$$T = (1 + C)\, M_0 \frac{V^2}{2} = -\frac{\rho}{2} \iiint (-\text{ grad } \phi)^2 \, dx \, dy \, dz \quad \ldots\ldots (1)$$

---

9 "Water Pressures on Dams During Earthquakes," by H. M. Westergard, Transactions, ASCE, 1933.

10 "Hydrodynamic Earthquake Forces on Submerged Structures," by J. S. McNown, Proceedings, Third Midwestern Conference on Fluid Mechanics, 1953.

11 "Virtual Mass and Acceleration in Fluids," by J. M. Stelson and F. T. Mavis, Transactions, ASCE, Vol. 22, 1957, pp. 518-530.

12 "Virtual Masses of Rectangular Plates and Parallelpipeds in Water, by Yee-Tak Yu, Journal of Applied Physics, November, 1945.

13 "Notes on Hydrodynamics," by Sir Charles Darwin, Proceedings, Camb. Phil. Soc. 49, 1953, pp. 342-354.

For three-dimensional flows the velocity potential has been determined explicitly only for a very limited category of geometrically prescribed objects. The added-mass coefficients of two separated spheres and of the lenses are the only ones determined analytically among those investigated herein. The flow around a lens appears to be first determined by J. Mehler.[14] Later H. Wagner,[15] W. A. Monaghan,[16] M. Shiffman and D. C. Spencer,[17] and L. E. Payne,[18] have studied it further. The added-mass coefficient of two parallel, separated, square, and infinitely long rectangular plates have not yet been determined analytically. The latter problem should not be confused with that one treated by J. S. McNown.[6]

A classical procedure for finding the flow due to the vertical motion of the two spheres is by the method of images. The flow produced by a single sphere moving alone in an infinite body of fluid is that created by a dipole of suitable strength placed at the center of the sphere. If two dipoles are situated at the centers of two spheres, in order to correct for their mutual interference and to correct the destroyed boundary condition, one has to introduce the corresponding images of each dipole and continue this process until a convergent expression for the potential function is obtained. If this potential function is introduced in Eq. 1, and necessary integrations are performed, one can solve for the added mass coefficient. Throughout this study C is referred to the displaced mass of the body.

For two completely separated spheres, the added-mass coefficient obtained in the manner described in the foregoing is deduced from the work[17] by Shiffman and Spencer:

$$C = \frac{3}{2} \sum_{k=1} \left((-1)^{k+1} \frac{\sin^3 \beta}{\sin^3 k\beta} - \frac{2}{3} \right) \quad \ldots\ldots\ldots\ldots (2)$$

When the spheres are tangent,

$$C = \frac{3}{2} \sum_{j=1} \left(\frac{(-1)^{j-1}}{j^3} - \frac{2}{3} \right) \quad \ldots\ldots\ldots\ldots (3)$$

The added mass for a lens-shaped body between two intersecting identical spheres is given by[17]

$$C = 3 \left(\frac{r_0}{R} \right)^3 H - 2(2 - \cos \beta) \cos^4 \frac{\beta}{2} \quad \ldots\ldots\ldots\ldots (4)$$

in which

$$H = \frac{1}{2} \left[\sum_{j=1}^{q-1} (-1)^{j-1} \csc^3 \frac{j n \pi}{q} + \frac{q}{2n} \sum_{k=1}^{n-1} (-1)^{k-1} \left\{ \csc z + \frac{q^2}{n^2} \frac{d^2}{dz^2} (\csc z) \right\}_{z = k q \pi / n} \right] \quad \ldots\ldots\ldots\ldots (5)$$

---

14 "Journal fur Mathematics," by J. Mehler, 68, 1868, pp. 134-150.
15 ZaMM 12, by H. Wagner, 1932, pp. 193-215.
16 R. A. E., Tech. Note Aero., by W. A. Monaghan, 1989, 1944.
17 "Flow of and Incompressible Fluid about a Lens," by M. Shiffman and D. C. Spencer, Quarterly of Applied Mathematics, Vol. V, No. 3, 1947, pp. 270-288.
18 Quarterly of Applied Mathematics, by L. E. Payne, Vol. X, 1952, pp. 197-204.

for $(n + q)$ odd, and

$$H = \frac{1}{q\pi}\left[\left(\frac{q^3}{6n^3} + \frac{q}{2n}\right) + \pi \sum_{j=1}^{q-1} (-1)^j \, j \csc^3 \frac{j n \pi}{q} + \frac{q}{2n} \sum_{k=1}^{n-1} (-1)^k \right\} z \csc z + \frac{q^2}{n^2} \frac{d^2}{dz^2} (z \csc z) \Bigg\} \Bigg] \quad \ldots\ldots\ldots\ldots\ldots\ldots (6)$$

for $(n + q)$ even and for $z = k q \pi/n$.

The results obtained from these and from previous equations have been recalculated and presented in Fig. 1, together with the rate of change of the added-mass coefficient with respect to the ratio B/R. The theoretical results obtained from Riabouchinsky's analysis[4] for two dimensional rectangular prisms are indicated by dashed lines on Fig. 2.

EXPERIMENTAL PROCEDURE

The experimental apparatus was designed to impart vibratory motion to connected pairs of spheres, parallel square and rectangular plates, and to lens-shaped bodies in such a manner that at all stages of motion the kinematic and kinetic characteristics of the experimental system and test objects could easily be determined.

A picture of the apparatus used and one sample object from each group tested are shown in Fig. 3. The test bodies were immersed in a rectangular tank, 80 in. square section, and 80 in. deep, filled with tap water. An 80 in. long small aluminum beam was simply supported on pivot bearings very carefully to eliminate end restraints. At the mid point and below the beam an elliptical aluminum ring (major axis 2 in., minor axis 1 in., thickness 0.10 in., width 0.50 in.) was securely attached to the beam with the major axis in the horizontal position. This ring constituted the elastic element for measuring the force directly. To indicate the ring deformations two pairs of SR-4 strain gages were glued at the ends of the major axis, on the inside and outside of the ring. The four strain-gage elements form the bridge which is led to a universal analyzer. By having four strain gages on the ring the sensitivity was increased and no corrections were needed for temperature changes. The universal analyzer is, in turn, relayed to one of the channels of a two-channel magnetic oscillograph. The ring was calibrated statically for both tension and compression before mounting it on the beam. Thereafter, the calibration was repeated before and after each run in the mounted position to make sure that no accidental changes occurred in the strain gages. The calibrations always reproduced and plotted on a straight line within the loading range. Furthermore, the system was calibrated dynamically. A known mass suspending in air was attached rigidly to the ring and then the beam was vibrated by means of a magnet-coil system. The frequencies were measured with sonometer and, also, with a universal counter and timer. Accelerations, displacements, and velocities were measured with a vibration meter (model M-I). Separate measurements of the latter kinematic variables also provided another check in the measurements since the velocity, displacement, acceleration, and frequency are related with a simple well-known expression in a harmonic motion. Using the force recorded by the

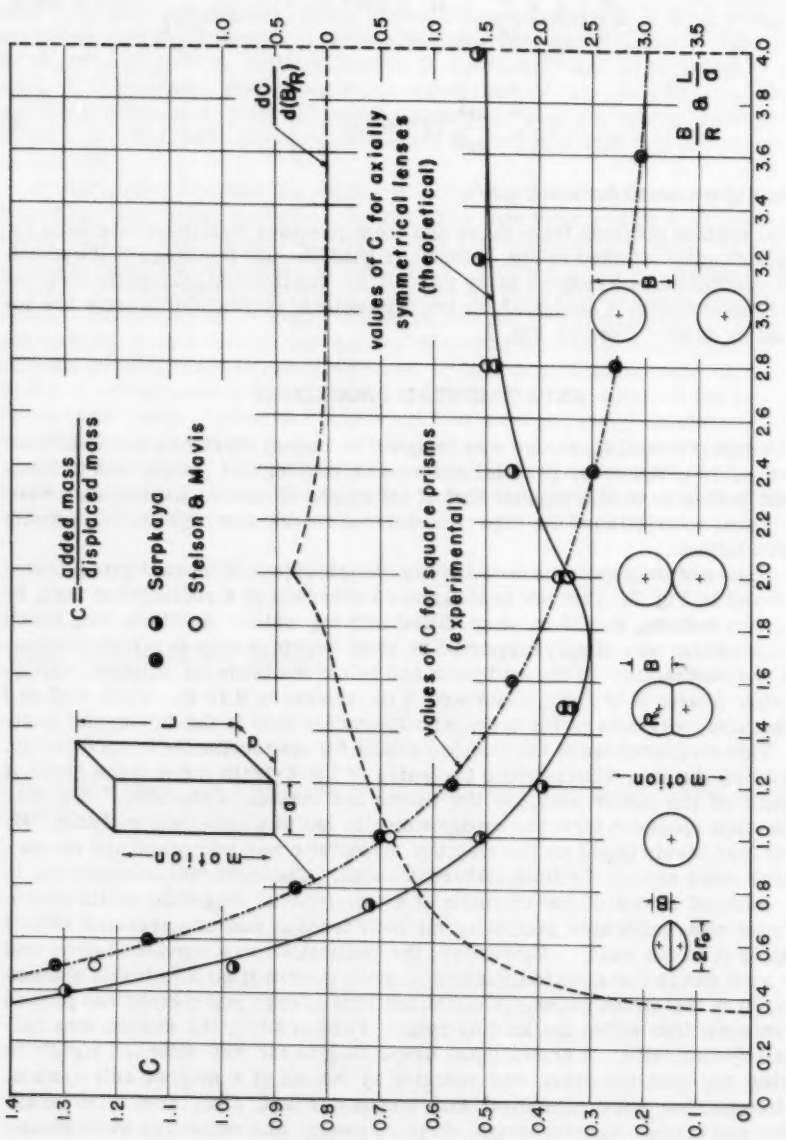

FIG. 1.—ADDED-MASS COEFFICIENTS FOR TWO SHPERES IN TANDEM AND FOR SQUARE PRISM

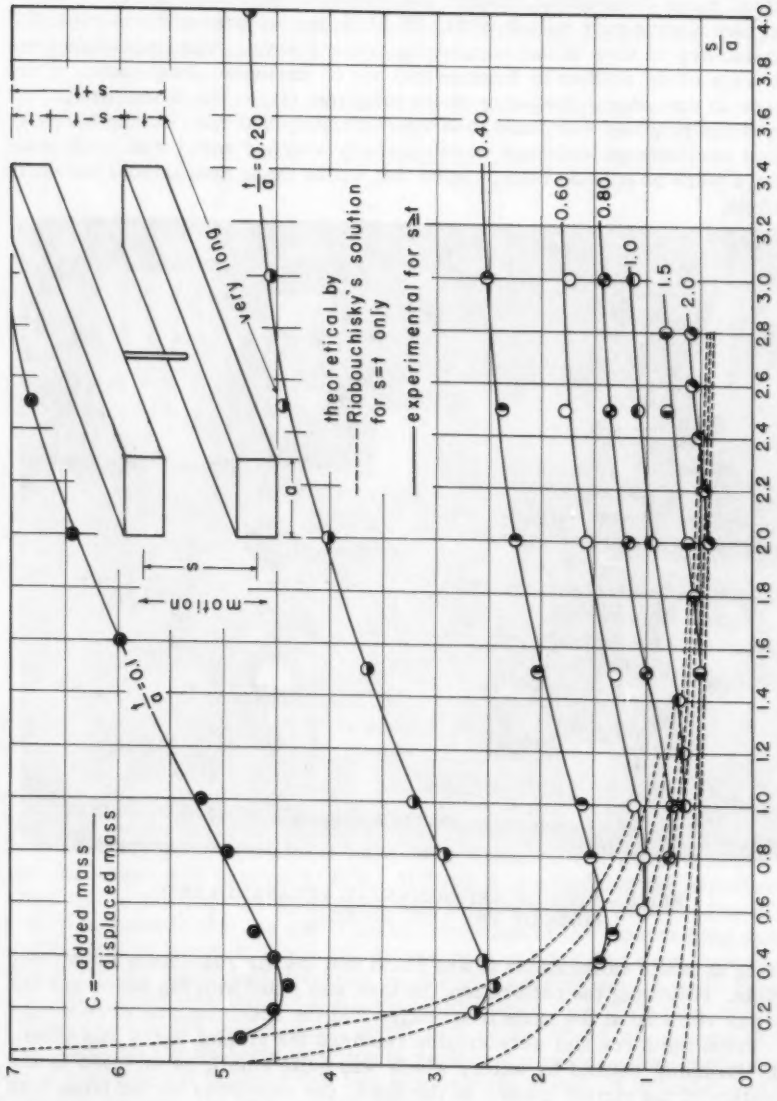

FIG. 2.—ADDED-MASS COEFFICIENT FOR TWO-DIMENSIONAL RECTANGULAR PRISMS SINGLY AND IN TANDEM

oscillograph and the acceleration measured, the total mass of the suspending rod and the mass of the sample body was calculated. Since the mass of the suspending rod was previously determined and remained constant throughout the experiment, the mass of the sample object was determined and compared with the actual mass determined through the measurement of its weight. Such a comparison always gave values within 1% of the actual mass and was regarded as satisfactory in view of the complexity of the system. The frequencies selected were close neither to fundamental nor to harmonic frequencies of the beam nor to the natural frequency of the elliptical ring. The fundamental frequency of the ring was computed to be approximately 850 cps. During each experiment oscilloscope tracings were carefully watched and it was made sure that there were no outside interference that would cause undesirable parasitic vibrations.

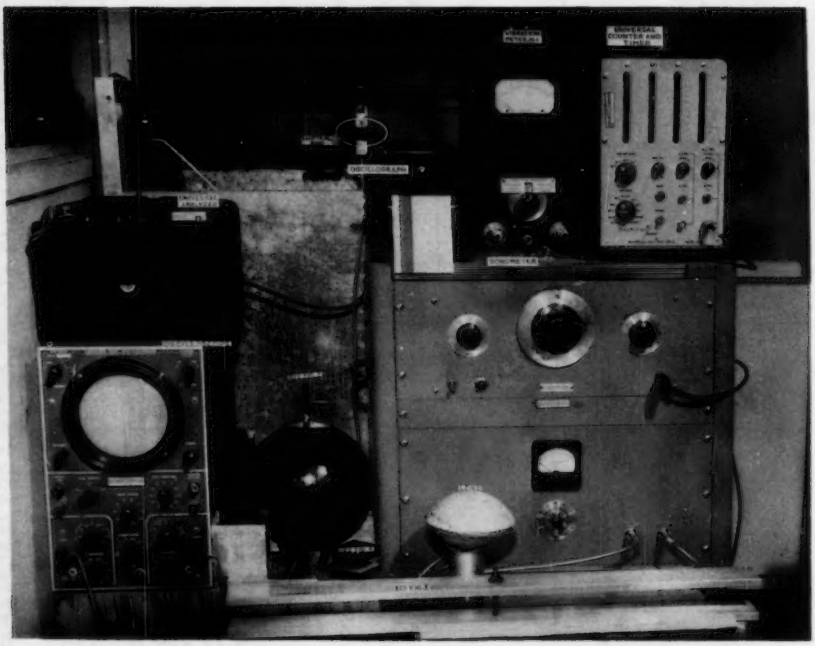

FIG. 3.—VIEW OF EXPERIMENTAL APPARATUS AND SOME OF THE TEST BODIES

During dynamic calibrations it was found that the air resistance is entirely negligible. Following the calibration, the tank was filled with tap water and the object was vibrated at the same frequencies and the accelerations were measured. From the force and acceleration readings the virtual mass was determined. Damping caused by water, which was quite small, is included in the computation of the virtual mass. In the tests, the velocities varied from 0.20 in. per sec to 0.60 in. per sec, the frequencies from 25 cps to 60 cps, and the accelerations from 40 in. per sec^2 to 400 in. per sec^2. Finally, it should be noted that the experiments were repeated several times for each test object for various frequencies within the frequency range tested. For a given object, no

appreciable difference has been noted between the added masses determined using different frequencies, that is, from 25 cps to 60 cps.

Test objects were constructed of brass, aluminum, and plaster of paris. Square prisms consisted of carefully sealed hollow aluminum blocks. Spheres were made of brass shell, the inside of which was filled with parafin wax. Lenses were made of plaster of paris and coated with parafin wax. The sizes of the objects tested are noted in Table 1.

TABLE 1.—DIMENSIONS OF TEST OBJECTS

Object	Item	Dimension, in inches									
Lenses	B	1.20		1.50		3.00		2.40		1.50	
	R	3.00		3.00		4.00		2.00		1.00	
Spheres	R	1.00		2.00		3.00		4.00			
Square prisms, s = t	L	1.5	1.8	2.4	3.0	3.6	4.8	4.8	5.6	5.4	3.6
	a	3.0	3.0	3.0	3.0	3.0	3.0	2.0	2.0	1.5	1.0
Parallel square prisms, s z t	t	0.20		0.40		0.60		0.80		1.00	2.00
	a	2.00		2.00		2.00		2.00		2.00	2.00
	s	For each, s/a varied with the connecting rod									
Parallel two-dimensional rectangular prisms		t and a same as for parallel square prisms. Length = 35 in.									

CONCLUSIONS

The added-mass coefficients for lenses and separated spheres obtained experimentally and theoretically are shown in Fig. 1. Also illustrated in Fig. 1, are the added-mass coefficients for square prisms which were obtained experimentally only. The points representing the latter coefficients comprise the dot-dash line, shown in Fig. 1. This dot-dash line is used later in Fig. 4, to define the asymptotic curves for various values of the parameter t/a. Also illustrated in Fig. 1, is a plot of the rate of change of the added-mass coefficient for lenses with respect to B/R. At first, it is noted that the experimental values are in satisfactory agreement with the theoretical values. The second point to be noted is that the added-mass coefficient of two intersecting spheres is minimum at about B/R = 1.75. If one can consider two such intersecting spheres as the equivalent potential model of a sphere and its wake together with two symmetrical vortices situated in the wake, one finds that during the unsteady motion the added-mass coefficient of the model drops from 0.50 to 0.30. It is not the writer's intention to replace the complicated unsteady motion of a sphere and of the vortex by a simple rigid model. It is mentioned here merely to point out the fact that the added-mass coefficient drops considerably as the wake grows longer. However, immediately after the shedding of the vortex, the motion becomes more complicated and at present nothing much can be said about the variation of C.

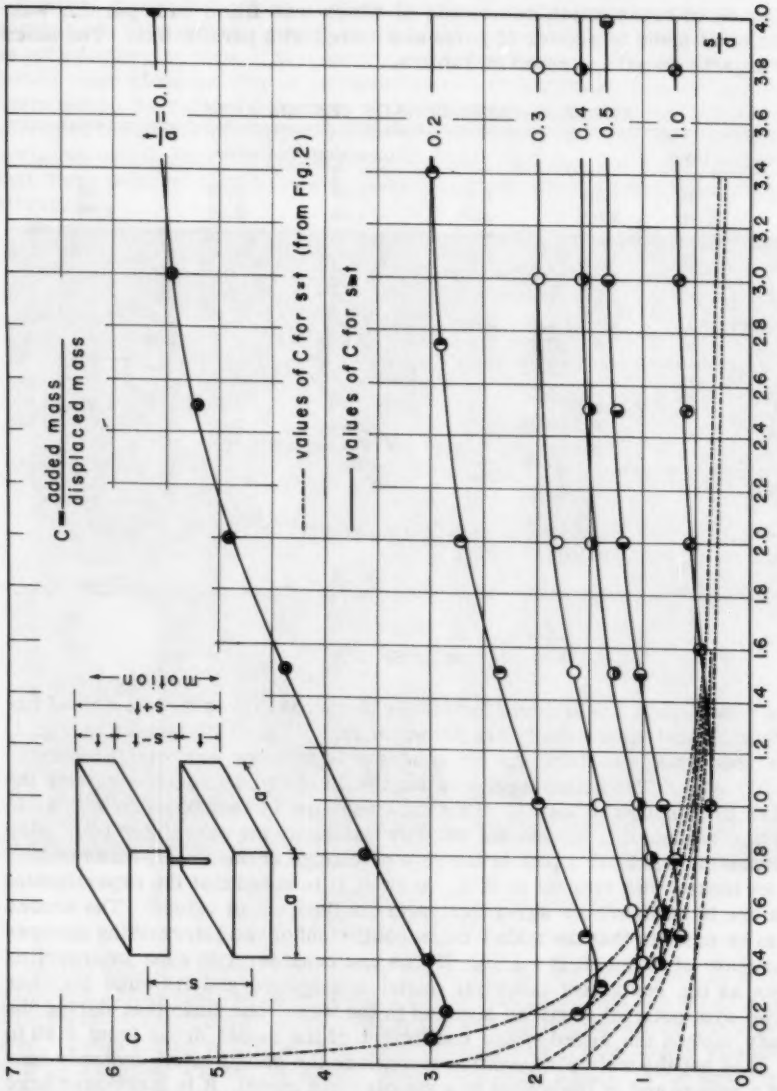

FIG. 4.—ADDED-MASS COEFFICIENT FOR SQUARE PRISMS SINGLY AND IN TANDEM

In Figs. 2 and 4 curves with dotted lines give the ratio of added mass to displaced mass for unslotted, two dimensional, right rectangular prisms and for full right square prisms, respectively, as a function of s/a, for constant values of t/a. Curves with full lines give the aforementioned ratio for the separated square and rectangular plates as a function of the same dimensionless ratios. As stated previously, the dotted lines in Fig. 2, are obtained from Riabouchinsky's analysis,[4] and the dot-dash lines in Fig. 4 are derived from the experimental curve shown in Fig. 1. The direction of the vibratory motion is also shown on the figures.

An examination of the figures reveals that as the plates are separated from each other but a very little distance, the added-mass coefficient decreases slightly, that is, the fluid between the plates behaves as if it were part of the solid full parallelpiped. As the plates are set farther apart, the added-mass coefficient increases, but always remains smaller than the added-mass coefficient of a single plate. Hence, when the distance between the plates is not too large in comparison with the width of the plate, there is mutual interaction of the flow patterns around the two plates. As the plates become farther apart, action becomes negligible and each plate behaves independently.

It should be noted that although the basic concepts of the subject matter contained herein have been expressed in similar ways by many others, the experimental data presented for the added mass of multiple spheres, lens-shaped bodies, and parallel square and rectangular plates is a new contribution.

ACKNOWLEDGMENTS

The experiments reported herein were conducted at the Hydrodynamics Laboratory of the Engineering Mechanics Department of the University of Nebraska. The writer wishes to express his appreciation to E. J. Marmo, Chairman of the Engineering Mechanics Department, for the financial assistance he has provided.

NOMENCLATURE

a	= width of a plate;
B	= half of the thickness of a lens measured in the direction of motion, (Fig. 1);
C	= added mass coefficient, (added mass/displaced mass);
H	= a function;
j, k, n, q,	= integers;
M_0	= displaced mass;
r_0	= radius of the circular plane surface generated by the intersection of two spheres. (Fig. 1);
R	= radius of a sphere;
s	= see Fig. 2;
t	= thickness of a plate;
T	= kinetic energy;

V = velocity of the undisturbed stream;

$x, y, z,$ = coordinate axes;

β = half of the exterior angle between the two intersecting spheres = $n \pi/q$;

ρ = density of fluid; and

ϕ = velocity potential function

Journal of the
ENGINEERING MECHANICS DIVISION
Proceedings of the American Society of Civil Engineers

STRESSES DUE TO THERMAL GRADIENTS IN REACTOR SHIELDINGS

By Melvin L. Baron,[1] A. M. ASCE, and Mario G. Salvadori,[2] M. ASCE

SYNOPSIS

The stresses due to a sudden rise in surface temperature on one side of a fixed ended arch with a rectangular cross-section are evaluated, taking into account the temperature variation in the interior of the arch. The results are extended to the case of a surface temperature which first increases linearly and then remains constant, by means of a Duhamel integral to the case of an arbitrary temperature applied to the surface of the structure.

INTRODUCTION

Nuclear reactors require shielding structures capable of serving their structural integrity in an environment which differs in many respects from that of other civil engineering structures. The necessarily massive dimensions of the shielding make it particularly sensitive to temperature changes and its structural design is often primarily governed by thermal stresses rather than by dead load and live loads. Thermal stresses can arise from:

a. Slow, cyclic, temperature variations due to natural causes.
b. Slow temperature variations due to normal operations.
c. Slow heat generation due to absorption of gamma rays.

Note.—Discussion open until November 1, 1960. To extend the closing date one month, a written request must be filed with the Executive Secretary, ASCE. This paper is part of the copyrighted Journal of the Engineering Mechanics Division, Proceedings of the American Society of Civil Engineers, Vol. 86, No. EM 3, June, 1960.

[1] Chf. Engr., Paul Weidlinger, Cons. Engr., New York, N. Y., and Adjunct Prof. of Civ. Engrg., Columbia Univ., New York, N. Y.

[2] Assoc., Paul Weidlinger, Cons. Engr., New York, N. Y., and Prof. of Civ. Engrg., Columbia Univ., New York, N. Y.

d. Sudden temperature rises (thermal shock) due to accidental causes in the reactor operation.

Temperature variations associated with a and b are normally sufficiently slow to allow steady state conditions with a corresponding linear gradient within the shielding to be assumed. The determination of the state of stresses can thus be obtained by well known engineering methods.

Case c leads to a nonlinear steady-state temperature gradient which can be determined if the energy absorption coefficient of the material is known. The corresponding state of stress can be found by the equations given in the section on strains due to thermal stresses.

A somewhat more difficult condition arises in case d, because the nonlinear transient temperature gradient due to the thermal shock cannot be given in a closed form valid for any time interval. On the other hand, the stresses in the shielding structure due to the kind of high intensity shock considered here, rise very rapidly, and the interest of the designer is restricted to the determination of the time when the stresses reach their greatest allowable value. Before this time is reached, provision must be made to reduce the temperature within the shielding by cooling, since in most instances it would be uneconomical to design the shielding to sustain very high intensity temperatures for extended periods. Since the maximum stress at early time is a tensile stress on the inner (hot) surface of the shielding, a reasonable criterion for allowable stress is that the tensile strength of the concrete not be exceeded beyond a depth equal to the coverage over the reinforcing bars. Under these conditions, the surface of the shielding may crack or spall, but its essential structural integrity is preserved.

For convenience, the time-temperature history at the inside surface of the shielding is first considered to be a step function, corresponding to a thermal pulse of zero rise time, and the corresponding temperature distribution in the arch is evaluated. However, as the containment sphere is normally separated from the reactor shielding by layers of air or other insulation, the temperature pulse will have a finite rise time with a linear or non-linear variation during this rise. Beyond the rise time, the surface temperature reaches and maintains a maximum value T_0 in the time period of interest.

Once the temperature distribution in the arch has been evaluated for the case of an applied step pulse (zero rise time), these results can be used as influence coefficients to determine the corresponding temperature distribution in the arch for an applied arbitrary temperature at its inside surface, by means of Duhamel integrals. Three cases of applied temperatures are considered in the subsequent sections: 1) a step pulse with zero rise time; 2) a pulse with a linear rise time; and 3) a pulse with an arbitrary nonlinear rise time.

The results obtained in the present study apply to the supporting arches of a reinforced concrete ribbed dome subjected to the above described temperature impacts on their inner surface. The outer surface remains at a constant temperature during the time period of interest.

Arches of shallow depth are considered, where the influence of the curvature on the temperature gradient can be neglected.[3] Direct thermal stresses due to the nonlinear gradient, together with end rotations and displacements of the arch are determined. Using these results, the end moments and thrust in the arch can be obtained for any support condition of full or partial fixity. A numerical example for a built-in symmetrical arch is presented.

[3] "Thermal Stresses in Curved Beams," by Bruno Boley and E. Barrekette, Journal of the Aeronautical Sciences, Vol. 25, No. 10, October, 1958.

TEMPERATURE GRADIENT DUE TO THERMAL SHOCK

Step Function with Zero Rise Time Applied to Inner Face of Arch.—If a free ended rectangular beam of depth 2c, and length 2L (Fig. 1), insulated on its lateral and end boundaries, has its boundary y = -c suddenly raised to a temperature T_o at a time t = 0 that is maintained for t > 0 while its boundary y = c is maintained at a temperature T = 0, its temperature distribution[4] at a time t can be considered to be a function of the y coordinate only and is given by the following expressions:[5]

Short Time Solution.—

$$T_S(y, t) = T_o \sum_{n=0}^{\infty} \left\{ \operatorname{erfc} \left[\frac{(2n+1)\ 2c - (c - y)}{2\sqrt{k\,t}} \right] - \operatorname{erfc} \left[\frac{(2n+1)\ 2c + (c - y)}{2\sqrt{k\,t}} \right] \right\} \quad \ldots\ldots\ldots\ldots \quad (1)$$

Complete Solution.—

$$T_S(y, t) = T_o \left\{ \frac{1}{2} \left(1 - \frac{y}{c} \right) + \frac{2}{\pi} \sum_{n=1}^{\infty} \frac{(-1)^n}{n} e^{-k\left(\frac{n\pi}{2c}\right)^2 t} \sin \frac{n\pi}{2} (1 - y/c) \right\} \quad \ldots\ldots \quad (2)$$

in which k (in square feet per hour) is the thermal diffusivity of the material of the beam and the function erfc ξ is the error function complement of ξ:

$$\operatorname{erfc} \xi = 1 - \operatorname{erf} \xi = \frac{2}{\pi} \int_{\xi}^{\infty} e^{-x^2}\, dx \quad \ldots\ldots\ldots \quad (3)$$

Eq. 2 shows that $T_S(y, t)$ approaches asymptotically a linear distribution. For early times the series of Eq. 1 converges so rapidly that for most practical cases, it is well represented by the first term, n = 0.

The temperature distribution of Eqs. 1 or 2 can be used with good approximation for arches, provided their radius of curvature R be large compared to their depths 2c.[3]

As a typical case, Fig. 2 shows the temperature distribution $T_S(y, t)$ for a reinforced concrete arch with a rectangular cross section, 5-ft deep. The value of the thermal diffusity "k" was taken as k = 0.33 sq ft per hr.

After 16-hr the maximum difference between the steady state temperature and $T_S(y, t)$, which occurs at y = 0, is less than 20%; after 32 hr, it is less than 2.5%. The error in $T_S(y, t)$ when only the first term of Eqs. 1 and 2 is used, is less than 1% for $t \leq 16$ hr.

The temperature distribution in an actual beam or arch, which is not insulated at the ends, is not a function of the y coordinate only, since there is heat

4 Not in the neighborhood of the ends of the beam.

5 "Conduction of Heat in Solids," by H. S. Carslaw and J. C. Jaeger, Clarenden Press, 1947, p. 250 ff.

flow at the ends in the axial direction x. Hence the temperature distribution of Eqs. 1 and 2 is a good approximation of the temperature in an arch everywhere except in the neighborhood of the ends. This neighborhood is small if 2c/R is small, which is the case for "long" arches.

Arbitrary Temperature Pulse T(t) Applied to the Inner Face of the Arch.—Let $V_S(y, t)$ be the temperature distribution in the arch due to a unit step temperature pulse applied to the inner face of the arch, that is, let $V_S(y, t)$ be given by Eq. 1 with T_o set equal to unity. Using these values as influence coefficients, the temperature distribution T(y, t) produced by an arbitrary temperature pulse

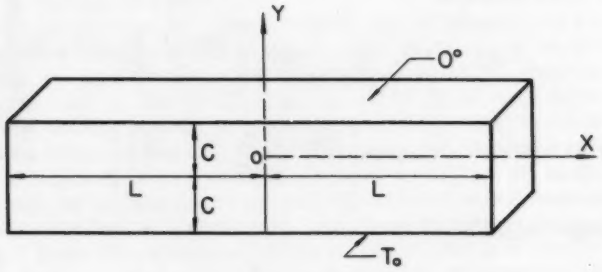

FIG. 1.—GEOMETRY

T(t) applied to the inner face of the arch can be evaluated by means of a Duhamel integral:

$$T(y, t) = \int_o^t \frac{dT(\tau)}{d\tau} \; V_S(y, t - \tau) \; d\tau \quad [\text{For } T(0) = 0] \quad \ldots . (4a)$$

or

$$T(y, t) = \int_o^t \frac{dT(\tau)}{d\tau} \left\{ \sum_{n=0}^{\infty} \text{erfc} \left[\frac{(2n+1)\,2c - (c - y)}{2\sqrt{k\,t}} \right] \right. \quad \ldots . (4b)$$

$$\left. - \text{erfc} \left[\frac{(2n+1)\,2c + (c - y)}{2\sqrt{k\,t}} \right] \right\} d\tau \quad \ldots \ldots \ldots . (4b)$$

Depending on the complexity of the function $\frac{dT(\tau)}{d\tau}$, the integral of Eq. 4 can be evaluated analytically, or numerically. In general, only the first term (n = 0) of the series expansion for $V_S(y, t)$ need be used, that is,

$$V_S(y, t) \approx \text{erfc} \frac{c\,(1 + y/c)}{2\sqrt{k\,t}} - \text{erfc} \frac{c\,(3 - y/c)}{2\sqrt{k\,t}} \quad \ldots . . (5)$$

thus considerably simplifying the integral in Eq. 4b.

Temperature Pulse T(t) With a Linear Rise Time Applied to the Inner Face of the Arch.—For the particular case of a linear pulse,

$$T(t) = \frac{T_o}{t_o} \; t \quad \ldots \ldots \ldots \ldots \ldots \ldots \quad (6)$$

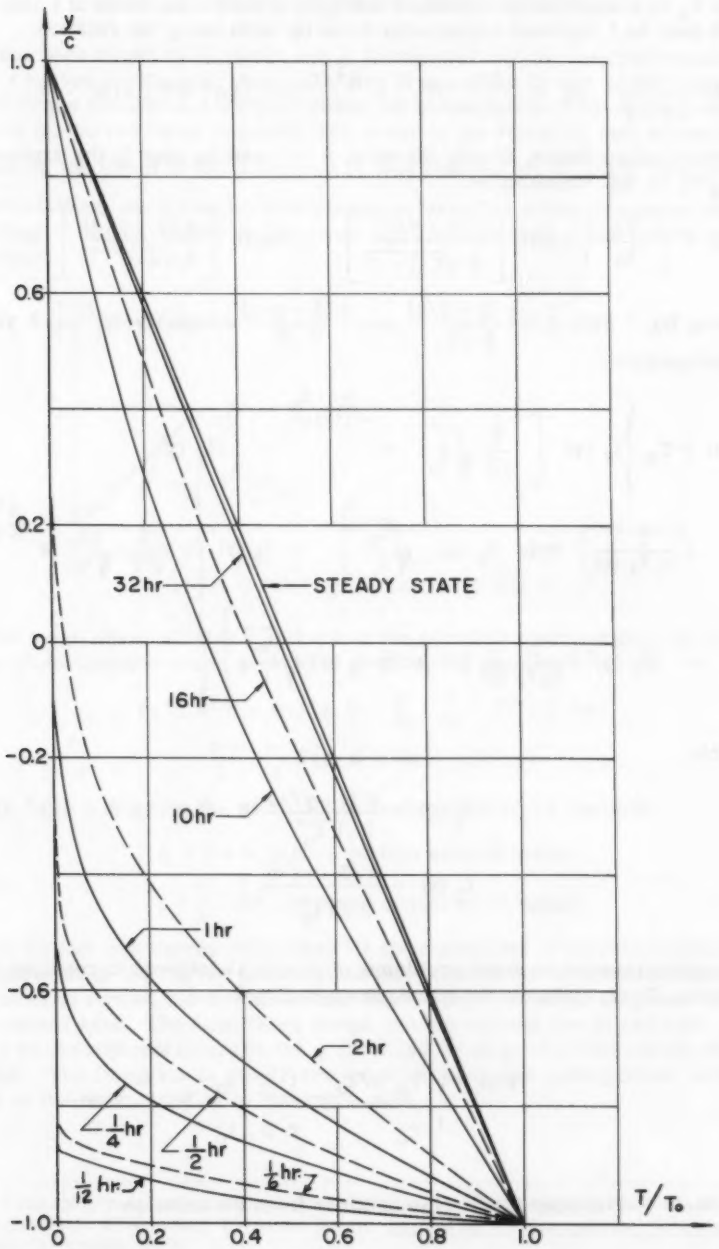

FIG. 2.—TEMPERATURE DISTRIBUTION T_S (y,t) IN ARCH

where T_o is a constant temperature and t_o is a particular value of t (Eq. 11), Eq. 4b may be integrated analytically term by term using the relation

$$\int_0^t \operatorname{erfc} \frac{A}{\sqrt{t-\tau}}\, d\tau = -\frac{2A}{\sqrt{\pi}}\sqrt{t}\; e^{-A^2/t} + \left[2A^2 + t\right] \operatorname{erfc} \frac{A}{\sqrt{t}} \quad \ldots (7)$$

For practical purposes, if only the term n = 0 need be kept in the expression for V_s (y, t), Eq. 4b becomes

$$T(y, t) = \int_0^t \frac{T_o}{t_o} \left\{ \operatorname{erfc}\left[\frac{c\,(1 + y/c)}{2\sqrt{k\,(t-\tau)}}\right] - \operatorname{erfc}\left[\frac{c\,(3 - y/c)}{2\sqrt{k\,(t-\tau)}}\right] \right. d\tau \quad \ldots (8)$$

Using Eq. 7 with $A = \frac{c\,(1 - y/c)}{2\sqrt{k}}$ and $\frac{c\,(3 - y/c)}{2\sqrt{k}}$ respectively, Eq. 8 yields upon integration,

$$T(y, t) = T_o \left\{ f_1(y) \left[-\frac{2}{\sqrt{\pi}}\sqrt{\frac{t}{t_o}}\; e^{-f_1^2(y)\frac{t_o}{t}} + \left(2f_1(y) + \frac{t}{t_o f_1(y)}\right) \operatorname{erfc}\, f_1(y)\sqrt{\frac{t_o}{t}} \right] + f_2(y) \left[-\frac{2}{\sqrt{\pi}}\sqrt{\frac{t}{t_o}}\; e^{-f_2^2\frac{t_o}{t}} + 2f_2(y) + \frac{t}{t_o f_2(y)}\right) \operatorname{erfc}\, f_2(y)\sqrt{\frac{t_o}{t}} \right] \right\} \quad \ldots (9)$$

in which

$$f_1(y) = \frac{c\,(1 + y/c)}{2\sqrt{k\,t_o}} \quad \ldots (10a)$$

$$f_2(y) = \frac{c\,(3 - y/c)}{2\sqrt{k\,t_o}} \quad \ldots (10b)$$

It is advantageous in some problems of practical interest to consider the distribution T_1 (y, t) due to the pulse shown in Fig. 3:

$$T(t) = \begin{cases} T_o\, t/t_o & t \le t_o \\ T_o & t > t_o \end{cases} \quad \ldots (11)$$

Using Eq. 9, the function T_1 (y, t) is obtained from the relation

STRAINS DUE TO THERMAL GRADIENTS T (y, t)

It has been shown by B. Boley and E. Barakette[3] that the longitudinal strains ϵ_x in a curved rectangular beam of radius R and depth 2c can be well approximated by the strains in a straight beam, for cases in which the depth to radius ratio of the curved beam is small. The error in the strain ϵ_x that arises from neglecting the effect of the curvature is less than 2% for $\frac{2c}{R} < 0.2$. For practical applications, many reactor shielding structures fall within this range; hence, the effect of the curvature of the beam will be neglected in the following development.

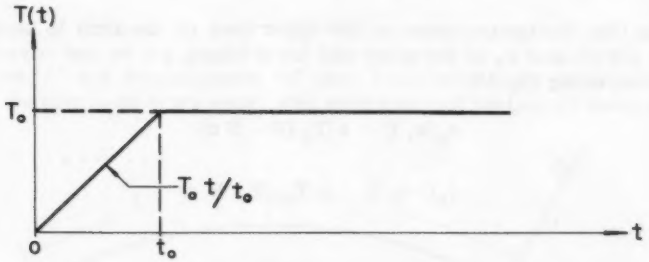

FIG. 3.—TEMPERATURE IMPUT-EQ. 11

The longitudinal strains ϵ_x, due to a temperature distribution T (y, t), in a beam of rectangular cross section is given by the relation[6,7]

$$\epsilon_x(y, t) = -\alpha T(y, t) + \frac{\alpha}{A} \int_A T(y, t)\, dA + \frac{\alpha y}{I} \int_A T(y, t)\, y\, dA + \alpha T(y, t) \quad \ldots\ldots\ldots\ldots (13)$$

where (with b denoting the width of the rectangular cross section)

$$A = 2\, c\, b \quad \text{(cross section area of beam)}$$
$$I = \frac{2}{3}\, b\, c^3 \quad \text{(Moment of Inertia of beam)} \quad \ldots\ldots\ldots (14)$$

and α (in feet per degree Fahrenheit) is the coefficient of thermal expansion of the material of the curved beam. The last term of Eq. 13 is the strain which produces no stress, due to the thermal expansion, of the fiber a distance y from the neutral axis. The first three terms are the strains due to restraint exercised by the adjacent fibers on the y-fiber and which produce the elastic stresses $E\Sigma$. The integrals in Eq. 13 are extended over the entire cross sectional area of the beam, leading to the expression,

---

[6] "The Determination of Temperature Stresses and Deflections in Two-Dimensional Thermoelastic Problems," by Bruno Boley, Journal of the Aeronautical Sciences, Vol. 23, No. 1, January, 1956.

[7] "Theory of Elasticity," by S. Timoshenko, McGraw-Hill Book Co., New York, 1954, p. 204.

$$\epsilon_x(y, t) = - \alpha\ T(y, t) + \frac{\alpha}{2c} \int_{-c}^{c} T(y, t)\ dy$$

$$+ \frac{3\ y}{2c^3} \int_{-c}^{c} T(y, t)\ y\ dy + \alpha\ T(y, t) \quad \ldots\ldots\ldots\ldots (15)$$

The strains at the upper and lower fibers, $y = \pm c$ respectively of the arch may be evaluated and will be used in the next section to determine the end rotations and displacements of the arch when the ends are considered to be free.

END ROTATIONS AND DISPLACEMENTS

Noting that the temperature on the upper face of the arch is kept at zero degrees, the strains ϵ_x at the upper and lower fibers, $y = +c$ and $-c$ respectively, become, using Eq. 15,

$$\epsilon_x(c, t) = \alpha\ T_o\ (P - N\ c)$$

$$\epsilon_x(-\ c, t) = \alpha\ T_o\ (P - N\ c) \quad \ldots\ldots\ldots\ldots\ldots (16)$$

where

$$P = \frac{1}{T_o\ A} \int_A T\ (y, t)\ dA = \frac{1}{2\ T_o\ c} \int_{-c}^{c} T(y, t)\ dy \quad \ldots\ldots\ldots (17)$$

$$N = \frac{1}{T_o\ I} \int_A T(y, t)\ y\ dA = \frac{3}{2c^3\ T_o} \int_{c}^{c} T(y, t)\ \ y\ dy \ldots\ldots (18)$$

and T_o is the maximum value to which the temperature pulse rises and is maintained.

The corresponding elongations $\delta(y, t)$ at the ends $x = \pm L$ of the arch of length $2L$ (Fig. 4), are given by

$$\delta(c, t) = \alpha\ L\ T_o\ (P + N\ c)$$

$$\delta(-c, t) = \alpha\ L\ T_o\ (P - N\ c) \quad \ldots\ldots\ldots\ldots\ldots (19)$$

Since the formulas for strain, Eqs. 13 and 15, have been derived on the assumption that sections plane before heating remain plane after heating,[6,7] the rotation at a given section x along the arch is given by

$$\theta\ (x) = \left[\frac{\epsilon_c - \epsilon_{-c}}{2\ c}\right] x = \alpha\ N\ T_o\ x \quad \ldots\ldots\ldots\ldots (20)$$

at $x = L$, the end rotation becomes:

$$\theta = \alpha\ N\ T_o\ L \quad \ldots\ldots\ldots\ldots\ldots\ldots (21)$$

Under the assumption of small displacements, the slope of the thermal deflection curve z(x) (Fig. 4) equals $\theta(x)$ so that

$$\frac{dz}{dx} = \theta\ (x) = \left[\frac{\epsilon_c - \epsilon_{-c}}{2\ c}\right] x = \alpha\ N\ T_o\ x \quad \ldots\ldots\ldots\ldots (22)$$

and by integration, the end displacement δ, at right angles to the arch, is given by

$$\delta = \int_0^L \theta\ (x)\ dx = \frac{\alpha\ L^2\ N\ T_o}{2} \quad \ldots\ldots\ldots\ldots\ldots (23)$$

The corresponding horizontal displacement at the end of the arch of central angle 2β becomes (Fig. 4)

$$a = \delta\ \sin\ \beta \quad \ldots\ldots\ldots\ldots\ldots\ldots (24)$$

The rotation "θ" and displacement "a" have been derived by considering the arch to be unrestrained at its ends. End moments and horizontal shears must

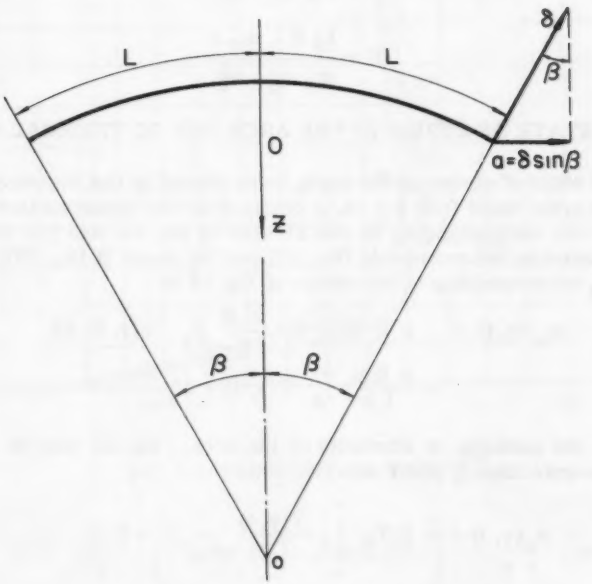

FIG. 4.—GEOMETRY OF ARCH

now be applied to the ends of the arch to force them back into their original fixed position.

END MOMENTS AND SHEARS

Let m_θ and h_θ be the moment and shear required to produce a unit rotation and zero horizontal displacement at the end of an arch of length 2L. Also, let m_a and h_a be the moment and shear required to produce a unit horizontal dis-

placement and no rotation at the ends of the arch. The four quantities m_θ, h_θ, m_a and h_a can easily be determined for any given arch by any of the usual structural methods available to the designer. The moments, M, and shears, H, required to produce end rotations and displacements, equal and opposite to those produced by the thermal gradient (θ and a), are given by the equations

$$\begin{aligned} m_\theta\ M + h_\theta\ H + \theta &= 0 \\ m_a\ M + h_a\ H + a &= 0 \end{aligned} \qquad \ldots\ldots\ldots\ldots\ldots\ldots (25)$$

$$\left(h_\theta = m_a\right)$$

Eqs. 25 are a statement that the ends of the arch are fixed. By similar methods, partially fixed or hinged arch moments and shears can be obtained. From Eq. 25,

$$M = \frac{h_\theta\ a - h_a\ \theta}{m_\theta\ h_a - h_\theta^2} \qquad \ldots\ldots\ldots\ldots\ldots\ldots (26)$$

$$H = \frac{h_\theta\ \theta - m_\theta\ a}{m_\theta\ h_a - h_\theta^2} \qquad \ldots\ldots\ldots\ldots\ldots\ldots (27)$$

FINAL STATE OF STRESS IN THE ARCH DUE TO THERMAL SHOCK

The final state of stress in the arch, is produced by the temperature pulse T (t) applied to the inner face y = -c, is obtained by the superposition of (a), the state of stress corresponding to the strains of Eq. 13, and (b), the state of stress produced by the moment M (Eq. 26) and the shear H (Eq. 27). The state of stress σ_x corresponding to the strain of Eq. 13 is

$$\sigma_x (y, t) = - \alpha\ E\ T(y, t) + \frac{\alpha\ E}{A} \int_A T(y, t)\ dA + \frac{\alpha\ E\ y}{I} \int_A T(y, t)\ y\ dA \qquad \ldots\ldots\ldots\ldots\ldots\ldots (28)$$

where E is the modulus of elasticity of the arch. Eq. 28 may be written in terms of the quantities N and P as

$$\sigma_x (y, t) = \alpha\ E\ T_o \left[- \frac{T(y, t)}{T_o} + P + N\ y \right] \qquad \ldots\ldots\ldots (29)$$

RESULTS FOR A STEP PULSE, $T(t) = T_o$

Substituting the n = 0 term of Eq. 1 into Eqs. 17 and 18, expressions for P and N are derived in terms of the integrals of the error function complements[8] (ierfc):

$$P = \frac{1}{\gamma} \left[\text{ierf}\ (0) - 2\ \text{ierfc}\ (\gamma) + \text{ierfc}\ (2\gamma) \right] \qquad \ldots\ldots\ldots (30)$$

---

[8] "Thermal Stresses in Curved Beams," Appendix II, "The Error Function and Related Functions," by Bruno Boley and E. Barrekette, Journal of Aeronautical Sciences, Vol. 25, No. 10, Oct., 1958.

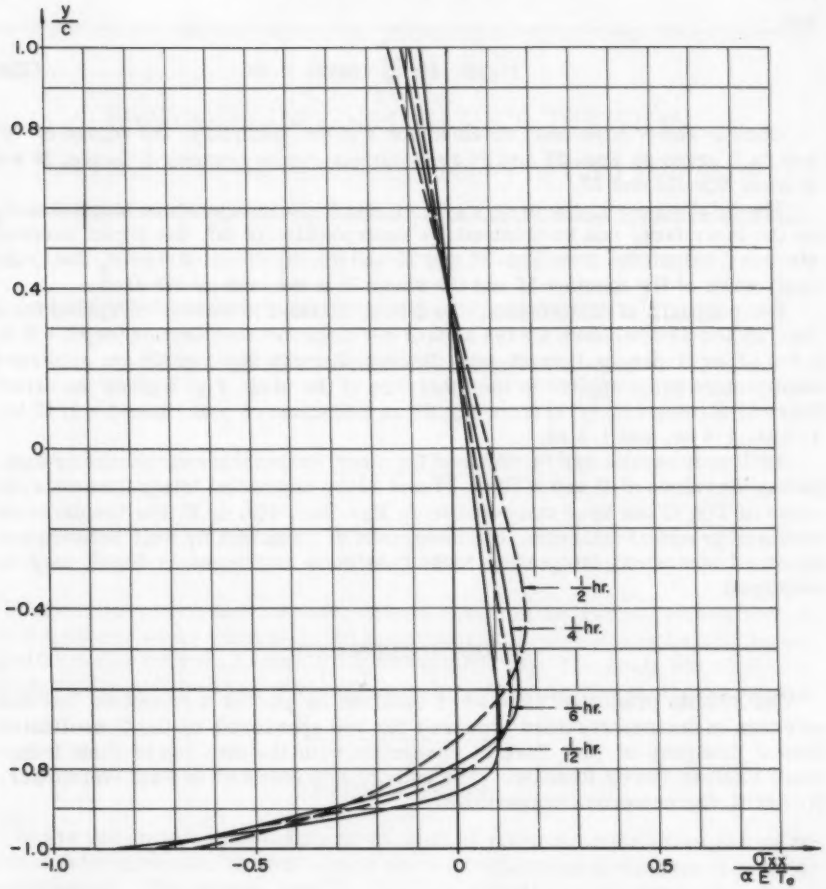

FIG. 5.—STRESS DISTRIBUTION $\frac{\sigma XX}{\alpha E\ T_O}$

$$N = \frac{6}{\gamma^2\ c}\left[i^2\text{erfc}\ (0) - i^2\text{erfc}\ (2\gamma)\right] - \frac{3}{\gamma\ c}\left[\text{ierfc}\ (0) + 2\text{ierfc}\ (\gamma) + \text{ierfc}\ (2\gamma)\right] \quad \ldots\ldots\ldots\ldots\ldots (31)$$

in which

$$\gamma = \frac{c}{\sqrt{k\ t}} \quad \ldots\ldots\ldots\ldots\ldots (32)$$

$$\text{ierfc}\ \xi = \int_{\xi}^{\infty} \text{erfc}\ z\ dz \quad \ldots\ldots\ldots\ldots\ldots (33a)$$

and

$$i^2\text{erfc}\ \xi = \int_{\xi}^{\infty} \text{ierfc}\ z\ dz \quad \ldots\ldots\ldots\ldots (33b)$$

Once P and N have been obtained for a given geometry, the values of "θ" and "a," given by Eqs. 21 and 24 respectively can be computed; hence, M and H from Eqs. 26 and 27.

The total stress in the arch, σ_x (y, t), due to the temperature step pulse T_o on the inner face, can be obtained by superposition of (a), the direct thermal stresses, calculated from Eqs. 28 and 29 and (b), the direct stress σ_x due to the application of the moment M and the shear H at the ends of the arch.

For purposes of illustration, the direct thermal stresses, computed from Eqs. 28 and 29 are shown for the arch of rectangular cross section (depth = 5 ft, k = 0.33 sq ft per hr.) which was discussed under the section on arbitrary temperature pulse applied to the inner face of the arch. Fig. 5 gives the direct thermal stresses σ_x (y, t) from Eq. 29 as a function of y at times t = 1/12 hr, 1/6 hr, 1/4 hr, and 1/2 hr.

Analogous results can be obtained for other temperature variations by computing the values of P and N (Eqs. 17 and 18) by numerical integration once the value of T(y, t) has been computed from Eqs. 4(a), 4(b) or 9. For temperature inputs of practical interests, the integrands are reasonably well behaved and standard numerical integration techniques such as Simpson's Rule[9] may be employed.

ACKNOWLEDGMENTS

The results presented here were obtained as part of a report on thermal stresses in nuclear reactors prepared for and sponsored by the Consolidated Edison Company of New York in connection with the erection of their Indian Point Nuclear Power Reactor. The authors are indebted to Paul Weidlinger, M. ASCE, for numerous suggestions.

9 "Numerical Methods in Engineering," by M. G. Salvadori and M. L. Baron, Prentice-Hall, 1952, New York, p. 70ff.

Journal of the
ENGINEERING MECHANICS DIVISION
Proceedings of the American Society of Civil Engineers

STRESSES AROUND RECTANGULAR OPENINGS IN A PLATE

By H. Boyd Phillips,[1] F.ASCE, and Ira E. Allen[2]

SYNOPSIS

Curves have been developed for determination of the normal stress around rectangular openings when subected to uniaxial or biaxial stress fields. Height to width ratios between 0.4 and 2.5 have been studied. The study was made experimentally utilizing the photoelastic interferometer method of stress analysis.

INTRODUCTION

In the design of massive structures, such as mass concrete dams, the problem of determining the state of stress around rectangular openings is frequently encountered. The opening may be a vertical elevator or access shaft, a horizontal or sloping gallery, or other such opening in the mass.

The stress distribution around openings in a uniform stress field has been investigated earlier[3,4,5,6]. However, those studies were for a uniaxial stress

Note.—Discussion open until November 1, 1960. To extend the closing date one month, a written request must be filed with the Executive Secretary, ASCE. This paper is part of the copyrighted Journal of the Engineering Mechaincs Division, Proceedings of the American Society of Civil Engineers, Vol. 86, No. EM 3, June, 1960.

[1] Engr., Design Div., U. S. Bur. of Reclamation, Denver, Colo.

[2] Engr., Design Div., U. S. Bur. of Reclamation, Denver, Colo.

[3] "Die Totale Zugkraft and Offnungen in Einem Einachsigen Druckspannungsfeld," by R. Hiltscher and B. Pant, Der Bauingenieur, Vol. 32, No. 12, December, 1957, pp. 470–474.

[4] "Stresses Around a Gallery-Determined by the Photoelastic Interferometer," by H. B. Phillips and C. N. Zangar, Proceedings, Soc. for Experimental Stress Analysis, Vol. VIII, No. 2, 1951, pp. 187-208.

[5] "Stress Analysis Applied to Underground Mining Problems—Part I," by W. L. Duvall, U. S. Dept. of the Interior, Bur. of Mines, Report R. I. 4192, March, 1948.

[6] "On the Stresses in the Neighbourhood of a Circular Hole in a Strip Under Tension," by R. C. J. Howland, Philosophical Transactions, Royal Soc. of London, Sec. A. Vol. 229, 1930.

field. This study was undertaken to simplify the determination of stress distribution for the design of reinforcement for rectangular openings of various height to width ratios and for a combination of stress fields.

For the preliminary design of a reinforcement around a gallery or other opening in a mass concrete dam, it is usually necessary to know only the net tensile force acting on the center lines of the opening. In the case of a horizontal gallery the tensile force is caused by the predominant dead load of the structure, and may be reduced by a horizontal compressive stress field caused by the reservoir load or the arch load in the case of an arch dam. For the final design, a stress determination along various lines radiating from the opening due to the two principal stress fields may be required.

Notation.—The letter symbols adopted for use in this paper are defined where they first appear and are arranged alphabetically, for convenience of reference, in the Appendix.

APPLICATION OF DATA

On Fig. 1 and 2 are curves for normal stress perpendicular to the center line of rectangular openings (having B to A ratios of 0.4 to 2.5) in an infinite plate due to uniform stress fields parallel to or perpendicular to the line. In Fig. 1 and 2, p indicates the intensity of the stress field acting on the opening in the direction indicated by the subscript. Figs. 1 and 2 are photoelastic interferometer stress analysis with B/A from 0.4 to 2.5 and D/A from 0.0 to 0.42. Fig. 1 shows the p_y stress field with σ_n along the Y-axis and Fig. 2 shows the p_x field with σ_n along the Y-axis. It was found in this study that the tensile stress normal to the center line due to a stress field parallel to the center line increased slightly with an increase in the B/A ratio. The increase was so slight, however, that for design purposes the same stress curve may be used for all B/A ratios studied (Fig. 1). Other investigators[3] have also reached this same conclusion. The compressive stress on the center line at the boundary of the opening due to a stress field perpendicular to it decreases rapidly with a decrease in B/A, falling below the maximum σ_n at a B/A ratio of approximately 0.5 (Fig. 2).

To find the net tensile force acting on the center line of a rectangular opening due to biaxial stress field, use the following procedure:

1. Determine B/A and k.
2. Using this B/A value, tabulate the σ_n/p_x values from the curves on Fig. 2.
3. Multiply the σ_n/p_x values by k.
4. Plot these k (σ_n/p_x) values as a curve on Fig. 1.
5. Determine the tensile area between the two curves.

This is the net tensile force in terms of p_y and A

As a numerical example, consider a horizontal rectangular gallery in a massive structure having a gallery width of 5 ft, a height of 7 1/2 ft, vertical compressive stress field of 100 psi, and a horizontal compressive stress field of 10 psi. The solution of this example is shown on Fig. 3.

Since rectangular openings having a B/A ratio of 1.5 are common in mass concrete structures, an extensive analysis was made of the stresses around

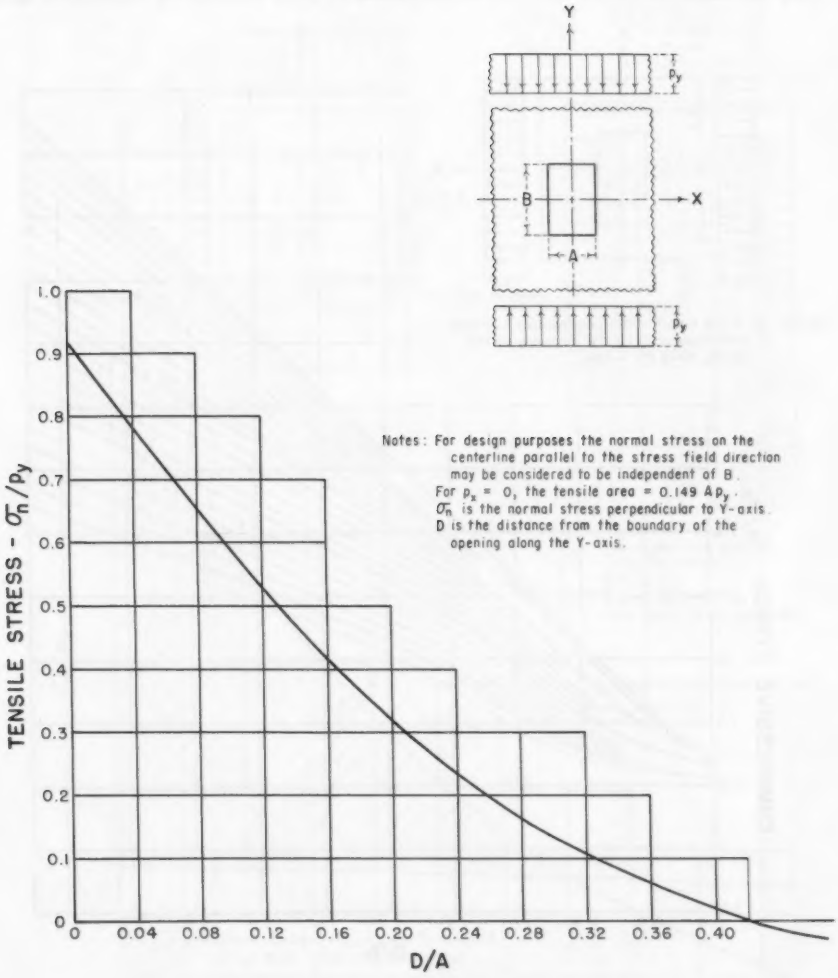

FIG. 1.—RECTANGULAR OPENINGS IN AN INFINITE PLATE

openings of this ratio. The results of this phase of the study are shown on Fig. 4 Table 1.

By other methods of analysis the normal and shear stresses, σ_x, σ_y, and τ_{xy}, are determined[7] at the point in the structure where the opening is to be located. They are assumed to be uniform stress fields of their respective intensities and

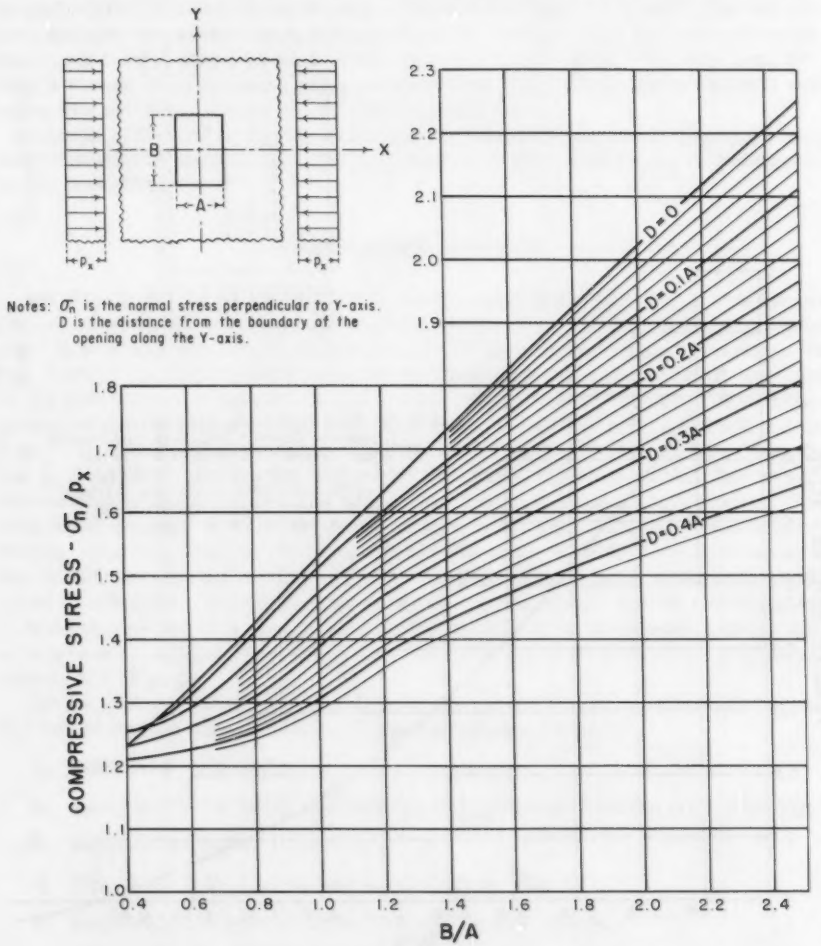

FIG. 2.—RECTANGULAR OPENINGS IN AN INFINITE PLATE

directions, p_x, p_y, and s_{xy}, acting on the opening. To determine the normal stress, σ_n, on the lines around the opening, multiply the stress coefficients tabulated on Fig. 4 by their respective intensities and sum the three resulting

[7] "Trial Load Method of Analyzing Arch Dams," Boulder Canyon Project Final Reports, Part V, Tech. Investigations, Bulletin 1, Bur. of Reclamation, 1938.

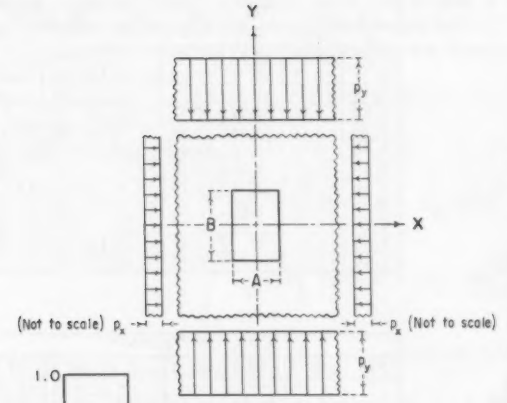

A = 5 feet
B = 7.5 feet
B/A = 1.5
p_y = 100 psi
p_x = 10 psi
k = p_x/p_y = 0.1

TABULATION FROM CURVES ON FIGURE 2

D/A	σ_n/p_x	$k\sigma_n/p_x$
0	1.78	0.178
0.02	1.77	0.177
0.04	1.76	0.176
0.06	1.75	0.175
0.08	1.73	0.173
0.10	1.72	0.172
0.12	1.71	0.171
0.14	1.69	0.169
0.16	1.68	0.168
0.18	1.66	0.166
0.20	1.65	0.165
0.22	1.63	0.163
0.24	1.61	0.161
0.26	1.59	0.159
0.28	1.57	0.157
0.30	1.55	0.155
0.32	1.53	0.153
0.34	1.51	0.151
0.36	1.49	0.149
0.38	1.47	0.147
0.40	1.45	0.145
0.42	1.43	0.143

The net tensile force = The shaded area between the two curves
= 0.0912 Ap_y
= 0.0912 (5) (100) (144)
= 6570 Lb/ft-length of gallery

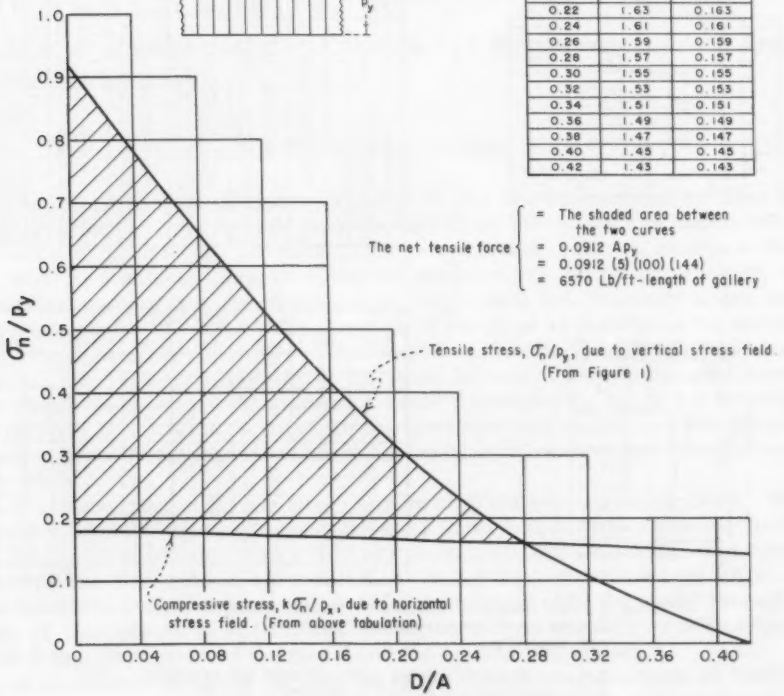

FIG. 3.—USE OF CURVES OF FIGS. 1 AND 2

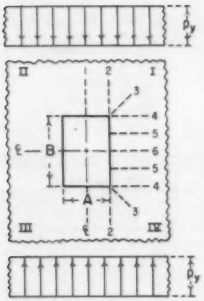

σ_n / p_y COEFFICIENTS						
D/A	LINE 1	LINE 2	LINE 3	LINE 4	LINE 5	LINE 6
0	−0.92	——	——	——	+1.49	+1.36
0.05	−0.75	+0.03	+1.06	+1.54	+1.46	+1.35
0.10	−0.59	−0.13	+0.85	+1.39	+1.42	+1.34
0.15	−0.44	−0.21	+0.76	+1.31	+1.38	+1.34
0.20	−0.32	−0.23	+0.71	+1.27	+1.33	+1.33
0.30	−0.13	−0.18	+0.64	+1.21	+1.27	+1.31
0.40	−0.02	−0.12	+0.59	+1.16	+1.22	+1.29
0.50	+0.04	−0.08	+0.58	+1.13	+1.18	+1.26
0.60	+0.07	−0.05	+0.56	+1.10	+1.16	+1.23
0.70	+0.09	−0.03	+0.54	+1.07	+1.13	+1.21
0.80	+0.10	−0.02	+0.53	+1.05	+1.10	+1.19
0.90	+0.11	0	+0.52	+1.04	+1.08	+1.18
1.00	+0.11	+0.01	+0.51	+1.03	+1.06	+1.17

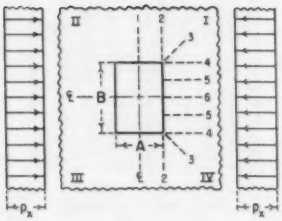

σ_n / p_x COEFFICIENTS						
D/A	LINE 1	LINE 2	LINE 3	LINE 4	LINE 5	LINE 6
0	+1.78	——	——	——	−0.89	−0.92
0.05	+1.75	+1.81	+1.32	+0.14	−0.78	−0.81
0.10	+1.72	+1.66	+1.12	−0.07	−0.66	−0.70
0.15	+1.69	+1.57	+0.99	−0.14	−0.55	−0.59
0.20	+1.65	+1.51	+0.89	−0.16	−0.43	−0.49
0.30	+1.55	+1.44	+0.77	−0.17	−0.24	−0.32
0.40	+1.45	+1.36	+0.70	−0.15	−0.14	−0.18
0.50	+1.36	+1.30	+0.65	−0.13	−0.08	−0.09
0.60	+1.28	+1.25	+0.61	−0.11	−0.05	−0.02
0.70	+1.23	+1.21	+0.59	−0.08	−0.02	+0.03
0.80	+1.19	+1.17	+0.57	−0.05	+0.01	+0.06
0.90	+1.16	+1.13	+0.55	−0.02	+0.03	+0.07
1.00	+1.14	+1.11	+0.54	+0.02	+0.05	+0.08

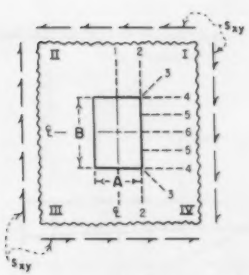

σ_n / s_{xy} COEFFICIENTS						
D/A	LINE 1	LINE 2	LINE 3	LINE 4	LINE 5	LINE 6
0	0	——	——	——	−0.95	0
0.05	0	−1.94	−2.77	−2.36	−1.00	0
0.10	0	−1.44	−2.20	−1.83	−0.99	0
0.15	0	−1.07	−1.89	−1.43	−0.93	0
0.20	0	−0.79	−1.69	−1.17	−0.85	0
0.30	0	−0.42	−1.45	−0.82	−0.65	0
0.40	0	−0.21	−1.28	−0.60	−0.43	0
0.50	0	−0.14	−1.18	−0.44	−0.27	0
0.60	0	−0.11	−1.11	−0.33	−0.17	0
0.70	0	−0.08	−1.06	−0.23	−0.10	0
0.80	0	−0.06	−1.02	−0.18	−0.06	0
0.90	0	−0.05	−0.99	−0.12	−0.03	0
1.00	0	−0.04	−0.98	−0.08	−0.02	0

Notes: D is the distance from the boundary of the opening along the line.
σ_n is the normal stress perpendicular to the line.
+ is compression.
− is tension.
σ_n/p_y and σ_n/p_x stresses are symmetrical about both centerlines.
σ_n/s_{xy} stress signs are as shown for Quadrants I and III, and opposite for II and IV.

FIG. 4.—PHOTOELASTIC INTERFEROMETER STRESS ANALYSIS FOR B/A = 1.5

stress effects. If instead of σ_x, σ_y, and τ_{xy} (the shear stress acting at 0, Fig. 6) the principal stresses, σ_I and σ_{II}, and their direction, α, are given, σ_I and σ_{II} may be rotated into σ_x, σ_y, and τ_{xy}.

As a numerical example of the use of the stress coefficients, consider a rectangular gallery having a height of 7 1/2 ft and a width of 5 ft in a massive structure with a maximum compressive principal stress field of 100 psi at 22 1/2°, counterclockwise from vertical, and a minimum compressive principal stress field of 10 psi.

Given then that; A = 5 ft, B = 7 1/2 ft, B/A = 1.5, σ_I = 10 psi, σ_{II} = 100 psi and, α = 22 1/2°.

Using the rotation equations:

$$\sigma_x = \sigma_I \cos^2 \alpha + \sigma_{II} \sin^2 \alpha \quad \ldots\ldots\ldots\ldots\ldots (1)$$

$$\sigma_y = \sigma_I \sin^2 \alpha + \sigma_{II} \cos^2 \alpha \quad \ldots\ldots\ldots\ldots\ldots (2)$$

$$\tau_{xy} = \left(\sigma_I - \sigma_{II}\right) \sin \alpha \cos \alpha \quad \ldots\ldots\ldots\ldots\ldots (3)$$

we obtain the following values: σ_x = 23.2 psi, σ_y = 86.8 psi and, τ_{xy} = -31.8 psi. For the tabulation of σ_n, see Table 1.

TECHNICAL DETAILS

The complete state of stress at any point in a two-dimensional problem is defined when the two principal stresses and their directions are known. The photoelastic polariscope provides only $(\sigma_I - \sigma_{II})$ and α, requiring another method, such as graphical integration, lateral extensometer, membrane analogy, or electrical analogy tray, to determine $(\sigma_I + \sigma_{II})$. On a free boundary where one principal stress is zero and the direction of the other is parallel to the boundary, the polariscope provides a very rapid method of determining boundary stress. For determining interior stresses, however, the photoelastic interferometer[8] is much more convenient because it provides σ_I, σ_{II}, and α directly. In addition, less load is required for the same accuracy as obtained with the polariscope, and time-edge effect has no appreciable influence on the optical measurements.

The material used for the model was an allyl diglycol carbonate resin. The variable height of the opening was from 0.2 in. to 1.25 in. with a constant width of 0.5 in. It was centered in a 5.8- by 5.8-in. plate 0.25-in.-thick. The opening with the B/A ratio of 1.5 was 0.6 in. by 0.9 in. in the same size plate. A compressive load of approximately 500 psi was applied to the model through a pair of multiple-element fluid load shoes, developed recently by the authors. Fig. 5 is a photograph of the model and the loading mechanism.

In an effort to evaluate the relation of the normal stress around an opening in a plate of finite dimensions to that of an infinite plate, the normal stress along the center lines parallel and perpendicular to the stress field direction

---

[8] "Photoelastic and Experimental Analog Procedures," by W. T. Moody and H. B. Phillips, U. S. Dept. of the Interior, Bur. of Reclamation, Engrg. Monograph No. 23, August, 1955.

were determined for a series of circular openings in a 5.8-in. by 5.8-in. plate. An analytical solution exists for the case of a circular opening in an infinite plate[9]. On the center line parallel to the stress field direction the normal stress determined experimentally was very near the analytical value until the diameter

TABLE 1.—RECTANGULAR OPENINGS IN AN INFINITE PLATE

LINE	D/A	σ_n STRESS DUE TO			σ_n †	
		σ_x	σ_y	τ_{xy}*	Quad. I	Quad. IV
1	0	+ 41	− 80	0	− 39	− 39
	0.05	+ 41	− 65	0	− 24	− 24
	0.10	+ 40	− 51	0	− 11	− 11
	0.15	+ 39	− 38	0	+ 1	+ 1
	0.20	+ 38	− 28	0	+ 10	+ 10
	0.30	+ 36	− 11	0	+ 25	+ 25
	0.40	+ 34	− 2	0	+ 32	+ 32
	0.50	+ 32	+ 3	0	+ 35	+ 35
	0.60	+ 30	+ 6	0	+ 36	+ 36
	0.70	+ 29	+ 8	0	+ 37	+ 37
	0.80	+ 28	+ 9	0	+ 37	+ 37
	0.90	+ 27	+ 10	0	+ 37	+ 37
	1.00	+ 26	+ 10	0	+ 36	+ 36
2	0	——	——	——	——	——
	0.05	+ 42	+ 3	+ 62	+ 107	− 17
	0.10	+ 39	− 11	+ 46	+ 74	− 18
	0.15	+ 36	− 18	+ 34	+ 52	− 16
	0.20	+ 35	− 20	+ 25	+ 40	− 10
	0.30	+ 33	− 16	+ 13	+ 30	+ 4
	0.40	+ 32	− 10	+ 7	+ 29	+ 15
	0.50	+ 30	− 7	+ 4	+ 27	+ 19
	0.60	+ 29	− 4	+ 3	+ 28	+ 22
	0.70	+ 28	− 3	+ 3	+ 28	+ 22
	0.80	+ 27	− 2	+ 2	+ 27	+ 23
	0.90	+ 26	0	+ 2	+ 28	+ 24
	1.00	+ 26	+ 1	+ 1	+ 27	+ 26
3	0	——	——	——	——	——
	0.05	+ 31	+ 92	+ 88	+ 211	+ 35
	0.10	+ 26	+ 74	+ 70	+ 170	+ 30
	0.15	+ 23	+ 66	+ 60	+ 149	+ 29
	0.20	+ 21	+ 62	+ 54	+ 137	+ 29
	0.30	+ 18	+ 56	+ 46	+ 120	+ 28
	0.40	+ 16	+ 51	+ 41	+ 108	+ 26
	0.50	+ 15	+ 50	+ 38	+ 103	+ 27
	0.60	+ 14	+ 49	+ 35	+ 98	+ 28
	0.70	+ 14	+ 47	+ 34	+ 95	+ 27
	0.80	+ 13	+ 46	+ 32	+ 91	+ 27
	0.90	+ 13	+ 45	+ 31	+ 89	+ 27
	1.00	+ 13	+ 44	+ 31	+ 88	+ 26
4	0	——	——	——	——	——
	0.05	+ 3	+ 134	+ 75	+ 212	+ 62
	0.10	− 2	+ 121	+ 58	+ 177	+ 61
	0.15	− 3	+ 114	+ 45	+ 156	+ 66
	0.20	− 4	+ 110	+ 37	+ 143	+ 69
	0.30	− 4	+ 105	+ 26	+ 127	+ 75
	0.40	− 3	+ 101	+ 19	+ 117	+ 79
	0.50	− 3	+ 98	+ 14	+ 109	+ 81
	0.60	− 3	+ 95	+ 10	+ 102	+ 82
	0.70	− 2	+ 93	+ 7	+ 98	+ 84
	0.80	− 1	+ 91	+ 6	+ 96	+ 84
	0.90	0	+ 90	+ 4	+ 94	+ 86
	1.00	0	+ 89	+ 3	+ 92	+ 86
5	0	− 21	+ 129	+ 30	+ 138	+ 78
	0.05	− 18	+ 127	+ 32	+ 141	+ 77
	0.10	− 15	+ 123	+ 31	+ 139	+ 77
	0.15	− 13	+ 120	+ 30	+ 137	+ 77
	0.20	− 10	+ 115	+ 27	+ 132	+ 78
	0.30	− 6	+ 110	+ 21	+ 125	+ 83
	0.40	− 3	+ 106	+ 14	+ 117	+ 89
	0.50	− 2	+ 102	+ 9	+ 109	+ 91
	0.60	− 1	+ 101	+ 5	+ 105	+ 95
	0.70	0	+ 98	+ 3	+ 101	+ 95
	0.80	0	+ 95	+ 2	+ 97	+ 93
	0.90	+ 1	+ 94	+ 1	+ 96	+ 94
	1.00	+ 1	+ 92	+ 1	+ 94	+ 92
6	0	− 21	+ 118	0	+ 97	+ 97
	0.05	− 19	+ 117	0	+ 98	+ 98
	0.10	− 16	+ 116	0	+ 100	+ 100
	0.15	− 14	+ 116	0	+ 102	+ 102
	0.20	− 11	+ 115	0	+ 104	+ 104
	0.30	− 7	+ 114	0	+ 107	+ 107
	0.40	− 4	+ 112	0	+ 108	+ 108
	0.50	− 2	+ 109	0	+ 107	+ 107
	0.60	0	+ 107	0	+ 107	+ 107
	0.70	+ 1	+ 105	0	+ 106	+ 106
	0.80	+ 1	+ 103	0	+ 104	+ 104
	0.90	+ 2	+ 102	0	+ 104	+ 104
	1.00	+ 2	+ 102	0	+ 104	+ 104

* Reverse sign for Quadrant IV.
† In psi.

of the opening approached 1 in., beyond which the experimental value exceeds the analytical value. On the center line perpendicular to the stress field direc-

9 "Theory of Elasticity," by S. Timoshenko, McGraw-Hill Book Co., New York, N. Y. 1934.

tion, the normal stress increased near the opening with increasing opening diameter in a manner that could be approximately related to the average normal stress on the line. The stress curve for the finite model plate width was higher at the opening than the analytical curve, falling below $\sigma_n/p = 1$ at the plate edge. The analytical curve, of course, approaches $\sigma_n/p = 1$ asymptotically. At some point then the two curves cross, and at this point the correction for the finite

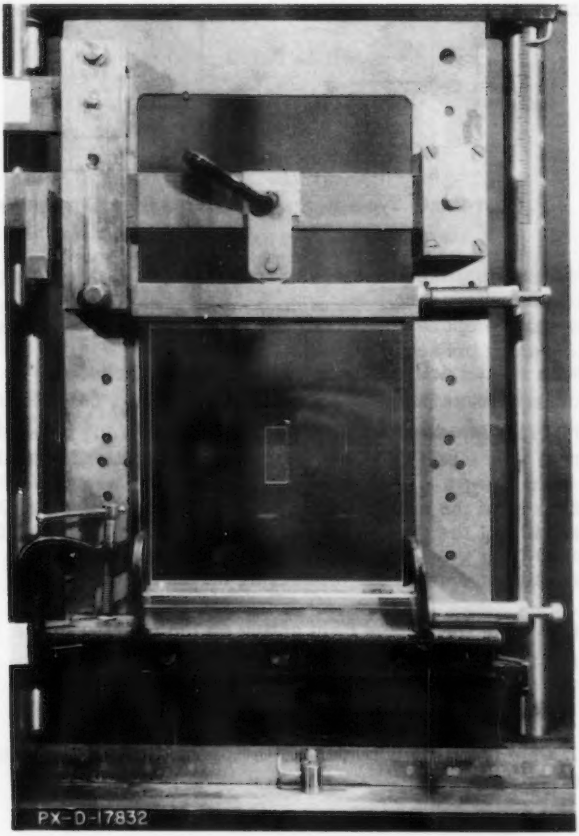

FIG. 5.—RECTANGULAR OPENINGS IN AN INFINITE PLATE

plate effect would be zero. This point varies with opening diameter, but for the corrections applied to the lines perpendicular to the stress field direction in this study it was assumed to be at D = B. The correction factor used at D = O was 1 divided by the average stress on the line, and varied linearly to 1 at D = B. Half the correction was applied to the lines at 45° to the direction of the stress field and no correction to the lines parallel to the stress field direction.

APPENDIX.—NOTATION

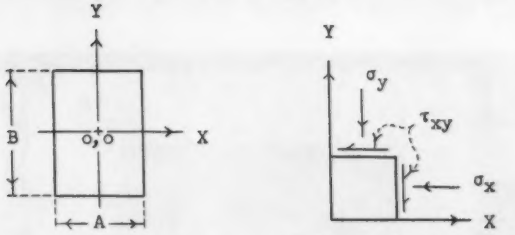

Coordinate System Positive Sign Convention

FIG. 6.—NOTATION SYSTEM

σ_x = Normal component of stress parallel to the X-axis acting at o, o with no opening present.

σ_y = Normal component of stress parallel to the Y-axis acting at o, o with no opening present.

τ_{xy} = Shear stress acting at o, o with no opening present.

σ_n = Normal stress perpendicular to the line being considered.

σ_I, σ_{II} = Principal stresses acting at o, o with no opening present.

α = Angle to the principal stress measured counterclockwise from the X-axis to σ_I; $0^\circ \leq \alpha < 90^\circ$.

p_x = Intensity of the stress field acting on the opening in the X-direction.

p_y = Intensity of the stress field acting on the opening in the Y-direction.

s_{xy} = Intensity of the shear stress field acting on the opening.

p_I = Intensity of the stress field acting on the opening in the direction of σ_I.

p_{II} = Intensity of the stress field acting on the opening in the direction of σ_{II}.

k = Ratio of p_x to p_y.

A = Dimension of the opening in the X-direction.

B = Dimension of the opening in the Y-direction.

D = Distance from the boundary of the opening along the line being considered.

Journal of the

ENGINEERING MECHANICS DIVISION

Proceedings of the American Society of Civil Engineers

CONTENTS

DISCUSSION

Note.—This paper is part of the copyrighted Journal of the Engineering Mechanics Division, Proceedings of the American Society of Civil Engineers, Vol. 86, No. EM 3, June, 1960.

ELECTRICAL ANALOG FOR EARTHQUAKE YIELD SPECTRA[a]

Discussion by John A. Blume

JOHN A. BLUME,[1] F. ASCE.—The research work reported by Messrs. Bycroft, Murphy, and Brown is of particular interest to the writer because of his having worked on the same problem from a different approach. The efforts by these investigators with the electrical analog constitute definite contributions to the storehouse of available information in earthquake research, particularly in inelastic dynamic response about which relatively little has been published.

There can be little remaining doubt that the history of damage, and lack of damage, in severe earthquakes cannot be reconciled unless energy loss and inelastic behavior are included as major factors.[2] Viscous damping, rubbing friction, and equivalent viscous damping[3] of composite materials and building elements are apparently of insufficient magnitude and effect to reduce elastic spectral responses from actual severe earthquakes to the yield values or even the ultimate strength values of buildings.[4] This is true for modern buildings designed under seismic codes, as well as for the traditional type of buildings.

A much more logical procedure than design by strength and elasticity alone is design, or refinement of design, by inelastic procedures that take into consideration the energy absorbing value of all materials and building elements. A simple method for doing this in normal structural design terminology has been presented by the writer.[4] This "reserve energy technique," that is general, in that it provides for any and all combinations of ductile, brittle, elasto-plastic, failing, or work hardening materials and building elements, will be applied herein to the elasto-plastic system the authors used in their research.

The first step of the procedure is to draw a static load-deflection curve to failure for the story or building under consideration. It should be noted that if such cannot be plotted, any mathematical or design procedure, no matter how rigorous, is merely a rough estimate that may lead to uneconomical designs or to inconsistent and unsatisfactory results in actual earthquakes. The additional value of most types of stress and of most building materials under rapid or dynamic loading as compared to static loading is roughly compensated for physically by the gradual but declining rate of deterioration of resistance under the repeated cycles of severe earthquake "loading" and yield excursions.

---

[a] October, 1959, by G. N. Bycroft, M. J. Murphy, and K. J. Brown.

[1] Pres., John A. Blume and Assocs., Research Div., and Francisco, Calif.

[2] "Structural Dynamics in Earthquake-Resistant Design," by John A. Blume, Proceedings, ASCE, Vol. 84, No. ST 4, July, 1958.

[3] "Frictional Effects in Composite Structures Subjected to Earthquake Vibrations," by L. S. Jacobsen, Dept. of Mech. Engrg., Stanford Univ., March 9, 1959, (California State Div. of Architecture, sponsor.)

[4] Closure to "Structural Dynamics in Earthquake-Resistant Design," by John A. Blume, Proceedings, ASCE, Vol. 85, No. ST 7, September, 1959.

Thus, static load tests can reasonably be used as a basis for constructing the required load-deflection diagrams that are actual approximations of the spring factor of the dynamic system. The spring factor may be linear, hardening, softening, elasto-plastic, or any combination. It should be plotted to the point of failure for the assumed initial force application.

The "reserve energy reduction coefficient," R, is the basis of reconciling any elastic design coefficient, C, with the elastic spectral earthquake response of a structure of elastic period T. Stated another way, R is the factor that reduces elastic spectral response acceleration to an equivalent value for elastic design modified (by R) for more realistic inelastic response values. R is based upon equating the kinetic energy of maximum response to the total available strain energy and energy dissipation value. The equation[4] for R for a single mass vibrating system is:

$$R_i = \frac{T_i}{T_d} \sqrt{\frac{D}{U_i - 0.5\,Hi}} \quad \ldots\ldots\ldots\ldots (1)$$

in which i is the subscript referring to the number or amount of any trial deflection of the structure or unit under consideration, T_d indicates the fundamental period, elastic state, T_i refers to the adjusted period at Δ_i, inelastic state, D is the elastic strain energy to the design unit stress, or the area under the diagram to Δ_D. (Fig. 1), U_i denotes the total area under the diagram up to trial deflection, i, and H_i refers to the "hump" area above a straight line from the origin to any point on the diagram at any deflection point, i.

For the special (elasto-plastic) case at hand, T_i will be considered equal to T_d, since the elasto-plastic system does not materially change its spring factor. The "hump" deduction, H_i (a design allowance for the possible softening or deterioration of resistance under repeated cycles), will be considered zero for this assumed perfectly elasto-plastic material with no deterioration. Thus, the expression becomes simply

$$R_i = \sqrt{\frac{D}{U_i}} \quad \ldots\ldots\ldots\ldots\ldots\ldots (2)$$

These values of R_i are initially assumed general for any earthquake spectrum and for any value of damping. This will be evaluated herein. The only remaining step is to consider the specific earthquake spectrum for any selected damping factor. Letting α equal the elastic spectral acceleration as a ratio to gravity, the equivalent (code) acceleration is $R_i\,\alpha i$. When $R_i\,\alpha i$ is equal to the design coefficient, C, the structure is barely adequate in energy dissipation value (at no safety factor), at deflection Δ_i. It is not necessary to assume value only to the yield point, since with more permanent yield or set (greater ductility factors) the structure can absorb much more energy. Thus, the authors' Fig. 16 does not indicate all important parameters, since the equivalent elasto-plastic accelerations would vary with the deflection beyond the yield point or the energy dissipation capacity. It was decided to plot ductility versus R_i.

Fig. 9 was utilized to obtain data for computing the authors' ductility factors, or deflection yield-point units. The maximum yield displacement was added to the elastic displacement, X_o and the sum divided by X_o. Values thus obtained for $\lambda = 0.20$ are shown in the first four columns of Table 1. The fifth and sixth columns show the determination of the equivalent "R" value from

Fig. 16, and the assumption that the design unit stress, including a one-third increase over normal (for earthquake loading), was 0.75 times the yield unit stress, which is a reasonable assumption for "elasto-plastic" mild steel. Columns 7 and 8 of Table 1 show the same data as for columns 5 and 6, but for another source of elastic data furnished the writer by the authors as part of another research program.[5] The variation in the values of columns 5 and 7 is to be noted. Columns 4, 6, and 8 are plotted on Fig. 1 together with other data.

Fig. 1 is a plot of elasto-plastic ductility factor versus the ratio of elasto-plastic spectral acceleration to elastic spectral acceleration, or R the "reserve energy reduction coefficient." The heavy solid line is R_i, calculated, as previously described, by the reserve energy procedure and Eq. 2. It is noted that the decrease of R from unity at design value to the yield point is due to the safety factor on a lineal basis, and beyond the yield point it is due to work done, or energy dissipation. Fig. 2 indicates these variations in the elastic response

TABLE 1.—DETERMINATION OF R AND DUCTILITY FACTOR

Period, T_i, in sec.	Fig. 9			Fig. 16		Blume-Sharpe-Elsesser	
	x_o, in in.	Maximum Yield Displacement, in in.	Computed μ, Ductility[a] factor	Lineal Acceleration, Ratio to g	R^a 0.75 x 0.24 / Col. (5)	Lineal Acceleration, Ratio to g	R^a 0.75 x 0.24 / Col. (7)
(1)	(2)	(3)	(4)	(5)	(6)	(7)	(8)
0.2	0.10	0.12	2.20	0.35	0.51	0.48	0.38
0.3	0.21	0.13	1.62	0.41	0.44	0.52	0.35
0.4	0.36	0.15	1.42	0.41	0.44	0.53	0.34
0.5	0.58	0.21	1.36	0.35	0.51	0.52	0.35
0.6	0.84	0.19	1.23	0.27	0.67	0.37	0.49
0.7	-	-	-	0.21	0.86	-	-
0.8	-	-	-	0.15	1.20	-	-

[a] Plotted in Fig. 1

and the four right-hand columns of Table 1 show the results for the two sets of analog data, both of which are plotted on Fig. 1 for the corresponding ductility factors. The general relationship to the R curve is fairly close for the authors' values, although the vertical scale variation between the new research program[5] previously referred to and Fig. 16 data is considerable.

The discussion of the authors' paper by Messrs. Berg and Thomaides became available to the writer at this stage of the comparison. Their digital computer results for the same elasto-plastic problem were then subjected to the same ductility and R factor calculations as those used for the authors' data. The results, also plotted on Fig. 1, show a somewhat better relationship to the

[5] "A Structural-Dynamic Investigation of Fifteen School Buildings Subjected to Simulated Earthquake Motion," by Blume, Sharpe, and Elsesser, for the State of California, Dept. of Pub. Wks., Div. of Architecture (being printed).

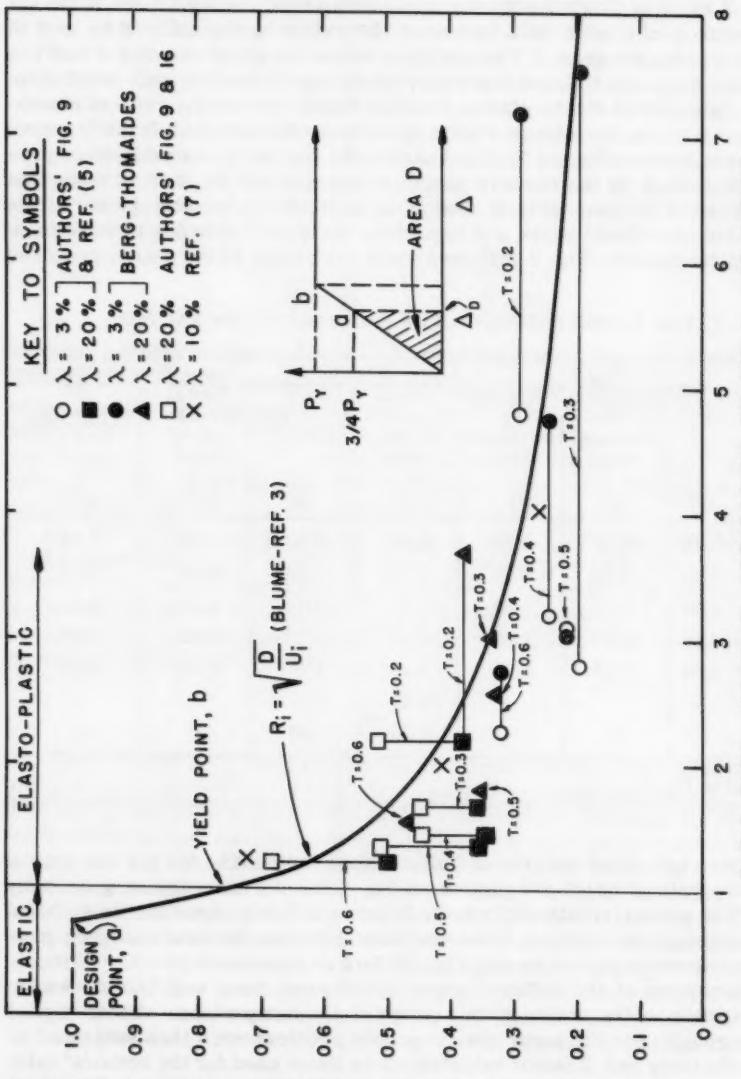

FIG. 1.—SINGLE-MASS ELASTO-PLASTIC SYSTEMS; EL CENTRO 1940

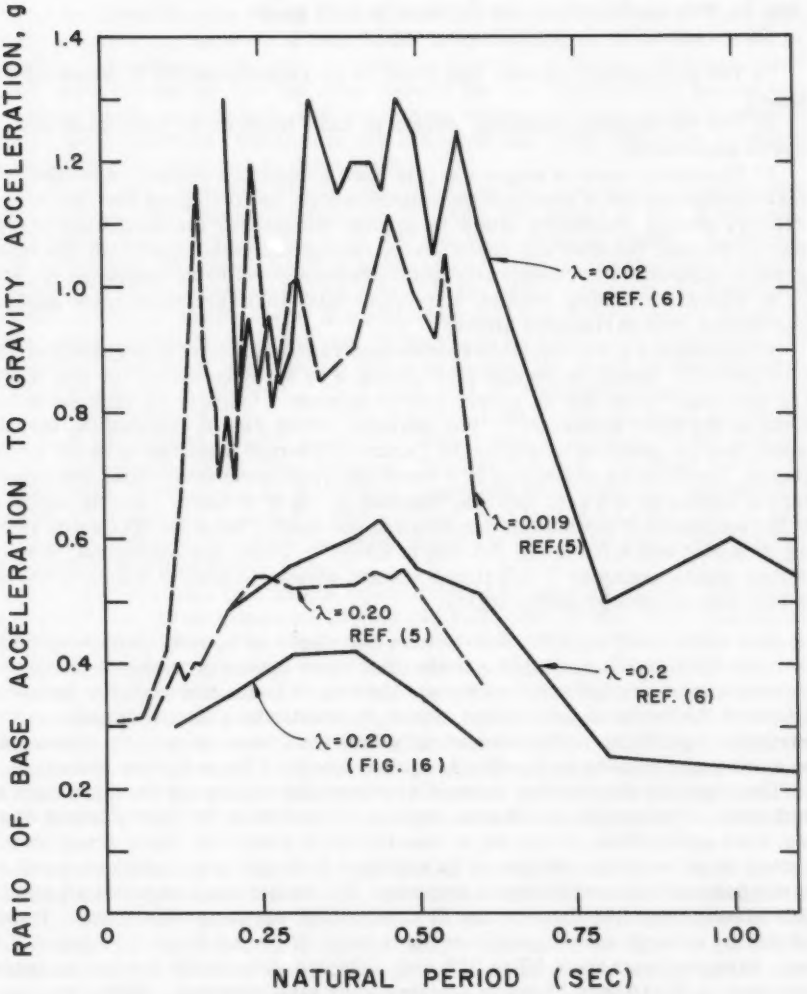

FIG. 2.—ELASTIC SPECTRA FOR EL CENTRO 1940 (N-S)

R curve, thus, providing some substantiation of the R curve and the Berg-Thomaides data. Still another set of data,[6] and perhaps the only other available set of inelastic data, was subjected to the same procedure and plotted on Fig. 1. The conformity to the R curve is very good.

Based upon Fig. 1, the following can be noted:

1) The parameter, period, has little or no relationship to R curve agreement;

2) The parameter, damping, seems to have little or no relationship to R curve agreement;

3) The compliance is so good in this case at least, as compared to the many other uncertainties in practical earthquake design, as to suggest that the simple reserve energy procedure might be applied directly to elasto-plastic energy design without the need for computer or analog analysis. Although the more general application to complex inelastic systems is yet to be compared to tests or to digital or analog results, the writer has, thus far, found good general agreement with earthquake history;

4) Any elastic acceleration response spectrum might be reduced to an equivalent inelastic design by simply multiplying α by R_i, determined for any limiting deflection ratio for an elasto-plastic system. (This is an inverse statement of the third statement.) For example, from Fig. 1, assume the single-mass design problem requires El Centro 1940-type resistance at no safety factor, the limiting deflection is 4 times the yield point deflection, the structure's period is 0.5 sec, and the damping is 5% of critical. The R factor is 0.29 regardless of period and damping and the elastic value for El Centro 1940, 5% damping and a period of 0.5 sec is 0.60g.[4] Then, the equivalent code or design elastic value at 1-1/3 times normal stress is simply 0.29 x 0.60g or 0.17g, with no energy safety factor.

It is to be noted as a word of caution that there are many other factors to be considered in actual design and also that these energy procedures for structures are recent considerations without the test of time. However, the inelastic approach to research and design seems to constitute a major assault on the earthquake problem. Time seems very important also, as may be attested to by earthquake results at Agadir, Arequipa, Mexico City and other places.

The apparent discrepancy in results between the analog and the digital work, and, also, between the two elastic system results from the New Zealand analog, need explanation, of course, to benefit future research. Some error is expected in all such operations as is apparent from the complexity of a major earthquake and the sensitivity of response. The writer has compared all available elastic response data for the El Centro 1940 north-south record. These efforts by several investigators cover a range of period from 0.10 sec to 3.5 sec, damping from about 2% to 20% and, although principally for single-mass systems, 2, 3, 10, and 15 mass systems were also included. There was fair agreement in some areas and considerable variation in others. In the long period, multi-mass range there are only two current sources one of which, the authors' electric analog, produces shears less than a recent digital source. The important point here is that the recent higher values, even if found to be more accurate, would not change but would instead reinforce the conclusions in the paper in which the multi-mass analog results were originally shown.[2]

---

6 "Intensity of Ground Motion During Strong Earthquakes," by G. W. Housner, Office of Naval Research, Contract N60NR-244, August, 1952.

In other words, all results to data indicate the vast gap between elastic values of response and code design values even at very high assumed damping values. The need for realistic energy dissipation design is abundantly clear.

It is believed that the writer's staff provided the shadowgraph or input data for the authors' analog work although this is not certain, since it was not mentioned by the authors. Several earthquake records, including El Centro 1940 (N-S), were developed into the form needed for the New Zealand analog and furnished to the Dominion Laboratory on an exchange basis, wherein certain results were returned. Whether or not the Dominion Laboratory has modified these graphs is not known to the writer.

Comparison of previous (1959) results[5] from the New Zealand analog with the Office of Naval Research program results[6] are shown in Fig. 2 and indicates fairly close agreement at both low and high damping values. However, subsequent (Fig. 16) analog results, also shown in Fig. 2, indicate considerable disparity from the previous analog data.[5] If the same shadowgraph were used for both series of analog tests, it would seem that any human errors would be minor compared to other problems. If the shadowgraphs were modified at the Dominion Laboratory, between the two test series, the graph as well as other factors should be considered. Two other sets of earthquake data were compared. The Olympia 1949 spectrum, made in 1959, by the analog,[5] compares very well with the Housner[6] record for 20% damping up to a 0.5 sec period, which is the limit of this run. However, the 20% damping spectrum for the El Centro 1934 (N-S), made on the analog, produces accelerations considerably greater than that for Housner's 20% curves[6] that is also to a 0.5 sec period. The Office of Naval Research program values, in this case, are approximately 50% to 75% of the analog values.

A further question that might be considered is whether or not the digital approach[7] has treated damping beyond the yield point in the same manner as did the authors. The authors apparently combined damping viscosity and energy dissipation beyond the yield, which procedure seems logical.

In the writer's opinion, actual damping values cannot safely be assumed to range from 10% to 20% as the authors state. Values have often been found[5,8] below 10% and even below 5% for low amplitudes. The use of 3% and 20% in the examples of this discussion above is for comparison purposes only and to cover a wide range of damping. The reserve energy procedure contemplates the normal use of only 5% as a reasonable maximum for non-yield and non-damage conditions.

A note of warning is also expressed about the sole use of the elasto-plastic assumption in research and design. Many materials and combinations of building materials[2,3,4] are not elasto-plastic or even good approximations to this convenient characteristic. The over-simplification of earthquake motion as simple harmonic motion some years ago was in some respects similar to over-simplifying inelastic response to the elasto-plastic. Both assumptions are convenient and very useful, but they may vary from actuality. Their limitations must be recognized.

---

7 "Effect of Inelastic Action on the Response of Simple Structures to Earthquake Motions," by R. M. Sheth, M. S. thesis under Dr. N. M. Newmark, Univ. of Illinois, Dept. of Civ. Engrg., 1959.

8 "Period Determinations and Other Earthquake Studies of a Fifteen-story Building," by John A. Blume, Chapter 11, Proceedings of World Conf. on Earthquake Engrg., June, 1956, E.E.R.I., Room 1039, 465 California St., San Francisco, Calif.

The discussion herein is not intended to be critical but to provide numerical data and other data for reconciliation of the apparent differences of certain analog and computer results. The finding and resolution of such differences is in itself a contribution to research and seems a proper basis for proceedings discussion. The electric analog is a valuable research tool which has advantages, (as well as disadvantages) over digital and other computers.

The authors are to be commended for their pioneering efforts in elasto-plastic spectral response with the electric analog. It is hoped that this work will be greatly extended after further evaluation of the procedures and equipment, and that, eventually, complex inelastic systems can be tested as well as elasto-plastic systems.

LATERALLY LOADED THIN FLAT PLATES[a]

Discussion by K. Yervant Terzian

K. YERVANT TERZIAN,[1] A. M. ASCE.—The author should be complimented for a concise research paper with important practical application and in particular for the accuracy of the results obtained utilizing relatively inexpensive equipment.

Referring to the section on rectangular plates, the writer carried out a series of tests[2] in 1954, using a rudimentary set-up, shown in Fig. T1, with a distributed load over the entire surface. The two long sides were always kept free, and the short sides were fixed or simply supported on knife edges. Because of the difficulties in setting the three parallel planes accurately, the writer only obtained the curvatures, or moments along the axis parallel to the free or long sides. The model used was Plexiglass 1-A, 6 in. by 9 in. by 1/4 in., coated with a very thin (molecular) coat of aluminum vapor in a vacuum chamber. The back of the plate was cemented to a rubber pad with attached nylon strings fastened through interconnected levers to lead weights, simulating a uniform load of 0.5 psi, in all cases.

The grid consisted of a series of black-nylon wires that were strung from a machined brass rod, looped over a second machined rod and weighted by small lead weights. By adjusting the two side plates holding the brass rod, the whole set-up was adjusted backwards and forwards and tilted.

The photographic equipment consisted of a camera with an F = 6 in. lens noted for its perfect spherical abberation correction.

The lighting arrangement consisted of two No. 2 floods with a white cardboard reflector set 2 in. behind the grid with a hole in the center for the camera lens. Arc lighting did not prove satisfactory.

Plans and elevations of the model mount and the grid are shown in Fig. T2.

For these experiments, a small flashlight was used to collimate the negative and model planes. An optical flat was then set in the grid plane by stringing it between two nylon wires. Thus, the grid plane was collimated parallel to the negative plane.

Using the presan system, two separate pictures, before load and after load, were taken and the grids were measured with a filar micrometer microscope. At the end of the experiment, the model plate was cut and milled in strips of 6 in. by 1/2 in. in order to determine the modulus of elasticity. The strips were cut lengthwise, crosswise, with and without the rubber backing. Load-deflection test consisted of a concentrated load at mid-span. The deflection

---

a October, 1959, by William A. Bradley.

1 Assoc., Lawrence T. Beck and Assocs., Philadelphia, Pa.

2 "A Photographic Method of Structural Analysis," by K. Yerrant Terzian, Master's Thesis, Univ. of Pennsylvania, 1954.

of the center was measured, the results plotted and the modulus of elasticity determined. The results showed that the rubber backing did not have any effect on the modulus of elasticity. The results obtained were corroborated using a finite-difference solution, but due to the unavailability of a digital computer at the time, the number of unknowns was limited.

As for a specific case, the results of the Experiment on a uniformly loaded plate, simply supported on two edges (short sides) and free on two opposite edges (long sides), are tabulated in Figs. 3 to 8. Photographs of the negative before load and after load enlarged 4.33 times are shown in Figs. 9 and 10, respectively. The results of this series of experiments showed that with the equipment used, results can be ascertained within a percentage error margin

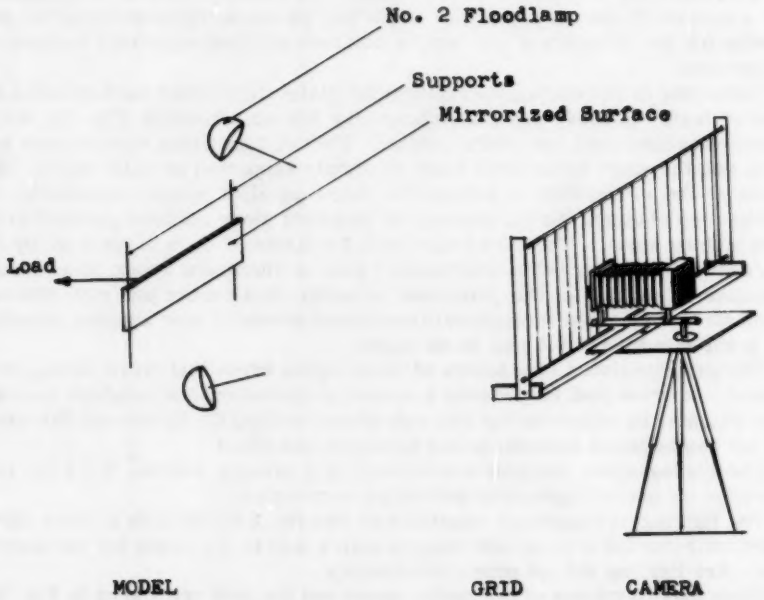

FIG. T1.—TEST SET-UP

of 10% to 15%. A commercial semi-automatic devise, involving expensive and complicated equipment of high accuracy, achieves far better results.

Mr. Bradley's work is very encouraging from the standpoint of deriving practical results for complicated problems without resorting to this commercial equipment. It could become a useful tool in a consulting office, particularly with the present tendency towards irregular column positions under a flat slab.

It would be very enlightening if the author would delve into the procedures followed to set up the equipment and to set the planes of the camera negative, grid, and model in their exact parallel positions. As a possible source of error, the suggestion of inaccurate collimation of the negative, model and grid planes may be worth discussing.

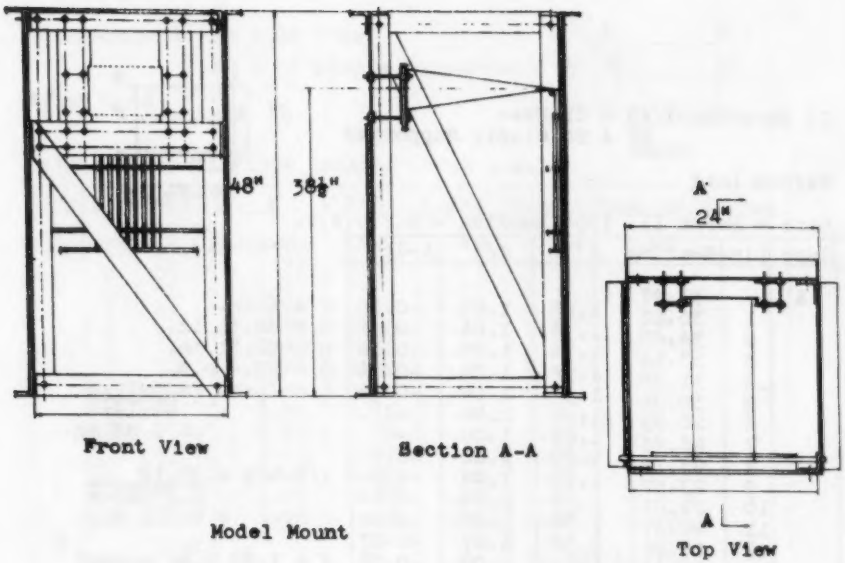

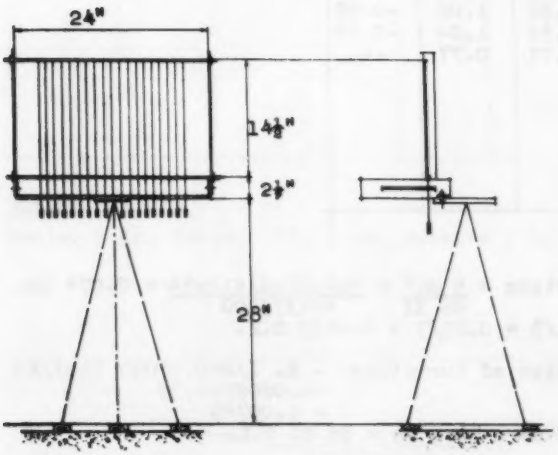

FIG. T2.—PLANS AND ELEVATIONS, MODEL MOUNT AND GRID SCALE

II Experiment AB & CD Free
AB & BD Simply Supported

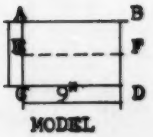

Before Load

Date - March 11, 1954 Loading - 0.5 p.s.i.

Supp	Line	Reading	J'	J/J'	1-J/J'
A		37.47			
	1	36.22	1.25	1.05	-0.05
	2	34.68	1.54	1.06	-0.06
	3	33.14	1.54	1.06	-0.06
	4	31.58	1.56	1.04	-0.04
	5	30.01	1.57	1.04	-0.04
	6	28.39	1.62	1.00	--
	7	26.76	1.63	1.00	--
	8	25.16	1.60	1.02	-0.02
	9	23.57	1.59	1.02	-0.02
	10	22.01	1.56	1.04	-0.04
	11	20.47	1.56	1.06	-0.06
	12	18.95	1.52	1.07	-0.07
	13	17.44	1.51	1.08	-0.08
	14	15.88	1.56	1.04	-0.04
	15	14.33	1.55	1.05	-0.05
	16	12.73	1.60	1.02	-0.02
	17	11.17	1.56	1.04	-0.04
B		9.46	1.71	0.77	--

F = 6 in.
h = 48.31 in.
p = 50.81 in.
O = 25.4 m.m.
q = (p+h) $F=\frac{99 \times 12 \times 6}{99 \times 12 \times 6}$
= 6.38 in.

$1/J=h+p = \frac{99.12}{6.38 \times 25.4}$
= 0.611 m.m.

J = 1.63 m.m. except at supports

DESIGN REQUIREMENT

Check on Max. Deflection = $\frac{5\ Ml^2}{48\ EI} = \frac{5 \times 4.23 \times 81 \times 12 \times 64}{48 \times 375000} = 0.074$ in.

which is less than t/3 = 0.25/3 = 0.0833 O.K.

Check on Minimum Radius of Curvature: - R. 1/R=0.02022 (1-J/K)
=0.02022x0.39
= 0.00789

R = 127 in. which is more than 2h = 96.62 O.K.

FIG. T3

II Experiment AB & CD Free
AB & BD Simply Supported

After Load

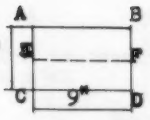

MODEL

Date - March 11, 1954 Loading - 0.5 p.s.i.

Supp	Line	Reading	K	J/K	1-J/K	Moment	Theorat	%Error
A		39.34						
	1	38.14	1.20	1.09	0.09	+0.22	0.00	
	2	36.45	1.69	0.96	0.04	1.09		
	3	34.60	1.85	0.88	0.12	1.95		
	4	32.56	2.04	0.80	0.20	2.50		
	5	30.23	2.33	0.70	0.30	3.26		
	6	27.75	2.48	0.66	0.34	3.80		
	7	25.27	2.48	0.66	0.34	4.01		
	8	22.81	2.46	0.66	0.34	4.23	5.14	17.7%
	9	20.50	2.31	0.71	0.29	3.80		
	10	18.30	2.20	0.74	0.26	3.26		
	11	16.19	2.11	0.77	0.23	3.04		
	12	14.21	1.98	0.82	0.18	2.28		
	13	12.31	1.86	0.88	0.12	1.74		
			1.26	1.04	0.04	0.00	0.00	
B		11.09						
						in lbs	in lbs	
		m.m.	m.m.					

MOMENT DIAGRAM

Scale: 1 in. Horiz. = 1.61 in. Model & 1 in Vert.= 5.43 in.-lbs. Model

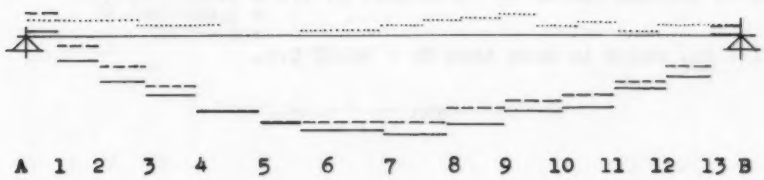

FIG. T4

Pl 1 - EF

II Experiment AB & CD Free
AB & BD Simply Supported

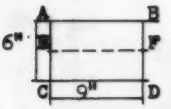

MODEL

Before Load

Date - March 11, 1954 Loading - 0.5 p.s.i.

Supp	Line	Reading	J'	J/J'	1-J/J'
E		38.68			
	1	37.35	1.33	0.98	+0.02
	2	35.81	1.54	1.06	-0.06
	3	34.21	1.60	1.02	-0.02
	4	32.61	1.60	1.02	-0.02
	5	31.04	1.57	1.04	-0.04
	6	29.42	1.62	1.00	--
	7	27.83	1.59	1.02	-0.02
	8	26.25	1.58	1.03	-0.03
	9	24.68	1.57	1.04	-0.04
	10	23.13	1.55	1.05	-0.05
	11	21.59	1.54	1.06	-0.06
	12	20.02	1.57	1.04	-0.04
	13	18.49	1.53	1.06	-0.06
	14	16.90	1.59	1.02	-0.02
	15	15.29	1.61	1.01	-0.01
	16	13.67	1.62	1.00	--
	17	12.03	1.64	0.99	+0.01
F		10.65	1.38	0.95	+0.05

F = 6 in.
h = 48.31 in.
p = 50.81 in.
O = 25.4 m.m.
q = (p+h) $F = \frac{99 \times 12 \times 6}{99 \times 12 \times 6} = 6.38$ in.

$1/J - \frac{h+p}{90} = \frac{99.12}{6.38 \times 25.4}$
$= 0.611$ m.m.

J = 1.63 m.m. except at supports

DESIGN REQUIREMENT

Check on Max. Deflection $= \frac{5}{48} \frac{Wl^2}{EI} = \frac{5 \times 3.91 \times 81 \times 12.64}{48 \times 375{,}000} = 0.068$ in.

which is less than t/3 = 0.25/3 - 0.0833 in. O.K.

Check on Minimum Radius of Curvature: R. 1/R = 0.02022(1-J/K)
= 0.02022x0.36
= 0.00726

R = 137 in. which is more than 2h - 96.62 O.K.

FIG. T5

II Experiment AB & CD Free
AC & BD Simply Supported

After Load

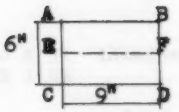

MODEL

Date - March 11, 1954 Loading - 0.5 p.s.i.

Supp	Line	Reading	K	J/K	1-J/K	Moment	Theorat	%Error
E		39.03						
	1	37.54	1.49	0.88	0.12	0.87	0.00	
	2	35.80	1.74	0.94	0.06	0.98		
	3	33.90	1.90	0.86	0.14	1.63		
	4	31.83	2.07	0.79	0.21	2.72		
	5	29.56	2.27	0.72	0.28	3.15		
	6	27.19	2.37	0.69	0.31	3.68		
	7	24.83	2.36	0.69	0.31	3.80		
	8	22.46	2.37	0.69	0.31	3.91	5.14	
	9	20.19	2.27	0.72	0.28	3.48		
	10	17.94	2.25	0.72	0.28	3.26		
	11	15.80	2.14	0.76	0.24	2.72		
	12	13.75	2.05	0.80	0.20	2.17		
	13	11.84	1.91	0.85	0.15	1.52		
F		10.79	1.05	0.85	0.15	0.98	0.00	
		m.m.	m.m.			in lbs.		

MOMENT DIAGRAM

Scale: 1 in. Horiz. = 1.61 in. Model & 1 in Vert.= 5.43 in.-lbs. Model

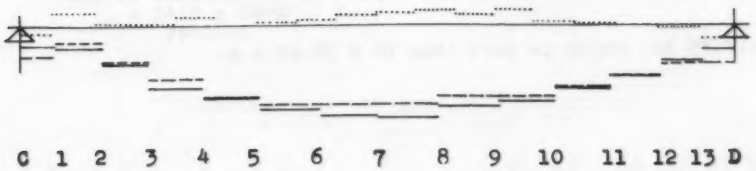

FIG. T6

Pl 1 - CD

II Experiment AB & CD Free
AB & BD Simply Supported

Before Load

Date - March 11, 1954 Loading - 0.5 p.s.i.

Supp	Line	Reading	J'	J/J'	1-J/J'
C		43.16			
			1.55	1.00	
	1	41.61	1.61	1.01	-0.01
	2	40.00	1.64	0.99	+0.01
	3	38.36	1.56	1.04	-0.04
	4	36.80	1.56	1.04	-0.04
	5	35.24	1.59	1.02	-0.02
	6	33.65	1.58	1.03	-0.03
	7	32.07	1.59	1.02	-0.02
	8	30.48	1.54	1.06	-0.06
	9	28.94	1.53	1.06	-0.06
	10	27.41	1.54	1.06	-0.06
	11	25.87	1.53	1.06	-0.06
	12	24.34	1.55	1.05	-0.05
	13	22.79	1.57	1.04	-0.04
	14	21.22	1.58	1.03	-0.03
	15	19.64	1.55	1.05	-0.05
	16	18.09	1.48	1.10	-0.10
	17	16.61	1.41	0.93	+0.07
D		15.20			

F = 6 in.
h = 48.31 in.
p = 50.81 in.
0 = 25.4 m.m.

$q = (p+h)\frac{F}{99x12x6} = \frac{99x12x6}{99x12x6} = 6.38$ in.

$1/J = \frac{h+p}{90} = \frac{99.12}{6.38 \times 25.4} = 0.611$ m.m.

J = 1.63 m.m. except at supports

DESIGN REQUIREMENT

Check on Max. Deflection $= \frac{5\ Ml^2}{48\ EI} = \frac{5x4.44x81x12x64}{48x\ 375000} = 0.077$ in.

which is less than t/3 = 0.25/3 = 0.0833 O.K.

Check on Minimum Radius of Curvature:- $R.\ 1/R = 0.02022\ (1-J/K)$
$= 0.02022 \times 0.42 =$
0.00849

R= 117.75 in. which is more than 2h = 96.62 o.k.

FIG. T7

II Experiment AB & CD Free
AB & BD Simply Supported
After Load

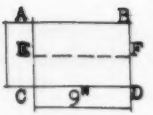

Date - March 11, 1954 Loading - 0.5 p.s.i.

Supp	Line	Reading	K	J/K	1-J/K	Moment	Theoret	% Error
C		40.54						
	1	39.22	1.32	0.99	0.01	+0.11	0.00	
	2	37.44	1.78	0.92	0.08	0.98		
	3	35.48	1.96	0.83	0.17	1.63		
	4	33.35	2.13	0.77	0.23	2.93		
	5	31.06	2.29	0.71	0.29	3.25		
	6	28.58	2.48	0.66	0.34	4.01		
	7	26.09	2.49	0.65	0.35	+4.44	5.14	13.6%
	8	23.62	2.47	0.66	0.34	4.34		
	9	21.24	2.38	0.68	0.32	4.12		
	10	18.88	2.36	0.69	0.31	3.80		
	11	16.63	2.25	0.72	0.28	3.47		
	12	14.66	1.97	0.83	0.17	2.39		
	13	12.96	1.70	0.96	0.04	1.41		
D		12.31	0.65	0.96	0.04	+0.33	0.00	
		m.m.	m.m.			in lbs.	in lbs.	

MOMENT DIAGRAM

Scale: 1 in. Horiz. = 1.61 in. Model & 1 in Vert.= 5.43 in.-lbs. Model

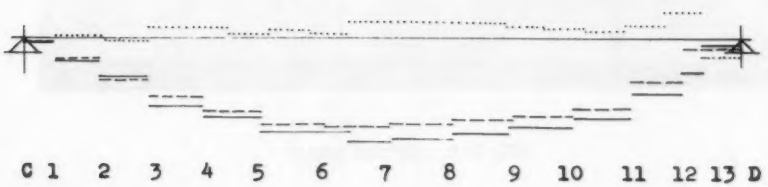

FIG. T8

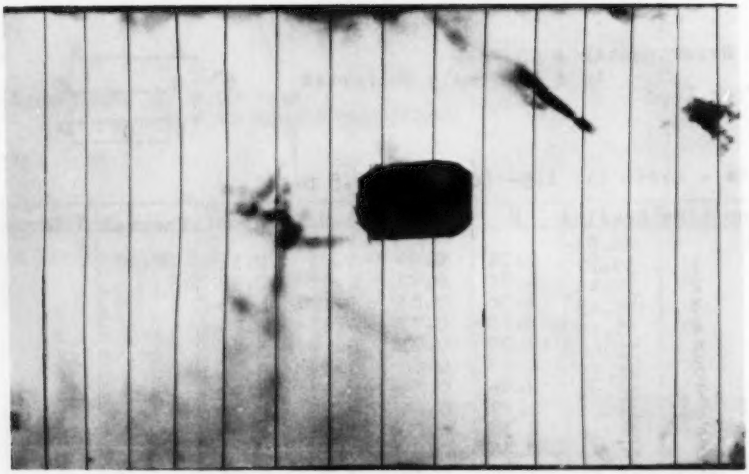

FIG. T9.—BEFORE LOAD

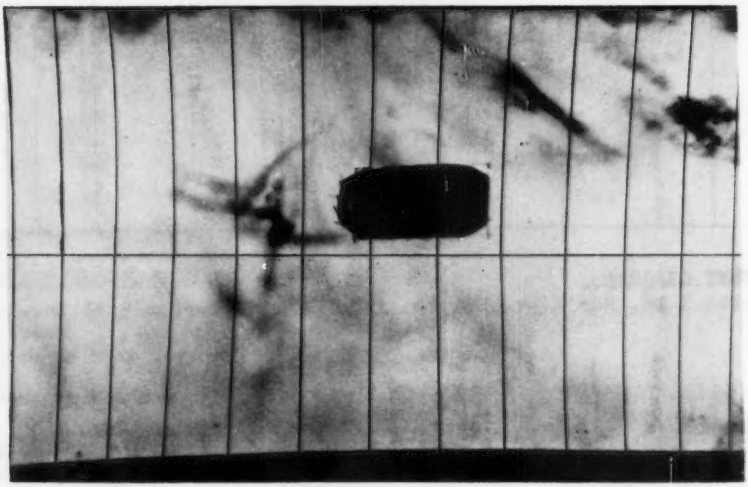

FIG. T10.—AFTER LOAD

With regard to large plate deflections, similitude equations would be difficult to satisfy with a plastic material corroborating a structural steel in the strain-hardening range.

It would be of great value to obtain influence surfaces by electronic digital computers using the finite difference solution for rectangular plates with varying degrees of skew, edge conditions, and continuous spans.

BEHAVIOR OF STRUCTURES DURING EARTHQUAKES[a]

Discussions by John A. Blume, and Edward Cohen and Samuel Weissman

JOHN A. BLUME,[1] F. ASCE.—The author's paper contains interesting averaged spectral response curves. It also brings together, for convenience, subject matter that has been treated in various previous papers and reports. Some of the subjects have been more extensively considered in certain other papers, the reference to which and to related sources might have been of interest to the reader in view of the general title.

The average spectrum curves (Figs. 7 and 8) are based upon the eight components of the four strongest ground motions yet recorded. The desirability of obtaining smooth curves, rather than the jagged curves of a single spectrum for low damping values, is recognized. However, a sense of complacency should not be developed from the fact that the records used by the author for this purpose are "the four strongest ground motions yet recorded." Recording history only goes back to 1933, a brief interval for random occurrences of this nature. It would be expected with the continued accurate recording of destructive ground motion that has been done by the Seismological Division of the U. S. Coast and Geodetic Survey (USGS), that many greater response spectra will become available with time. The San Francisco 1906 earthquake, as one example that was not recorded, was an earthquake of much greater energy release and presumably much greater effect on structures (or on spectral response) than any of those recorded thus far. The use of averages is, therefore, not yet recommended for ultimate design procedures unless good judgment allowances are made for the variations in intensity, epicentral distance, and the geological and soil conditions that would be expected with a more adequate sampling of earthquake ground motion.

The variations in response for various epicentral distances and soil conditions has been considered previously.[2,3] The writer has done considerable thinking about this matter and is of the opinion that the greater-intensity close-epicenter shocks yet to be accurately recorded could well create "spike" or impact effects on records that could accentuate short period response considerably. Moreover, the far-epicenter shocks could have a much greater resonant response on long period structures than has been shown on spectra thus far. The Mexico City and the Taft earthquakes indicated this effect. The author's Fig. 9 is, thus, very interesting to the writer who had constructed an

---

[a] October, 1959, by George W. Housner.

[1] Pres., John A. Blume and Assocs. Research Div., San Francisco, Calif.

[2] "Effects of Ground on Earthquake Motion," by B. Gutenberg, Bulletin of the Seis. Soc. of Amer., Vol. 47, July, 1957, pp. 221-250.

[3] "Structural Dynamics in Earthquake-Resistant Design," by John A. Blume, Proceedings, ASCE, Vol. 85, No. ST 4, July, 1958, and Closure, September, 1959.

"absolute maximum" spectrum of possible spectra, or a so-called "spectragraph," on the basis of response calculations to hypothetical impact pulses and repeating (resonant) cycles from possible future shocks and the detailed study of existing spectra, supplemented by estimates and plain guesses. The purpose was to provide a limiting value for a standard earthquake rating for structures of all types.[3] It is expected and hoped that such velocity values never occur. Fig. 1 shows this "spectragraph" as well as other spectra including certain of the author's values. Any of these can be converted to acceleration by $A = \frac{2\pi V}{T}$ in which A is the acceleration and V denotes velocity. All curves shown are for 5% of critical damping, a value that has been suggested by the writer as a logical value for normal design purposes. Most structures, especially buildings, seem to have about a 5% non-damaging damping capacity and more than this cannot, generally, be justified in the so-called elastic range. Much greater energy dissipation capacity may be present, but this is an inelastic problem for which other considerations are indicated depending upon the type of motion—steady state[4] or other and the materials involved. The 0% damping spectrum has little use in design applications.

The writers "spectragraph" or suggested absolute curve for rating purposes is the upper line, (a). As previously suggested,[3] this energy is roughly 2.3 times El Centro 1940. Thus, $2.77(T)^{1/4} \sqrt{2.3}$ or $1.83(T)^{1/4}$, curve (b), is plotted as an approximation to El Centro 1940 (NS). Curve (c), interpolated spectral values for 5% n, and curve (b) are in close agreement except in the very short period range in which, perhaps, none of the curves shown are accurate. The author's "average" velocity spectrum is the lowest curve and 2.7 times this is his suggested curve for El Centro 1940. Although curves (b), (c) and the author's El Centro average are very similar in shape, there is a definite spread in velocity values, much of which may be due to the process of averaging from 8 records and then factoring back to the original; and some is, of course, due to averaging both components for El Centro 1940.

It would seem that the writer's suggested relationship, velocity equals $1.83(T)^{1/4}$ is both simple and reasonably accurate for design purposes for El Centro 1940 (N-S). Of course, other factors, F in velocity equals $F(T)^{1/4}$, could be applied for other earthquakes or damping values. For T values less than 0.15 or 0.20 sec, more detailed data will shortly be available.[5] If a factor of 3.5 were applied to the author's average curve of Fig. 7, almost perfect coincidence with the writer's curve (b) would be obtained except in the short period range where the writer has allowed for the greater close-epicenter shocks than have been recorded in this manner.

The curves in Fig. 9 are Taft 1952, Hollywood 1952, and San Francisco 1957, respectively, all of which are for no damping. From Fig. 7 it can be seen that the short period hump characteristics of Taft curve A disappear with damping. In fact, at 5% damping, the Taft curve would plot as 1.6 times the "average" shown on Fig. 1.

The author mentions the effect of damping and the value of cracking, rubbing, and plastic yield of composite building structures and the anomalies be-

---

4 "Frictional Effects in Composite Structures Subjected to Earthquake Vibrations," by L. S. Jacobsen, Dept. of Mech. Engrg., Stanford Univ., March 9, 1959. (California State Div. of Architecture, sponsor).

5 "A Structural Dynamic Investigation of Fifteen School Buildings Subjected to Simulated Earthquake Motion," by Blume, Sharpe, and Elsesser, for the State of California, Dept. of Pub. Wks., Div. of Architecture. (being printed)

tween observed behavior and design values of old buildings and he discusses the damage to a structure as a means for absorbing energy and the survival of these structures being "not so much a matter of static lateral strength as a question of whether the structure can continue to absorb appreciable energy during its vibrations." He also compares a complex, traditional-type building to a simple roof and column structure. These matters have been extensively and numerically considered elsewhere.[3] The Alexander Building has been extensively studied for many years[6] and qualitative and numerical values of the energy dissipation capacity have been determined.[3,4]

The author states that the results of such analysis (overstressed non-linear vibration) are not yet in a form to be used for design and he suggests an approximate method for assumed elasto-plastic behavior based upon average spectral velocity. There is a general method for aseismic design in any type of inelastic response (including actual failures of elements) that is in a form for design and it is also in terms that are familiar to the structural designer. This method involves only simple mathematics and a knowledge of the force-deflection characteristics of the structure or a basic unit of same. If the force-deflection or spring factor characteristics are not known or cannot be estimated up to failure, no method of inelastic design or energy dissipation design can be consistently reliable, no matter how rigorous the analysis. This procedure, termed the "reserve energy technique," has been found to be a simple but effective basis for design or prediction of structural response, drift and damage. Although it is so far only suggested for use to modify or analyze structures first designed under static codes, it seems to have interesting possibilities.[5,7] It can also be used to evaluate "plateau" or multi-stage resistance, to provide value against collapse in severe emergencies, to account for period variations with damage, and to evaluate condition after damage.

The authors Eqs. 18, 19, 21, and 22 are based upon average spectral velocities. Although the simplicity of this is recognized and often justified, the variations that occur in velocity with period (Figs. 5, 6, 7, and the writer's Fig. 1) can be appreciable, especially for a value that is squared to obtain kinetic energy. It would also appear that some nominal damping value, say 5% of critical, should be used for velocity (or acceleration) in energy design procedures. A normal hysteresis loop about both sides of the no-load point on a force-deflection curve would account for this, or its equivalent, by trading on energy lost in the form of heat rather than to damage or permanent set. Assuming 5% for this purpose, and using the author's Fig. 7 values as well as curve (b), Fig. 1, a comparison is obtained as shown in Table 1 for which there is a 5% damping value. It is to be noted that the required energy dissipation values vary considerably with period. A simple device for improving the relative results is to use the writer's velocity approximation (Fig. A), modified for the "El Centro type" earthquake. Thus, the total energy requirement would be $\frac{0.12\ W}{2.3}\sqrt{T}$, or $0.052\ W\sqrt{T}$, column 4. On this basis, the energy dissipation requirement, D, would become $D = 0.052\ W\sqrt{T} - V$. V is neglected as minor in the comparisons of Table 1. The 0.10 ft-lb energy requirement would develop at T = 3.7 sec, which is a long period.

---

6 "Period Determinations and Other Earthquake Studies of a Fifteen-Story Building," by John A. Blume, Chapter 11, Proceedings of the World Conf. on Earthquake Engrg., June, 1956, EERI, Room 1039, 465 California St., San Francisco, Calif.

7 Discussion of "Electrical Analog for Earthquake Yield Spectra," by John A. Blume, Proceedings, ASCE, Vol. 86, No. EM 3, June, 1960.

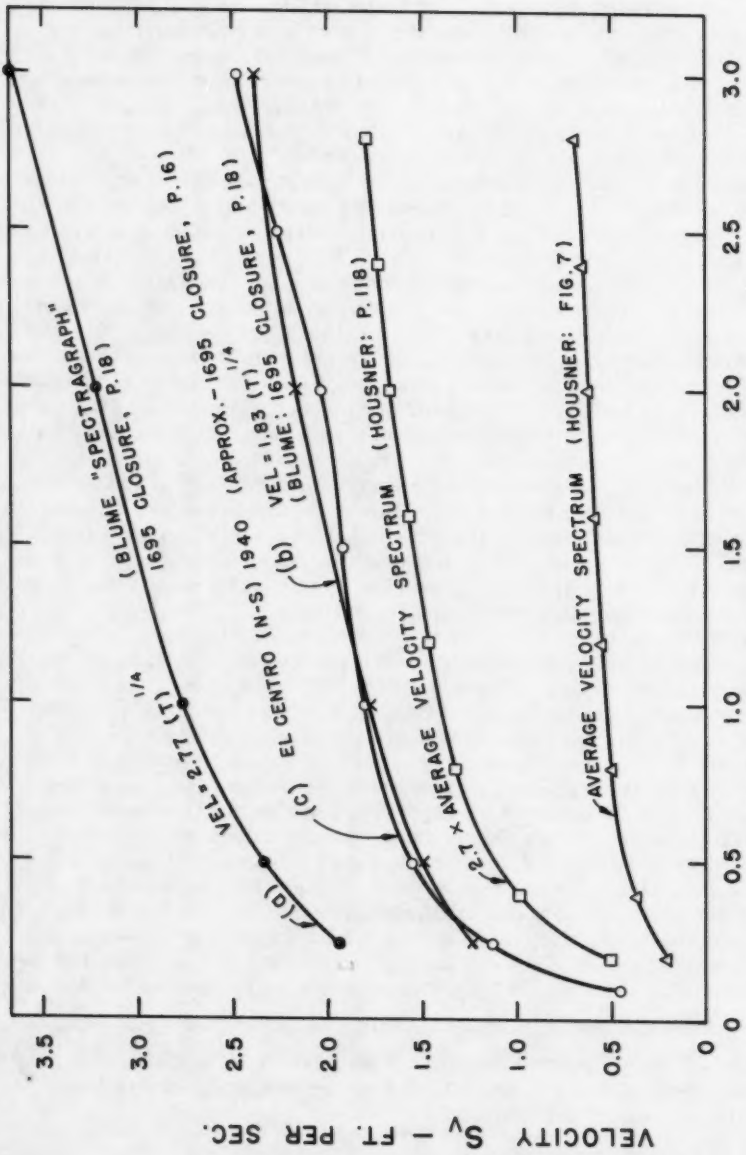

FIG. 1.—COMPARISON OF VELOCITY SPECTRA, n = 5%

Column 3 represents the energy requirements using the author's averaged El Centro 1940 velocities and column 4 the writer's El Centro 1940 N-S velocities. There is a variation between the two, but what is even more significant, a considerable variation in either case from a constant value such as 0.10 ft-lb of energy per pound weight of structure. Most buildings, of a few stories, would be in the 0.5 sec or less period range.

The spectral response curves can be valuable in design as well as in comparing earthquakes. Code design requirements, although constantly improving,

TABLE 1.—VELOCITY AND ENERGY REQUIREMENTS FOR EL CENTRO 1940

T_1 seconds (1)	Sv From Fig. 7; n = 5% (2)	$D = \frac{(2.7\ Sv)^2 W}{2g}$ (3)	From Curve (b) $D = 0.052W\sqrt{T}$ (4)
0.1	----	----	0.016W
0.5	0.40	0.019W	0.037W
1.0	0.52	0.033W	0.052W
2.0	0.61	0.045W	0.073W
3.0	0.68	0.056W	0.090W
3.7	----	----	0.10W

are not, in the writer's opinion as in the author's conclusion, adequate for the final design of unusual, very slender, very tall, or very critical structures. Modern aseismic design or analysis should deal numerically as well as intuitively with energy requirements, yield deflection, and damage under various degrees of severity and probability.

The research work being done on school buildings for the California State Division of Architecture, indicates that there can be a considerable variation of the type and amount of earthquake resistance for different buildings designed under the same code and, also, that the short period range of the spectrum (0.05 to 0.20 sec) needs more attention to the design and analysis of the numerous low buildings.

EDWARD COHEN,[8] F. ASCE and SAMUEL WEISSMAN,[9] A. M. ASCE.—The author has presented a timely paper describing the application of response spectra to aseismic design. The proposal to have two design criteria in seismically active areas, one to avoid damage from frequent earthquakes and the second to avoid collapse from earthquakes of maximum anticipated severity, deserves serious consideration.

Several years ago, the senior writer proposed[10] a similar procedure in which he postulated a "standard" and a "maximum" earthquake. Designs for the "standard" earthquake having a probable recurrence period of 50 yr would limit damage to negligible or minor, easily repaired, amounts. For the "maximum"

8 Assoc., Ammann and Whitney, Cons. Engrs., New York, N. Y.

9 Structural Designer, Ammann and Whitney, Cons. Engrs., New York, N. Y.

10 "Rational Analysis of Earthquake Distortions," by E. Cohen, Presented at the Centennial of Engrg. Convocation, Symposium of the Amer. Geophysical Union, Chicago, Ill., September 12, 1952.

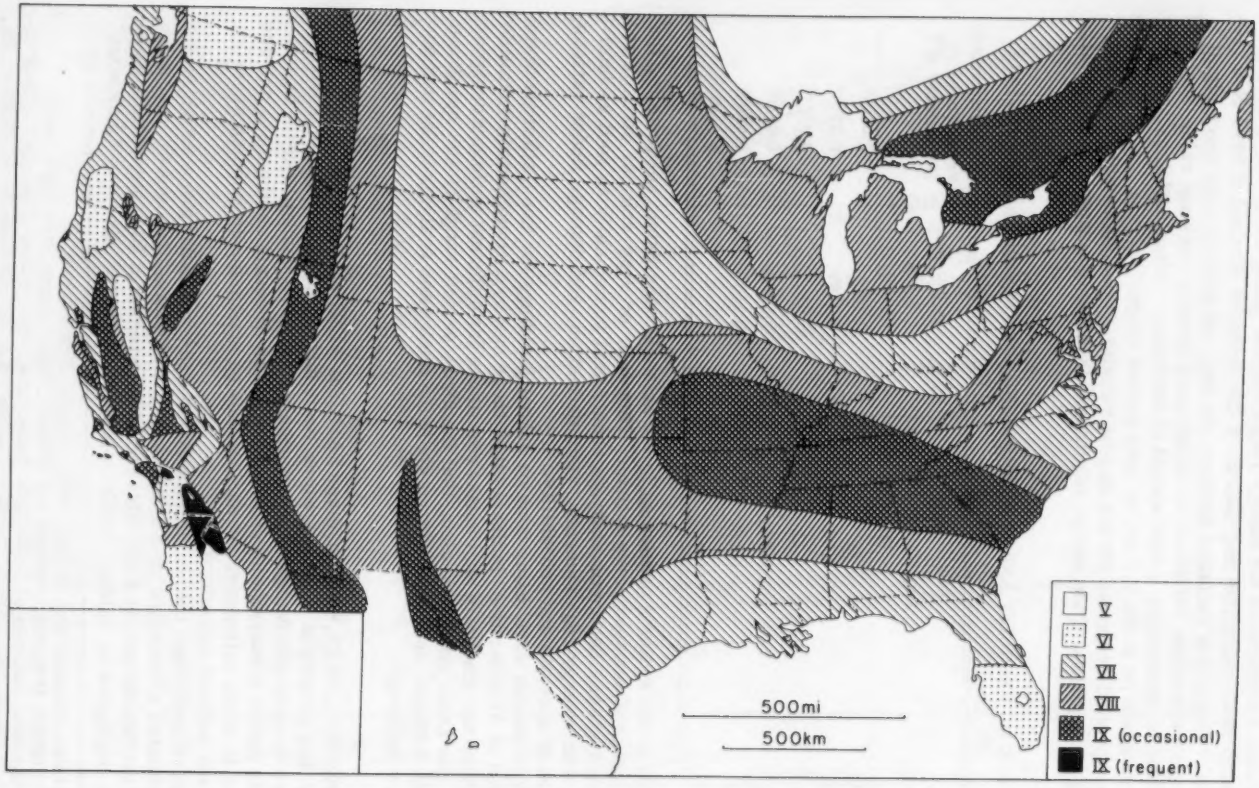

FIG. 1.—SEISMIC REGIONALIZATION OF THE UNITED STATES SHOWING ZONES OF GIVEN PROBABLE MAXIMUM INTENSITY

earthquake the structure would be allowed to approach incipient collapse. Distortions and ultimate strength would be the controlling design criteria rather than allowable stress. Recent studies and investigations indicate that our knowledge of structural strength and behavior under dynamic loads is adequate for this purpose.

The "standard" and "maximum" earthquakes would be defined by synthesized ground motions consistent with the geology in the vicinity of the building or by response spectra for the standard earthquake. However, methods of predicting the standard and maximum earthquakes appeared to be beyond the state of the art. One of the implications of building codes, which seems to be condoned to some extent by the author's discussion, is that the maximum anticipated earthquake is the maximum experienced earthquake. This is contrary to general engineering practice relative to the prediction to other recurring physical phenomena which cannot be predicted on a sound theoretical basis and probably unlikely except in very active seismic regions.

C. F. Richter has described[11] a study which shows promise of progress in the direction of actual "risk zoning." Unfortunately, this excellent paper has not had wide distribution in civil engineering circles, as yet. Richter reports that proposals similar to that of the senior writer were made in Russia in 1949, high intensity regions (greater than Mercalli VIII) being divided into areas with probable recurrence times of 1) centuries, 2) decades, 3) years. Although such "risk zoning" is still some time off, Richter has prepared a regional map (Fig. 1) of probable maximum intensity for the United States which should be of considerable interest to the profession.

It may be of interest to note that the ground motions associated with nuclear weapons bursts are currently being considered in the design of protected facilities. The problems encountered are, in many ways, similar to those of earthquake engineering and procedures of the type suggested by the author are currently being used to analyze structures and shock isolation systems. However, the physical characteristics of the ground shocks differ from those of an earthquake.

Ground motion from nuclear bursts may be induced by two distinct processes: (1) air-induced shock, and (2) ground-transmitted shock. The ground-transmitted shock is a direct conversion of hydrodynamic energy into mechanical energy in the vicinity of the explosion. Nuclear-weapons-test data has indicated that the air-induced shock effects are substantially larger than the ground-transmitted effects for most cases in current design pressure regions. The air-induced shock is caused by the blast wave traveling over the ground surface. The characteristics of the blast wave in terms of intensity, propagation velocity, and variation with time are functions of the weapon size, height of burst and distance from ground zero. This air blast wave impulse loading on the ground surface results in predominantly single pulse ground motions.[12]

Fig. 2 shows records of typical vertical free-field acceleration versus time in gravity units for the 1 ft and 5 ft depth below the ground surface. These

---

11 "Seismic Regionalization," by D. F. Richter, Calif. Inst. of Tech., Contribution No. 897, December, 1958.

12 "Underground Shock Environment Data and Application to the Design of Underground Structures," by E. Cohen and S. Weissman, Proceedings of the 28th Symposium on Shock, Vibration, and Associated Environments, Office of the Dir. of Defense, Research and Engrg., Washington 25, D. C., February, 1960.

were obtained during a nuclear weapons test at the Nevada Test Site[13] for a 40 kiloton weapon at the 200 psi over-pressure range. As seen in Fig. 2 the acceleration records are characterized by single sharp peaks of acceleration (182 and 54.2 gravities) preceded and followed by minor disturbances. The duration of the peak downward acceleration pulse is in the order of 8 millisec for the 1-ft depth and 18 millisec for the 5-ft depth. The total durations are about 0.18 sec which are approximately equal to the air blast duration. These curves are typical of free-field accelerations in both the vertical and horizontal directions in that there is rapid attenuation of acceleration and decrease of frequency with depth. The single sharp acceleration pulse corresponds to a ground displacement which is also essentially a predominant single displacement pulse. This differs from typical earthquake motion in that the frequency

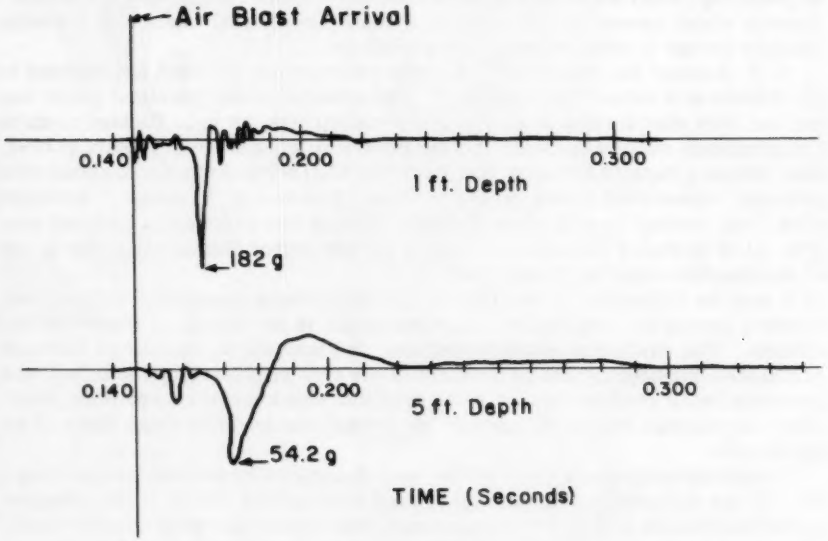

FIG. 2.—VERTICAL FREE—FIELD GROUND ACCELERATION VERSUS TIME, NEVADA TEST SITE; W=40 KT, p=219 PSI

and intensity of acceleration is much higher, having a single sharp peak, rapid decay and considerable attenuation with depth in the upper layers.

Fig. 3 shows vertical displacement shock spectra recorded at the Nevada Test Site[14] for 10 to 40 kiloton weapon yields at 116 to 146 psi pressure regions, by multi-frequency reed gages with approximately one-half per cent of critical damping. Peak displacements of the gages were recorded near the ground surface (2-ft depth) in the free field and in a shallow buried structure.

13 "Ground Acceleration, Stress and Strain at High Incident Overpressures," by L. M. Swift, D. C. Sachs, and F. M. Sauer, Project 1.4, Operation Plumbbob, ITR 1404, Stanford Research Inst., Menlo Park, Calif., 1957, (Classified).

14 "Ground Shock Environment—Measurement and Application," by M. V. Barton, GM-TR-293-A, Space Tech. Lab., The Ramo-Wooldridge Corp., Los Angeles, Calif., December 11, 1957.

As indicated by the spectra there is considerable attenuation of the free-field responses by the shelter. Fig. 4 is a vertical acceleration spectrum derived from average displacement responses of Fig. 3. The responses increase as the frequency increase reaching a peak at about 150 cps and decreasing in the higher frequency range. It is significant to note that the range of most earth-

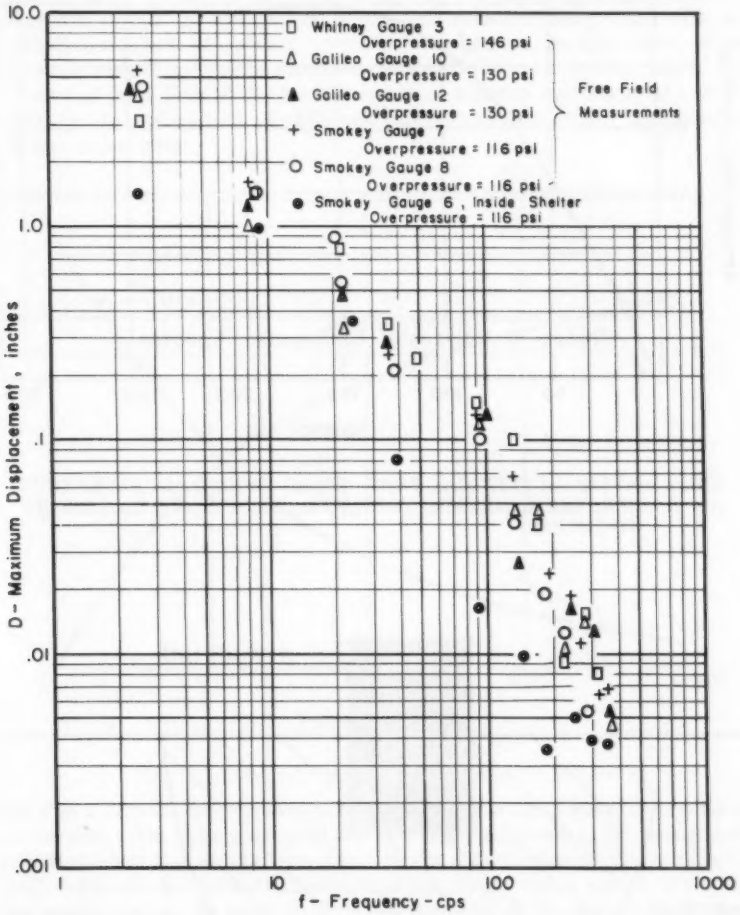

FIG. 3.—VERTICAL DISPLACEMENT SHOCK SPECTRA, NEVADA TEST SITE; W = 10 KT TO 40 KT

quake spectra would fit into the small area indicated near the origin of the acceleration spectrum curve. Although data is limited it appears that response records of a particular ground shock gage do not exhibit as complicated a form as the earthquake spectra. This is the result of oscillators of all frequencies responding to the predominant single pulse, whereas earthquake spectra may be representative of resonant responses at the particular frequency range close

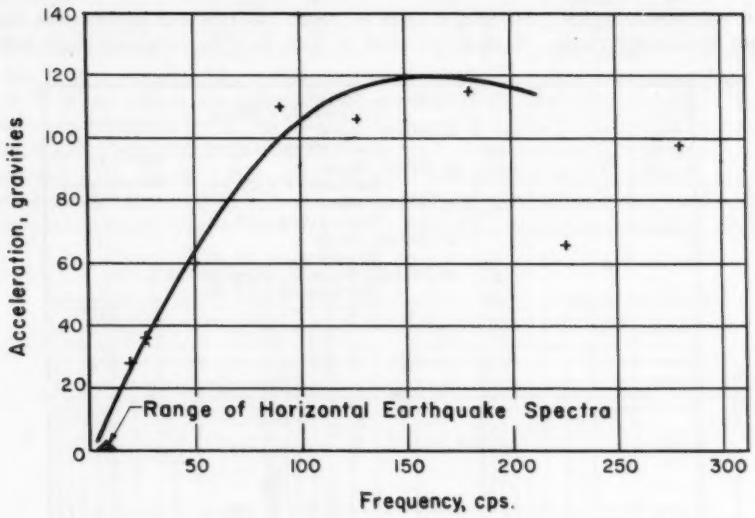

FIG. 4.—AVERAGE VERTICAL FREE—FIELD GROUND ACCELERATION SPECTRUM, NEVADA TEST SITE; W = 10 TO 40 KT, p = 116 PSI TO 146 PSI

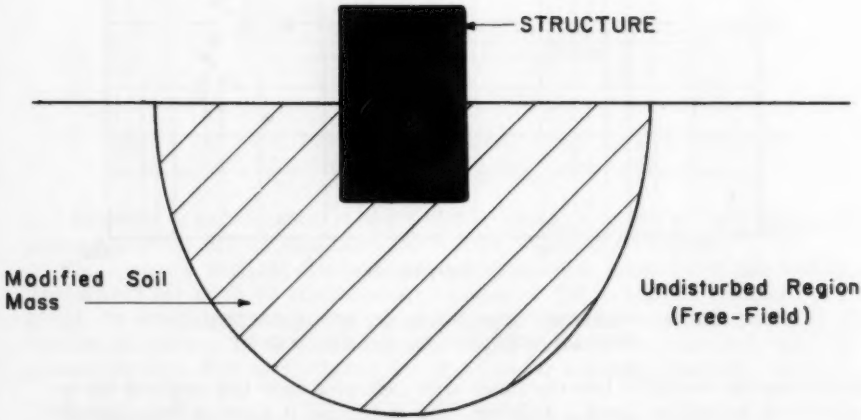

FIG. 5.—SCHEMATIC REPRESENTATION OF STRUCTURE IN A GROUND SHOCK OR EARTHQUAKE FIELD

to the frequencies of the ground vibration. For the same reason, structure damping is not as important in this case as in the case of earthquakes.

It is important to note that spectra obtained from free-field ground motion data (motion not affected by the presence of a structure) may not be the actual motion of the ground at the base of a multi-story building or surrounding a hard buried structure.[15] This is particularly true for the high frequency portion of the spectra in that the interaction of the structure and the ground will, in effect, modify the actual vibrations induced by the ground. In blast induced shock this effect is magnified by the sharp variation of the motion with depth. Thus, ground motion data obtained in the basement of a particular structure may not be applicable to structures of different mass, configurations and frequency even in the same area.

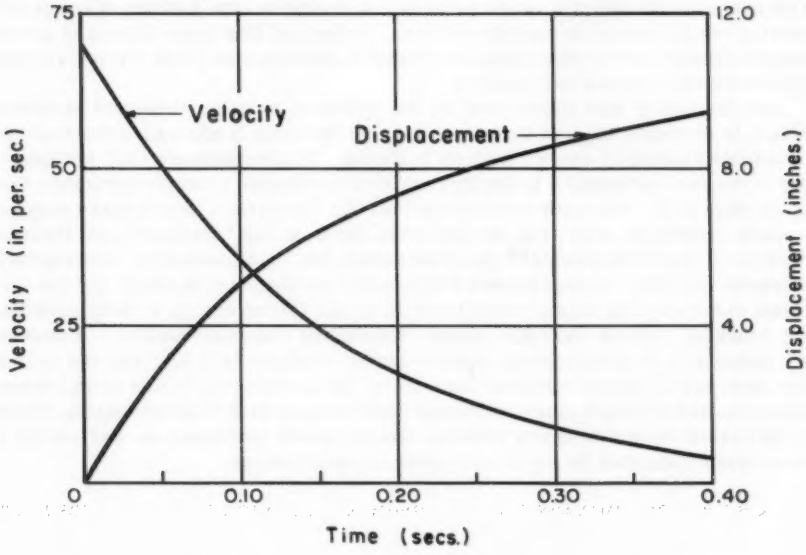

FIG. 6.—DISPLACEMENT AND VELOCITY PULSE

Fig. 5 is a schematic representation of a structure in a general ground shock or earthquake field. The motion of the soil mass adjacent to the structure will be modified from that in the free-field by the interaction of the structure and the soil. Although the free-field response spectrum which exists in the undisturbed region cannot be used directly for analysis of the structure, it may be applied to the overall system, including the adjacent soil mass if the system is and remains elastic. It may also be used for elastic structures where the ground interaction may be neglected or approximated. For elasto-plastic, non-linear or discontinuous structures a free-field spectrum, without further analysis, has only limited value. However, a synthesized ground motion curve consistent with both the spectrum and observed motions is useful.

15 "Comprehensive Numerical Method for the Analysis of Earthquake Resistant Structures," by C. S. Whitney, B. G. Anderson, and M. G. Salvadori, Proceedings, ACI, September, 1951, Vol. 48, pp. 5-28.

Such ground motions have been synthesized in the case of nuclear ground shock by approximating the ground motion as a single displacement or velocity pulse.[16] Fig. 6 shows a displacement and velocity pulse which was derived from the average response spectrum of Fig. 4. This pulse, applied to a series of single degree of freedom oscillators, would result in the peak responses of the spectrum for the frequencies below 100 cps which includes the range of application to most structures. A velocity pulse having a rise time to the peak value may be derived to conform more closely in the higher frequency area if required. The displacement curve is of the same type observed in test records. Using such a pulse a consistent analysis may be performed by numerical integration taking into account elasto-plastic, non-linear and discontinuous behavior.[12,15,17]

The longer duration and more periodic nature of the earthquake ground motion prevents the use of a single pulse and a complete time history of the ground motion would have to be considered in an analysis of this type. Trains of ground displacements of varying frequency could be determined from typical recorded earthquake motion and spectra.

As discussed and illustrated by the author a suitably designed structure which is stressed beyond the yield point by dynamic loads will absorb an appreciable amount of energy without collapse. It also appears that because of the increased earthquake intensity required to collapse a ductile structure than to damage it, the strength requirements of the "maximum" earthquake may not greatly exceed or may even be less than those of the "standard" earthquake. Studies of blast resistance[18] have indicated that it is feasible to substantially increase the blast overpressure required to produce collapse of the conventional structures by minor modifications in the initial design to fully mobilize the inherent lateral strength and or ductility of the construction. However, the validity of a design based upon dynamic analysis is a function not only of the accuracy of the calculations but also of the consistency of the actual mass, stiffness, and strength magnitudes and distributions with those assumed. Where large plastic distortions are allowed unanticipated increases or variations in these quantities may be as catastrophic as deficiencies.

---

16 Developed by V. Chobotov, Space Tech. Labs., Inc., Also, See Reference 3.

17 "Impulsive Motion of Elasto-Plastic Shear Buildings," by E. Cohen, L. Levy, and L. Smollen, Transactions, ASCE, Vol. 122, 1957, p. 293.

18 "Design of Balst Resistant Construction for Atomic Explosions," by C. S. Whitney, B. G. Anderson, and E. Cohen, Proceedings, ACI, Vol. 51, March, 1955, pp. 589-683.